PALEOCEANOGRAPHY OF THE SOUTH ATLANTIC OCEAN FROM THE MIDDLE EOCENE THROUGH THE OLIGOCENE

By

GREGORY A. MEAD

A DISSERTATION PRESENTED TO THE GRADUATE SCHOOL
OF THE UNIVERSITY OF FLORIDA IN PARTIAL FULFILLMENT
OF THE REQUIREMENTS FOR THE DEGREE OF
DOCTOR OF PHILOSOPHY

UNIVERSITY OF FLORIDA

1995

This Dissertation is dedicated to the memories of my Grandmother Minnie Morris and my Mother Shirley Lopez, Father Daniel Weiss, and Step-father Bruce Mead.

ACKNOWLEDGMENTS

I would like to thank first my advisor and friend, Dr. David A. Hodell, and the rest of my committee, Drs. Paul F. Ciesielski, Douglas S. Jones, Neil D. Opdyke, and Claire L. Schelske, for (at various times) advice, encouragement, and financial support. Drs. G. W. Brass, J. P. Kennett, D. V. Kent, K. G. Miller, J. S. Oslick, E. Thomas, J. D. Wright, and J. C. Zachos contributed valuable comments on the chapters. The idea for the *Braarudosphaera* study was initiated in a class led by Dr. E. L. (Jerry) Winterer. Dr. Kennett also supplied the washed samples from ODP Hole 689B, and Dr. Zachos allowed me to use unpublished data from ODP Hole 748B. It is impossible to thank Ray Thomas enough for keeping the equipment running. Rich Cooke, Jason Curtis, Dr. Ann Heatherington, Vicky Mejia, and Dr. Paul Mueller also helped materially in the laboratory. Richard Crockett was the Scanning Electron Microscope technician. Hallie Smith produced the drafted figures.

My fellow Micropaleo lab students, Alex Amigo, Jennifer Callahan, Jason C., Jose Garrido, Rick Greenfield, Anon Vayavananda, and Kathy Venz, were invaluable sources of advice, commentary, brain-storming, and entertainment. I thank them, along with all those who worked in the lab, Soraya Balmes, Gail Beals, Belinda Seidel Breidenbach, Gil Butler, Rich C., Charlotte Davison, Sabine Eppler, Paul Gremillion, Binhe Gu, Alexandra Isern, Vicky M., Danny Müller, Mark Mulligan, Tamara Mullis, Sarah Palmer, Mark

Schult, Laura Stanley, Loni Terry, Jang Vayavananda, Ana Vrba, and Doug Wilder, for their friendship and for making the lab a pleasant (if at times distracting) place to work and study.

In addition, I especially thank Gail B., Kim D'Arcy and Paul Meyers, Vic Divenere (also for teaching me recorder), Ken Gilland, Lori Guthrie, Jack Holt, George Houston, Paul (the Mac Master) Kirk, Nancy Mullins (also for the loan of her printer), Mark S., Ana V., and Mick and Julie Whitelaw for their companionship, understanding, and friendship over the years I've been here.

I want also to thank all my family, and my extended families, the Abrams and the Beals, for their support and love during this (at times) seemingly endless endeavour.

I also thank the Gainesville Cycling Club, the Gainesville Area Fiddle Jam and Fast Molasses, and the J. J. Finley Ultimate players for helping keep me healthy (more or less) and sane (more or less).

Finally, I thank my cat Trash, and my other 4-footed friends, Harold, Rhett, Yoda, and Barclay, for their unquestioned and unending affection.

This research was supported by National Science Foundation grants OCE-8858012 and DPP-8717854 and by the Donors of the Petroleum Research Fund administered by the American Chemical Society.

PREFACE

The late Paleogene (middle Eocene through Oligocene) was an important time in the Earth's biogeographic, paleoclimatic, paleogeographic, and paleoceanographic history. It marked the transition between the warm Cretaceous and early Paleogene, and the cooler Neogene [Miller et al., 1991a,b]. The continents of the Earth were approaching the present positions, as Australia and India moved northward, the Atlantic Ocean continued to widen, and the Tethys progressively constricted [Dercourt et al., 1986]. It was during this time that major seaways opened around Antarctica [Kennett et al., 1972], allowing the Antarctic to cool to the point where glacial ice could eventually build up.

A band of siliceous deposition widened as a result, and the planetary temperature gradient increased, causing more restricted biogeographic zonation. Deep thermohaline circulation in the oceans also developed at this time.

In the Oligocene, a series of deposits in the Atlantic and Indian Oceans (Braarudosphaera oozes) suggest that unusual conditions repeatedly occurred, for reasons that are poorly understood. Biostratigraphic markers are relatively rare in the Oligocene, leading to poor resolution in stratigraphy.

Isotopic studies of geochemical tracers have been important parts of research into this time period in the oceans. Progressive oxygen isotopic enrichment of planktic and benthic microfossils has documented oceanic cooling, mostly of high latitudes, with a major shift in the earliest Oligocene suggesting probable glaciation (confirmed by the finding of ice rafted debris in Indian Ocean drill holes [Zachos et al., 1992b]) and cooling, especially of bottom waters. Additional glaciations have been postulated during the Oligocene as a result of other $\delta^{18}O$ enrichments. An inversion in the usual $\delta^{18}O$ gradient in two sites just off the Antarctic coastline has been interpreted to result from the production of warm saline bottom water in the Eocene and warm saline deep water with an underlying psychrosphere [Kennett and Stott, 1990].

The oceanic record of carbon isotopes has shown that changes have occurred more uniformly, with less geographic variability. The changes have been inferred to be overall reservoir changes rather than basin-to-basin fractionation. The low paleogeographic variation has been suggested to be due to low productivity, especially during the Oligocene [Miller, 1992; Wright and Miller, 1993].

The balance between continental weathering of ^{87}Sr-rich rocks and hydrothermal weathering of ^{86}Sr-rich oceanic crustal rocks controls the marine $^{87}Sr/^{86}Sr$ ratio preserved in foraminiferal shells. The middle to late Eocene $^{87}Sr/^{86}Sr$ ratio was held low at a near constant level, indicating a stable continental weathering to hydrothermal weathering ratio, with domination by the hydrothermal component. A transition to steadily increasing conditions in the late Eocene has been used to infer increased continental weathering rates, either through increased mountain building [Richter et al., 1992] or increasing glaciation [Oslick et al., 1994]. Not incidentally, the steadily increasing $^{87}Sr/^{86}Sr$ values also allow improvements in Oligocene stratigraphic resolution, as biostratigraphic events can be dated more precisely even in the absence of magnetostratigraphy, and as the ratio itself can provide a unique date once the curve is correlated to the Geomagnetic Polarity Time Scale (GPTS).

This dissertation is composed of four chapters, which serve to examine aspects of late Paleogene paleoceanography. It is concentrated in the South Atlantic, but many of its conclusions may be extrapolated world-wide.

Since the research in this dissertation refers back to several older data sets, most dated magnetostratigraphically, the first chapter presents a compilation and correlation of the 12 comprehensive GPTSs developed since 1968. The correlations enable conversion of dates generated under older time scales to newer ones. The correlation table has been placed on-line at the National Geophysical Data Center to enable other researchers to have easy access to it.

Strontium isotope stratigraphy from the middle Eocene through the Oligocene is the topic of Chapter 2. A well dated, nearly continuously deposited and recovered section from Ocean Drilling Program (ODP) Hole 689B, a key high latitude site, was used to generate a fairly high resolution (166 ky/sample) $^{87}Sr/^{86}Sr$ record. This record was used in two ways. First, the $^{87}Sr/^{86}Sr$ record was used to form a refined strontium isotope stratigraphy from the mid Eocene to the end of the Oligocene. This will allow further researchers to correlate biostratigraphic markers to the GPTS. Second, the record forms the basis for modelling experiments to determine the tectonic changes controlling the marine $^{87}Sr/^{86}Sr$ ratio. Since both hydrothermal activity [Edmond et al., 1979; Owen and Rea, 1985; Lyle et al., 1987] and mountain building [Raymo and Ruddiman, 1992] can have implications for affecting the Earth's climatic history, it is important to understand what these changes are.

The third chapter uses $\delta^{18}O$ and $\delta^{13}C$ to examine deep circulation changes in the Antarctic and South Atlantic Oceans, especially with respect to Warm Saline Deep Water. It uses pre-existing data from ODP Sites 689 and 690 [Kennett and Stott, 1990] with new data from ODP Sites 699 and 703 to examine the vertical $\delta^{18}O$ and $\delta^{13}C$ distribution in this region during the late Paleogene, and examines the changes in circulation which may have taken place during those times, the loci of deep- and bottom-water formation, and the influence of glaciation.

The final chapter examines the genesis of *Braarudosphaera* oozes in the South Atlantic by examining $\delta^{13}C$ and $\delta^{18}O$ records from mid-South Atlantic Deep Sea Drilling Project sections. These data are analyzed in terms of their possible relationships to vital effects, productivity, shallow- and intermediate-depth circulation, and how the circulation may have been affected by Oligocene glaciation.

Collectively, these studies have two purposes. First, they act to improve stratigraphic correlation and resolution in marine sections of the late Paleogene. Second, these studies are intended to help delineate circulation in shallow, intermediate, and deep parts of the South Atlantic, and to help us understand how this circulation affected and was affected by changes in the Earth's paleoclimatic, paleogeographic, paleoceanographic, and paleotectonic regimes.

TABLE OF CONTENTS

page

ACKNOWLEDGMENTS....iii

PREFACE....v

ABSTRACT....xii

CHAPTERS

1 THE CORRELATION OF GEOMAGNETIC POLARITY TIME SCALES....1

- Introduction....1
- Calibration of the Time Scales....5
- Correlation Between Time Scales....13
- Discussion....21
- Conclusion....26

2 CONTROLS ON THE $^{87}Sr/^{86}Sr$ COMPOSITION OF SEAWATER FROM THE MIDDLE EOCENE TO OLIGOCENE: HOLE 689B, MAUD RISE, ANTARCTICA....28

- Introduction....28
- Methods And Materials....33
- Results....43
- Discussion....50
- Conclusion....92

3 LATE EOCENE TO OLIGOCENE VERTICAL OXYGEN ISOTOPIC GRADIENTS IN THE SOUTH ATLANTIC: IMPLICATIONS FOR WARM SALINE DEEP WATER....95

- Introduction....95
- Methods....99
- Results....113
- Discussion....121
- Conclusion....151

4 OLIGOCENE BRAARUDOSPHAERA OOZES AND CHALKS: GENESIS AND PALEOCEANOGRAPHIC IMPLICATIONS FROM ISOTOPIC ANALYSES OF FINE FRACTION AND FORAMINIFERA....154

- Introduction....154
- Methods....166
- Results....171
- Discussion....204
- Conclusion....220

APPENDICES

A LARGE DATA TABLES....223

- 1 Correlated Geomagnetic Polarity Time Scales from 1968 to 1994....224

2 Sr, O, C Isotope and Sr/Ca Data, ODP Hole 689B....239
3 Oxygen and carbon isotope analyses of *Cibicidoides* spp. for ODP Hole 703A....253
4 Oxygen and carbon isotope analyses of *Cibicidoides* spp. for ODP Hole 699A....262
5 Oxygen and carbon isotope data from DSDP Site 363, cores 5, 6, and 7....269

B DETAILED METHODS AND DERIVATIONS....276

1 Instructions for obtaining and using on-line data tables....277
2 Strontium extraction method....280
3 Operating instructions for thermal ionization mass spectrometer....282
4 Preparation of foraminifera for oxygen and carbon isotopic analysis....287
5 Derivation of equations....291

REFERENCES....294

BIOGRAPHICAL SKETCH....315

Abstract of Dissertation Presented to the Graduate School of
the University of Florida in Partial Fulfillment of the
Requirements for the Degree of Doctor of Philosophy

PALEOCEANOGRAPHY OF THE SOUTH ATLANTIC OCEAN FROM THE MIDDLE EOCENE THROUGH THE OLIGOCENE

By

GREGORY A. MEAD

May, 1995

Chairman: Dr. David A. Hodell
Major Department: Geology

In middle Eocene through Oligocene time, the Earth experienced major changes, including major plate tectonic events and the transition from relatively warm conditions to polar ice and high planetary thermal gradients. These paleoclimatic and tectonic events led to changes in the isotope geochemistry of the oceans, the basis for this dissertation.

Marine microfossil $\delta^{18}O$ evidence suggests that the warmest temperatures of the Cenozoic were during the early Eocene. Planktic and deep-sea benthic foraminiferal $\delta^{18}O$ data suggest that temperatures began to decrease from that time in a series of rapid changes separated by periods of relative stasis. Despite these Eocene climatic changes, the marine $^{87}Sr/^{86}Sr$ ratio stayed relatively constant, implying that the balance between continental erosion and hydrothermal input to the oceans was unchanging.

During the Eocene, $\delta^{18}O$ data from Ocean Drilling Program (ODP) Sites 689 and 690 show a reversal in the normal temperature gradient, interpreted as mid-water warm, salty deep waters underlying cooler, fresher, shallow waters. Additional data from ODP Sites 699 and 703 show that at least by the late middle Eocene, this warm, saline deep water mass extended to abyssal depths.

Strontium isotopic data from ODP Site 689 show that in the late Eocene (about 35.5 Ma), a profound, sudden change in the crust's geochemical balance occurred as marine $^{87}Sr/^{86}Sr$ ratios began to rise rapidly, probably as hydrothermal alteration decreased relative to continental weathering. The timing of this event suggests that it was not due to increased continental weathering due to either glaciation or uplift. In the earliest Oligocene (about 33.5 Ma), marine $\delta^{18}O$ values increased by about $1^{o}/oo$ at all paleodepths in the deep South Atlantic, indicating an increase in continental ice volume and/or lower temperature. This change, estimated to be due 35% to increased Antarctic ice volume and 65% to temperature decrease, left the ocean's vertical temperature structure unchanged. Oxygen isotopic evidence suggests that at this time, glacial ice became semi-permanent on Antarctica, waxing and waning through the mid-Oligocene and beyond.

During the Oligocene, repeated _Braarudosphaera_ oozes were deposited. These unusual deposits may have resulted from upwelling of cold, low-salinity, nutrient-rich water originating from melting of an Antarctic ice shelf during glacial/interglacial transitions.

CHAPTER 1

THE CORRELATION OF GEOMAGNETIC POLARITY TIME SCALES

Introduction

Knowledge in geology advances with time, just as it does with all sciences. However, geology differs from other sciences in that the baseline by which all other data are calibrated, the geologic time scale, changes as the knowledge changes. In most cases, the ordering of events in the geologic time scale does not change. However, spacing between events does change. This causes our understanding of rate-dependent geologic processes to change (e.g., sedimentation rates, frequency of glaciations, tectonic plate motions, or evolutionary rates) [Kominz, 1984; Delaney and Boyle, 1988].

The geologic time scale, especially among marine geologists, is calibrated to the marine magnetic anomaly pattern (the Geomagnetic Polarity Time Scale, GPTS) for the past 100 Ma or so. Since the advent of plate tectonic theory [Vine and Matthews, 1963] when it was realized that marine magnetic anomalies (MMA) are created during the seafloor spreading process, several different GPTSs based on the MMA pattern have been developed, beginning with the pioneering time scale of Heirtzler et al. [1968]. A GPTS is based on the concept that seafloor anomalies record the history of geomagnetic polarity reversals. Time scales based on MMAs differ in a number of ways, including the particular anomaly pattern used, the method of dating tie-points within the pattern, the method used in dating anomalies between tie-points, the radiometric decay constant used for radiometric dates, and the particular anomalies included or excluded from the time scale.

Since 1968, at least 12 different, comprehensive, geomagnetic polarity time scales covering the last 80 or 100 Ma (back to Anomalies 33 or 34) have been constructed, along with a host of partial time scales which cover smaller parts of the polarity record. As a result, comparing studies which use different time scales can be difficult, because events may be dated at different times which may be simultaneous, or events which appear to be simultaneous may in fact be diachronous.

Unfortunately, the problem is worsened by the fact that in very few of the revisions are direct comparisons made between the revised and older time scales. Usually, the ages of periods of normal polarity are given, often with little or no identification. Since revisions often distort some of the polarity intervals, and insert or delete others, it becomes a non-trivial matter to determine which polarity interval of one time scale is correlative to a polarity interval of another time scale.

This paper attempts to give a comprehensive correlation of 12 geomagnetic polarity time scales over the past 26 years. It does not in general discuss the relative merits of each time scale. Comparisons of preceding time scales generally can be found in each successive revision, but especially in Ness et al. [1981] and Harland et al. [1990]. This paper instead is meant to be a resource by which investigators can calibrate studies which use different time scales, or to bring older studies up to date. It presents a brief description of the method used for calibration of each time scale to geochronology, and a graphic and tabular correlation of the time scales to one another. The means by which time scales are correlated are discussed, and ambiguous regions are noted. In addition, during the preparation of this paper, a total of 6 errors were identified in 5 published time scales. They are listed in Table 1-1 along with the way that the errors were identified. In most cases, it is unlikely that researchers re-entering the time scales for their own uses would not notice them, but they are presented here for the sake of completeness. Finally, to help others avoid the onerous task of typing in each of the time scales for their own use, a copy of the table which correlates the time scales will be placed on-line (see Appendix A1) so that it may be downloaded for the use of other researchers (see Appendix B1 for instructions).

TABLE 1-1

List of typographical errors in published Geomagnetic Polarity Time Scales

Time Scale	Datum	Incorrect Date	Correct Date	How Error Was Recognized
HDHPL68	Within 1r	1.93	0.93	Out of order
TM76	Top 5^{III}	12.49	16.49	Out of order
MD79	Top 12	33.32	33.22	Not correctly converted from LKC77.
NLC81	Within 17	38.57	39.57	Out of order
NLC81	Within 17	38.64	39.64	Out of order
GTS82	Top of Jaramillo	0.92	0.90	Supposed to be identical with MD79.

Calibration of the Time Scales

The Heirtzler et al. [1968] (HDHPL68) time scale was based on a single magnetic anomaly record from the South Atlantic, the V-20SA magnetic profile from about 30°S, on the western side of the Mid Atlantic Ridge. Heirtzler et al. [1968] examined several magnetic profiles from the Atlantic, Pacific, Indian, and Antarctic Oceans and concluded that the South Atlantic was most likely to have undergone spreading at a constant rate. This anomaly profile was to become the standard, with modifications, for most subsequent time scales. Only two dates for the profile were used: 0 Ma for the center of the Mid Atlantic Ridge, and 3.35 Ma for the Gauss/Gilbert boundary [Doell et al., 1966]. This resulted in a calculation of 1.9 cm/yr as a spreading rate, which they extrapolated to the entire anomaly pattern. The result was an age of 76.33 Ma for the top of Anomaly 32, and a slightly adjusted age of 3.37 Ma for the Gauss/Gilbert boundary. The ages of normal polarity intervals are presented in their Table 1 without identification, although the major anomalies are identified graphically in their Figure 3 (which in some cases differs from the table; see the last two normal polarity intervals in their table and figure, for instance). Despite the extrapolation of constant spreading rates to more than 22 times the length of the dated portion of the anomaly pattern, the HDHPL68 time scale has remained within a few percent of succeeding time scales.

Tarling and Mitchell [1976] (TM76) revised the HDHPL68 time scale in two major ways. First, they introduced additional radiometric calibration points from sedimentary sequences for the anomaly pattern. They dated the top of Anomaly 6 at 19.5 Ma, with Anomalies 13, 24, and 30 centered at 35, 48, and 64-65 Ma, respectively. They then linearly corrected all reversal boundaries to these tie points. Secondly, they inserted additional polarity intervals into Anomaly 2 based on reversals found in deep sea sections, and into Anomaly 5 based on reversals found in deep sea sections and in MMA patterns by Blakely [1974]. They designated additional polarity intervals with superscript roman numerals such as Anomalies 2^{I}, 5^{IV}, etc. As with the HDHPL68 time scale, ages of normal polarity intervals are not identified in the tabular listing of ages, only graphically.

A widely used major revision of the GPTS was developed by LaBrecque et al. [1977] (LKC77). They started with the original HDHPL68 time scale, and added an additional calibration point at the base of Anomaly 29 of 64.9 Ma. This was based on an age of 65 Ma for the Cretaceous/Tertiary (K/T) boundary, which was found just below Anomaly 29 in a section at Gubbio, Italy [Lowrie et al., 1976]. They also used a more recent [Dalrymple, 1972] age for the base of the Gauss (Anomaly 2A) of 3.32 Ma, adjusted the length of Anomaly 4A, included the short reversed intervals in Anomaly 5 of Blakely [1974], inserted an extra reversal in Anomalies 23 and 24, spliced in a revised sequence from Anomalies 29 to 34, and most importantly, removed Anomaly 14 from the GPTS, which was not found in most anomaly patterns. In addition, LKC77 used radiometric ages directly for anomalies younger than 2A [Klitgord et al., 1975], and extrapolated the GPTS through Anomaly 34, to 108.17 Ma. The new time scale was presented with brief identification of periods of normal polarity in both tabular and graphic form. This time scale re-appeared in the Larson et al. [1982] time scale, with extensions to the Mesozoic by Larson and Hilde [1975] and Van Hinte [1976a,b].

Later in 1977, new decay constants were adopted for K/Ar dating [Steiger and Jäger, 1977]. All subsequent time scales used the new decay constants in calculating K/Ar dates. To take into account the new decay constants, Mankinen and Dalrymple [1979] (MD79) revised the LKC77 time scale by recalculating each of the LKC77 time scale datums to new values. They presented their results in a side-by-side comparison to the LKC77 time scale, along with anomaly identifications, simplifying conversion from one to the other time scale. MD79 further revised the late Neogene (5-0 Ma) based on additional radiometric dates later in their paper (their Figure 3); those dates are presented in the 5-0 Ma portion of this compilation.

A comprehensive review of previous time scales, along with the development of a new one, was presented by Ness et al. [1980] (NLC80). The new NLC80 time scale was based in general on the LKC77 time scale corrected to the new K/Ar decay constants, but used segments from several other time scales to adjust the length of anomalies, and to insert a few new reversals. Yet another terminology was used in the NLC80 time scale, with decimal numbers, and then primes, to designate successively smaller intervals after the main anomaly numbers. A total of 4 calibration points, plus the present, were taken from a wide variety of sources, and dates were interpolated between them. Anomaly 2.3'(o) (for "older end") was fixed at 3.40 Ma, with dates extrapolated to Anomaly 3.4; Anomaly 4.1'(y) was fixed at 7.81 Ma; Anomaly 24(o) was fixed at the Paleocene/Eocene boundary (54.9 Ma); and the K/T boundary, just below Anomaly 29(o), was fixed at 66.7 Ma. The study compared in graphical form the dated anomaly sequences and time scales used in all the previous studies discussed in the present paper, as well as several more fragmentary sequences. A synthetic anomaly profile was generated which facilitates comparison to other anomaly sequences. Major anomalies and correlations between the various time scales were made (and in general are followed in this paper) although a few ambiguities remained. Dates attached to the anomaly patterns were unfortunately printed in a font so small as to be nearly unreadable.

Another time scale appeared just a year later by Lowrie and Alvarez [1981] (LA81). This time scale used a total of 11 biostratigraphically defined calibration points (geologic period boundaries), from Italian pelagic sections (as well as the 0 Ma point), to modify the LKC77 time scale, corrected for new K/Ar decay constants. The biostratigraphic correlations allowed them to adjust the positions of the anomaly boundaries to agree with additional radiometric dates. As in most other time scales, the ages between calibration points were determined by linear interpolation. Most of the anomaly boundaries were identified in the table of ages provided.

A geologic time scale covering the entire Phanerozoic was published in 1982 by Harland et al. (GTS82). It dated MMA from the present back into the Mesozoic, although for the sake of consistency it is reported here only through Anomaly 34. From 5-0 Ma, radiometric dates were used to fix reversal boundaries. From 83-5 Ma, GTS82 is based on MMA, modified from LA81. Two modifications were made. First, the Paleocene and Eocene boundary calibration points were removed because they implied improbably rapid spreading rate changes. Points at the beginning and ends of the Paleocene and Eocene were kept, however. The second modification was to place the K/T boundary at 65 Ma; some other adjustments were made to reduce apparent spreading rate changes as well. Overall, NLC80 was stretched between the new calibration points from 10.3 to 83 Ma, NLC80 was used directly for 3.4 to 10.3 Ma, and MD79 was used directly from 0-3.4 Ma.

An extremely widely used time scale was next published by Berggren et al. [1985a] (BKFV85). The same time scale has appeared as Berggren et al. [1985b,c] separately for the Paleogene and Neogene, and, with extensions, in Kent and Gradstein [1986] (back to the Jurassic). The major advance of this time scale was that it integrated biochronologic, magnetochronologic, and radiochronologic data into a single time scale. The BKFV85 time scale used fewer calibration points than some of the recently preceding time scales, only 6 (plus the present). The younger ends of Anomalies 2A, 5, 12, 13, 21, and 34 were fixed at 3.40, 8.87, 32.4, 34.6, 49.5, and 84.0 Ma, respectively, by reference to a host of different studies. Three best-fit line segments were constructed from these data, from 0 to 10.42 Ma (the base of Anomaly 5), from 10.42 to 56.14 Ma (the base of Anomaly 24), and 56.14 to 84 Ma (the top of Anomaly 34). Ages for the other paleomagnetic boundaries were interpolated from LKC77 and reported in tabular and graphical form, with most intervals of normal polarity identified. Perhaps most importantly, BKFV85 also correlated marine calcareous planktonic biostratigraphic zonations to the GPTS for the entire Cenozoic. BKFV85 used the chron nomenclature introduced by LaBrecque et al. [1983], with a "C" prefix designating the time during which a given normal and reversed anomaly couplet was created, and a "N" or "R" designating the polarity of the Earth's field at the time within the chron.

Haq et al. [1988] (HHV88) recognized that using a single MMA pattern or a patchwork of MMA patterns strung together suffers from the problem that spreading rate changes may not be taken into account. In addition, errors in radiometric dates of calibration points may introduce errors in calculated spreading rates. To overcome these uncertainties, HHV88 plotted numerous radiometric dates against MMA patterns from 3 ocean basins - the North and South Pacific and the South Atlantic. They calibrated the MMA to best-fit age-to-length lines, and then stacked (i.e., averaged) the ages of the tops of the major anomalies from each basin to arrive at their time scale. The time scale has a coarse resolution, with only the tops of Anomalies 1 to 32, 5A to 5E, and 6A to 6C listed.

Harland et al. [1990] (GTS89) modified the original HDHPL68 anomaly spacing by splicing in parts from the several different sources, and adjusting spacing using MMA pattern segments from fast spreading ridges. To date this modified HDHPL68 record, GTS89 used numerous radiometric dates to define 3 best-fit line segments, from 0 to 3.4 Ma, 9 to about 50 Ma, and about 50 to about 85 Ma. No data was used for 3.4 to 9 Ma. These 3 line segments were used to constrain and convert the modified MMA pattern of HDHPL68, resulting in the new time scale. No correlation to previous time scales is shown. However, through an intermediate step (2 tables), GTS89 does provide an exact match to HDHPL68, except for Anomalies 4A through 5, which are "very different."

Cande and Kent [1992] (CK92) used two new approaches in constructing their new time scale. One of the techniques was the creation of a synthetic MMA pattern in order to remove the problems associated with using a single MMA pattern (V-20SA) as a standard. Cande and Kent [1992] stacked different segments of MMA patterns from the South Atlantic to reduce the noise and error associated with a single MMA pattern, using from 5 to 9 different MMA patterns for every part of the time scale from Anomaly 1 to 34. They next assumed that spreading rates were not necessarily constant but instead smoothly varying, and fitted 9 points (finite rotation poles from Cande et al. [1988]) plus the ridge axis with a cubic spline function. Their aim was to reduce the apparent spreading rate changes in the synthetic MMA record. They also identified numerous "tiny wiggles" (their Table 7) which they did not include in the main time scale (their Table 6). Some of the tiny wiggles they identified (C2r.2r-1, C5n.2n-1 to -3, C5Dr-1, and C13n1) are included in Appendix A1 of this work, because they are commonly observed in previous time scales. The second technique use by CK92 was to use two astronomically tuned dates (0.780 Ma for the Bruhnes/Matuyama boundary and 2.600 Ma for the Matuyama/Gauss boundary) of Shackleton et al. [1990] and Hilgen [1991]. These dates were obtained by assuming that Milankovitch periods seen in geologic records are known more precisely and accurately than radiometric dates over the same intervals, and counting back to magnetic reversals in these records. Interestingly, tuned ages used in this time scale and the Cande and Kent [1995, in press] time scale are all older than radiometric ages by 5 to 10%. It has been suggested that this is due to an error in the decay constant of Steiger and Jäger [1977] [Shackleton et al., 1990] or to diffusional loss of radiogenic Ar [Hilgen 1991].

Cande and Kent [1995, in press] (CK95) is modified in two ways from the CK92 timescale. The later part uses a total of 19 additional tie-points added according to the astronomical time scales of Hilgen [1991] from the base of C3n.4n to the base of C2An.1n and Shackleton et al. [1990] from the top of C2An.1n to the present. The early part was adjusted so that the Cretaceous/Tertiary (K/T) boundary falls at 65 Ma, and another cubic spline used to fit the data from the top of C34n to the base of C3n.4n as with CK92. Because of the use of different cubic splines in CK92 and CK95, the difference between the two time scales varies sinusoidally between ±0.2 my except near the K/T boundary, when CK95 is over 1 my younger than CK92. This time scale will be incorporated into a comprehensive revision [Berggren et al., in preparation] of Cenozoic microfossil datums [Kent, personal communication].

Correlation Between Time Scales

Ideally, every time a new time scale was published, each period of normal and/or reversed polarity would be completely identified so as to facilitate comparison to older and newer time scales. Failing that, it would be helpful if the polarity intervals in each time scale were of equal number and of roughly equal relative size. Both of these possibilities are rarely seen.

Another option would be to have each time scale correlated by referring back to the original anomaly pattern each is based upon. Unfortunately, the anomaly patterns are rarely published, and are presented in only 3 of the papers discussed here (HDHPL68, NLC80, and CK92). It is clear that these papers, each published 12 years apart, are easily correlated by comparison of the anomaly patterns (Figure 1-1), despite the different methods used to construct them.

In lieu of the above choices, pattern matching must be done, similar to the way magnetostratigraphic records in sedimentary sequences are matched to the GPTS. The comparison is made easier because, at least in this case, the entire record is in fact present. This has been done graphically in two of the papers discussed, NLC80 and CK92. NLC80 presented their new time scale correlated to other partial and comprehensive time scales (their Figure 2), with a few lines of correlation, and much of their technique is followed here in Figure 1-2. Few lines of correlation were presented, leaving a great deal of ambiguity in the correlations. CK92 used a different method, displaying each polarity record as a series of lines shifting back and forth

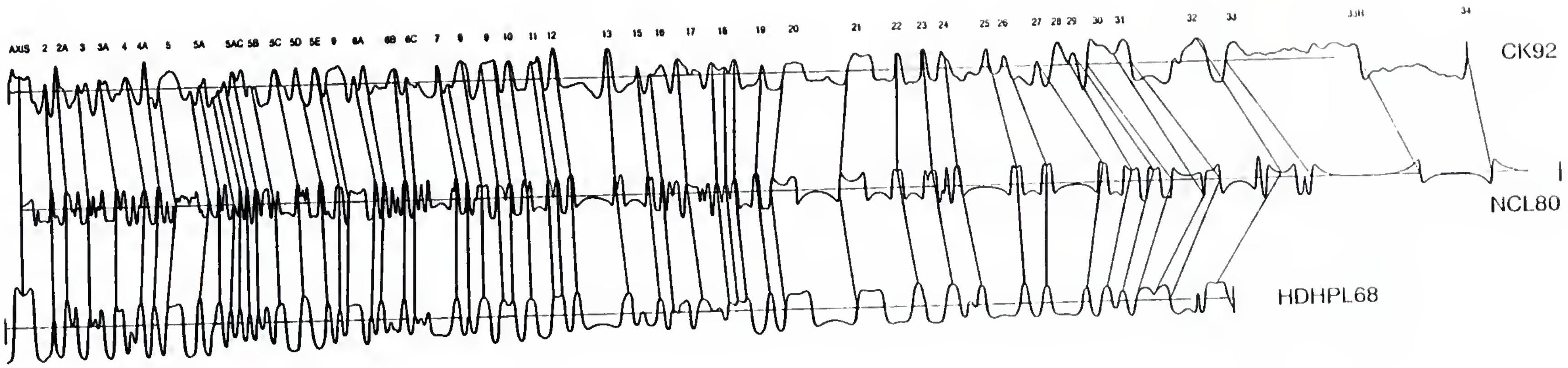

Figure 1-1: Marine Magnetic Anomaly patterns from HDHPL68, NLC80, and CK92. The MMA patterns from HDHPL68 and NLC80 are synthetic. The MMA pattern from HDHPL68 was constructed using the identified anomalies found in profile V-20SA, while the MMA pattern from NLC80 was constructed with the modified magnetic anomaly sequence used to define the timescale itself. The MMA from CK92 is the sum of between 5 and 9 anomaly patterns from the South Atlantic. Note the excellent correspondence, despite the different methods used to construct each MMA pattern.

Figure 1-2: Correlated paleomagnetic intervals from 12 time scales. Black indicates an interval of normal polarity; white indicates an interval of reversed polarity. Lines indicate tops and bottoms of equivalent polarity intervals. In the region from 34 to 64 Ma, some lines are dotted or dashed. The differences are merely to help guide the eye. The abbreviated headings are explained in the text.

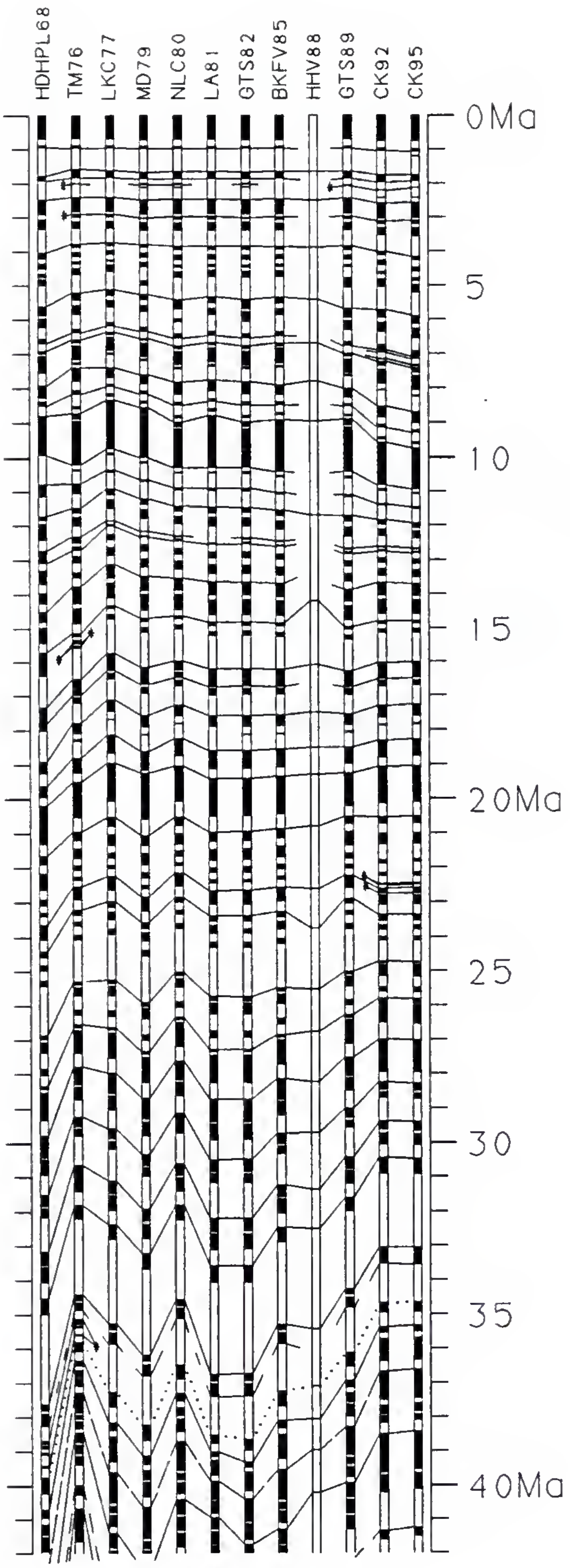
HDHPL68
TM76
LKC77
MD79
NLC80
LA81
GTS82
BKFV85
HHV88
GTS89
CK92
CK95
0Ma
5
10
15
20Ma
25
30
35
40Ma

Figure 1-2--continued

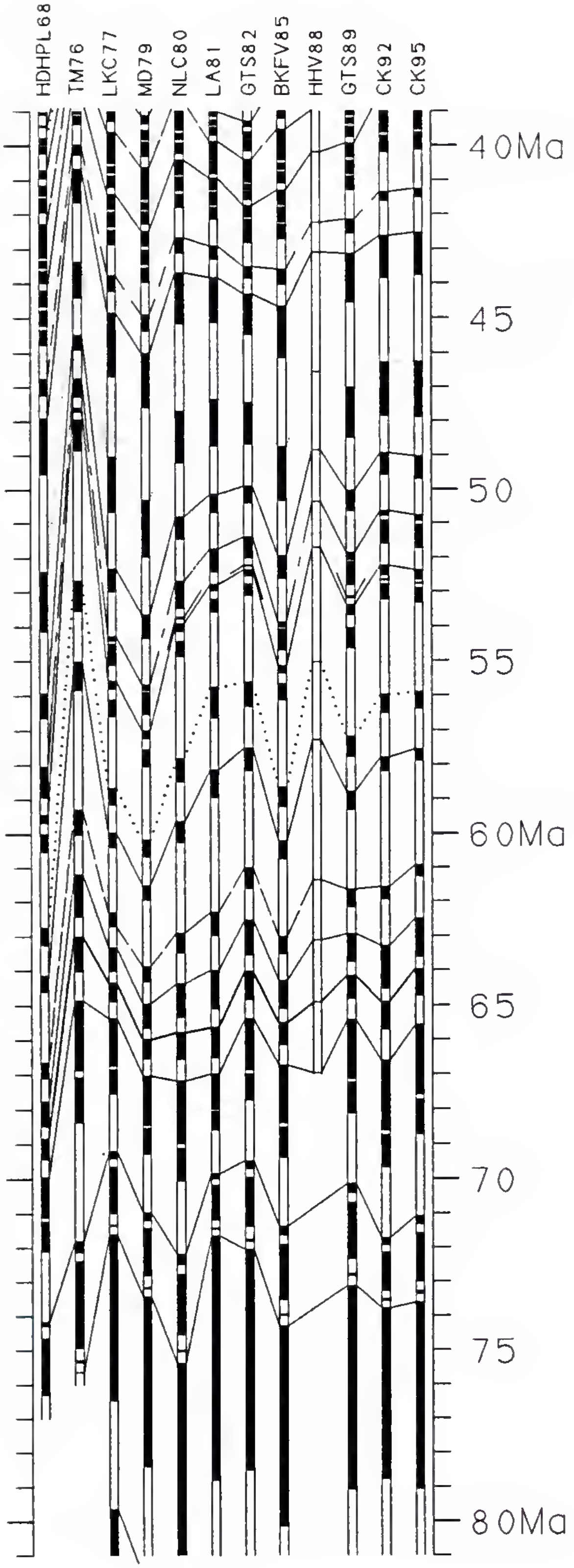

Figure 1-2--continued

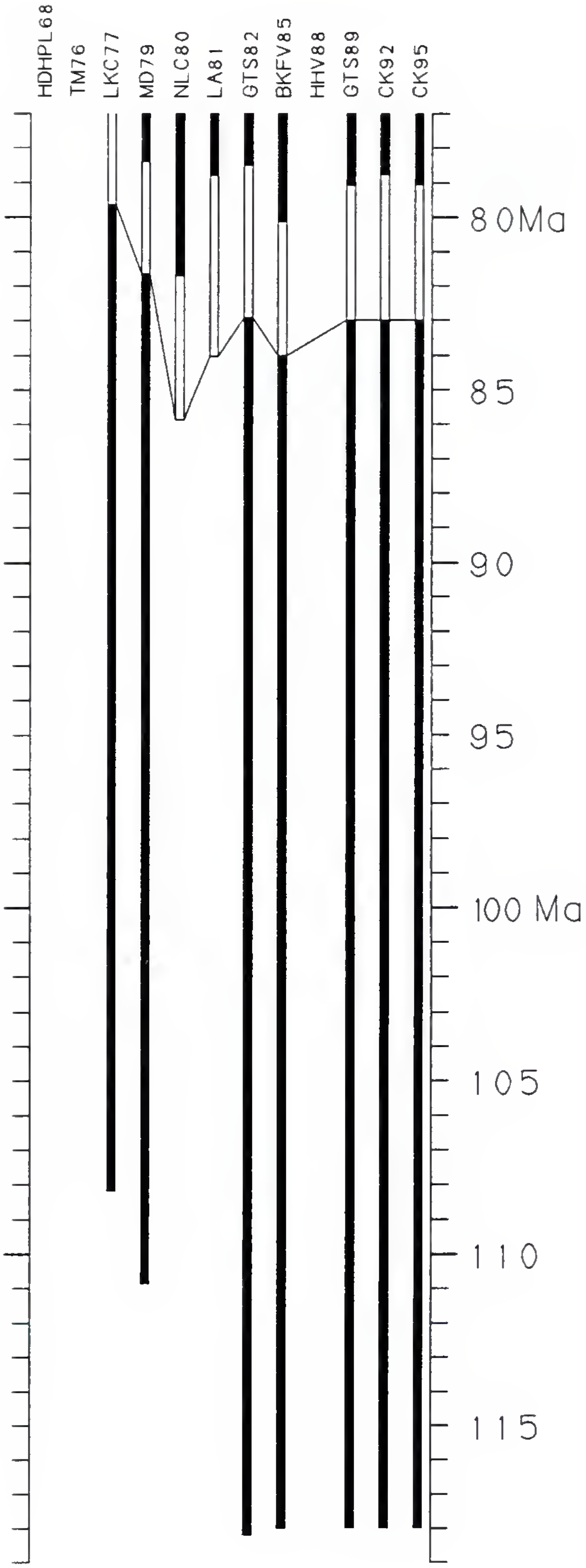

from the right (Normal polarity) to the left (Reversed polarity) for their time scale and 5 preceding time scales.

In this case, no lines of correlation were used, and the figure was published at such a small scale that fine-scale correlations cannot be made.

A hierarchy of methods is used in this paper to correlate the time scales. First and foremost, the authors' designation of a polarity interval, if present, was used to make a first-order correlation. Although not all time scales were published with identifying labels in the table of ages, generally accompanying figures could be used for the same purpose. Second, in the absence of sufficient labeling (and it should be noted that only GTS82, CK92, and CK95 time scales had sufficient unique identifiers for all periods of normal and/or reversed polarity), the relative lengths of the polarity intervals (i.e., pattern matching) were used to make correlations. This method succeeded in making almost all of the detailed correlations left after the first-order correlations. The ambiguities that remain generally result from multiple short reversed or normal events which are not present in all time scales, and whose relative position cannot be used to determine which of the multiple events may or may not be present in a particular time scale.

The result is Appendix A1 and Figure 1-2. Within Figure 1-2, lines of correlation are drawn for the tops of each major polarity chron, with additional lines drawn to clear up any residual ambiguities. Asterisks (*) indicate the ambiguities which remain.

Discussion

A GPTS is usually used to date stratigraphic sequences. An age model for a sequence is developed using identifiable magnetostratigraphic events within the GPTS, or biostratigraphic datums that are calibrated to the GPTS. Sample ages are then calculated by linear interpolation from the position of samples within the stratigraphic sequence. Linear interpolation will also generally be used to make the conversion between one time scale and another. Two factors must be taken into account when converting between time scales, however.

First, in constructing a conversion table of two GPTSs from Appendix A1, only dates (i.e., paleomagnetic chrons) common to both time scales can be used. For example, if conversion is made between the BKFV85 and CK92 time scales, Chron C2r.2r-1 is present only in CK92, not in BKFV85, and must be left out of a conversion table. Similarly, Chron C23R-1, found in NLC80, GTS82, and GTS89, is not present in either BKFV85 or CK92. Obviously, Chron C23R-1 cannot be used in the conversion table, either. Therefore, Appendix A1 must be edited to remove the unusable chron intervals.

Second, even an edited Appendix A1 cannot in general be used to convert ages from one time scale to another directly from the nearest two dates common to both time scales. The reason is that the age model used to date the samples, usually generated from paleomagnetic boundaries, usually only uses selected polarity transitions in a time scale. Since the relationship between time scales is usually not linear, the age model must be converted, and that converted age model used to determine ages directly from stratigraphic sequences. For example, suppose columns 2 and 3 of Table 1-2 show the depths and ages of several samples in a given stratigraphic sequence, using the BKFV85 time scale. If the datums listed in column 1 are known, then the ages of the samples can be easily converted by using the relationship of BKFV85 to CK92 for all points, and are listed in column 4. But if only 2 datums, the top of C12 and the top of C20, are known (e.g., because of coring disturbance or lithologic problems in the section between those datums), then the age model used to calculate ages from the depths would consist of only 2 points, 32.46 Ma at 12.46 m, and 44.66 Ma at 24.66 m, and ages calculated by linear interpolation between those points. Converting those dates to 30.452 Ma and 42.629 Ma of CK92, respectively, and using linear regression to calculate the new dates would result in the ages given in column 5, which differ from the column 4 ages by up to 0.844 Ma (Column 6), a potentially significant error. The reason that the differences exist is that the relationship between BKFV85 and CK92 is not linear in this interval (Figure 1-3).

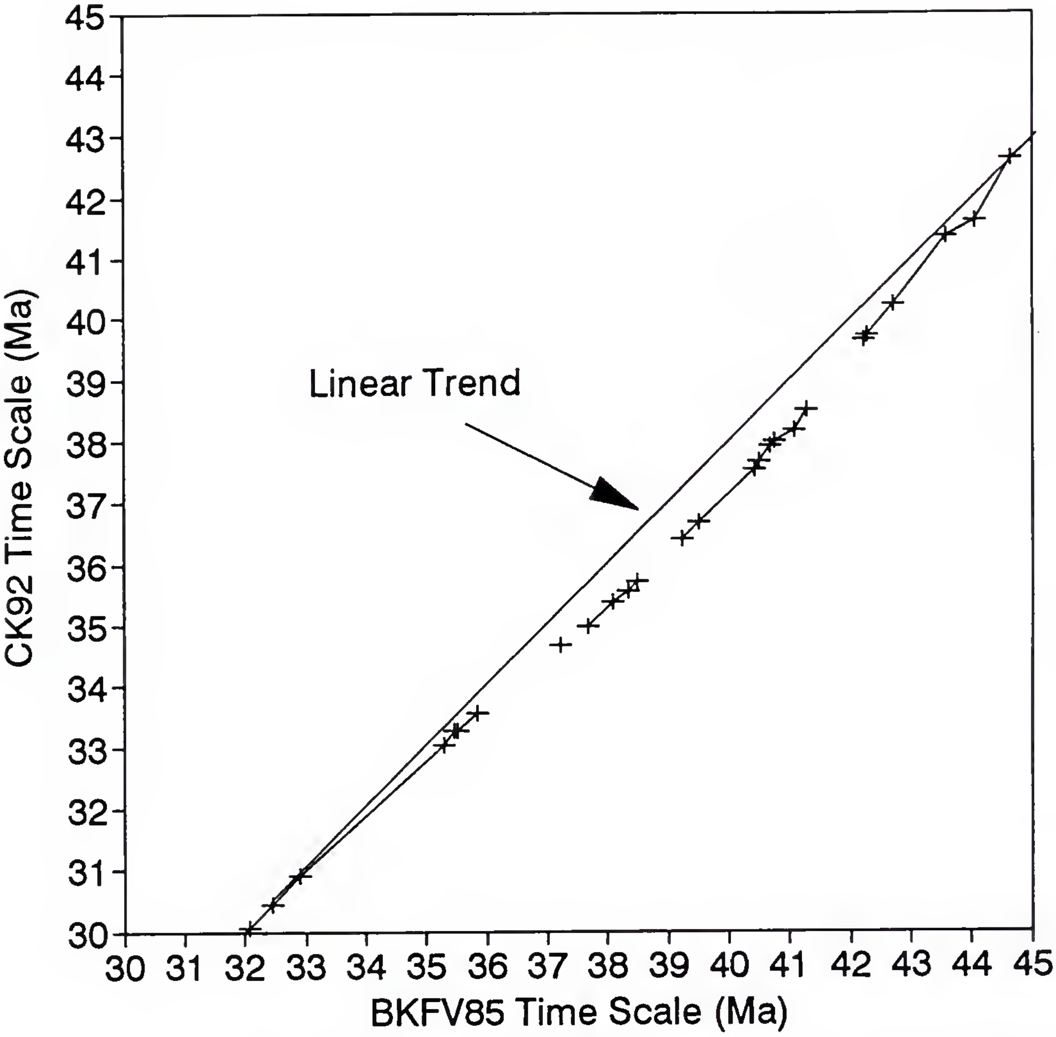

Figure 1-3: The CK92 time scale plotted against the BKFV85 time scale from 30-45 Ma. Note that the relationship is not linear.

For a similar reason, if biostratigraphic datums are being used that have originally been dated paleomagnetically, then to re-calculate the ages of those datums, the original citation must be re-examined, and the ages of the biostratigraphic datums re-calculated based on the age model used in the original citation. Then the new ages of the biostratigraphic datums can be used in a given age model to calculate ages at a particular site.

Therefore, the following steps must be taken in order to convert a series of dated samples from one GPTS to another. First, Appendix A1 of this paper must be edited to remove polarity boundaries not common to both time scales in question. Second, using linear interpolation, the age model originally used to calculate ages for the samples must be converted from the original time scale to the new one. Finally, the newly converted age model may be used to calculate ages of the samples.

The set of steps listed above raises two additional points. In many papers, ages are given without reference to a particular time scale and/or the age model used to calculate those ages. Without this information, it is impossible to evaluate the synchroneity or diachroneity of events within one study with those of another. Therefore, in any geologic study, both the time scale and the age model used should be explicitly stated.

It is of course highly unlikely that the CK92 time scale will be the final word in GPTSs. The utility of

TABLE 1-2

Example of a conversion from one time scale to another

1 Datum	2 Sample Depth (m)	3 Age (BKFV85)	4 Direct Age (CK92)	5 Age-Model Age (CK92)	6 Difference
top C12	12.46	32.46	30.452	30.452	0.000
top C13	15.29	35.29	33.050	33.277	0.227
top C15	17.24	37.24	34.669	35.223	0.554
top C16	18.10	38.10	35.368	36.081	0.713
top C17	19.53	39.53	36.665	37.509	0.844
top C18	21.29	41.29	38.500	39.265	0.765
top C19	23.60	43.60	41.353	41.571	0.218
top C20	24.66	44.66	42.629	42.629	0.000

future time scale revisions would be greatly enhanced if they included a detailed point-by-point comparison to at least one previous version of the GPTS, probably the most recent preceding one.

Conclusion

Since the development of the first comprehensive GPTS in 1968, numerous time scales have been developed based on the sequence of reversals of the Earth's magnetic field. Twelve GPTSs are examined in this paper and correlated to each other as well as possible. The correlations are presented graphically and in table form. Some ambiguities remain, but the correlations should enable conversion from one time scale to another.

Direct conversion from one time scale to another cannot in general be used to re-calculate ages within a stratigraphic section. Instead, the original age model used to calculate ages must be converted, and the new age model must then be used to calculate ages within the stratigraphic section. The reason is that the relationship between GPTSs is rarely linear, and it would be very unusual for every reversal boundary to be identified in any given stratigraphic section.

The need for this paper results from the fact that most revisions of the GPTS do not include detailed, useful comparisons to previous versions of the GPTS. Users of future revisions would be helped if the authors of those revisions would include a detailed comparison to at least one pre-existing version.

CHAPTER 2

CONTROLS ON THE $^{87}Sr/^{86}Sr$ COMPOSITION OF SEAWATER FROM THE MIDDLE EOCENE TO OLIGOCENE: HOLE 689B, MAUD RISE, ANTARCTICA

Introduction

The time from the middle Eocene through Oligocene saw major changes in the Earth's climatic and biotic realms. During this time, the transition from "Greenhouse" to "Icehouse" conditions occurred [Miller et al., 1991a,b]. For example, ice rafted debris (IRD) from Antarctic glaciers first appeared on the Kerguelen Plateau in the earliest Oligocene at about 35.8 Ma (Berggren et al., 1985 time scale), coeval with the world wide increase in $\delta^{18}O$ values of marine carbonates [Zachos et al., 1992b; Breza and Wise, 1992; Barrera and Huber, 1993]. By the late Eocene, the planetary thermal gradient increased [Keigwin and Corliss, 1986; Zachos et al., 1992a]. Major plate tectonic events in the middle Eocene to Oligocene include the opening of the Drake Passage [Barker and Burrell, 1977], the progressive closure of the Tethys and uplift of the Alps [Dercourt et al., 1986], collision of the Indian subcontinent with Eurasia and subsequent uplift of the Himalayan-Tibetan Plateau [Harrison et al., 1992], and a middle Eocene change in the direction of motion of the Pacific plate [Van Andel et al., 1975; Clague et al., 1975; Kennett et al., 1985].

The ratio of ^{87}Sr to ^{86}Sr in the oceans is a function of the balance between continental weathering via riverine input, dissolution of marine carbonates, and hydrothermal exchange with mid-ocean ridge basalts [Palmer and Elderfield, 1985]. When biogenic marine carbonates precipitate, the $^{87}Sr/^{86}Sr$ ratio of ocean water is preserved with no fractionation as Sr substitutes diadochically for Ca. The Sr isotopic composition of the oceans is constant at any given time due to the long residence time of Sr in the oceans (about 2.5 Ma [Hodell et al., 1990]). The $^{87}Sr/^{86}Sr$ ratio thus has great potential as a stratigraphic tool. Although the controls on the Sr budget of the ocean are thought to be well understood [Palmer and Elderfield, 1985], the actual factors that influence changes in the $^{87}Sr/^{86}Sr$ seawater curve are often difficult to determine [Hodell, 1994].

The ratio of ^{87}Sr to ^{86}Sr in marine carbonates has changed irregularly through the Phanerozoic [Burke et al., 1982, Hess et al., 1986], and increased, with some intervals of stasis, throughout the Cenozoic [Palmer and Elderfield, 1985, Koepnick et al., 1985, Hess et al., 1986]. During the Eocene, oceanic $^{87}Sr/^{86}Sr$ ratios were approximately constant, although somewhat variable, and averaged from about 0.7077 to 0.7078 [DePaolo and Ingram, 1985, Hess et al., 1986]. In the late Eocene, oceanic $^{87}Sr/^{86}Sr$ ratios began to increase, rising fairly linearly to about 0.7082 at the end of the Oligocene with a slope reported at from 34×10^{-6}/m.y. [Miller et al., 1988] to 29×10^{-6}/m.y. [Hess et al., 1989]. The transition to more rapidly increasing Oligocene values is not well documented, however. Lower resolution studies [Burke et al., 1982; Koepnick et al., 1985; Palmer and Elderfield, 1985; Hess et al., 1986] place the change between 40 and 35 Ma, according to the Berggren et al. [1985] time scale. The most complete published $^{87}Sr/^{86}Sr$ records available for the Oligocene do not reach the transition and/or are not paleomagnetically dated [Miller et al., 1988; Hess et al., 1989]. In addition, Site 522 (analyzed by Miller et al. [1988]) is at least partially recrystallized [Hess et al., 1989]. Finally, the resolution of the two studies was not particularly high (about 0.4-0.5 m.y./sample), especially in light of recent studies that suggest short term $^{87}Sr/^{86}Sr$ variation [Capo and DePaolo, 1990; Dia et al., 1992; Clemens et al., 1993].

The cause of the inflections in the $^{87}Sr/^{86}Sr$ curve in the late Eocene is not known. There are a number of tectonic and environmental factors that may have influenced the input of Sr into the oceans near this time. Glaciation occurred on Antarctica in the earliest Oligocene, which could have increased the weathering rates on that continent [Zachos et al., 1992b; in preparation]. Uplift of the Himalayan-Tibetan Plateau following the collision of India with Eurasia may have increased continental weathering rates

[Richter et al., 1992]. In addition, major sea level drops in the middle Eocene, earliest, "mid", and late Oligocene occurred [Haq et al., 1988], and the Carbonate Compensation Depth (CCD) deepened near the Eocene/Oligocene boundary [Van Andel et al., 1977], possibly reflecting a change in oceanic circulation, shallow/deep calcium carbonate fractionation, or continental weathering rates. Plate reorganization in the Pacific may also have affected the hydrothermal component and/or direction of plate convergence [Lyle et al., 1987].

This paper presents the $^{87}Sr/^{86}Sr$ record from the middle Eocene to Oligocene of ODP Hole 689B (Maud Rise, near the coast of Antarctica; Figure 2-1). The purpose of this study is (1) to refine the Sr isotope curve during the middle Eocene-Oligocene, (2) to help calibrate Antarctic biostratigraphy to the Geomagnetic Polarity Time Scale (GPTS), and (3) to improve our understanding of geochemical cycling of Sr during that time. In addition, additional oxygen and carbon isotopes of Cibicidoides were analyzed in order to cross calibrate the results from the work of Kennett and Stott [1990] and Chapter 3, and to improve the resolution of the $\delta^{18}O$ and $\delta^{13}C$ records from Hole 689B. This site contains a nearly continuous and well preserved calcareous and siliceous biostratigraphic record of the Eocene to Oligocene, from very high latitudes. As such, it constitutes a vital tie-point for biostratigraphic

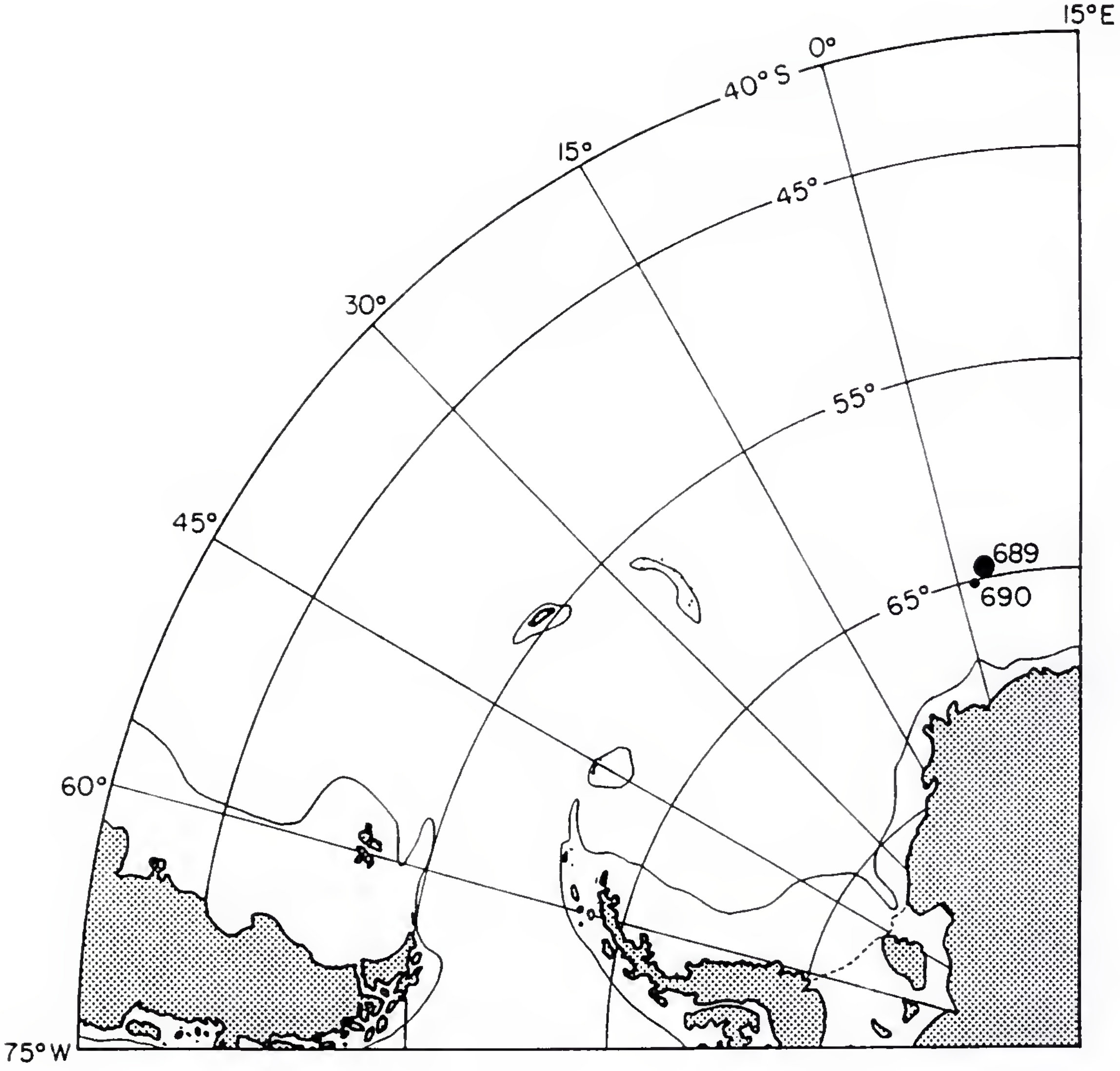

Figure 2-1: Location map, showing ODP Site 689 and nearby Site 690.

correlation. It also is an important site for biogeographic and isotopic paleoceanographic studies [Barker, Kennett et al., 1988, 1990; Chapter 3 of this dissertation].

Methods And Materials

Stratigraphy

Cenozoic stratigraphy is currently in a state of change, with the standard time scale of Berggren et al. [1985] (BKFV85) being replaced by Cande and Kent [1992] (CK92). Ages in this paper will be given using the newer time scale, although the BKFV85 ages are reported in the data tables as well as the newer CK92 ages. Where appropriate, BKFV85 ages are given in parentheses.

The age model used is based on the magnetostratigraphy of Spieß [1990] and the age model of Kennett and Stott [1990], modified to the CK92 time scale (Table 2-1, Figure 2-2). Modifications have been made to these models in a few instances discussed below.

First, an unconformity exists at 161.54 mbsf that was not recognized by Kennett and Stott [1990] but was identified by Spieß [1990]. Without this hiatus, it is difficult to reconcile the pattern of normal and reversed polarity events between about 135 and 190 mbsf. This unconformity has been added, with the ages of the upper and lower surfaces (defined by extrapolation of sedimentation

TABLE 2-1

Age Model of ODP Hole 689B

Depth (mbsf)	Preferred Model Datums	BKFV85 Age (Ma)	CK92 Age (Ma)	
60.40,	Top C5Dr-2	18.14	17.893	
61.76,	Base C5Dr-2	18.56	18.317	
65.50,	Hiatus, ≤Base C5En	19.09	18.817	
65.50,	Hiatus, by extrap.*1	20.05	19.770	
66.86,	Hiatus, ≤Base C6n	20.45	20.162	
66.86,	Hiatus, ≥Top C7n1r	25.60	24.772	
67.11,	Top C7n-2	25.67	24.826	
75.97,	Base C8n	27.74	26.533	SK
79.46,	Top C9n	28.15	27.004	SK
91.93,	Base C10n	30.33	28.716	SK
103.37,	Base C11n	32.06	30.071	SK
106.87,	Base C12n	32.90	30.915	SK
116.71,	Top C13n	35.29	33.050	S
119.69,	Base C13n	35.87	33.543	SK*3
124.09,	Top C15n	37.24	34.669	
125.07,	Base C15n	37.68	34.959	
128.32,	Top C16n	38.10	35.368	K
134.02,	Base C16n-1	38.79	35.977	

TABLE 2-1--continued

Depth (mbsf)	Preferred Model Datums	BKFV85 Age (Ma)	CK92 Age (Ma)	
135.75,	Top C17n	39.53	36.665	K*4
152.73,	Base C17n3	41.11	38.183	SK
153.70,	Top C18n	41.29	38.500	SK*5
161.17,	Top C18r-2	42.73	40.221	S
161.54,	Hiatus, by extrap.*2	42.80	40.312	S
∼∼∼∼∼∼	∼∼∼∼∼∼∼∼∼∼∼∼	∼∼∼∼∼∼	∼∼∼∼∼∼	∼∼
161.54,	Hiatus, by extrap.*1	43.66	41.387	S
163.16,	Base C19n	44.06	41.617	SK
165.55,	Top C20n	44.66	42.629	SK
171.11,	Base C20n	46.17	43.868	S
183.23,	Top C21n	48.75	46.284	S

S: Datum from Spieß [1990].
K: Datum from Kennett and Stott [1990].
*1: Age calculated by assuming constant sedimentation rate from underlying section.
*2: Age calculated by assuming constant sedimentation rate from overlying section.
*3: Datum listed by KS90 as Top C13n.
*4: Age listed by KS90 as 39.52 Ma.
*5: Age listed by KS90 as 41.21 Ma.

Figure 2-2: Magnetostratigraphy and interpretations, $^{87}Sr/^{86}Sr$ and $\delta^{18}O$ from ODP Hole 689B, plotted against depth.

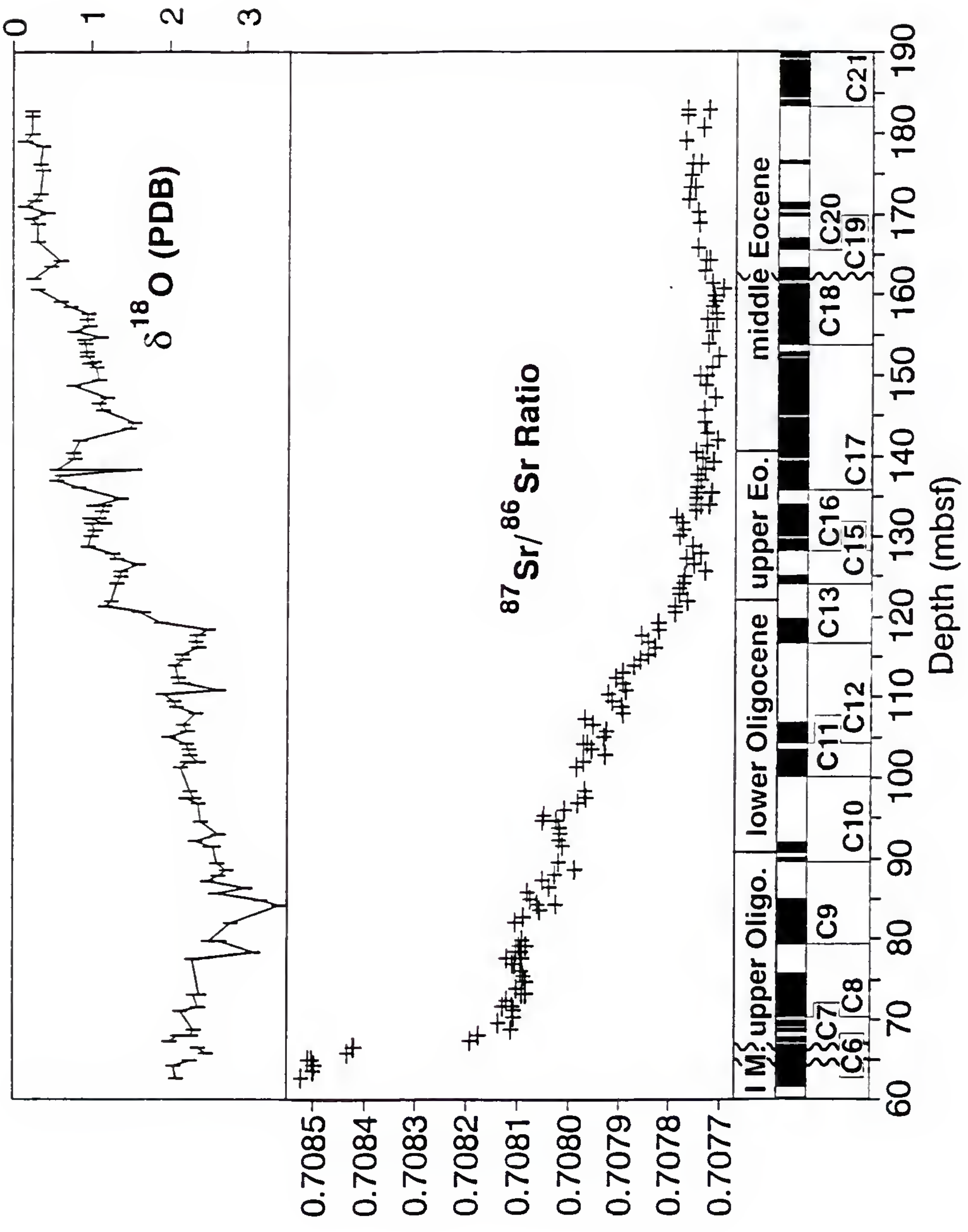
0
1
2
3
δ18O (PDB)
87Sr/86Sr Ratio
0.7085
0.7084
0.7083
0.7082
0.7081
0.7080
0.7079
0.7078
0.7077
l M.
upper Oligo.
lower Oligocene
upper Eo.
middle Eocene
C6
C7
C8
C9
C10
C11
C12
C13
C15
C16
C17
C18
C19
C20
C21
60
70
80
90
100
110
120
130
140
150
160
170
180
190
Depth (mbsf)

rates to the position of the unconformity) converted from the BKFV85 to CK92 time scale.

Second, there is a disagreement between the age models from 128.33 to 137.77 mbsf (lower upper Eocene). The series of polarity intervals identified as Chrons C15n-1/2 to C15r-2 by Spieß [1990] are identified as Chrons C16n-1 to C16r-3 by Kennett and Stott [1990]. The CP15b/CP15a calcareous nannofossil boundary (recognized at 131.7-132.7 mbsf by Wei and Wise [1990]) is closely associated with the C15n-1/2 to C15r-2 boundary [Berggren et al., 1985], and this controls Spieß's [1990] position of that paleomagnetic boundary at 134.02 mbsf. However, Wei [1991] and Wei and Wise [1992] showed that the first occurrence of Isthmolithus recurvus, which defines the CP15b/CP15a boundary, occurs somewhat earlier in the Southern Ocean, within C16. Using Spieß's [1990] identification also introduces large distortions into the sedimentation history, with sudden jumps in the sedimentation rates within C15n and C16n. As a result, I accept the chron assignments of Kennett and Stott [1990] in this interval. This chron assignment also re-defines the normally magnetized interval between 124.09 and 125.07 mbsf from a normal within C13r-2 [Spieß, 1990] to C15n, considerably improving the pattern match between the magnetic stratigraphy and the seafloor magnetic anomaly record.

Finally, two unconformities occur in the upper part of the section: one at approximately 66.86 mbsf and the other at about 65.5 mbsf. Only the lower one is recognized paleomagnetically [Spieß, 1990]. The second falls within a normally magnetized interval and was identified only through the use of biostratigraphy [Gersonde and Burckle, 1990]. Neither hiatus is recognized by Kennett and Stott [1990]. However, both are clearly identified by the use of Sr isotope stratigraphy (see RESULTS). The $^{87}Sr/^{86}Sr$ ratio of sediments within the short normally-magnetized interval between the unconformities (about 0.70843) indicates that the age is approximately 20 Ma [Hodell and Woodruff, 1994], assignable to Chron C6n [Cande and Kent, 1992]. The sediments immediately above the upper unconformity have a $^{87}Sr/^{86}Sr$ ratio of about 0.70851, and are approximately 18.7 Ma [Hodell and Woodruff, 1994], assignable to Chron C5En [Cande and Kent, 1992].

Materials

Benthic and planktic foraminifera from the >250µm, >212µm, or >150µm fraction (depending on abundance) were picked from washed (>63µm) samples from Hole 689B. Preservation of foraminifera is generally good [Stott and Kennett, 1990, Kennett and Stott, 1990]. In addition, analysis of interstitial waters from Hole 689B [Egeberg et al., 1990] indicates unusually low recrystallization rates of carbonate. To further check the degree of preservation, Sr/Ca ratios were measured as well (see Results).

The sampling interval is somewhat variable, ranging between 0.5 and 3 m, or from 50 to 660 ky. The average sampling interval was 0.96 m or 166 ky. Below 142 mbsf, the sampling interval was coarser, with one sample per 1.44 m or 211 ky, while above that depth, the sampling interval averaged one per 0.81 m or 134 ky. Because the amplitude of the $^{87}Sr/^{86}Sr$ signal is much smaller below 135 mbsf, the lower sampling rate below 142 mbsf is adequate to delineate the $^{87}Sr/^{86}Sr$ curve.

The samples were ultrasonically cleaned in methanol to remove adhering fine debris and dried in a 60°C oven. They were then dissolved in 1 to 2 ml of 0.25 N HCl for about 1 hour at 200-250°C, then dried under a laminar flow hood. Sample sizes range from about 1.3 to 10.0 mg. Strontium concentrations were about 2000 ppm according to isotope dilution techniques, and about 1350 ppm according to atomic absorption spectrophotometry, giving sample Sr masses of 1.8 to 20 μg.

Ion exchange columns, made of Teflon shrink-tubing and packed with ElChroM Industries, Inc. Sr-selective crown ether resin, were used to extract strontium from the samples. All extractions were made under a laminar flow hood. A modification of the method of Pin and Bassin [1992] was used with slightly differing volumes of HNO_3 and H_2O (Appendix B2). Yields were approximately 75%, with excellent separation of Sr from Ca [Pin and Bassin, 1992].

Mass Spectrometry

Strontium isotopes

All Sr samples were analyzed in a VG Micromass 354 thermal ionization mass spectrometer in dynamic mode (instructions for operation are listed in Appendix B3). Samples were loaded onto oxidized Ta single filaments by dissolving the extracted Sr in 2-3μl of 0.5 N H_3PO_4 acid.

An analysis of NBS-987 was run with each turret of 14 samples. Analyses of 17 NBS-987 standards averaged 0.710240, with an uncertainty (2 standard deviations or 2σ) of ±0.000022. All samples are normalized to NBS-987 = 0.710235 and $^{86}Sr/^{88}Sr = 0.1194$. Samples for which the $^{86}Sr/^{88}Sr$ ratio was determined to be less than 0.1194 are assumed to have been fractionated and those values were not reported.

To examine reproducibility of the results, two different types of replicates were analyzed. Separate analyses of planktonic and benthic foraminifera were made in 17 samples. The $^{87}Sr/^{86}Sr$ ratios of planktonic foraminifera averaged $8x10^{-6}$ (σ=$20x10^{-6}$) higher than those of benthic foraminifera, showing no systematic difference between Sr isotopic ratios of the different types. Because in some cases less than perfectly preserved specimens of foraminifera had to be picked due to lack of sample, I also analyzed the difference between well preserved and poorly preserved (visibly damaged, probably dissolved) specimens when possible (5 cases). The $^{87}Sr/^{86}Sr$ ratios of well preserved specimens averaged only $2x10^{-6}$ ($\sigma=13x10^{-6}$) higher than those of poorly preserved specimens, which, despite the small number of analyses, suggests that no systematic difference exists between Sr isotopic ratios of differentially preserved specimens. The poor preservation of some foraminiferal tests is attributed to dissolution rather than recrystallization. The average difference of all 22 replicates is $16x10^{-6}$ ($\sigma=12x10^{-6}$), not much larger than the standard deviation of the NBS-987 standard.

Oxygen and carbon isotopes

Well-preserved specimens of the benthic foraminiferal genus Cibicidoides were picked from the washed >150μm fraction of 35 samples from Hole 689B. Standard methods were used to prepare and analyze the carbonate (see Chapter 3). The samples were analyzed in a VG Prism triple collector mass spectrometer with an automated preparation system. Of the 35 samples run, 14 were replicate analyses of samples run by Kennett and Stott [1990] in an attempt to calibrate their data with that of Chapter 3. The analytical precision of standards (1σ) was ±0.029 for $\delta^{13}C$ and ±0.067 for $\delta^{18}O$.

Atomic Absorption Spectrophotometry

A Perkin-Elmer 3100 Atomic Absorption Spectrometer was used to measure Sr/Ca ratios. About 50 μg of carbonate (typically 3-6 foraminifera) was dissolved in 5 ml of 0.5 N Optima (trace metal grade) nitric acid. The Ca concentrations (on the order of 3 ppm by weight) were measured in flame mode, while the Sr measurements (on the order of 10 ppb by weight) were analyzed using the graphite furnace, on the same aliquot of sample. Both sets of measurements were compared to standard absorbance curves to calculate concentrations. Results are reported in both mass and molar ratios (Appendix A2).

Results

Strontium Isotopic Measurements

From the base of the section analyzed in this study (183 mbsf) to 133.2 mbsf, the value of the $^{87}Sr/^{86}Sr$ ratio shows little variability, averaging 0.707735 (σ=0.000018) (Figure 2-2, Appendix A2). When plotted against age, the $^{87}Sr/^{86}Sr$ ratios remained steady or possibly decreased slightly from an average of 0.707754 (σ=0.000014) at 46.2 Ma to the middle Eocene hiatus beginning at 41.4 Ma (162.54 mbsf) (Figure 2-3). By the time sedimentation resumed at 40.3 Ma, the $^{87}Sr/^{86}Sr$ ratio had dropped to near 0.70771. The $^{87}Sr/^{86}Sr$ ratio averages 0.707728 (σ=0.000015) between 40.3-35.9 Ma (161.4-133.25 mbsf), but rose slightly during this interval, at a rate of about $8x10^{-6}$/m.y. This rise is poorly constrained, with a regression coefficient (R^2) of only 0.459. None of the variability within this section is

Figure 2-3: ODP Hole 689B strontium isotope data compared to the model curves, plotted against age. The time scale used is that of Cande and Kent [1992]. Curving dotted lines on either side of the regressions are the 95% confidence interval of the regresssion. Upward curving lines are the 95% confidence intervals for ages calculated from the $^{87}Sr/^{86}Sr$ ratio of one sample.

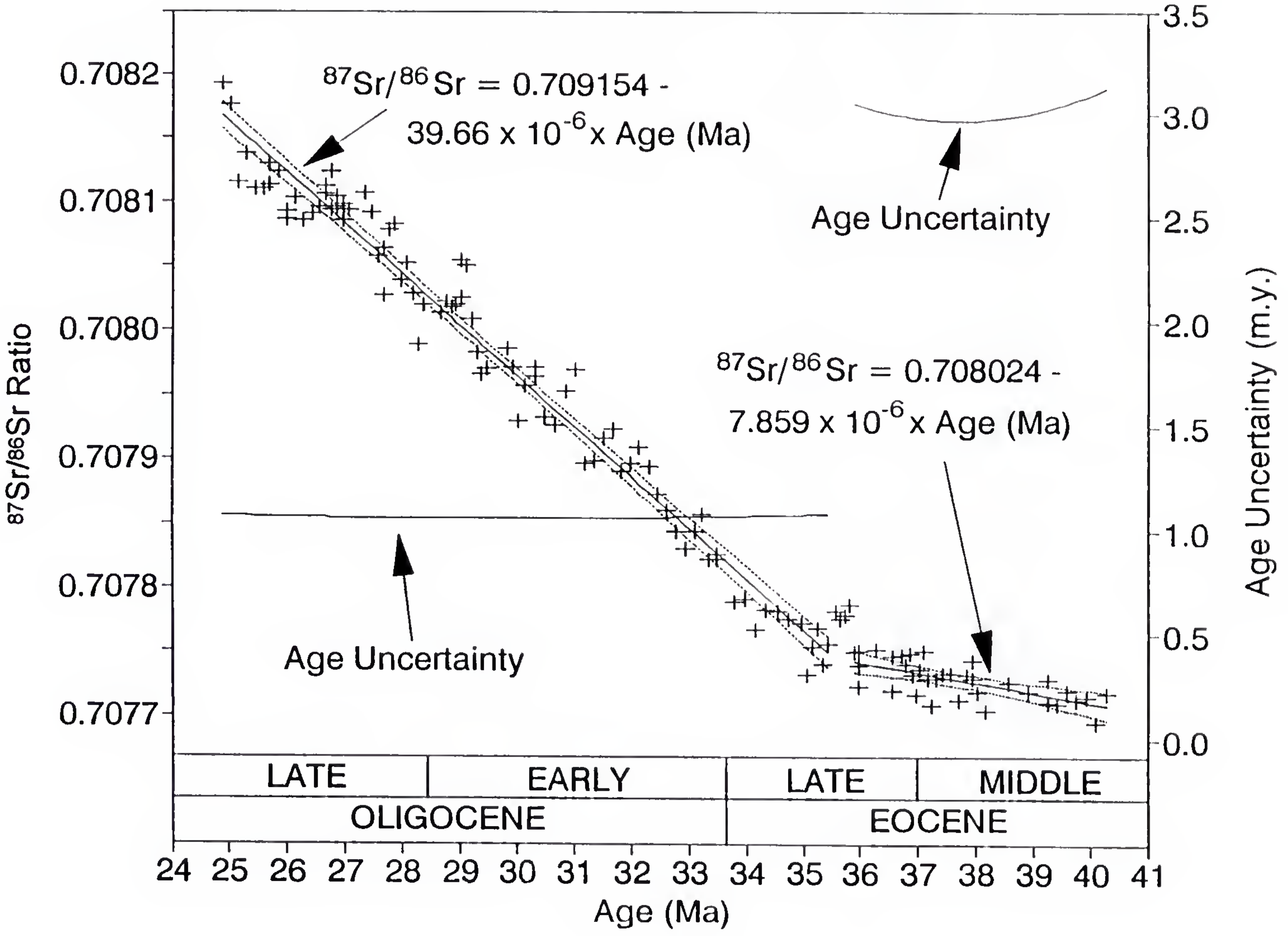
$^{87}Sr/^{86}Sr = 0.709154 - 39.66 \times 10^{-6} \times Age (Ma)$
Age Uncertainty
$^{87}Sr/^{86}Sr = 0.708024 - 7.859 \times 10^{-6} \times Age (Ma)$
Age Uncertainty
$^{87}Sr/^{86}Sr$ Ratio
0.7082
0.7081
0.7080
0.7079
0.7078
0.7077
Age Uncertainty (m.y.)
3.5
3.0
2.5
2.0
1.5
1.0
0.5
0.0
LATE
EARLY
LATE
MIDDLE
OLIGOCENE
EOCENE
24 25 26 27 28 29 30 31 32 33 34 35 36 37 38 39 40 41
Age (Ma)

likely to be of stratigraphic utility, because the total range is so small.

During the late Eocene, a brief increase occurred in four samples from 35.8-35.6 Ma (132.52-130.25 mbsf), with the $^{87}Sr/^{86}Sr$ ratio rising to a constant 0.70778 (σ=0.000005) before falling again to about 0.70775 (Figure 2-3). Although the increase is very consistent in this site, it must be confirmed before any interpretations can be drawn from it.

A steady rise began in the late Eocene at about 35.5 Ma (128.8 mbsf, 38.2 Ma BKFV85), with $^{87}Sr/^{86}Sr$ ratios rising to near 0.70812 by 25.2 Ma (68.8 mbsf), at a rate of 40×10^{-6}/m.y. This increase is well constrained, with R^2 = 0.972. Two samples above 68.8 mbsf (25.0-24.8 Ma; 68.12 and 67.37 mbsf) show somewhat higher $^{87}Sr/^{86}Sr$ ratios of about 0.70818, suggesting the possibility of another small hiatus. Across the hiatus in sedimentation from 24.8 to 20.2 Ma (66.86 mbsf), $^{87}Sr/^{86}Sr$ ratios increased sharply to 0.70843 at 20 Ma. Another sudden jump in the ratio occurred across the unconformity from 19.8 to 18.8 Ma (65.50 mbsf), to an average of 0.70851 between 18.8 Ma and the top of the section at 18.5 Ma (62.87 mbsf), confirming the unconformity identified by Spieß [1990] and Gersonde and Burckle [1990].

Oxygen and Carbon Isotopic Measurements

In general, the purpose of the additional 35 isotope measurements was to improve the resolution of the curve of

Kennett and Stott [1990], in particular near the earliest Oligocene oxygen isotope shift. This was successfully done, constraining the shift to between 118.44 and 121.30 mbsf (33.33 to 33.96 Ma CK92, 35.63 to 36.37 Ma BKFV85) (Appendix A2, Figure 2-2). The shift in this section has a duration somewhat longer than reported elsewhere [e.g., Kennett and Shackleton, 1976; Oberhänsli et al., 1984; Zachos et al., 1992a; Barrera and Huber, 1993; Chapter 3], lasting about 0.6 m.y. During this time, the $\delta^{18}O$ values rise from approximately 1.19^{o}/oo to 2.51^{o}/oo PDB, with the increase delineated by 4 separate samples (two of which are replicated from Kennett and Stott [1990]).

The difference between samples measured in 14 replicates by this study and those measured by Kennett and Stott [1990] is statistically insignificant. Values for $\delta^{18}O$ averaged 0.07^{o}/oo (σ=0.29) lower in this study than Kennett and Stott [1990], while values for $\delta^{13}C$ averaged 0.03^{o}/oo (σ=0.18) higher in this study than in Kennett and Stott [1990]. These differences are insignificant compared to an analytical error of ±0.1^{o}/oo for stable isotopic measurements.

Strontium/Calcium Ratios and Diagenetic Alteration

Strontium to calcium ratios were measured to assess the effects of diagenesis in this section. Recrystallization of calcite results in lower Sr/Ca ratios than in biogenic calcite because of the lower distribution coefficient of authigenically precipitated calcite present in slowly altering limestone as compared to rapidly precipitating biogenic calcite [Lorens, 1981]. Measurement of Sr/Ca ratios can therefore be used to evaluate the degree of recrystallization [Hess et al., 1986]. Sr/Ca ratios of 42 samples were measured from ODP Hole 689B (Figure 2-4, Appendix A2) to evaluate recrystallization in this section. The Sr/Ca ratios of the samples averaged 3.4 (σ=±0.6) μg/mg (mass ratio) or 1.5 (±0.3) mmol/mol (molar ratio). The Sr/Ca ratios rise very slightly up section, from 2.9 (±0.3) μg/mg (mass ratio) or 1.3 (±0.1) mmol/mol (molar ratio) in the bottom 20 m to 3.7 (±0.5) μg/mg (mass ratio) or 1.7 (±0.2) mmol/mol (molar ratio) in the top 20 m of section. These values are comparable or higher than those reported by other studies [Graham et al., 1982; Hess et al., 1986,1989; Barrera et al., 1991; Egeberg et al., 1990] Figure 2-4 and I therefore conclude that the ^{87}Sr/^{86}Sr ratios of the samples used in this study have not been altered by diagenesis.

The ^{87}Sr/^{86}Sr and Sr/Ca ratios of bulk carbonate (Egeberg et al. [1990]) correspond well with values measured on cleaned foraminiferal calcite (Figure 2-4) as well. Bulk carbonate, with a large component of fine fraction carbonate, tends to be more susceptible to diagenetic alteration than coarse fraction carbonate [Garrison, 1981]. The fact that ^{87}Sr/^{86}Sr ratios of bulk carbonate (at least for the 4 measurements of Egeberg et al. [1990]) and

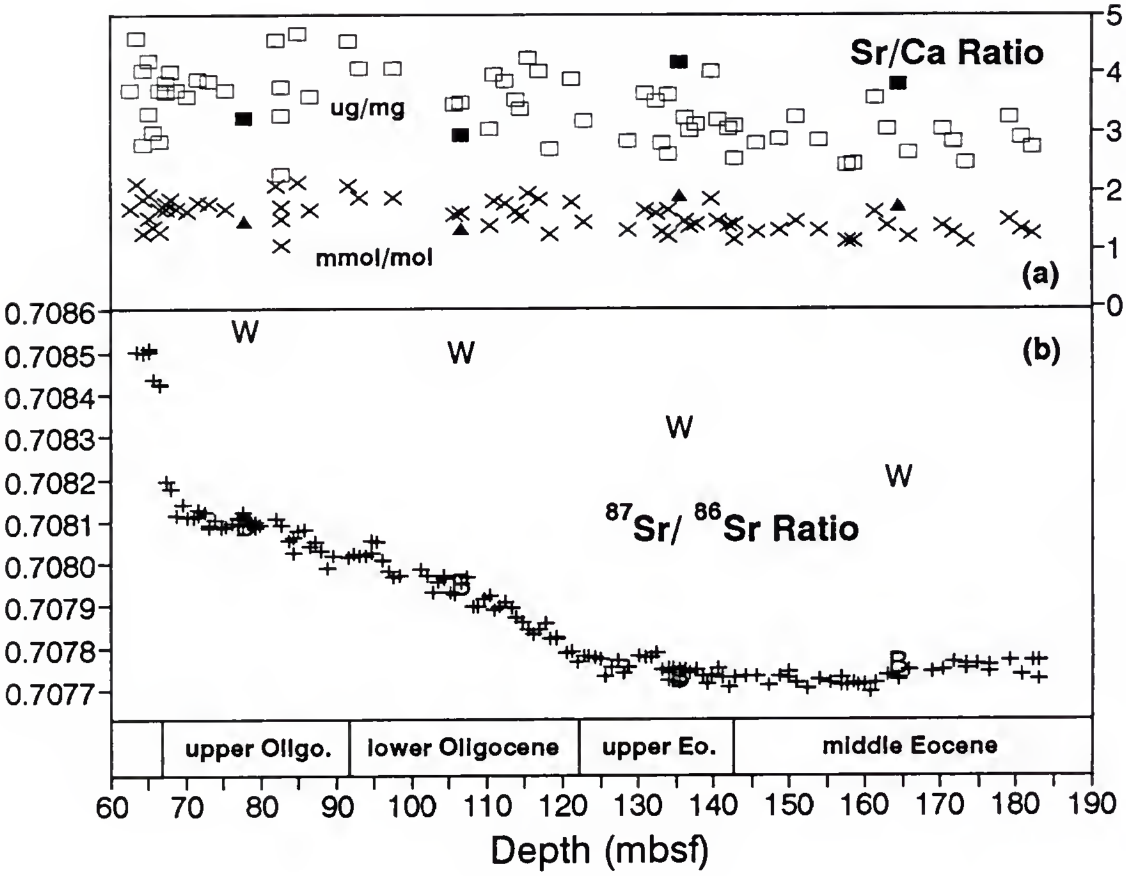

Figure 2-4: Strontium geochemical measurements.
a: X's and empty boxes are Sr/Ca ratios in mmol/mol and μg/mg measured on cleaned foraminiferal samples (this study), respectively, while solid triangles and boxes are Sr/Ca ratios in mmol/mol and μg/mg measured on bulk carbonate from Egeberg et al. [1990].
b: Crosses are ^{87}Sr/^{86}Sr ratios measured on cleaned foraminiferal samples (this study), while W's and B's are interstitial water and bulk carbonate ^{87}Sr/^{86}Sr ratios, respectively, from Egeberg et al. [1990].

$^{87}Sr/^{86}Sr$ ratios of foraminiferal calcite are so similar suggests that little or no diagenetic alteration of these carbonates has occurred. Lastly, the high $^{87}Sr/^{86}Sr$ ratios of interstitial water (Figure 2-4) and relatively low concentrations of interstitial Sr also argue for low rates of recrystallization in ODP Hole 689B [Egeberg et al., 1990]. If recrystallization had occurred, porewater $^{87}Sr/^{86}Sr$ values would be much lower and bulk carbonate ratios would be higher. Egeberg et al. [1990] concluded that pore waters at Site 689 displayed an almost complete lack of recrystallization.

Discussion

Strontium Isotope Stratigraphy

Strontium isotope stratigraphy is used today in two primary ways: for determining ages of marine samples based on their measured $^{87}Sr/^{86}Sr$ ratio, and for investigating geochemical cycling of strontium on the Earth's surface [Hodell, 1994]. The variation in $^{87}Sr/^{86}Sr$ has been described using regression analyses, either linear [McKenzie et al., 1988; Miller et al., 1988, 1991a; Hess et al., 1989; Hodell et al., 1989, 1990; Oslick et al., 1994] or curvilinear [Miller et al., 1991a; Hodell and Woodruff, 1994; Oslick et al., 1994]. Oslick et al. [1994] suggested that in the absence of a theory mandating a polynomial (curvilinear) fit, the simpler linear regression should be used. The present study uses line segments and linear regression to model the data because of the relative simplicity of the method and because linear regression seems to fit these data well.

I use two linear regressions to model the data. First, a regression for the Site 689 data from 40.3-35.8 Ma (42.8-38.6 Ma BKFV85) was calculated. This regression, with 35 data points, is

$$^{87}Sr/^{86}Sr = 0.708024 - 7.8588\times10^{-6} \times Age\ (Ma) \qquad (1)$$

but gives a rather poor fit ($R^2 = 0.459$) as previously noted, and a standard error of 11×10^{-6}. The equation can be inverted for the purposes of age calculation to

$$Age\ (Ma) = 90093.124 - 127245.848 \times {}^{87}Sr/^{86}Sr \qquad (2)$$

and is valid for values of $^{87}Sr/^{86}Sr$ from 0.707707 to 0.707743. Second, I calculated a regression for the data from 35.5-24.8 Ma (38.3-25.4 Ma BKFV85). This regression equation, with 86 data points, is

$$^{87}Sr/^{86}Sr = 0.709154 - 39.6584\times10^{-6} \times Age\ (Ma) \qquad (3)$$

and gives an excellent fit ($R^2 = 0.972$), and a standard error of 21×10^{-6}. The equation can be inverted to

$$\text{Age (Ma)} = 17881.554 - 25215.329 \times {}^{87}\text{Sr}/{}^{86}\text{Sr}. \qquad (4)$$

and is valid for values of ^{87}Sr/^{86}Sr from 0.707746 to 0.708171. The two regressions cross at a calculated age of 35.535 Ma and a ^{87}Sr/^{86}Sr ratio of 0.707745. I do not evaluate the 4 data points from 35.8-35.6 Ma, which fall off of both these trends. Figure 2-3 shows the fit of this model to the data.

In order to evaluate the reliability of this curve in examining controls on the marine ^{87}Sr/^{86}Sr ratio and in predicting ages of samples, two statistical analyses of the regressions were performed. The first analysis calculates the 95% confidence interval of the regression itself (i.e., the uncertainty in the estimate that the regression correctly models the actual increase in marine ^{87}Sr/^{86}Sr ratios). The second analysis calculates the uncertainty in age calculations made from one or more ^{87}Sr/^{86}Sr analyses of an unknown sample. In the first analysis, I follow the procedures outlined in Draper and Smith [1981], as suggested by Miller et al. [1991a] in calculating uncertainties in the regression. I use the exact solution in calculating uncertainty in age estimation due to regression uncertainty rather than the approximate solution used by Miller et al. [1991a] because the calculations show that the approximate solution slightly underestimates the uncertainty. In addition, $(2F)^{\frac{1}{2}}$ was used instead of the t statistic. This allows the 95% confidence curve for the entire regression to be calculated rather than the 95% confidence interval for a given point in the regression [Draper and Smith, 1981, p.31] (Figure 2-3). In the second case, the procedure outlined in Miller et al. [1991a, equation 6] is used to calculate the uncertainty in age determinations.

A caveat in these calculations is that they are based on the assumption that $^{87}Sr/^{86}Sr$ measurements are distributed normally about each point on the regression. If there is small-scale structure along the line, as suggested by several recent studies [Capo and DePaolo, 1990; Dia et al., 1992; Clemens et al., 1993; Oslick et al., 1994], then deviations from the regression are systematic. In this case, calculations of ages and uncertainty using a regression will be invalid.

The linear regression for the interval from 40.3 to 35.8 Ma shows a rather low regression coefficient ($R^2=0.459$). This, coupled with the low slope in this interval, results in a high uncertainty of the regression and raises the question of whether the slope differs significantly from zero. A t-test of the regression [Draper and Smith, 1981] was used to test this hypothesis. The t-test shows that the slope is significantly different from zero, at the 99.9% confidence level, despite the low coefficient. A t-test of the interval from 35.5-24.8 Ma, with a much greater slope and higher regression coefficient, not surprisingly also shows that the slope differs significantly from zero at this confidence level.

The uncertainty in the regression from 40.3 to 35.8 Ma ranges from a minimum of ±4.9x10^{-6} near the middle of the interval to ±8.6x10^{-6} and ±10.9x10^{-6} at the upper and lower ends of the interval, respectively (Table 2-2). The corresponding age uncertainties are not quite symmetrically distributed about the regression line because of the curve of the lines of uncertainty, but are about ±1.37, ±0.71, and ±1.76 m.y. for the upper, middle, and lower parts of the interval, respectively (Figure 2-3). These calculations do not take into account the uncertainty in ^{87}Sr/^{86}Sr measurements, however. Given the 2σ uncertainty in ^{87}Sr/^{86}Sr measurement of ±22x10^{-6} (comparable to a 95% confidence interval), and a slope of 7.86x10^{-6}/m.y., we can divide the uncertainty by the slope to obtain an estimate of the measurement uncertainty. We arrive at an uncertainty of about ±2.80 m.y. due to the measurement uncertainty. Applying the formula given by Miller et al. [1991, eq. 6], which more rigorously calculates the uncertainty in age calculations based on a number of ^{87}Sr/^{86}Sr measurements, the uncertainty for one measurement of an unknown sample at the 95% confidence interval is approximately ±3 m.y., and decreases by about a third for 3 measurements. Clearly, the uncertainty in this interval (with a total duration of only 4.5 m.y.) makes this regression useless for precise age calculations.

For the upper (35.5-24.8 Ma) interval, the corresponding uncertainties due to the regression in

TABLE 2-2

Uncertainties in regression, due to measurement error, and due to age calculation from regression

Age Range:	35.5-24.8 Ma			42.8-35.8 Ma		
Slope:	39.66×10^{-6}/my			7.86×10^{-6}/my		
Part of Curve:	Upper	Middle	Lower	Upper	Middle	Lower
Uncertainties:						
Regression:						
$^{87}Sr/^{86}Sr$ ($\times10^{-6}$)	±10.6	±5.7	±12.0	±8.6	±4.9	±10.9
Age (m.y., total)	0.53	0.29	0.61	2.74	1.43	3.53
From Measurment Error (m.y.):	±0.55	±0.55	±0.55	±2.80	±2.80	±2.80
95% Confidence Interval (m.y.):						
1 measurement:	±1.08	±1.06	±1.08	±3.05	±2.97	±3.13
3 measurements:	±0.64	±0.62	±0.65	±1.90	±1.76	±2.01

$^{87}Sr/^{86}Sr$ are somewhat larger, at $\pm 10.6 \times 10^{-6}$, $\pm 5.7 \times 10^{-6}$, and $\pm 12.0 \times 10^{-6}$. Due to the higher slope, however, the age uncertainties due to the regression are smaller, and are about ±0.27, ±0.14, and ±0.30 Ma for the upper, middle, and lower parts of the curve, respectively (Table 2-2, Figure 2-3). The age uncertainty obtained by dividing 2σ uncertainty by the slope is ±0.55 m.y. Uncertainty based on 1 measurement is about ±1.1 m.y. at the 95% confidence level, decreasing to about ±0.6 m.y. for 3 measurements, suggesting that regression error is less important than errors in $^{87}Sr/^{86}Sr$ ratios in calculating ages for this part of the curve.

Comparisons with Other Records

Three studies have used $^{87}Sr/^{86}Sr$ records for the latest Eocene to Oligocene to calculate linear regression of $^{87}Sr/^{86}Sr$ ratio vs. age [Miller et al., 1988; Hess et al., 1989; Oslick et al., 1994]. In addition, a fourth study [Zachos et al., in prep.] has also generated a record from the middle Eocene up to the earliest Miocene. In comparing these records (from DSDP and ODP sites) to the Site 689 data, two modifications were made. For records originally calibrated to the BKFV85 time scale, sample ages were converted from the BKFV85 time scale to the CK92 time scale in one of two ways. If magnetostratigraphy of a site was available, a new age model tied to the CK92 time scale was used to calculate ages. If magnetostratigraphy of a site was not available, sample ages were calculated by comparison of the magnetic anomaly tie points used by the BKFV85 and CK92 age models. The new time scale can significantly change the pattern observed in the marine $^{87}Sr/^{86}Sr$ ratios. For example, the inflection identified by Hess et al. [1989] at 26 Ma (BKFV85) is even more notable when the Hess et al. [1989] record is calibrated to the CK92 time scale, where the inflection is dated at near 24.8 Ma. Coincidentally, this is near where the continuous portion of the record ends, and so the slope change is not recognized in the data from Hole 689B. Second, all $^{87}Sr/^{86}Sr$ results from these studies were normalized to the standard value of 0.710235 for NBS-987. For example, Miller et al. [1988] reported a $^{87}Sr/^{86}Sr$ ratio of 0.710250 for NBS-987; therefore, 0.000015 was subtracted from their data. Hess et al. [1989] used the Eimer and Amend standard, which converts to a value of 0.710220 for the NBS-987 standard; therefore 0.000015 was added to all of their data. Oslick et al. [1994] reported a $^{87}Sr/^{86}Sr$ ratio of 0.710255 for NBS-987; therefore, 0.000020 was subtracted from their data.

In general, the records are quite similar, with the greatest differences occurring during the early Oligocene and late Eocene (Figure 2-5). With one exception, the data suggest that the increase in $^{87}Sr/^{86}Sr$ ratios began earlier, but initially at a lower rate, than previous studies. Data from ODP Hole 748B [Zachos et al., in prep.] also suggests that a lower rate of increase in $^{87}Sr/^{86}Sr$ began in the middle or

Figure 2-5: Sr isotope data from ODP Hole 689B (crosses), compared to the Sr curves of Miller et al. [1988] (Holes 522 and 549A), Hess et al. [1989] (Holes 516, 516F, and 563), Hodell and Woodruff, [1994] (Hole 289, labelled Hodell & W. 1994), Oslick et al. [1994] (Hole 747B), and Zachos et al. [in prep.] (Hole 748A, labeled Zachos .. in prep.).

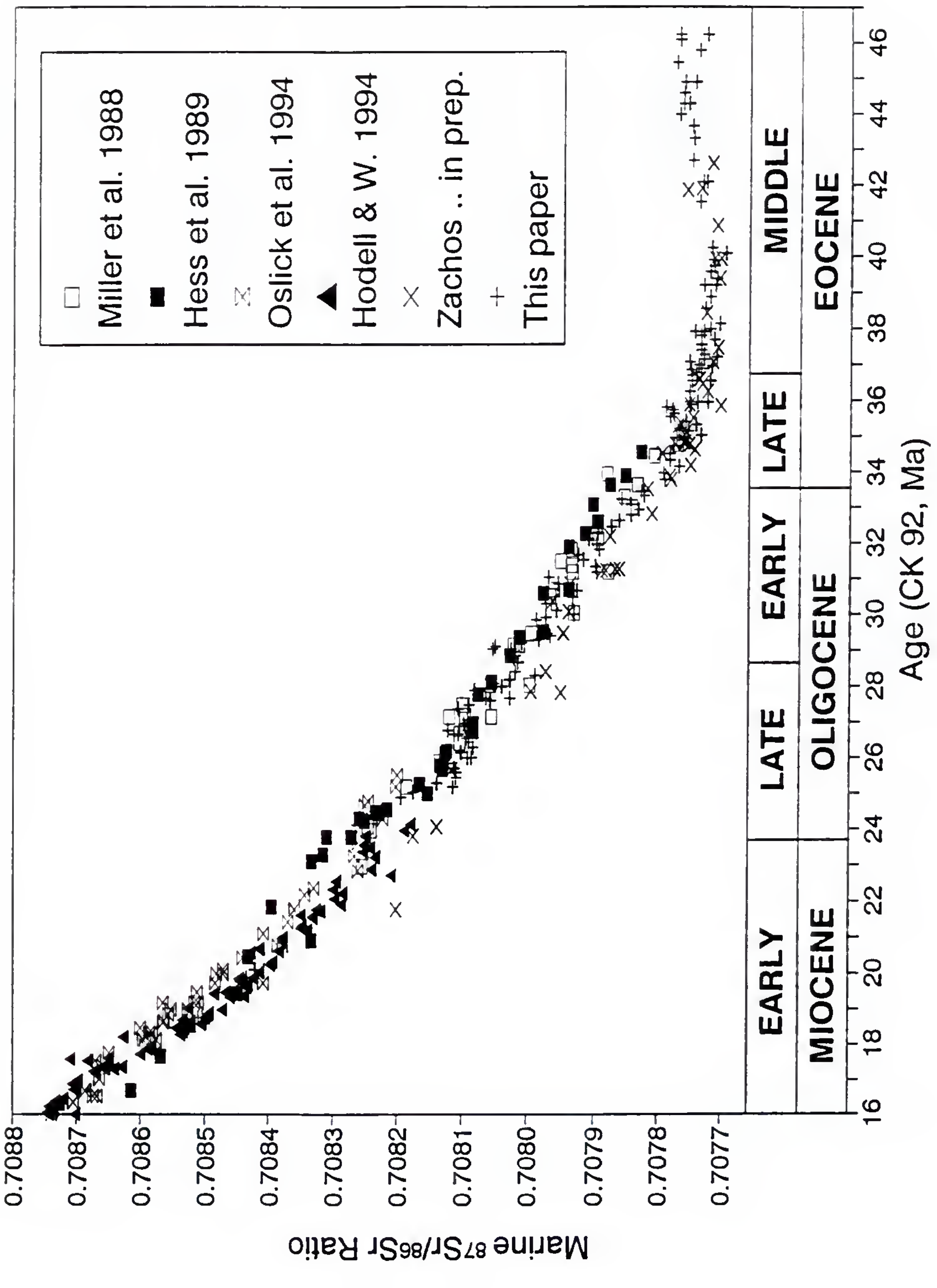
Marine 87Sr/86Sr Ratio
0.7088
0.7087
0.7086
0.7085
0.7084
0.7083
0.7082
0.7081
0.7080
0.7079
0.7078
0.7077
Age (CK 92, Ma)
16
18
20
22
24
26
28
30
32
34
36
38
40
42
44
46
EARLY
LATE
EARLY
LATE
MIDDLE
MIOCENE
OLIGOCENE
EOCENE
□ Miller et al. 1988
■ Hess et al. 1989
⊠ Oslick et al. 1994
▲ Hodell & W. 1994
× Zachos .. in prep.
+ This paper

late Eocene, but the resolution of this record is low compared to that of Hole 689B. I recalculated the linear regressions of Miller et al. [1988] and Hess et al. [1989], and include the regressions of Oslick et al. [1994] for comparison to this model (Figure 2-6). The regressions of the different records give quite similar results, with the exception that the regression of Hess et al. [1989] does not match the other regressions in the late Eocene to early Oligocene. This suggests that there may be a problem with the age model used by Hess et al. [1989]. Alternatively (see Figure 2-5), there may not be enough points in the data set to adequately constrain the early part of the records from sites 516 and 563. It is interesting to note also that there is a very consistent offset between the data of Miller et al. [1988] and the data, even after normalization. The data of Oslick et al. [1994] are offset on average by about the same amount. The results in the present study are consistently about 15×10^{-6} below those of Miller et al. [1988] and Oslick et al. [1994]. This offset is in the same direction, but not quite as large as that observed by Hodell and Woodruff [1994]. Oslick et al. [1994] attributed the offset between data from the University of Florida (Site 588; Hodell and Woodruff [1994]) and Rutgers (Hole 747A) to errors in stratigraphic correlation. However, Holes 689B and 522 [Miller et al., 1988] are well constrained by magnetostratigraphy. This does not guarantee that the

Figure 2-6: Regressions from Miller et al. [1988], Hess et al. [1989] (both converted to CK92), and Oslick et al. [1994] compared with the regression curve from ODP Hole 689B.

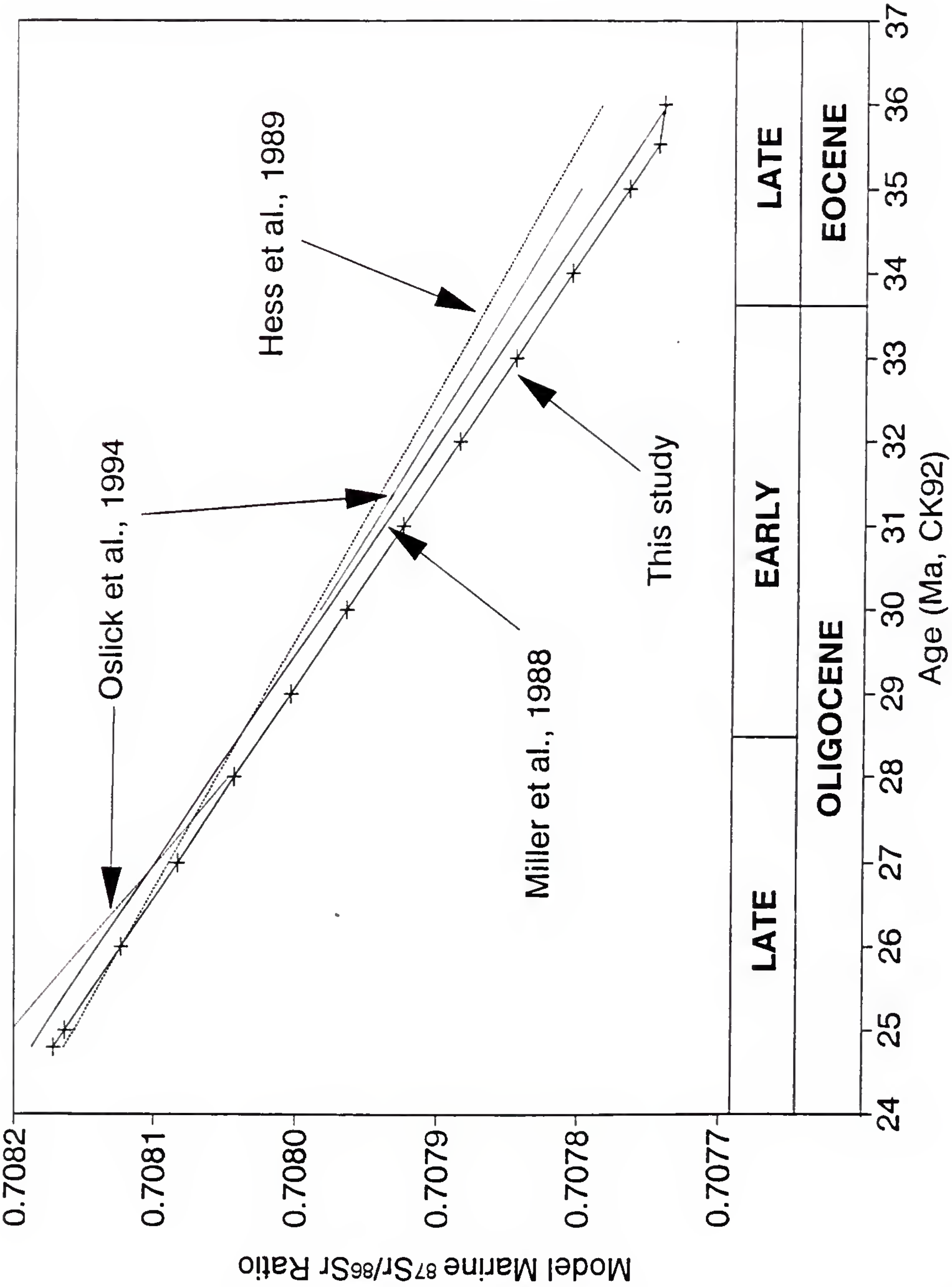
Model Marine 87Sr/86Sr Ratio
0.7082
0.7081
0.7080
0.7079
0.7078
0.7077
Age (Ma, CK92)
24
25
26
27
28
29
30
31
32
33
34
35
36
37
Oslick et al., 1994
Hess et al., 1989
Miller et al., 1988
This study
LATE
EARLY
LATE
OLIGOCENE
EOCENE

correlation between these sites is correct, as small unconformities and mis-identifications can be present which would not be visible in the magnetostratigraphy, but it makes it less likely that mis-correlations are the cause of the offset between the holes. As yet, the reasons for the offsets between laboratories remain unknown.

Some small scale variability can be seen in the record from Hole 689B, with local peaks in $^{87}Sr/^{86}Sr$ values at 35.8-35.6 (as previously mentioned), 31.0, 29.0, and 26.6-27.5 Ma, and a period of rapid rise from 33.0 to 32.1 Ma (Figure 2-3). All of these values are within the expected measurement error, and thus their significance is suspect. However, they are all represented by more than one measurement. Very small scale, high frequency variability in $^{87}Sr/^{86}Sr$ ratios has been reported in the Plio-Pleistocene and related to glacial/interglacial changes [Capo and DePaolo, 1990; Dia et al., 1992; Clemens et al., 1993], but these variations remain controversial. In addition, Oslick et al. [1994] identified several episodes of small scale $^{87}Sr/^{86}Sr$ variability in the Oligocene and Miocene, and suggested that they lagged deglaciation events by approximately 0.9-1.4 m.y. Whether the specific 32 and 28 Ma events identified by Oslick et al. [1994] correlate with the 31 Ma (or 33 to 32 Ma) and 29 Ma events identified here is unknown, but the high quality magnetostratigraphy in the two sections involved (DSDP Hole 522 and ODP Hole 689B) makes it unlikely. It is possible that finer scale variation does exist in this core, but more detailed studies will have to be undertaken to confirm this.

Controls on the $^{87}Sr/^{86}Sr$ Curve

Several possible controls on the strontium isotopic composition of the ocean have been identified. Most of them depend on changing inputs or $^{87}Sr/^{86}Sr$ ratios from continental erosion (i.e., riverine input) of one type or another. Some sources of strontium may be dismissed as a control almost immediately. Dissolution of marine carbonates only buffers seawater $^{87}Sr/^{86}Sr$ ratios from changing, and cannot be invoked as a control [Hodell et al., 1989]. This also eliminates changes in the CCD as a forcing mechanism. Input into the ocean from continental erosion has a $^{87}Sr/^{86}Sr$ ratio considerably above that of modern seawater (0.7119 vs 0.7092, Palmer and Edmond, 1992], and it has been argued that as a result it is much easier to change the seawater $^{87}Sr/^{86}Sr$ ratio by altering that source than by altering hydrothermal input or carbonate dissolution. Different proposed ways of changing the Sr input from the continents are: (1) by opening a previously isolated Arctic Ocean, with inputs from the Canadian and Siberian shields, (2) by increasing erosion through the effects of the changes in glaciation [Armstrong, 1971; Hodell et al., 1990; Miller et al., 1991a; Oslick et al., 1994; Zachos et al., in prep.], or (3) by increasing erosion via uplift of mountain ranges such as the Himalayan-Tibetan Plateau [Raymo et al., 1988; Hodell et al., 1989, 1990; Edmond, 1992; Richter et al., 1992]. Hydrothermal input is usually considered to change too slowly to be effective [Palmer and Elderfield, 1985; Elderfield, 1986]. However, the difference between the $^{87}Sr/^{86}Sr$ ratio of hydrothermal input (0.703) and the Eocene seawater $^{87}Sr/^{86}Sr$ ratio (0.7077) is even greater than between riverine input and seawater $^{87}Sr/^{86}Sr$ ratio (0.0047 vs. 0.0042), so hydrothermal input is also considered as a way of significantly changing the marine $^{87}Sr/^{86}Sr$ ratio.

To investigate these controls, I used the method of Hodell et al. [1989], which solves the box model of Palmer and Elderfield [1985] for non-equilibrium conditions, to investigate possible changes in fluxes. In calculating initial conditions, I assumed present day fluxes for carbonate dissolution and hydrothermal exchange, use the present day $^{87}Sr/^{86}Sr$ ratio for hydrothermal exchange and riverine input. The $^{87}Sr/^{86}Sr$ ratio for riverine input (0.7119) should probably be lower in the absence of input from the Himalayan-Tibetan Plateau [Palmer and Edmond, 1992]. However, by using the higher value, river flux is allowed to vary more conservatively. I assume that prior to the increase in marine $^{87}Sr/^{86}Sr$ in the middle Eocene, the oceans were in equilibrium at 0.707707. This allows us to use 0.707707 as the $^{87}Sr/^{86}Sr$ ratio of carbonate dissolution (Table 2-3). I can then calculate the equilibrium riverine flux as a starting point. At equilibrium, the riverine flux

TABLE 2-3

Model Parameters, Stable Latest Eocene Values

	Modern Values	Arctic Opening Model Arctic	Arctic Opening Model non-Arctic	Glacial Model	Uplift Model Model 1	Uplift Model Model 2	Hydrothermal Model
Fluxes (10^9 mol Sr/yr):							
Riverine	33.3[a]	1.00[a]	14.328[g]	14.818[g]	14.818[g]	15.058[g]	33.3[a]
Hydrothermal	13.202[b]	0.4388[b]	12.76[b]	13.2[b]	13.2[b]	13.2[b]	29.659[g]
Carbonate	3.4[a]	0.1130[a]	3.287[a]	3.4[a]	3.4[a]	3.4[a]	3.4[a]
Arctic Connection (post-conn.)			20.0[e]				
$^{87}Sr/^{86}Sr$:							
Riverine	0.7119[a]	0.7128[a]	0.7119[a]	0.7119[a]	0.7119[a]	0.711539[g]	0.7119[a]
Hydrothermal	0.703[c]	0.703[c]	0.703[c]	0.703[c]	0.703[c]	0.703[c]	0.703[c]
Carbonate	0.7084[a]	0.709811[f]	0.707707[h]	0.707707[h]	0.707707[h]	0.707707[h]	0.707707[h]
Glacial				0.715[i]			
Seawater	0.709172[d]	0.709811[g]	0.707707[h]	0.707707[h]	0.707707[h]	0.707707[h]	0.707707[h]
NBS-987	0.710235[d]						

TABLE 2-3--continued

a: From Palmer and Edmond (1989), with Arctic and non-Arctic values partitioned if necessary according to their respective areas (from Knauss, 1978).

b: Calculated from non-equilibrium equations, with Arctic and non-Arctic values partitioned if necessary according to their respective areas (from Knauss, 1978).

c: From Richter et al. (1992).

d: From Hodell et al. (1990).

e: Approximately 1/100 of Gulf Stream.

f: Defined from Arctic Seawater equilibrium value.

g: Calculated from equlibrium equations.

h: Defined from Hole 689B average for late Eocene.

i: Approximate Gondwana value from Palmer and Edmond (1989).

in the middle Eocene is calculated to be less than 15×10^9 moles Sr/yr, about half of today's riverine flux of 33.3×10^9 moles Sr/yr.

I model the marine $^{87}Sr/^{86}Sr$ curve as a series of straight line segments. This method of modeling can create artificially abrupt changes in fluxes at changes in slope of the marine $^{87}Sr/^{86}Sr$ curve, but is simpler to model and easier to understand than using a continuously varying model. Each step in the model is approximated by a portion of an exponential curve. As a result, it is important to use a time step which is small relative to the residence time in order to accurately approximate the model. I use a step of 0.1 m.y., less than 5% of the residence time of 2.5 Ma for the modern ocean [Hodell et al., 1990] to 3.4-4.0 m.y. for the Eocene and Oligocene (this study, as a result of smaller riverine fluxes).

Arctic opening model

Plate tectonic reconstructions of the opening of the Norwegian-Greenland Sea suggest that opening occurred along a fracture zone, leading to a gateway effect in which the Arctic was suddenly put into communication with the North Atlantic Ocean over a short period of time. Prior to 72 Ma (Cretaceous), the North Atlantic Ocean had not yet begun to form and the region between Scandinavia and Greenland was closed with no intervening ocean floor. The first extension in the Arctic region is believed to have begun at Chron 30 time [Rowley and Lottes, 1988] and the oldest seafloor anomaly to be identified in the North Atlantic and Eurasian basins is Anomaly 24 [Vogt et al., 1981], at about 53 my [Cande and Kent, 1992], of early Eocene age. A close connection is maintained between Greenland and Europe (Svalbard) during the Eocene as Svalbard was transformed eastward relative to Greenland along the Greenland fracture zone. At Anomaly 13 time (33.4 Ma), the contact between Svalbard and Greenland was tenuous and the final separation between the European and American plates may have occurred at this time. This disagrees with interpretations of Lawver et al. [1990] which suggested a later opening (15-10 Ma). However, as we shall see below, only a small opening would be necessary to have a large effect on marine $^{87}Sr/^{86}Sr$ ratios. Because the seafloor in the North Atlantic and the Arctic Ocean would have been at depths of over 4000 m, the opening may have occurred rapidly, over hundreds or thousands of years. The motion of the Arctic basin may have occurred similar to a sliding door, allowing water from the surface to 4 km depth to be released suddenly into the Atlantic Ocean.

This sudden influx of cold deep water should produce severe erosion of abyssal sediments in the North Atlantic Ocean. Severe erosion is, in fact, observed beginning in earliest Oligocene time (C13) (e.g., the reflector R4 of Miller and Tucholke [1983]). If the Arctic had been isolated up to that point, it would then have mixed with the world ocean, and added its riverine input, hydrothermal exchange, and carbonate dissolution to those of the World Ocean.

By using a few assumptions about those sources (Table 2-3), we can calculate what the equilibrium $^{87}Sr/^{86}Sr$ ratio of a closed Arctic Ocean would have been (0.709811) and what riverine input into the world ocean (in the absence of Arctic input) would be at the equilibrium marine isotopic value of 0.707707 (14.328×10^9 moles Sr/yr, as opposed to 14.818×10^9 moles Sr/yr with Arctic input). At the point when the marine $^{87}Sr/^{86}Sr$ ratio begins to increase, I model the connection between the Arctic Ocean and the world ocean as a small flux between the two oceans, on the order of 1/100 of the flux of Sr carried by the Gulf Stream. I then use the non-equilibrium model of Hodell et al. [1989] to model the response of the world ocean to these new inputs (Figure 2-7a).

Rather than recreating the marine Sr isotope curve, it is clear that there are fundamental differences between the modelled and the real curve. First, there is an immediate, sudden jump in the world ocean $^{87}Sr/^{86}Sr$ ratio, as the isotopically more radiogenic Arctic Ocean mixes with the world oceans, even with the relatively small flux between the two. Secondly, the modelled marine $^{87}Sr/^{86}Sr$ ratio asymptotically approaches equilibrium with the new riverine input from the Arctic Ocean, rising steeply at first, then less steeply as time goes on. The modelled Arctic Ocean

Figure 2-7. Modelled response of marine $^{87}Sr/^{86}Sr$ ratio to different forcing functions.

a: Opening of the Arctic Ocean, compared to the actual marine $^{87}Sr/^{86}Sr$ ratio.
b: Change in Sr flux from Antarctic glaciation.
c: Change in riverine Sr flux and in both riverine Sr flux and isotopic ratio.
d: Change in hydrothermal Sr flux.

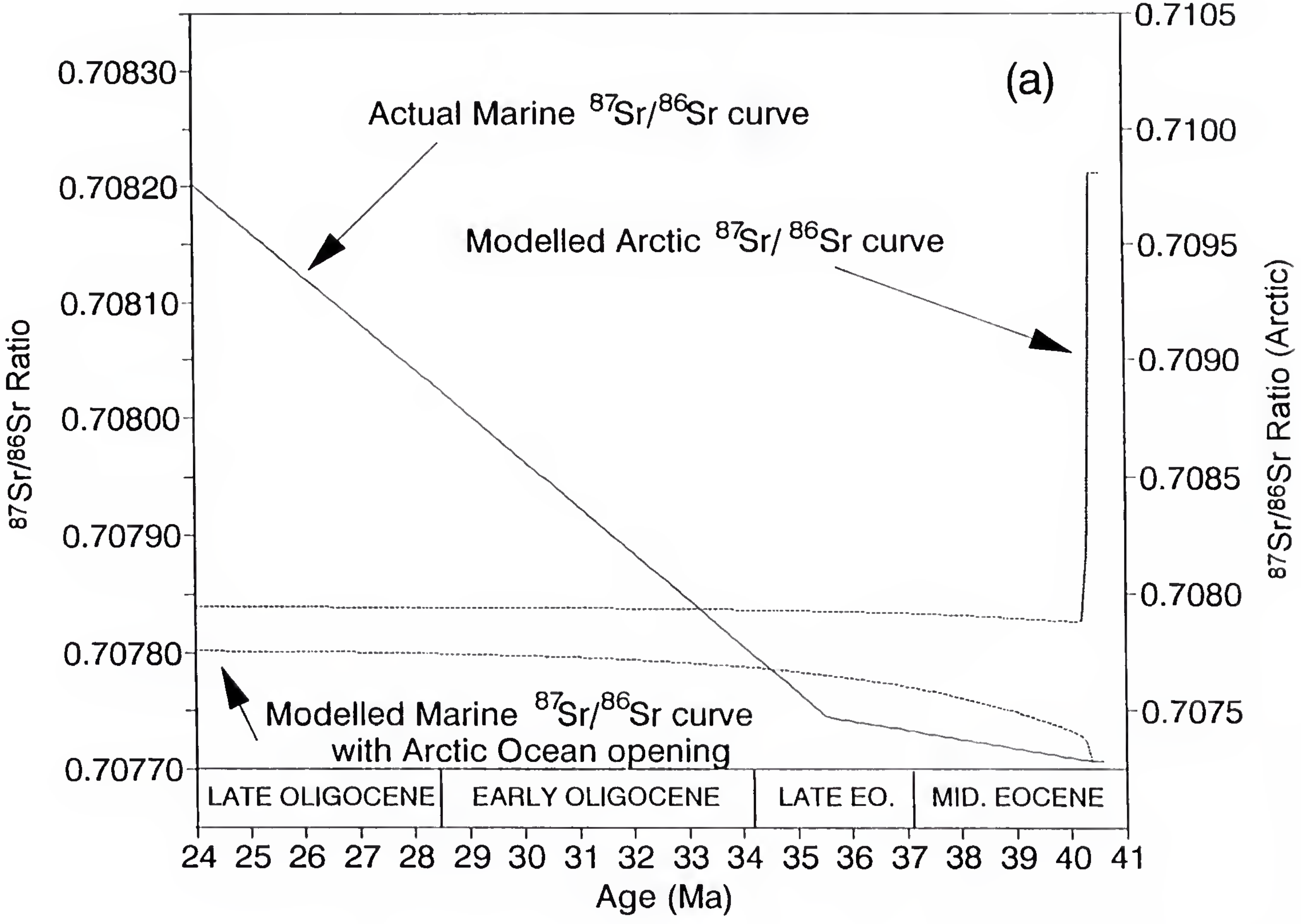
(a)
Actual Marine $^{87}Sr/^{86}Sr$ curve
Modelled Arctic $^{87}Sr/^{86}Sr$ curve
Modelled Marine $^{87}Sr/^{86}Sr$ curve with Arctic Ocean opening
$^{87}Sr/^{86}Sr$ Ratio
0.70830
0.70820
0.70810
0.70800
0.70790
0.70780
0.70770
$^{87}Sr/^{86}Sr$ Ratio (Arctic)
0.7105
0.7100
0.7095
0.7090
0.7085
0.7080
0.7075
LATE OLIGOCENE
EARLY OLIGOCENE
LATE EO.
MID. EOCENE
24 25 26 27 28 29 30 31 32 33 34 35 36 37 38 39 40 41
Age (Ma)

Figure 2-7--continued

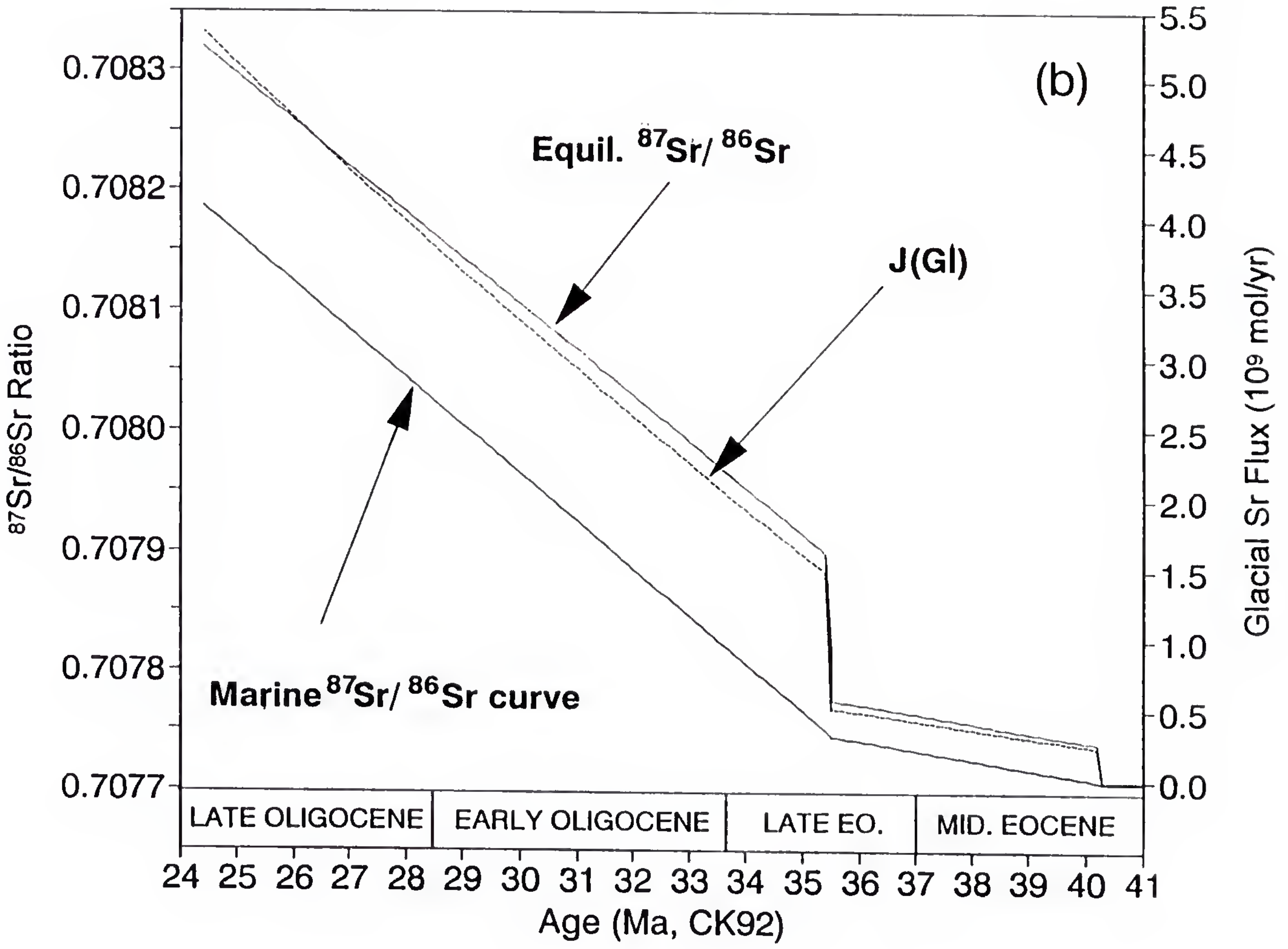

Figure 2-7--continued

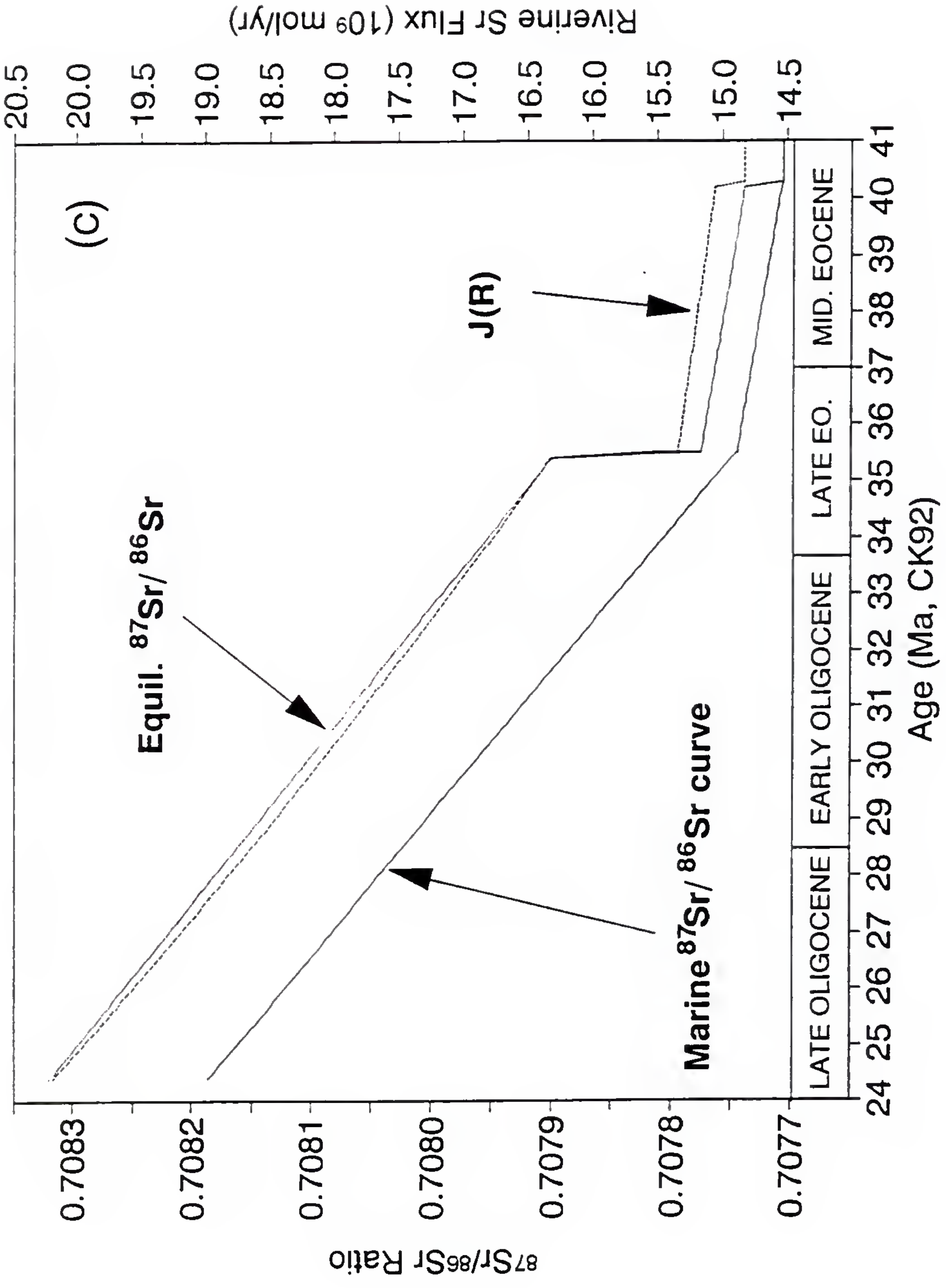

Figure 2-7--continued

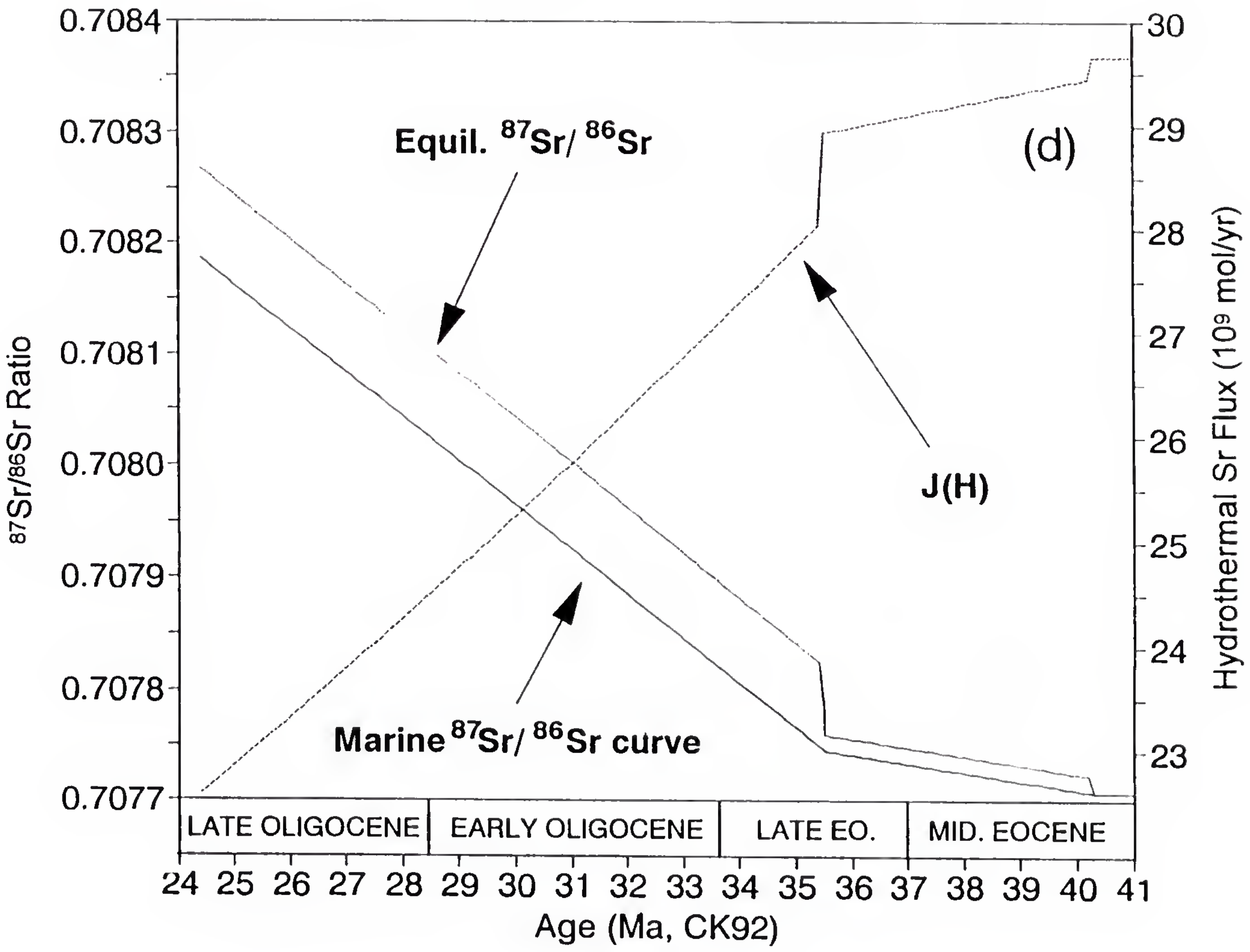

$^{87}Sr/^{86}Sr$ ratio decreases suddenly and then asymptotically approaches equilibrium with the world ocean. It is clear that this model cannot adequately explain the nearly linear increase in marine strontium isotope composition from 35 to 26 Ma. It is also clear that strontium isotopic measurements of Arctic carbonate sediments may help to constrain the time of connection of this basin to the world ocean.

Glaciation model

Recent evidence suggests that glaciation on Antarctica began near the time that the marine $^{87}Sr/^{86}Sr$ ratio began to increase, and that glaciation may in fact be a cause for the rising $^{87}Sr/^{86}Sr$ ratios of seawater [Armstrong, 1971; Hodell et al., 1990; Miller et al., 1991a; Hodell, 1994; Oslick et al., 1994; Zachos et al., in prep.]. It has been known for some time that a major increase occurred in $\delta^{18}O$ at about 33.4-33.6 Ma (35.7-35.9 of BKFV85). The cause was originally suggested to be the onset of cold bottom water production [Shackleton and Kennett, 1975] and more recently, due to the onset of Antarctic glaciation [Matthews and Poore, 1980]. A pulse of IRD has been found on the Kerguelen Plateau [Zachos et al., 1992b; Breza and Wise, 1992; Barrera et al., 1994] and in lesser amounts on the Maud Rise [Ehrmann and Mackensen, 1992], which coincided with the earliest Oligocene increase in $\delta^{18}O$ values. This suggests that glaciation on Antarctica reached the coastline at least briefly at about 33.4-33.6 Ma. At this time, benthic foraminiferal $\delta^{18}O$ records suddenly increased by about 1 $^{o}/oo$, then decreased by about 0.3-0.4 $^{o}/oo$ [Miller et al., 1987; Zachos et al., 1992b; Chapter 3]. This suggests a sudden advance, followed by a retreat of continental ice sheets.

Other evidence may point to a somewhat earlier onset of glaciation. Sedimentological studies of ODP Legs 113 and 119 [Ehrmann and Mackensen, 1992] suggest that glaciers may have affected Antarctica as early the late middle Eocene, 43.3 Ma (45.5 Ma BKFV85), with a further expansion near the middle/late Eocene boundary at about 37.1 Ma (40 Ma). Somewhat controversial evidence of terrigenous grains first occurred on the Kerguelen Plateau and possibly the Maud Rise in the middle Eocene from 43.3-39.1 Ma [Wise et al., 1992], suggesting ice-rafting events during the Eocene. In addition, massive diamictites drilled in Prydz Bay, Antarctica, and interpreted as till deposits [Ehrmann et al., 1992] have been tentatively dated between 37.9 and 34.8 Ma (40.8-37.5 Ma), suggesting a late middle to late Eocene age for Antarctic glaciation. An increase of chlorite and kaolinite at the expense of smectite on the Maud Rise in the late Eocene is suggested to have resulted from increased physical weathering on Antarctica attributed to increased Antarctic glaciation [Ehrmann and Mackensen, 1992; Robert and Chamley, 1992], although a moderate, humid climate is still postulated for that time. The major sedimentologic evidence cited by Ehrmann and Mackensen [1992] still suggests the major onset of glaciation in the earliest Oligocene at about 33.5 Ma. This is the time when the largest change from smectite to illite occurs in marine clay mineral assemblages, indicating a change from chemical to physical weathering conditions on Antarctica [Ehrmann et al., 1992].

In modeling the effects of glaciation on Antarctica, equilibrium values for riverine input, hydrothermal exchange, and carbonate dissolution (Table 2-3) are used. As a rough average $^{87}Sr/^{86}Sr$ of typical "Gondwana" shields, 0.715 is used by averaging the values for rivers from Australia and southern Africa [Palmer and Edmond, 1989]. I use this value for a new, glacial erosion input (holding riverine input, hydrothermal exchange, and carbonate dissolution constant at their equilibrium values; Table 2-3) and calculate the glacial erosive flux of Sr necessary to produce the observed record, using the non-equilibrium method of Hodell et al. [1989] (Figure 2-7b).

In this case we can compare the model's predicted glacial activity with the observed indications of glaciation. The comparison is not encouraging. The onset of modelled glaciation occurred at 40.4 Ma, defined by the time when the marine $^{87}Sr/^{86}Sr$ began to increase, and rose from a low of just 0.24×10^9 to 0.52×10^9 moles Sr/yr by 35.5 Ma (Figure 2-7b). The modelled glacial Sr flux then jumped to 1.50×10^9 moles Sr, about 1/10 of the riverine flux of

14.8×10^9 moles Sr/yr, reflecting the increased slope of the $^{87}Sr/^{86}Sr$ curve, and finally rose to a high of 5.19×10^9 moles Sr/yr by 24.8 Ma. In contrast, most sedimentologic and oxygen isotopic evidence points to a somewhat later onset of glaciation, at about 33.5 Ma, 2 m.y. later than the first increase in marine $^{87}Sr/^{86}Sr$ [Rea, 1992 and this study]. This glaciation, rather than starting at low intensity and gradually increasing over the next 8 m.y. or so, as suggested by the strontium isotopic modelling, seems to have been episodic based on oxygen isotopic evidence, with maxima at about 33, 29, and 24 Ma (35, 31, 25 Ma; Miller et al., 1987, 1991a; Wise et al., 1991].

Oslick et al. [1994] also examine the possibility that glaciation and the $^{87}Sr/^{86}Sr$ curve are related. They identified 6 events in the Oligocene and Miocene in which very small scale $^{87}Sr/^{86}Sr$ (from ODP Hole 747A) increases lag deglacial events by 0.9 to 1.4 m.y. The deglaciation events were defined by decreases in $\delta^{18}O$ values that followed previously identified glacioeustatic episodes [Miller et al., 1991b, Wright and Miller, 1992]. They attribute the overall rise in marine $^{87}Sr/^{86}Sr$ ratios in the Oligocene and the shorter scale $^{87}Sr/^{86}Sr$ increases in the Miocene to glaciation, with the overall rise in the Miocene due to uplift of the Himalyan-Tibetan Plateau. The 0.9 to 1.4 m.y. lag in response is attributed to the long residence time of the oceanic Sr reservoir.

I disagree with this interpretation on three points. First, the long residence time of Sr will create a lag between the initial $^{87}Sr/^{86}Sr$ response and its final equilibrium value, not between the driving mechanism (weathering of the Antarctic craton during deglaciation [Oslick et al., 1994]) and initial response of marine $^{87}Sr/^{86}Sr$ values. If in fact the lagged association between deglaciations and $^{87}Sr/^{86}Sr$ increases is real, another mechanism must be invoked to delay the release of radiogenic Sr to the ocean until 0.9 to 1.4 m.y. after the deglaciation. Second, as stated above, the continued rise in marine $^{87}Sr/^{86}Sr$ ratios implies a gradually increasing level of glacial weathering throughout the Oligocene (Figure 2-7b). Evidence for glaciation in the Oligocene instead suggests a more episodic behavior. Unless the amplitude of these episodic glaciations slowly increased (which is not implied by $\delta^{18}O$ records) or unless weathering on the Antarctic craton gradually increased during each deglacial episode (perhaps through dissolution of gradually increasing deposits of finely ground, easily weathered cratonic till [Hodell et al., 1990, B. Opdyke, pers. comm., 1994]), it would not be possible to produce the observed $^{87}Sr/^{86}Sr$ curve from Oligocene glaciation. Third, the inflection to a high slope of the $^{87}Sr/^{86}Sr$ curve clearly begins before the first glaciation event cited by Oslick et al. [1994] (about 35.5 Ma vs. about 33.5 Ma). The time of onset of the slower rise in $^{87}Sr/^{86}Sr$ began even earlier, around 40 Ma.

Even if interpretations of sedimentologic evidence suggesting earlier onset of glaciation are correct, it may be hard to ascribe the increase in marine $^{87}Sr/^{86}Sr$ to glaciation. Two factors support this conclusion. First, the $^{87}Sr/^{86}Sr$ ratio in river water draining continental shields under most circumstances is likely to be lower than the bulk ratio of the shield rocks, because the minerals containing highly radiogenic $^{87}Sr/^{86}Sr$ ratios are more resistant to erosion [Palmer and Edmond, 1992; Edmond, 1992]. Higher (more radiogenic) $^{87}Sr/^{86}Sr$ ratios are present in minerals with high Rb contents (i.e., containing incompatible monovalent cations such as potassium feldspar, sodic plagioclase, and muscovite) which are also fairly resistant to weathering. Biotite has been suggested as one mineral containing highly radiogenic Sr which is easily weathered in glacial deposits, but the amount of Sr contained in biotite is low [Blum and Erel, 1995]. Less radiogenic $^{87}Sr/^{86}Sr$ ratios are generally present in more easily weathered minerals containing divalent cations such as calcic plagioclase and olivine. Strontium isotopic ratios derived from shield areas are therefore usually either not high enough, or with strontium fluxes too low, to control the marine $^{87}Sr/^{86}Sr$ ratio [Edmond, 1992]. For example, the marine $^{87}Sr/^{86}Sr$ ratio of rivers draining the Canadian Shield averages only 0.7111, with more radiogenic ratios present in rivers with lower Sr concentrations [Wadleigh et al., 1985]. Special circumstances must be invoked, such as deep-seated metamorphic homogenization, for rivers with high $^{87}Sr/^{86}Sr$ to also have large Sr fluxes [Edmond, 1992]. Second, although the increase in illite in the late Eocene suggests climatic deterioration possibly associated with glaciation, it is suggestive of glaciation precisely because it indicates a change in the mode of weathering, from chemical to physical. This, however, may not necessarily reduce the amount of Sr weathered from the craton, because mechanical grinding by glaciers may lead to enhanced chemical dissolution [Armstrong, 1971; Hodell et al., 1990]. There is evidence that chemical denudation rates of cations in glacial environments are high [Reynolds and Johnson, 1972], and it is likely that the temporary glacial events suggested for the Oligocene were temperate (wet based) in nature.

Uplift model

The Himalayan-Tibetan Plateau system is unique in a number of ways. First, it is the highest mountain range on Earth, with an average elevation of 5000 m [Raymo and Ruddiman, 1992]. Second, rivers draining it have high $^{87}Sr/^{86}Sr$ ratios for the flux of Sr that they carry [Palmer and Edmond, 1989, 1992]. It has been suggested that the anomalous co-occurrence of high $^{87}Sr/^{86}Sr$ ratios with high Sr fluxes in Himalayan rivers is due to unique tectonic aspects of the region [Palmer and Edmond, 1992; Edmond, 1992]. Uplift of the Himalayan orogen followed unusually deep seated metamorphism due to the collision of India with Eurasia and subsequent crustal thickening, allowing radiogenic Sr (formerly trapped within hard-to-weather Na- and K-bearing silicates) to be remobilized into easier-to-weather Ca-silicates [Edmond, 1992]. Uplift exposes more, and deeper, continental crust to weathering, and because of mass wasting in areas of high relief, fresh rock is repeatedly exposed to continued weathering. As a result, several studies [Raymo et al, 1988; Hodell et al., 1989, 1990; Raymo and Ruddiman, 1992; Richter et al., 1992; Hodell and Woodruff, 1994] have suggested that uplift of the Himalayas controls the marine $^{87}Sr/^{86}Sr$ ratio during the Cenozoic by increasing the amount of continental weathering and delivery of radiogenic Sr to the world's oceans.

Raymo et al. [1988], Hodell et al. [1989, 1990], and Raymo and Ruddiman [1992] suggested Himalayan control of marine Sr isotopic ratios during the Neogene. Richter et al. [1992] suggested that this control extended back to the Paleogene, with the first effects of the uplift on marine $^{87}Sr/^{86}Sr$ ratios occurring at about 37 Ma (40 Ma BKFV85, their date for the first increase in the Sr isotopic ratio). They modelled the increase using a non-equilibrium model in which riverine input of Sr controls the marine $^{87}Sr/^{86}Sr$ curve. I re-calculated the curve for this time period for a number of reasons. First, the model is based on the data from Hole 689B, which is more highly refined than previous records. Second, the time-step used by Richter et al.

[1992], 1 m.y., was too small to accurately portray the large changes in flux implied by the data. An example of this is the change in $^{87}Sr/^{86}Sr$ ratios that occurred in the late Eocene. The sudden change in slope of the marine $^{87}Sr/^{86}Sr$ curve implies that large and rapid changes in marine $^{87}Sr/^{86}Sr$ ratios occurred at this time. By using a 1 m.y. time step, they underestimated these changes. Third, the model used by Richter et al. [1992] ignores the effect of carbonate dissolution in calculating fluxes. Although small, this flux is significant, and leaving out its buffering effect [Raymo and Ruddiman, 1992] on the Sr isotope budget gives underestimates of the fluxes necessary to change the marine $^{87}Sr/^{86}Sr$ curve. Fourth, I re-calculate the curve based on the new Cande and Kent [1992] time scale. These calculations are based on rates-of-change, which are sensitive to changes in time scale [Delaney and Boyle, 1988].

I model the change in two ways. Richter et al., [1992] noted that in increasing erosion from the Himalayan-Tibetan Plateau, both riverine Sr flux and $^{87}Sr/^{86}Sr$ may change. I first assume that world riverine $^{87}Sr/^{86}Sr$ stays constant at the current value, 0.7119 [Palmer and Edmond, 1989]. The result is that a small jump in flux occurred, from the equilibrium value of 14.82×10^9 to 15.06×10^9 mcles Sr/yr at the beginning of the increase in $^{87}Sr/^{86}Sr$ at 40.4 Ma. The riverine flux gradually rose to 15.34×10^9 moles Sr/yr by 35.5 Ma. At that time, a sudden increase in riverine strontium flux occurred, from 15.34×10^9 to 16.32×10^9 moles Sr/yr, an increase of about 6.4%. The sudden jump is probably an artifact resulting from the modelling of the data as having a sudden change in slope, from nearly stable $^{87}Sr/^{86}Sr$ values to steadily increasing values. If instead of suddenly changing, the marine $^{87}Sr/^{86}Sr$ ratio ramps gradually up to increasing values, the increase in riverine flux would be more gradual. The model flux grows steadily from 35.5 Ma to a maximum of 20×10^9 moles Sr/yr at 24.8 Ma (Figure 2-7c, Table 2-3). For the second model, I assume that the riverine Sr flux began to increase slowly, as the Himalayas were uplifted, but that the $^{87}Sr/^{86}Sr$ ratio of the rivers draining the Himalayas was higher, such that the Sr flux increased from an equilibrium value of 15.06×10^9 moles Sr/yr. In this case, it is a simple equilibrium calculation to determine what the riverine $^{87}Sr/^{86}Sr$ ratio would have been before the increase. Using equilibrium calculations, if the Eocene riverine Sr flux was 15.06×10^9 moles Sr/yr, the riverine $^{87}Sr/^{86}Sr$ ratio must have been 0.711833. These results are similar to the results of Richter et al. [1992], except that (1) the calculated fluxes are higher, and (2) the timing of course is different, in part because of the different time scales, and in part because of the different $^{87}Sr/^{86}Sr$ curves employed.

Superficially, this seems to be a reasonable simulation of the events leading to the change in marine $^{87}Sr/^{86}Sr$ from the Eocene through the Oligocene. The next step is to determine whether this is a realistic model for the uplift of the Himalayas. Richter et al. [1992] cited evidence for the collision of India with Eurasia beginning at about 50 Ma (BKFV85), and increased uplift at about 20 Ma (BKFV85). Convergence rates between India and Eurasia decreased suddenly about 50 Ma (BKFV85)[Richter et al., 1992]. This might suggest that the uplift could have begun somewhere in between these times, specifically at the time when the marine $^{87}Sr/^{86}Sr$ ratio began to increase. Richter et al. [1992] calculated that enough crust has eroded from the Himalayan-Tibetan Plateau since the collision to account for the increase.

The next point to consider is whether the timing is correct. Several recent studies on tectonism in the Himalayan region suggest that the uplift did not begin until the latest Oligocene or Neogene. These studies use $^{40}Ar/^{39}Ar$ closure dates [Harrison et al., 1993; McFarlane, 1993] and U-Pb dates [Parrish and Hodges, 1993] to date the first large episode of Himalayan deformation at 27-19 Ma. In addition, Rea [1992] examined mass accumulation rates (MAR) in the Indian Ocean and found that most of the accumulation occurred after 16 Ma. Even after 16 Ma, there was little correlation between MAR and the Sr isotope curve. He concluded that runoff from the Himalayan region cannot explain the increase in marine $^{87}Sr/^{86}Sr$ before 16 Ma, and is not the only control after 16 Ma.

These studies all suggest that perhaps the uplift of the Himalayas is not the controlling factor in the marine Sr budget during the Paleogene. They suggest that, despite the decrease in convergence rates at about 50 Ma, hard collision leading to extensive uplift did not begin until 20-30 m.y. later, after marine $^{87}Sr/^{86}Sr$ ratios began to increase.

Hydrothermal model

Besides continental input, the other major control on marine strontium isotopic ratios is hydrothermal activity at mid-ocean ridges. At hydrothermal vents, seawater strontium exchanges with strontium in mid-ocean ridge basalts (MORB). No net change in concentration occurs [Edmond et al., 1979], but the marine $^{87}Sr/^{86}Sr$ reaches equilibrium with $^{87}Sr/^{86}Sr$ of MORBs at 0.703 [Richter et al., 1992]. In most models of marine $^{87}Sr/^{86}Sr$ ratios through geologic time, hydrothermal activity is (1) assumed to be directly correlated to spreading rates [Owen and Rea, 1985; Richter et al., 1992; Rea, 1992] and/or (2) assumed to be only slowly varying as a result [Hodell et al., 1989, 1990, Miller et al., 1991a, Richter et al., 1992]. Calculations of rates of crustal generation [Kominz, 1984] do seem to show only slow changes through time, although they need to be recalibrated to the CK92 time scale. If hydrothermal activity and rates of crustal generation are not in fact related, however, this correlation obviously cannot be used.

If there were a simple relationship between these parameters, a correlation between spreading rates and rates of accumulation of hydrothermal sediment near the spreading ridges would be expected. Several studies suggest instead that the relationship between hydrothermal activity and rates of crustal generation is not as simple as has been previously assumed. Owen and Rea [1985] and Lyle et al. [1987] found Neogene maxima of MAR of iron-rich hydrothermal sediments in the Pacific up to 20 times greater than minima (and 10 times greater than present values). These changes in hydrothermal MAR were uncorrelated with, and much larger than, spreading rate changes. Instead, maxima in hydrothermal MAR occurred at times of tectonic reorganization such as ridge jumps and changes in ridge reorientation. These maxima and minima are regional rather than global in extent, while the marine Sr signal is a response to, among other things, the integrated global hydrothermal signal. However, the assumed spreading rate - hydrothermal activity signal would also be an integrated one. The lack of correspondence with spreading rates and the positive correspondence with times of tectonic reorganization strongly suggests that we should not look to spreading rates as the controlling relationship with hydrothermal activity.

We can then look to MAR of hydrothermal sediments as indicators of hydrothermal activity in the Paleogene. There is some evidence that timing of hydrothermal activity in the

Eocene and Oligocene, as delineated by MAR of hydrothermal sediments and other hydrothermally-related sediment factors, does indeed support the hypothesis of hydrothermal control of marine $^{87}Sr/^{86}Sr$ ratios. Owen and Rea [1985] found decreased MAR of Fe, opal, and $CaCO_3$, and decreased Sr/Ca (which is not found in the Hole 689B data set) in the Oligocene relative to the Eocene, although their data are sparse. Leinen [1987, 1989] also showed decreased hydrothermal deposition in the Oligocene of the North Pacific relative to the Eocene. Hydrothermal sedimentation on Broken Ridge (Indian Ocean) decreased by a factor of 2 across a late Eocene/early Oligocene unconformity [Owen and Zimmerman, 1991].

There is considerable geologic evidence of a major tectonic reorganization in the Pacific in the middle Eocene. A bend in hotspot lineations, especially the Hawaii-Emperor seamount chain, occurred in the middle Eocene [Van Andel et al., 1975, Clague et al., 1975, Kennett et al., 1985] and has been dated paleomagnetically and radiometrically at 41-43 Ma [Vogt, 1975, Clague et al., 1975]. A major reorganization such as this would be expected to cause widespread cracking of the oceanic crust as re-alignment of spreading centers occurred [Lyle et al., 1987]. Hydrothermal activity from this, combined with widespread seafloor volcanism during the Eocene [Owen and Rea, 1985] would tend to keep the marine $^{87}Sr/^{86}Sr$ ratio depressed through the Eocene. Subsequent to this, a decay in hydrothermal activity would allow the marine $^{87}Sr/^{86}Sr$ ratio to rise as the effect of high riverine $^{87}Sr/^{86}Sr$ ratios began to predominate.

The timing of these events suggests that it would be useful to model the changes in hydrothermal input that would be necessary to give the observed change in marine $^{87}Sr/^{86}Sr$. I begin by using present day values (Table 2-3) for riverine input and carbonate dissolution and for riverine and hydrothermal $^{87}Sr/^{86}Sr$, with $^{87}Sr/^{86}Sr$ of carbonate dissolution at the equilibrium late Eocene marine $^{87}Sr/^{86}Sr$ (0.707707), and calculate the hydrothermal Sr input necessary to reach the equilibrium late Eocene marine $^{87}Sr/^{86}Sr$. The value obtained is 29.66×10^9 moles Sr/yr, about 2.25 times larger than the present value. This increased flux is well within the range of values suggested by the studies on hydrothermal sediment MARs. Note that in addition, if riverine input was less, as has been suggested [Richter et al., 1992], the hydrothermal flux would not need to be even this high. I then use the non-equilibrium model of Hodell et al. [1989] and allow hydrothermal input to change rather than riverine or glacial input (Figure 2-7d). At 40.4 Ma, a drop from 29.66×10^9 to 29.44×10^9 moles Sr/yr occurs as the increase in marine $^{87}Sr/^{86}Sr$ ratios begins. The hydrothermal flux decreases slowly until 35.5 Ma, when it drops suddenly from 28.94×10^9 to 28.04×10^9 moles Sr/yr, at the same time as the slope of the marine Sr curve increases. Hydrothermal flux decreases more quickly, falling to 22.78x10^9 moles Sr/yr by 24.8 Ma.

The results of the model do not exactly mirror changes seen in hydrothermal sedimentation as delineated by Owen and Rea [1985], Leinen [1987, 1989] and Owen and Zimmerman [1991]. However, it is important to note that these were regional rather than global studies. Geochemical indicators such as Li/Ca or Sr/Ca ratios in marine sediments may give a global record. These indicators suggest that hydrothermal flux changed by less than a factor of 2 during the Cenozoic [Delaney and Boyle, 1988], which disagrees with the results from the present model, although they do not discount the effect entirely.

It is, of course, simplistic to suggest that any of the models discussed above would act alone to totally control the marine strontium isotope curve. Richter et al. [1992] allowed hydrothermal input to vary as a function of spreading rates while calculating the changes in riverine runoff necessary to obtain the observed marine $^{87}Sr/^{86}Sr$ record. Although from the above discussion spreading rate records cannot be used to constrain hydrothermal input, this type of model, where more than one input varies, is clearly the most likely to realistically simulate the real world. In addition, the actions of the different inputs on each other will need to be addressed as well. For instance, the effects of hydrothermal activity on climate may effect the Sr cycle. Owen and Rea [1985] noted that increased hydrothermal activity in the early Eocene may have led to an enhanced greenhouse effect through the addition of CO_2 to the atmosphere. As hydrothermal activity decreased later in the Eocene, not only would marine $^{87}Sr/^{86}Sr$ values tend to increase, but by cooling of the climate system, glaciation would be encouraged, possibly further increasing marine $^{87}Sr/^{86}Sr$ values through increased continental weathering. The increase in marine $^{87}Sr/^{86}Sr$ values through the Oligocene is fairly steady, rather than pulse-like, suggesting the forcing factor(s) have long time constants [Hess et al., 1989] and that more than a single, sudden increase or decrease in a given parameter is responsible (Figure 2-7). One way this could have occurred would be for a succession of events to have taken place, each of which would tend to increase the marine $^{87}Sr/^{86}Sr$ composition.

Conclusion

Strontium isotope stratigraphy offers an additional dating tool for time periods during which the ratio of ^{87}Sr to ^{86}Sr in the oceans increases rapidly. One such interval is the Oligocene. Ocean Drilling Program Hole 689B offers an excellent, high resolution $^{87}Sr/^{86}Sr$ record in a section with a good paleomagnetic record and low diagenetic alteration.

The Sr isotopic composition of seawater is controlled by input of Sr from 3 sources: continental weathering through riverine flux, hydrothermal alteration, and dissolution of seafloor carbonates. Any of these inputs may be altered to control the marine $^{87}Sr/^{86}Sr$ curve, although carbonate dissolution is primarily a buffer and cannot realistically be expected to have a controlling effect.

Three different models (glaciation, uplift, hydrothermal) are evaluated for their effect on marine Sr ratios. Each of the 3 models can be forced to produce the marine $^{87}Sr/^{86}Sr$ curve, but each has drawbacks. The glaciation model suffers from the fact that either (1) the timing of glaciation, especially the onset of glaciation, is not yet well constrained, (2) the time constant of observed glaciation is too short to explain the constant slope of the $^{87}Sr/^{86}Sr$ curve over a 10 m.y. time period, (3) the type of erosion caused by glaciation may not be able to provide sufficient radiogenic Sr. The uplift model suffers from the fact that sedimentologic and geochronologic evidence [Rea, 1992] suggests that the timing of the uplift was too late to have caused the increase in marine $^{87}Sr/^{86}Sr$ ratios. The hydrothermal model suffers from the fact that insufficient changes in hydrothermal activity appear to have occurred [Delaney and Boyle, 1988], although I show here that the effects of hydrothermal activity may be larger than previously assumed.

The correct solution to the question of what controlled the marine $^{87}Sr/^{86}Sr$ curve during the late Eocene to Oligocene (and indeed the entire Cenozoic) may rest in a combination of these factors. Some of these factors may be linked, such as hydrothermal activity and glaciation [Owen and Rea, 1985] or uplift and glaciation [Raymo and Ruddiman, 1992; Raymo et al, 1988] while others may not be so linked, such as a decrease in hydrothermal activity in the Paleogene followed by Neogene uplift [Rea, 1992].

CHAPTER 3

LATE EOCENE TO OLIGOCENE VERTICAL OXYGEN ISOTOPIC GRADIENTS IN THE SOUTH ATLANTIC: IMPLICATIONS FOR WARM SALINE DEEP WATER

Introduction

The history of paleoclimate during the Tertiary has been one of stepwise cooling since the early Eocene [Shackleton and Kennett, 1975]. A great deal of evidence suggests high (10-15°C, McKenna, 1980; Wolfe, 1980] oceanic temperatures near the poles in the early Eocene, including faunal, floral [Estes and Hutchinson, 1980; McKenna, 1980; Wolfe, 1980], and oxygen isotopic evidence [Shackleton and Kennett, 1975, Douglas and Savin, 1975, Miller et al., 1987]. The oxygen isotopic evidence has been somewhat equivocal, however, because the oxygen isotopic ratio of biogenic calcite is affected both by temperature and by the oxygen isotopic composition of seawater (and hence ice volume and salinity). Shackleton and Kennett [1975] and Savin et al. [1975] suggested that a 1 $^{o}/oo$ increase in $\delta^{18}O$ values during the earliest Oligocene was due to a decrease in high-latitude temperature and the production of cold bottom water, with another increase in the middle Miocene due to the first permanent accumulation of ice on East Antarctica. In contrast, Matthews and Poore [1980] re-interpreted the oxygen isotopic signal to suggest that the earliest Oligocene oxygen isotopic increase was due to ice accumulation on East Antarctica and that a cooling of bottom waters caused the middle Miocene $\delta^{18}O$ increase. Further work has failed to resolve this question although a consensus [Wise et al., 1991] is emerging of at least limited Oligocene glaciation, particularly in light of recent discoveries of earliest Oligocene ice-rafted debris [Zachos et al., 1992b, Barrera and Huber, 1993]. Neither interpretation has considered in detail the implications of the theories on deep ocean circulation.

Production of deep and bottom waters today results from evaporation, cooling, and sea-ice formation at high latitudes. As a result, the deep water in the oceans is cold and moderately saline. Chamberlin [1906] and Brass et al. [1982] pointed out that during times when the planetary temperature gradient was small and polar regions were warmer than today, cold, dense water could not have been produced at high latitudes. Instead, Brass et al. [1982] suggested, based on modeling, that production of warm, highly saline water in low-latitude marginal seas may have produced Warm Saline Deep Water (WSDW) which would have been the densest water in the oceans in the absence of cold, dense water.

A recent study [Kennett and Stott, 1990], which analyzed benthic foraminiferal oxygen isotopes from Ocean Drilling Project Sites 689 (paleodepth ~1400 m) and 690 (paleodepth ~2200 m) (Figure 3-1), provided the first

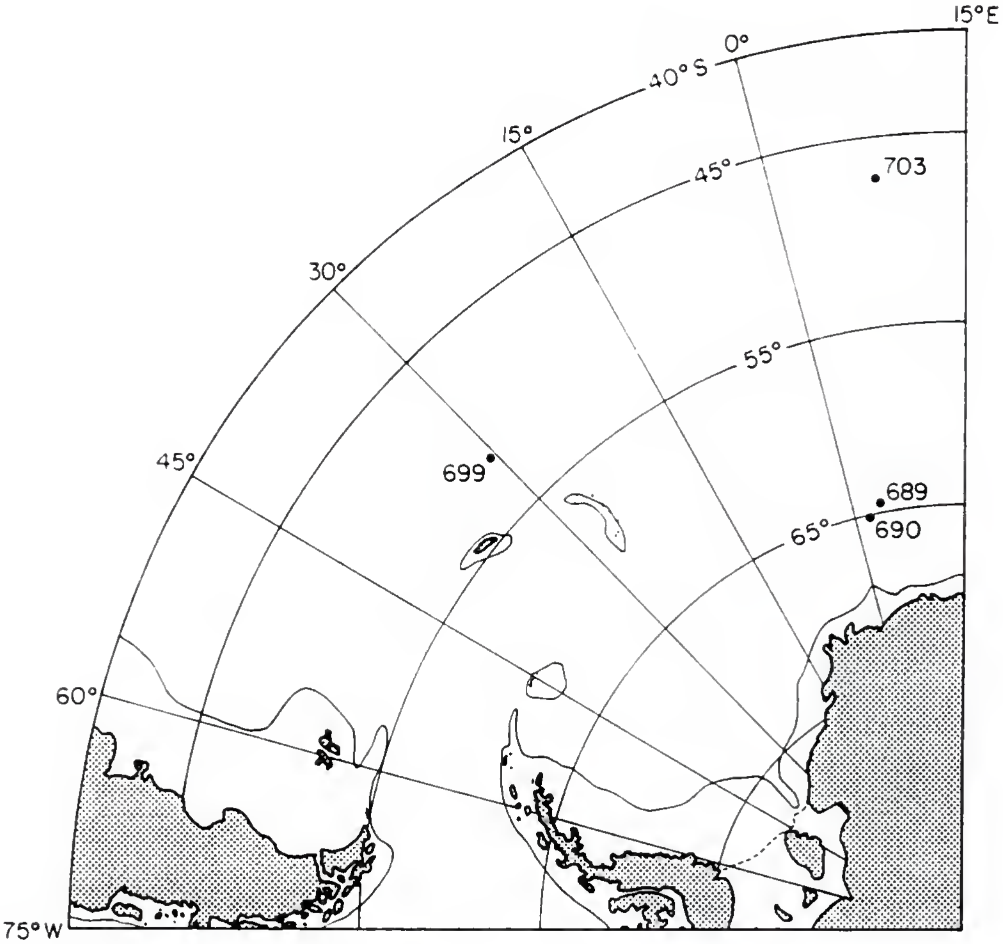

Figure 3-1: Location map of Ocean Drilling Program Sites 689, 690, 699, and 703.

evidence for a Paleogene deep circulation quite different from that of the late Neogene. Neogene to Recent deep circulation, with cold bottom water, results in a pattern of decreasing temperature with increasing depth in the ocean. Because $^{18}O/^{16}O$ ratios in biogenic calcite increase with decreasing temperature, analysis of Recent benthic foraminiferal oxygen isotopic ratios shows a pattern of increase $\delta^{18}O$ with depth, resulting in a positive ($\delta^{18}O$ vs. depth) gradient. Instead of this configuration, Kennett and Stott [1990] found that at several times in the late Eocene and during much of the Oligocene, the gradient of benthic foraminiferal $\delta^{18}O$ vs. depth reversed, indicating increased temperatures with increased depth. They suggested that this temperature inversion could be explained by the presence of Warm, Saline Deep Water produced in lower latitudes. Their "Proteus" scenario began with WSDW sporadically bathing Site 690 in the Eocene. Kennett and Stott [1990] suggested that in the Oligocene ("Proto-Oceanus"), the production of Proto-Antarctic Bottom Water (Proto-AABW) raised the WSDW up to the level of Site 690, creating a near-permanent oxygen isotopic inversion. In the late Oligocene, the establishment of modern ("Oceanus") circulation occurred, with the dominance of AABW in the oceans.

Kennett and Stott [1990] speculated that the onset of AABW formation began after the earliest Oligocene oxygen isotopic enrichment, but in the absence of direct data from a deep-water site, this hypothesis has gone untested. To test this hypothesis, we need to determine whether the reversed isotope gradient is present at other sites with different depths, in order to better outline the bathymetric, geographic, and temporal extent of WSDW. Secondly, we need to test whether or not Proto-AABW may have been present below the WSDW in the Oligocene. If in fact the production of Proto-AABW below WSDW begins at the earliest Oligocene oxygen isotope shift, it should be signalled by the establishment of a trend of increased $\delta^{18}O$ (decreased temperatures) with increasing depth below the WSDW-AABW boundary.

Leg 114 of the Ocean Drilling Program drilled two holes that help address these questions. Hole 703A was drilled in relatively shallow (1796 m) water on the Meteor Rise, sampling mid-water paleodepths, and Hole 699A was drilled in deeper water (3705 m), sampling abyssal water masses (Figure 3-1]. I analyzed the isotopic composition of benthic foraminiferal calcite from these two sites to delineate, in conjunction with Sites 689 and 690, the vertical water mass structure of the South Atlantic during the late Eocene to Oligocene, from ~42 to 26 Ma.

Methods

Age Model

The age models used by Kennett and Stott [1990] for Sites 689 and 690 are based on magnetostratigraphy [Spieß, 1990; Hamilton, 1990] and planktonic foraminiferal biostratigraphy [Stott and Kennett, 1990], and were calibrated to the Berggren et al. [1985] time scale. This time scale was used rather than the newer Cande and Kent [1992] geomagnetic polarity time scale because of the lack of calibration (as yet) of biostratigraphic datums to the newer time scale. An alternative to the Kennett and Stott [1990] age model has been developed for Site 690 by Thomas et al. [1990] that is significantly different in some respects. In most cases, these differences have little effect on oxygen isotopic conclusions, with 1 m.y. averages differing by 0.22 ^{o}/oo or less. The only major difference occurs with respect to an unconformity near 91-94 mbsf. Kennett and Stott's [1990] isotopic data suggest that the position of the unconformity should be nearer to 93.20 mbsf as opposed to the 91.58 mbsf level suggested by Thomas et al. [1990]. If the Thomas et al. [1990] position is used, the earliest Oligocene isotopic shift occurs below the unconformity, at an age greater than 38.5 Ma. Because this isotopic shift is known to occur very near 36 Ma [Oberhänsli et al., 1984; Miller et al., 1988, Zachos et al., 1992a], I accept the position of the unconformity at 93.20 mbsf. Unfortunately, biostratigraphic and magnetostratigraphic studies [Spieß, 1990; Hamilton, 1990; Stott and Kennett, 1990; Thomas et al., 1990; Wei, 1991] do not delineate the boundary ages well enough to determine which of the ages of the unconformity is correct. I provisionally accept the remainder of the Kennett and Stott [1990] age model. This is a key site for Antarctic paleoceanography, and more work is needed to define better the age of sediments at this site.

A combination of paleomagnetic datums [Hailwood and Clement, 1991a, b] and calcareous nannofossil biostratigraphic markers were used to construct the age models for Sites 699 and 703 (Table 3-1). The ages were derived from the Berggren et al. [1985] time scale. The datum levels below 35.9 Ma in Site 699 and the lowest two datum levels in Site 703 are biostratigraphic rather than magnetostratigraphic. This might lead to doubts about the age resolution, especially in the high sedimentation rate zone between the first appearance datums (FAD) of the calcareous nannofossils Reticulofenestra oamaruensis and Ismolithus recurvus (Site 699). However, Wei [1991, 1992] has shown these datums to be reliable markers for the latitudes from 47°S to 65°S. Similarly, Wei [1991, 1992] found the 41.0 Ma biostratigraphic datum (FAD Chiasmolithus oamaruensis) and the nearly correlative datum just below (Last Appearance Datum (LAD) C. solitus, 41.4 Ma) also to be reliable biostratigraphic markers.

One unconformity in Site 699 and four unconformities in Site 703 were identified within the time represented by the isotopic records. In Site 699, an unconformity was identified between 33.9 and 33.0 Ma, marked by the joint LADs of C. oamaruensis and I. recurvus between 254.33 and

TABLE 3-1

Age models for ODP holes 699A and 703A

699A

Depth (mbsf)	Age (Ma)	Datum
127.69±0.15	25.97	C7N/C7R
137.09±0.05	26.38	C7R/C7AN
140.38	26.56	C7AN/C7AR
143.84±0.10	26.86	C7AR/C8N
145.73±0.08	26.93	C8N.1
146.21±0.04	27.01	C8N.2
156.14±0.10	27.74	C8N/C8R
166.95±0.75	28.15	C8R/C9N
182.69±0.35	29.21	C9N/C9R
189.34±0.10	29.73	C9R/C10N
192.55±0.10	30.03	C10N.5
193.05±0.10	30.09	C10N.6
198.35±1.55	30.33	C10N/C10R
208.09±0.25	31.23	C10R/C11N
216.05±0.75	32.06	C11N/C11R
249.70	32.90	C12N/C12R
253.64±0.70	33.00±0.02	
- - - - - -	- - - - - -	- - - - - -
253.64±0.70	33.94±0.14	
284.55±0.86	35.87	C13N2/C13R2

Table 3-1--continued

699A

Depth (mbsf)	Age (Ma)	Datum
321.28	38.16	FAD *Reticulofenestra oamaruensis*
330.70	38.40	FAD *Ismolithus recurvus*
350.56	41.00	LAD *Chiasmolithus oamaruensis*

703A

Depth (mbsf)	Age (Ma)	Datum
22.72±0.37	19.35	C5ER/C6N
31.35±0.10	20.45	C6N/C6R
32.59±0.05	20.88	C6R/C6AN
36.54±0.09	21.16	C6AN.3
39.14±0.10	21.38	C6AN.6
39.44±0.30	21.40	
~~	~~~~~	~~~~~~~~~~
39.44±0.30	23.22	
40.00±0.10	23.27	C6BN/C6CN
41.89±0.05	23.44	C6CN.2
44.54±0.40	23.55	C6CN.3
45.99±0.25	23.79	C6CN.6

Table 3-1--continued

703A		
Depth (mbsf)	Age (Ma)	Datum
52.95±0.55	24.03	
52.95±0.55	25.79±0.10	
56.00±0.04	25.97	C7N/C7R
57.25±0.05	26.38	C7R/C7AN
57.40	26.56	C7AN/C7AR
58.00±0.05	26.86	C7AR/C8N
63.40±0.10	27.74	C8N/C8R
64.00	28.15	C8R/C9N
65.89±0.05	29.21	C9N/C9R
67.81±1.49	29.47	
67.81±1.49	30.21±0.31	
78.34±0.10	31.23	C10R/C11N
79.35±0.10	31.58	C11N.4
80.30±0.15	31.64	C11N.5
86.02±1.02	32.06	11
90.99±1.35	32.46	top C12
95.74±0.40	32.90	C11R/C12N
107.52	34.80	LAD Ismolithus recurvus
109.70	35.15±0.01	

Table 3-1--continued

703A

Depth (mbsf)	Age (Ma)	Datum
109.70	37.10±0.05	
130.70±0.05	38.10	16
146.50±0.55	38.79	C16N.5
154.95±0.10	39.24	C16N/C16R
173.71	41.00	FAD *Chiasmolithus oamaruensis*

252.94 mbsf. There is a 1.4 m uncertainty in the position of this unconformity, below which the sedimentation rate was 16.0 m/m.y., but even when this uncertainty and the uncertainty in the age of the base of the unconformity (±0.14 m.y.) are taken into account, the range of possible sedimentation rates is only 14.6 to 17.7 m/m.y. Age assignments of samples will not vary by more than 0.28 m.y. (the total uncertainty in the age of the base of the unconformity). In Site 703, a hiatus is present across the Eocene/Oligocene boundary between 37.1 and 35.0 Ma. The lower age of this unconformity is based on a combination of biostratigraphic and magnetostratigraphic factors, combined with an age extrapolated from sedimentation rates. The younger age is extrapolated from the sedimentation rate defined by the LAD of I. recurvus and the C12N/C12R paleomagnetic boundary. Another unconformity occurs between 30.4 and 29.5 Ma, for which the lower boundary is defined by another extrapolation between the C12N/C11R and C11N/C10R boundaries. The third unconformity, between 25.8 and 24.0 Ma, is defined at the base by an abundance of Rocella vigilans and at the top by a combination of biostratigraphic and magnetostratigraphic datums. The last unconformity, between 23.2 and 21.4 Ma, is defined by extrapolation of sedimentation rates based on paleomagnetic datums.

The age models of Sites 699 and 703 were based on a different set of biostratigraphic datums than Sites 689 and 690. The planktonic foraminiferal faunas of the Leg 113 sites are different from that of the Leg 114 sites, resulting in different biostratigraphic zonations [Stott and Kennett, 1990]. Calcareous nannofossil biostratigraphy [Wei and Wise, 1990] was primarily used to guide the magnetostratigraphy of the Leg 113 sites [Spieß, 1990]. Several of the reliable markers used by Wei [1991, 1992] are present in both sets of sites, suggesting to us that mis-correlations, if any, between these sites are small.

Subsidence Models

Paleodepths of the sites were calculated using the thermal subsidence model of Parsons and Sclater [1977]. Paleodepths were calculated with isostatic corrections made using sediment densities presented in the site reports [Barker, Kennett et al., 1988a; Ciesielski, Kristofferson et al., 1988]. Hayes [1988] recently recalculated subsidence constants for the South Atlantic, and found that different segments and sides of the South Atlantic mid-ocean ridge subsided at different rates. Subsidence constants were taken from Hayes [1988] if applicable; otherwise an average value of 300 was used [Hayes, 1988; Table 3-2). A computer program was written to isostatically correct for sediment loading, and oceanic crustal subsidence was calculated with a crossover age of 30 Ma separating "young" and "old" crust (as defined by the differing styles of subsidence).

Average wet bulk density between each successive isotopic measurement was multiplied by the depth difference

TABLE 3-2

Parameter List for Subsidence Calculations.

Site	Crustal Age (Ma) (Ma)	Present Depth (m)	Total Sediment Thickness (mbsf)	Subsidence Constant (m/m.y.$^{0.5}$)	Depth at Zero Age (m)
689	84.0[a]	2080	320	300[f]	-495
690	84.0[a]	2914	332[d]	300[f]	325
699	100[b]	3705.5	740[e]	380[g]	775
703	60[c]	1796.1	364	290h	-310

Unless otherwise noted, all water depths and sediment thicknesses are from site reports in Initial Reports [Kennett et al., 1988a; Ciesielski, Kristoffersen et al., 1988]. Sources: (a) Kennett and Stott [1990] and Barker, Kennett et al. [1988b] note that the oldest sediments correlate with the Campanian/Maestrichtian boundary (74.5 Ma). However, Shipboard Scientific Party [1988a] suggest a Cenomanian age for basement, while Shipboard Scientific Party [1988b] suggest 10 Ma of subaerial exposure after formation at Site 689. I therefore use an age of 84 Ma for the formation of basement at this site. (b) Assumed to be the same age as nearby Site 700, dated by Kristoffersen and LaBrecque [1991]. (c) Raymond et al. [1991]. (d) Hole 690 (297.3 mbsf maximum penetration) was abandoned an estimated 25-45 m above basement (Shipboard Scientific Party, 1988b]. I use 35 m as an average value,resulting in a total sediment load of 332 m. (e) An estimated 700 m of seismically defined sediment overlies an approximately 80 m thick basal unit (Shipboard Scientific Party, 1988c]. Basement is not well defined and is assumed to be midway within the basal unit. (f) Revised average value Hayes [1988] for the entire ocean was used for these sites because revised values for the Southern Ocean were not available. (g) Western basin of the southern-Southern Atlantic (Zone C of Hayes [1988]). (h) Eastern basin of the southern-Southern Atlantic (Zone C of Hayes [1988]).

between each measurement and summed to get the isostatic loading, and the isostatic corrections were made assuming a mantle density of 3.30 g/cm^3 and seawater density of 1.03 g/cm^3. If drilling did not reach basement, the depth-to-basement was taken from seismic data in the site reports: 332 mbsf for Site 689 [Barker, Kennett et al., 1988a,b] and approximately 740 mbsf for Site 699 [Ciesielski, Kristofferson et al., 1988]. Densities of these deeper sediments were assumed to be equal to the average of the lowermost few density measurements. All sites were assumed to have subsided according to the Parsons and Sclater [1977] model. The only difference was that the starting or maximum depths were different based on the present depth, and calculations were based on the parameters presented in Table 3-2. Subsidence curves are plotted in Figure 3-2.

Isotopic Methods

Well-preserved specimens of Cibicidoides were picked from the washed >150μm fraction of samples from Holes 699A and 703A and prepared using standard methods (detailed instructions may be found in Appendix B4). Organic carbon was removed from the picked specimens by either crushing and roasting at 375°C for 1 hour (part of 703A samples) or by reaction in 12.5% H_2O_2 for 1/2 to 1 hr (part of 703A and all 699A samples). No significant difference was found in results from these two methods of pretreatment. Specimens were ultrasonically cleaned in methanol for 10-20 seconds to

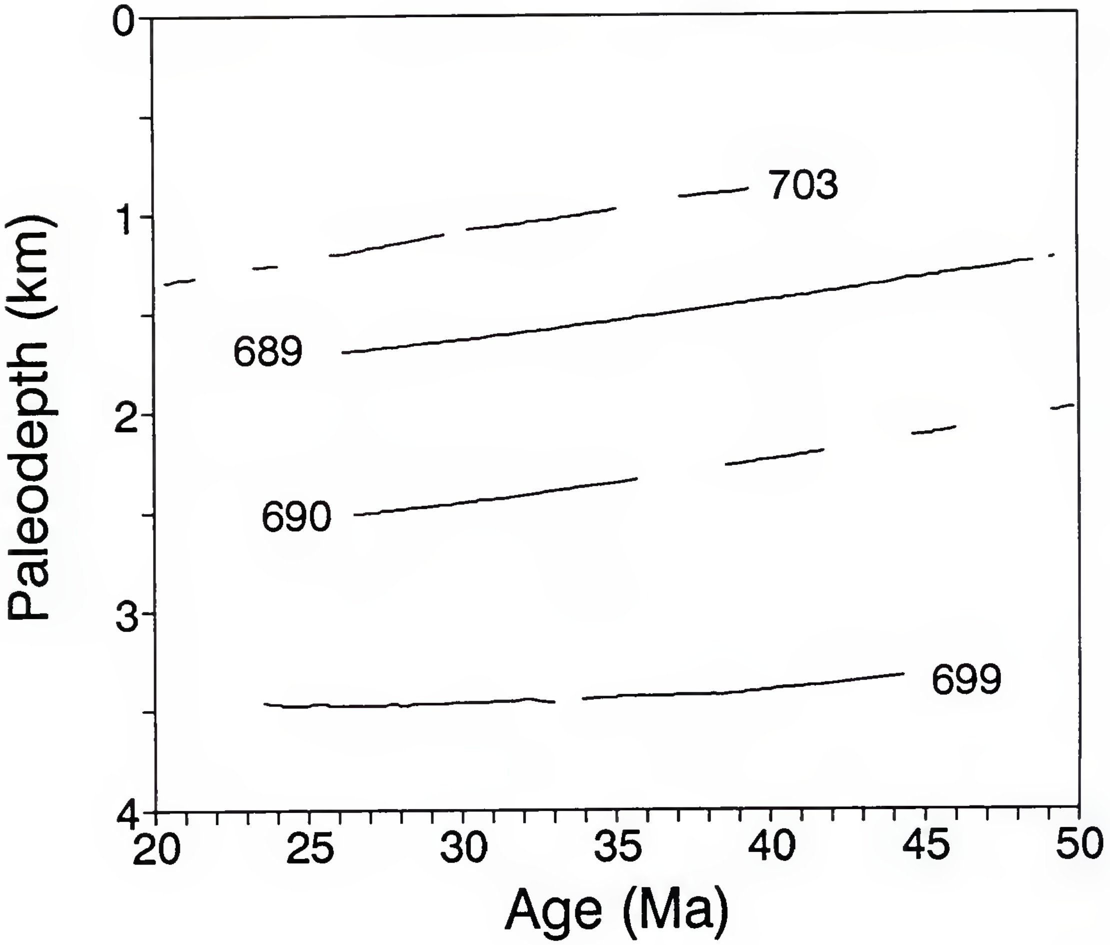

Figure 3-2: Subsidence curves for the sites used in this study, calculated by the method of Parsons and Sclater (1977).

remove adhering debris, and examined microscopically to ensure the effectiveness of the treatment.

Specimens were reacted in 100% orthophosphoric acid at either 70 or 90°C to release CO_2 in an automated preparation system. The released CO_2 was analyzed in a VG Prism triple collector mass spectrometer. Isotopic standards were Carrara Marble and NBS-19, corrected to Pee Dee Belemnite [Hodell et al., 1989]. Precision (1 standard deviation) was $\pm 0.13^{o}/oo$ and $\pm 0.05^{o}/oo$ for oxygen and carbon isotopes, respectively, for the Carrara Marble standard and $\pm 0.09^{o}/oo$ and $\pm 0.04^{o}/oo$, respectively, for the NBS-19 standard. A total of 14% of all sample analyses were replicated. The mean difference between replicate pairs (or standard deviation when more than 2 replicates were made) was $0.16^{o}/oo$ for $\delta^{18}O$ and $0.12^{o}/oo$ for $\delta^{13}C$.

This study includes isotopic results from ODP Sites 689 and 690, produced by Kennett and Stott [1990], and Sites 699 and 703 from this study. Interlaboratory calibration, especially with reference to possible offsets, is therefore a concern. To reduce this possibility, both data sets have been calibrated to PDB by using the same intermediate standards (NBS-19 and NBS-20) or have been intercalibrated with that standard via Carrara Marble. Repeated analyses of NBS-19 and NBS-20 in our laboratory are not significantly different from the results of Kennett and Stott [1990] or the standard values of Coplen et al. [1983] (Table 3-3).

TABLE 3-3

Comparison of isotopic analyses of NBS-19 and NBS-20

NBS-19	$\delta^{13}C$	$\delta^{18}O$
Coplen et al. (1983) standard value	1.92	-2.19
Hodell et al., 1989	1.90	-2.19
Kennett and Stott, 1990	1.92	-2.19

NBS-20		
Coplen et al. (1983) standard value	-1.06	-4.14
Hodell et al., 1989	-1.10	-4.19
Kennett and Stott, 1990	-1.06	-4.14

Values from Hodell et al., 1989 are those used for this study, and the values for Kennett and Stott, 1990 were provided by J. P. Kennett (1990, personal communication).

Results

Subsidence Curves

Table 3-4 presents a synopsis of paleodepths at 26, 30, 35, and 40 Ma for the 5 sites. The four ODP sites show non-overlapping paleodepths (Figure 3-2). Note that the minimum separation between any two of these sites is 495 m (Sites 689 and 703 at 26 Ma), so that even if a total error of as much as 495 m is present in any pair of the paleodepth calculations, the relative depths of Sites 689, 690, 699, and 703 will remain the same.

The Maud Rise, on which Sites 689 and 690 are located, is an aseismic ridge, making assumptions of normal oceanic subsidence [Parsons and Sclater, 1977] an oversimplification [Thomas, 1989]. However, as noted above, even errors in depth estimates of more than a half kilometer will not change the ordination of the ODP sites. In addition, these estimates are comparable to estimates derived by other methods [Thomas, 1989, 1990, 1992, written comm. 1991].

Oxygen Isotopes

Site 703

The isotopic record of 162 samples from Hole 703A extends from 39.6 to 20.4 Ma (159.13-30.72 mbsf) (Appendix A3, Figure 3-3). The average sampling interval is 0.79 m (80 ky, excluding unconformities). The upper Eocene portion of the $\delta^{18}O$ record averages ~1°/oo. The earliest Oligocene

TABLE 3-4

Paleodepths of Sites 689, 690, 699, and 703

Site	26 Ma	30 Ma	35 Ma	40 Ma
703	1206	1093	981	865
689	1701	1638	1543	1438
690	2518	2455	2356	2240
699	3480	3466	3431	3401

Depths at selected times, based on subsidence curves calculated using parameters in Tables 3-1 and 3-2.

Figure 3-3: Oxygen and carbon isotopic records from ODP Sites 699 and 703, plotted against age. Gaps in records indicate positions of unconformities.

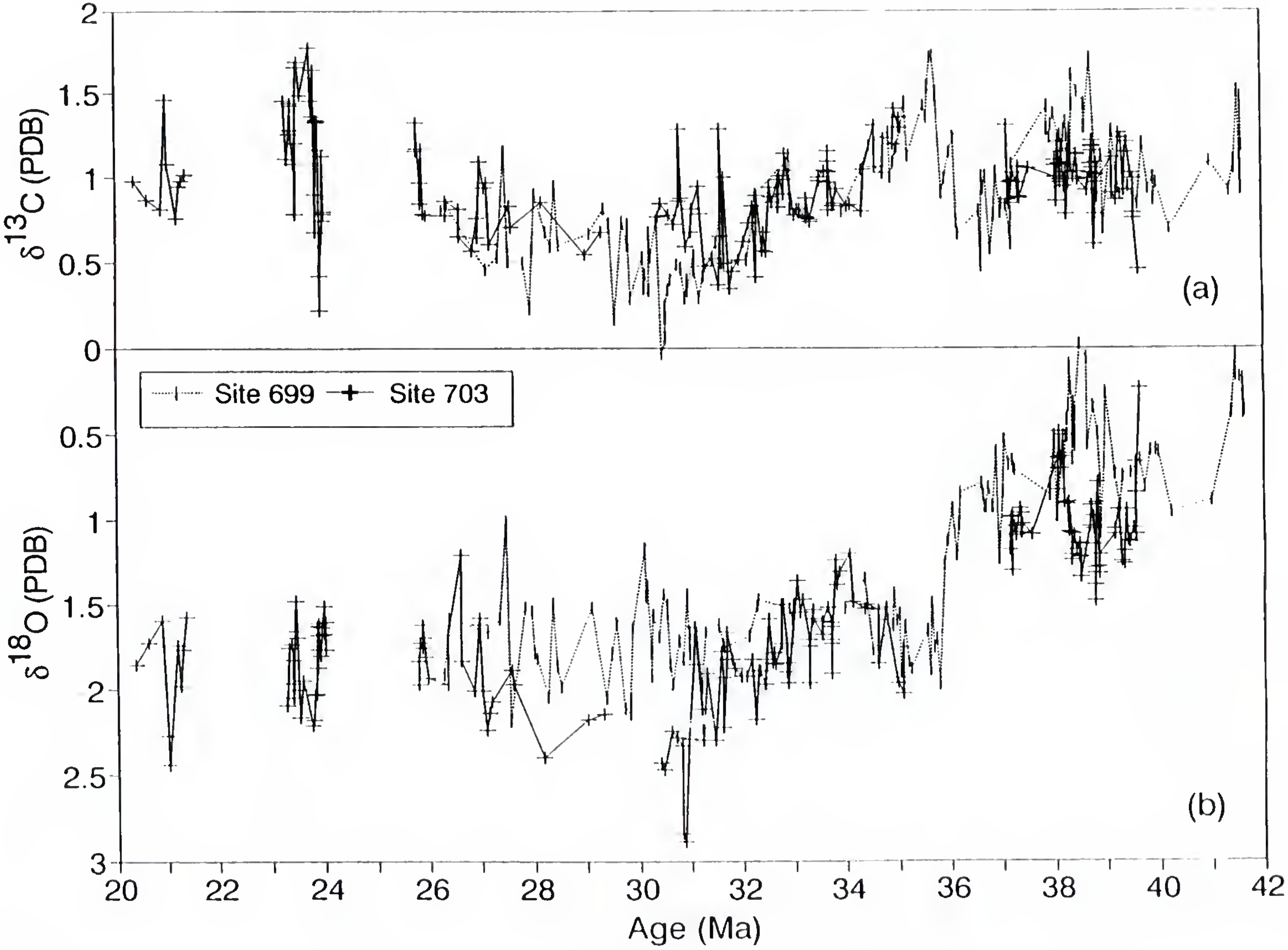
2
1.5
1
0.5
0
$\delta^{13}C$ (PDB)
(a)
Site 699
Site 703
0.5
1
1.5
2
2.5
3
$\delta^{18}O$ (PDB)
(b)
20
22
24
26
28
30
32
34
36
38
40
42
Age (Ma)

oxygen isotope shift is ~0.5^{o}/oo, smaller than the usual 1.0^{o}/oo seen in most areas of the deep sea. After the earliest Oligocene oxygen isotope increase, which occurs within the unconformity present between 37.10 and 35.2 Ma (109.30 to 109.85 mbsf), $\delta^{18}O$ values decreased from near 2^{o}/oo to about 1.6^{o}/oo until 33.0 Ma (96 mbsf), an increase of 0.6^{o}/oo over Eocene values.

Near 32 Ma, $\delta^{18}O$ values began to increase, reaching peak values of over 2.8^{o}/oo from 30.8 to 30.9 Ma. A decrease to 2.2-2.5^{o}/oo follows to the unconformity at 67.81 mbsf (30.2 Ma). When sedimentation resumed (at 29.3 Ma), $\delta^{18}O$ values generally decreased from a maximum of 2.4^{o}/oo near 28 Ma to 1.7-1.8^{o}/oo between 27.0 and 25.8 Ma (59.0-52.95 mbsf), after which another unconformity occurred. During the short period of sedimentation between this unconformity and the next at 39.44 mbsf, sediments are present with ages ranging from 24.0 to 23.2 Ma. In this interval, $\delta^{18}O$ ratios increased from initial values of 1.7^{o}/oo to near 2.0^{o}/oo from 23.8 to 23.5 Ma, and then decreased back to 1.6-1.8^{o}/oo. Above the unconformity at 39.44 mbsf, this record extends from 21.4 Ma, when sedimentation resumed, to 20.4 Ma (30.72 mbsf). Oxygen isotope ratios average about 1.9^{o}/oo in this interval, including one value of 2.44^{o}/oo at 21 Ma.

Site 699

The Hole 699A record (Appendix A4, Figure 3-3) begins at 41.6 Ma (356.35 mbsf) and continues to 26.3 Ma (134.71 mbsf), with a total of 130 samples and an average sampling interval of 111 ky (1.72 m). The record ends at 134.71 mbsf because not enough carbonate is present above this level for isotopic analysis. Initial $\delta^{18}O$ values are lower than those of equivalent age in Hole 703A despite the greater paleodepth of Hole 699A. Beginning at 41.6 Ma, $\delta^{18}O$ values average 0.2 to 0.3^{o}/oo, increasing to 0.7 to 0.8^{o}/oo between 39 to 36 Ma (288 mbsf). The earliest Oligocene oxygen isotope shift occurs between 35.87 and 35.77 Ma (284.60 and 283.02 mbsf). Additional unpublished oxygen isotopic data from analysis of Stilostomella aculeata reveal that the shift is further constrained between 35.87 and 35.82 Ma (284.60 and 283.79 mbsf), suggesting that the change occurs on a time scale of 50 ky or less. The rapidity of the shift is in agreement with data from other sites [Kennett and Shackleton, 1976; Oberhänsli et al., 1984, Zachos et al., 1992a, Barrera and Huber, 1993]. At Site 699, the oxygen isotopic shift is larger than in Site 703, with a magnitude of about 1^{o}/oo, comparable to most benthic oxygen isotopic signals found in other regions (North Atlantic - Miller and Fairbanks, 1983; South Atlantic - Poore and Matthews, 1984, Corliss et al., 1984, Oberhänsli and Toumarkine, 1985, Keigwin and Corliss, 1986, Miller et al., 1987, 1988;

Pacific - Keigwin, 1980, Corliss et al., 1984, Miller and Thomas, 1985; Indian Ocean - Corliss et al., 1984, Zachos et al., 1992a,b, Barrera and Huber, 1993].

Initial post-shift $\delta^{18}O$ values average $1.76^{o}/oo$, thereafter averaging mostly between 1.55 and $1.81^{o}/oo$ to 26.3 Ma. Greater values of $\delta^{18}O$ are generally found at 36-35 Ma and 31-28 Ma. Values commonly exceed $1.8^{o}/oo$, suggesting glacial conditions [Miller and Fairbanks, 1983; Miller et al., 1985b, 1987]. Oxygen isotopic ratios of 2.0-$2.15^{o}/oo$ are found especially between 29.85-29.7 Ma. High frequency variability is seen in the Site 699 oxygen isotopic record, with values varying by $\pm 0.5^{o}/oo$. However, due to the generally low sampling interval, it is difficult to interpret this variability. The oxygen isotopic values in Site 699 are generally comparable to or lower than those of Site 703, despite the considerably greater paleodepth of Site 699. In addition, the average values from Site 699 are lower than those found in either Sites 689 or 690.

Carbon Isotopes

Site 703

Initial $\delta^{13}C$ values average $\sim 1^{o}/oo$ from the base of the record to the upper Eocene-lower Oligocene unconformity at 109.30 to 109.85 mbsf. Above the unconformity, $\delta^{13}C$ values increase to as much as $1.41^{o}/oo$ for a period of about 680 ky (4.2 m). After this interval, $\delta^{13}C$ values decrease first to between 0.8 and 0.9^{o}/oo by ~34 Ma, to a minimum of ~0.5^{o}/oo at 31.4 Ma, and then increase again to ~0.8^{o}/oo at the unconformity at 30.2 Ma.

During the unconformity-bounded interval between 29.5 and 25.8 Ma (67.81-52.95 mbsf), $\delta^{13}C$ values remained at about 0.7-0.8^{o}/oo until increasing to over 1.1^{o}/oo just before the upper unconformity. After sedimentation resumed at 24.0 Ma, carbon isotopic ratios decreased rapidly from values near 0.9^{o}/oo to as low as 0.22^{o}/oo by 24.0 Ma, before increasing again to maximum values of between 1.33 and 1.77^{o}/oo from 23.9 to 23.5 Ma. Carbon isotopic ratios decreased again to between 0.7 and 1.45^{o}/oo just before the unconformity. The record above the unconformity from 21.4 to 20.4 Ma averages ~1^{o}/oo, with one short interval of high $\delta^{13}C$ associated with high $\delta^{18}O$ values at 21 Ma.

Site 699

Results for Site 699 are generally similar to those of Site 703. From 41.6 to 39.2 Ma (356.35 to 337.1 mbsf), $\delta^{13}C$ averaged ~1^{o}/oo. A sudden increase, not seen in Site 703, began at this point and continued until 38.7 Ma (333 mbsf) to values as high as 1.7^{o}/oo. Afterwards a decrease to preceding values occurred, reaching values of ~0.8 to 1.0^{o}/oo by 37.2 Ma (306.1 mbsf). Coeval with the earliest Oligocene $\delta^{18}O$ increase beginning at about 35.8 Ma (284 mbsf), another short-term increase, similar to that seen in Site 703, occurred with $\delta^{13}C$ increasing to between

$1.49^{o}/oo$ and $1.77^{o}/oo$ until 35.5 Ma (279 mbsf). Carbon isotopic ratios average $1.0-1.2^{o}/oo$ until the hiatus at 33.9 - 33.0 Ma (253.64 mbsf). With the onset of renewed sedimentation at 33 Ma (253.64 mbsf), $\delta^{13}C$ values began to decrease from about $1^{o}/oo$ to a brief minimum of $0^{o}/oo$ at about 30.5 Ma. Values averaged near 0.5 to $1.0^{o}/oo$ thereafter, with high frequency variability of about $0.5^{o}/oo$.

Discussion

Comparison of the two oxygen isotopic records (Figure 3-3) reveals that during most of the time from 26 to 42 Ma (the time during which overlap occurred between the Site 689, 690, 699 and 703 records) an inversion in the $\delta^{18}O$ gradient was present, with lighter $\delta^{18}O$ values deeper in the water column. This configuration is similar to that reported by Kennett and Stott [1990]. Oxygen (Figure 3-4a) and carbon (Figure 3-4b) isotopic records of sites 689, 690, 699, and 703 plotted together reveal that strong $\delta^{18}O$ gradients were present between the sites during most of this interval, but there was little difference between the $\delta^{13}C$ signals. The four $\delta^{18}O$ (Figure 3-5a) and $\delta^{13}C$ (Figure 3-5b) data sets (uncorrected Cibicidoides) as a function of paleodepth and time have been contoured, to better observe the changes taking place during this interval. I used weighted 1 m.y. averages of each of the 4 isotopic data sets to decrease effects of uncertain dating, high frequency

Figure 3-4: Isotopic records from ODP Sites 689, 690, 699, and 703 for the time period 26-42 Ma. a: $\delta^{18}O$. b: $\delta^{13}C$.

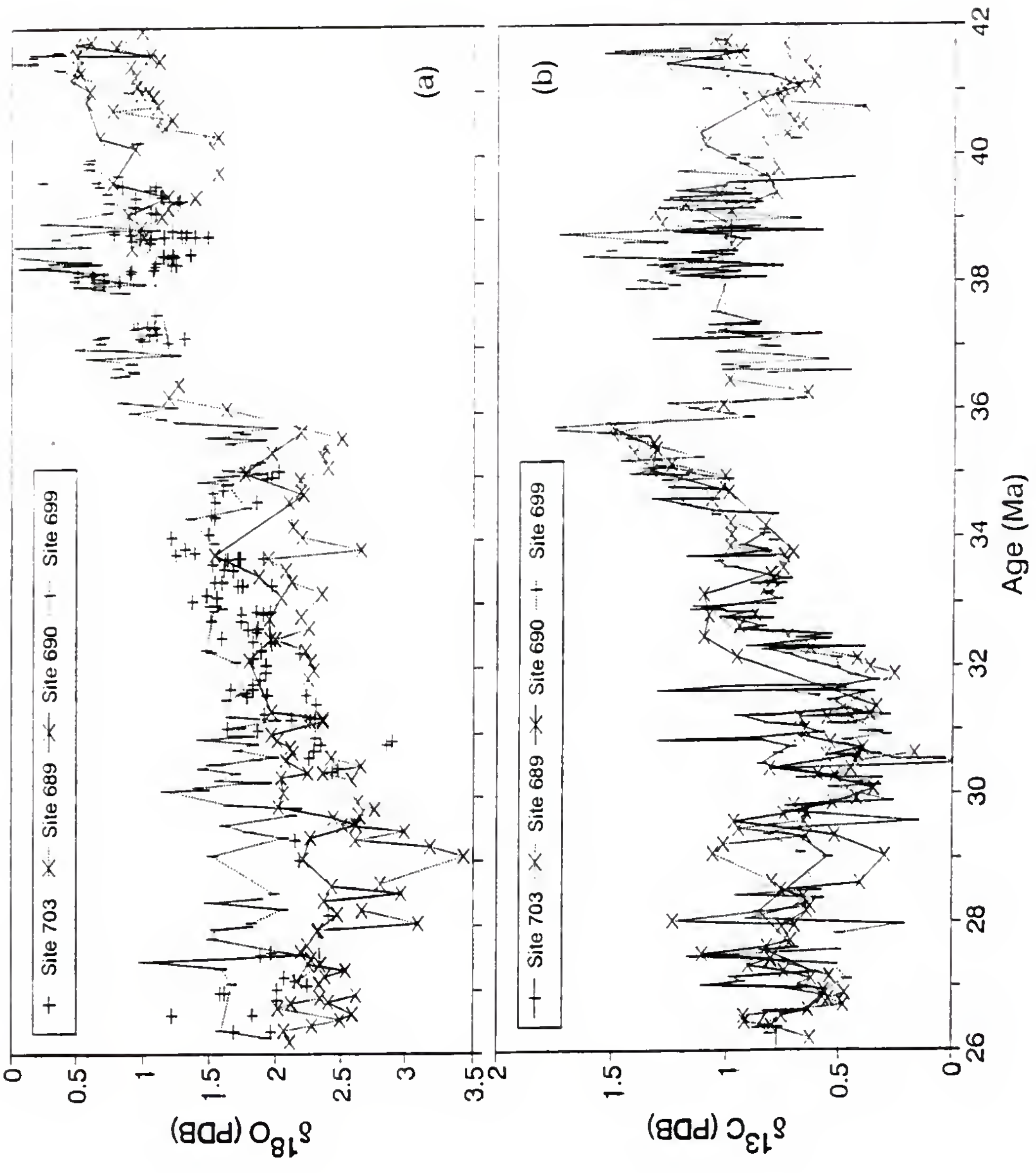
(a)
(b)
Site 703
Site 689
Site 690
Site 699
δ18O (PDB)
δ13C (PDB)
0
0.5
1
1.5
2
2.5
3
3.5
2
1.5
1
0.5
0
Age (Ma)
26
28
30
32
34
36
38
40
42

Figure 3-5: Isotopic data plotted against age and paleodepth for ODP Sites 689, 690, 699, and 703, contoured on the basis of the ODP sites. a: $\delta^{18}O$ - Note the near-permanent $\delta^{18}O$ minimum near the paleodepth of Site 689, indicating a temperature minimum. Oxygen isotopic ratios decrease downward to maximum paleodepths, indicating the presence of a warmer, more saline deep water mass. b: $\delta^{13}C$ - Note the relative lack of vertical gradients at all times, and the enrichment in $\delta^{13}C$ over the 36-35 Ma interval.

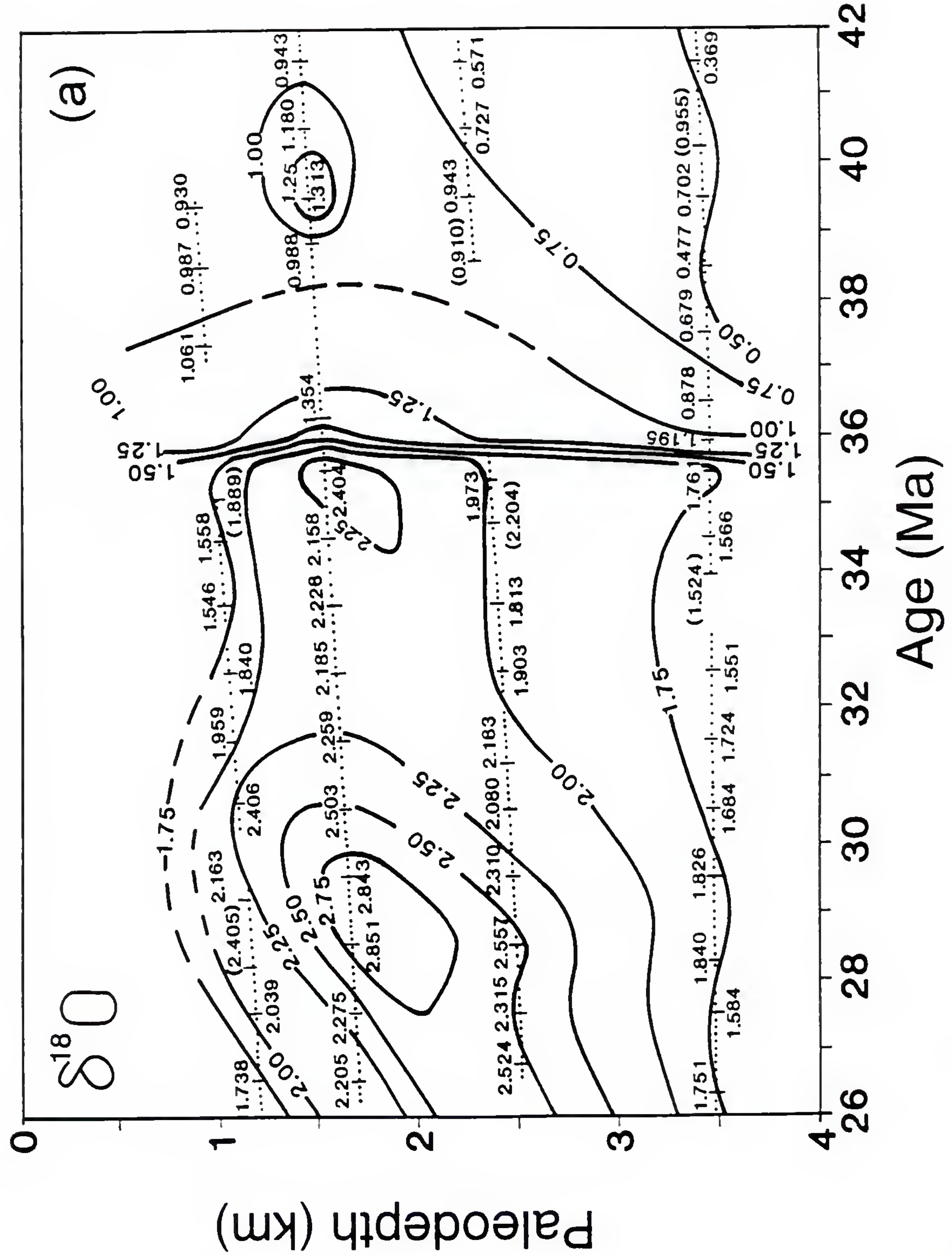
δ18O
(a)
Age (Ma)
Paleodepth (km)
26
28
30
32
34
36
38
40
42
0
1
2
3
4
1.75
2.00
2.25
2.50
2.75
1.50
1.25
1.00
0.75
0.50
1.738
2.039
(2.405)
2.163
1.959
1.840
1.546
1.558
(1.889)
2.406
2.205
2.275
2.851
2.843
2.503
2.259
2.185
2.228
2.158
2.404
2.524
2.315
2.557
2.310
2.080
2.183
1.903
1.813
(2.204)
1.973
1.751
1.584
1.840
1.826
1.684
1.724
1.551
(1.524)
1.566
1.76
1.195
0.878
0.679
0.477
0.702
(0.955)
0.369
1.354
1.061
0.987
0.930
0.988
1.313
1.180
0.943
(0.910)
0.943
0.727
0.571

Figure 3-5--continued

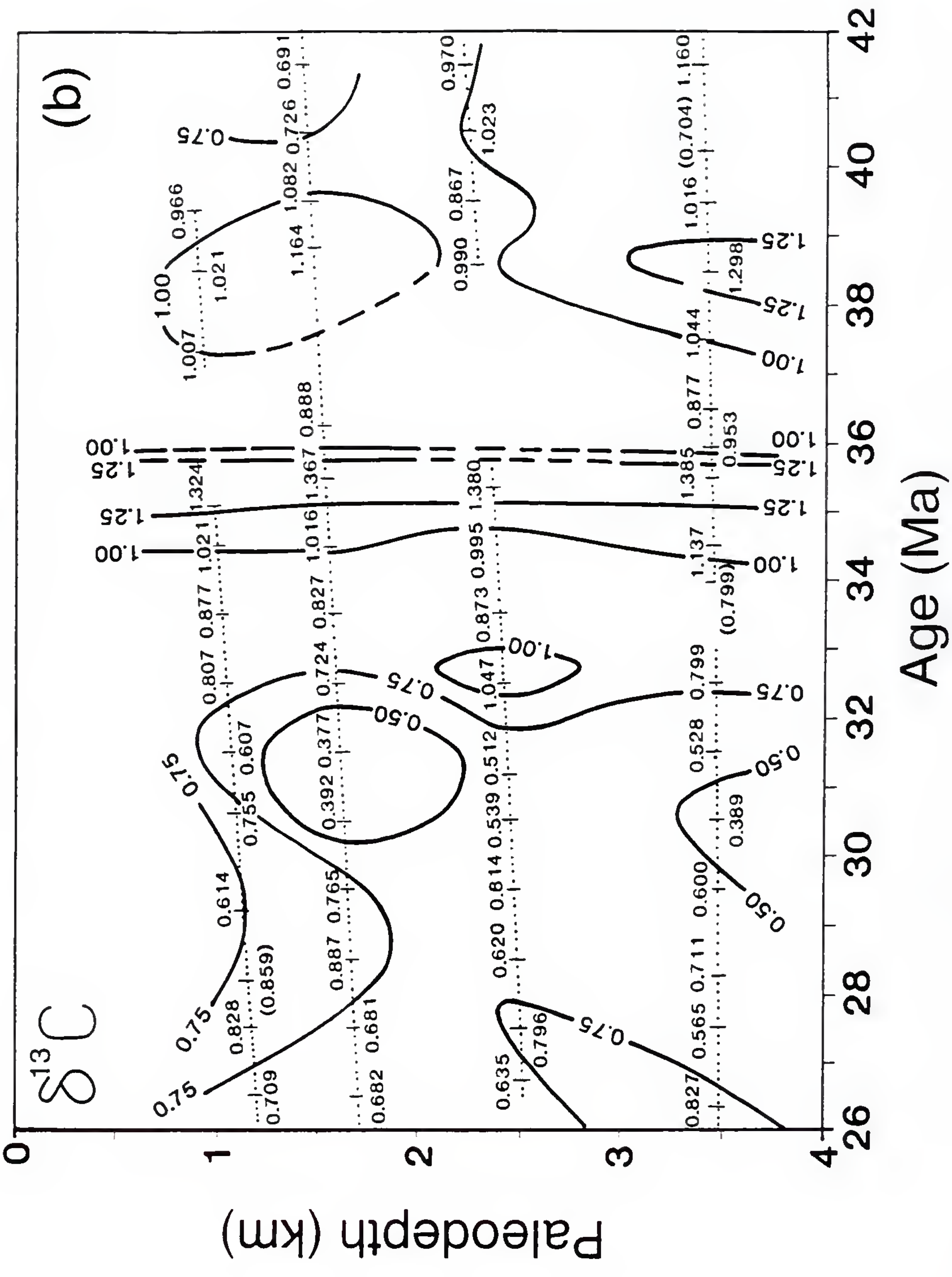

variability, and noise in the isotopic signal. In calculating weighted averages, replicate analyses were first averaged, then data in 100 ky intervals were averaged, and finally the 100 ky values were combined into 1 m.y. averages. The only part of the data not treated in this way were the data on either side of the earliest Oligocene oxygen isotopic shift in Site 699. Data on opposite sides of the shift were averaged separately. The 1 m.y. averages were weighted in this way in order to eliminate bias based on unequal sample distributions within each 1 m.y. interval. This also has the unfortunate effect of reducing the amplitude of some of the maxima and minima when the duration of the extreme values is substantially less than 1 m.y. For example, peak $\delta^{13}C$ values of over 1.7 $^{o}/oo$ at ~35.6 Ma in Site 699 are not apparent in the contoured data.

Beginning at 42 Ma (before the Site 703 record begins), an oxygen isotopic gradient of about 0.6$^{o}/oo$ existed between Site 689 (1.4 km paleodepth, 0.94$^{o}/oo$) and Site 699 (3.4 km paleodepth, 0.37$^{o}/oo$). Except for one measurement from Site 699A at 40.24 Ma, this gradient is maintained at 0.5-0.6$^{o}/oo$ from 42 to 31 Ma. From 31 to 28 Ma, the gradient between Sites 689 and 699 strengthened to between 0.8 and 1.0$^{o}/oo$. At this time, the core of the high $\delta^{18}O$ values, initially always present at Site 689 (1.3-1.6 km paleodepth) seems to have increased in depth, to about 2.5 km, with the core of greater $\delta^{18}O$ (cooler temperatures) near the depth of Site

690. By 26 Ma, the magnitude of the gradient also weakened slightly to 0.7-0.8^{o}/oo.

The gradient between high $\delta^{18}O$ values at Site 689 and lower values at the overlying Site 703 was 0.4^{o}/oo at the beginning of this overlapping sequence, decreasing to 0^{o}/oo from 40 to 38 Ma. Data are not present for both sites from 38 to 35 Ma, but by 35 Ma, a gradient was well established, with magnitudes of 0.6 to 0.7^{o}/oo until 33 Ma, decreasing to 0.1^{o}/oo by 30 Ma. From 30 to 29 Ma, the gradient increased to 0.7^{o}/oo. Following only a single data point for the 29-28 Ma interval in Site 703 and the deepening of the colder core, the magnitude of the gradient between Sites 703 and 690 increased from 0.3^{o}/oo to 0.8^{o}/oo again.

This pattern extends Kennett and Stott's [1990] identification of inverted oxygen isotope gradients to greater depths, suggesting the presence of a warmer water mass down from paleodepths of ~2100-2400 m to nearly 3500 m. However, alternative explanations for these gradients must first be addressed. I have identified three alternative possibilities.

First, the gradients could be artifacts of interlaboratory calibration errors, since the new results have generally (for a given age) lower $\delta^{18}O$ values than the results of Kennett and Stott [1990]. However, because of the intercalibration already discussed and because the gradients are generally larger than the uncertainty, I feel this cannot be the cause of the gradients.

Errors in dating could be a source of these gradients as well. One of the reasons for averaging 1 million-year increments was to help eliminate small errors in dating. Examination of the gradients shows that except near the earliest Oligocene oxygen isotope shift, even errors in dating of one million years would not change the character of the gradients. Near the earliest Oligocene, dating is well constrained by the position of the oxygen isotope shift, which has been shown to be synchronous world wide [Corliss et al., 1984, Poore and Matthews, 1984; Miller et al., 1985b; Oberänsli and Toumarkine, 1985; Corliss and Keigwin, 1986; Miller et al., 1988].

A third possible reason for these isotopic patterns is a latitudinal mixing effect. Water masses mix with overlying and underlying water masses during northward and southward transport in the Atlantic, changing composition and temperature. It is possible that the reason for the lower $\delta^{18}O$ ratios found in Sites 699 and 703, is that they contain a larger northerly component than Sites 689 and 690 simply because they are located 15° to the north. To evaluate this, I constructed equilibrium oxygen isotopic profiles using modern hydrographic data from near the site locations [Bainbridge, 1981a, 1981b, Ostlund et al., 1987]. I calculated equilibrium $\delta^{18}O$ values using the temperatures and oceanic $\delta^{18}O$ values at the modern location and paleodepths of the 4 sites at 4 different times (39.5, 35.5, 30.5, and 26.5 Ma), corrected to the Cibicidoides offset of

$-1.02^{o}/oo$ [Graham et al., 1981]. I use a correction factor of $-1.02^{o}/oo$ rather than the more commonly used $-0.64^{o}/oo$ because, except for Shackleton and Opdyke [1973], most investigations into taxa-specific fractionation of oxygen isotopes have found an offset of about $-1^{o}/oo$ between the $\delta^{18}O$ of Cibicidoides and of equilibrium calcite [Duplessy et al., 1970, Belanger et al., 1981, Graham et al., 1981]. Figure 3-6 shows that indeed a latitudinal effect may be present. Equilibrium $\delta^{18}O$ values of Site 699, corrected to Cibicidoides, are seen to be up to about $0.25^{o}/oo$ lower than that found at the position and paleodepths of Site 689. This is primarily due to the warmer in-situ temperatures of Site 699 (1.0°C) than those at Site 689 (-0.3°C). However, isotopic gradients between these sites during the Late Eocene and early Oligocene are nearly always at least twice the $0.25^{o}/oo$ seen in the present day situation. In addition, while the calculated $\delta^{18}O$ values for the present-day show lower $\delta^{18}O$ in Site 703 than at Site 699 (as would be expected for a shallower site) the oxygen isotopic composition at Site 699 is lighter than at Site 703 during most of the 14 m.y. time period when the two records overlap. Another consideration is that low latitudinal thermal gradients in surface waters during the Eocene and Oligocene relative to today would reduce the total range of temperatures seen in the ocean [Keigwin and Corliss, 1986, Zachos et al., 1992a]. These factors lead us to believe that the gradients seen between the Maud Rise and Sites 703

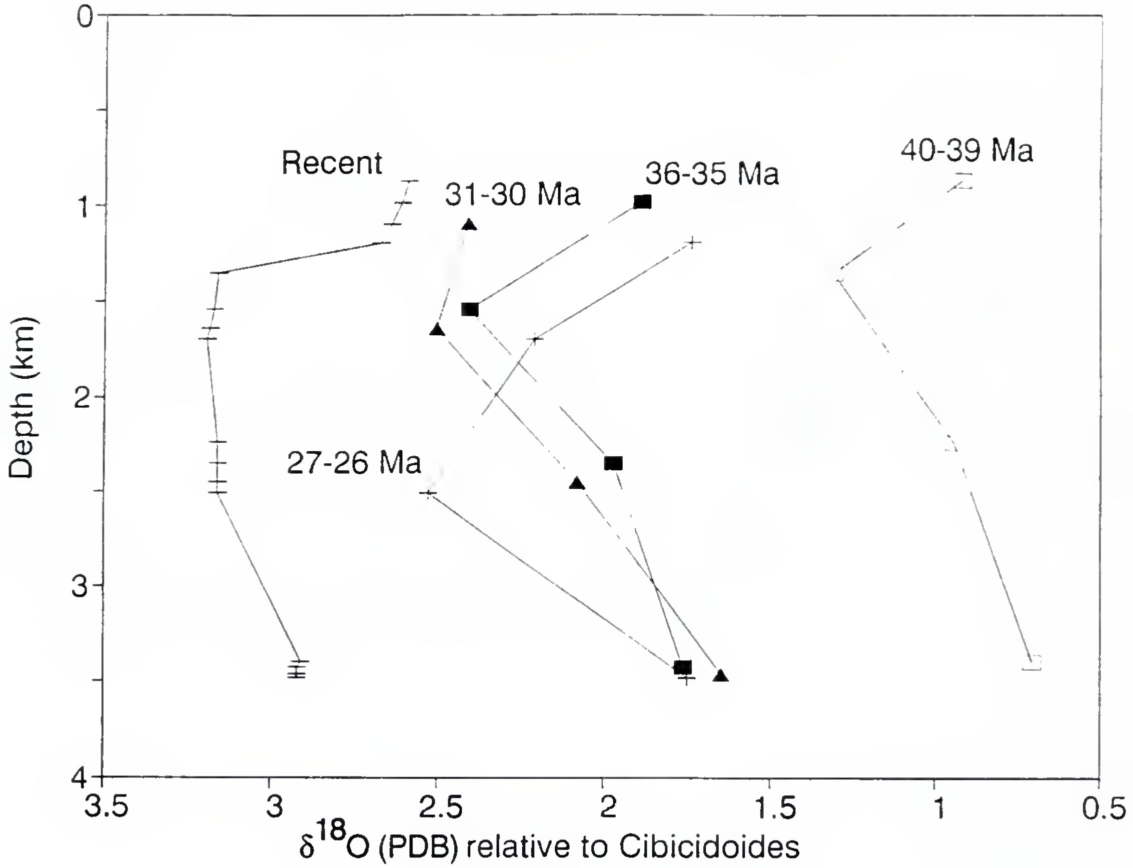

Figure 3-6: Vertical oxygen isotopic gradients from Cibicidoides for the present (calculated based on hydrographic data and an offset from equilibrium calcite of -1.02°/oo by Cibicidoides), and for the time periods 40-39 Ma, 36-35 Ma, 31-30 Ma and 27-26 Ma. Gradients are larger in the Paleogene sections than in Recent sections, indicating that any latitudinal mixing effect is not solely responsible for the gradients seen in the Paleogene sections.

and 699 are in fact real, although perhaps up to 0.25°/oo smaller than indicated in Figure 3-6. I conclude that this evidence supports a warmer, more highly saline water mass underlying a cooler, less saline water mass in the South Atlantic during most of the period from 42 to 26 Ma.

Circulation Patterns

Kennett and Stott [1990] suggested that the reason for the strengthened inversion present after the Eocene/Oligocene boundary is the onset of Antarctic Bottom Water (AABW) formation, and a "Proto-Oceanus" configuration. If this was the case, we would expect to see an eventual cooling of deep water and an increase in $\delta^{18}O$ somewhere deeper than Site 690. These data do not confirm or deny this. We find instead a continuous and permanent (at least to 26 Ma) $\delta^{18}O$ inversion from ~1500m to ~3400m paleodepth. I interpret the configuration to show, from 42-28 Ma, a core of cooler water centered near 1500 m (the paleodepth of Site 689) with temperatures increasing upward to Site 703 and downward from Site 689 through Site 690 and at least to the paleodepth of Site 699 (3400-3500 m). A mixing zone between the cooler water at Site 689 and the warmer water at Site 699 would have been present, but if a discrete boundary layer was present, it is not identifiable within the resolution of this study. At 28 Ma, there is a suggestion that this core of cooler water may have begun to deepen somewhat. If proto-AABW was present in the Oligocene, it must have been present at greater paleodepths than we find at Site 699 (3400-3500 m).

Examination of the carbon isotopic composition of foraminiferal calcite at these 4 sites may be useful in understanding deep circulation during this period. Today, substantial vertical and horizontal gradients exist in $\delta^{13}C$ in the Atlantic Ocean [Kroopnick, 1980]. This is a result of mixing of younger North Atlantic Deep Water with Antarctic Bottom Water. There is little effect of aging on NADW because the residence time of water in the Atlantic basin is short [Broecker, 1979]; thus, the relatively high $\delta^{13}C$ of NADW is a useful tracer throughout the Atlantic [Kroopnick, 1985; Oppo and Fairbanks, 1987; Charles and Fairbanks, 1992]. A vertical section of carbon isotopes (Figure 3-5b), constructed in the same way as Figure 3-5a, shows that almost no vertical gradient existed during most of the 16 m.y. time interval examined in this paper. Two possible reasons for this are that the deep southern ocean could have been well mixed during this time, or that there could indeed have been a singular source of deep water production. However, the presence of the oxygen isotope gradients renders both of these explanations unlikely. Previous studies have shown that during most of the late Eocene and Oligocene, there was little difference between carbon isotope records from different oceans, as well as small surface-to-deep carbon isotopic gradients [Miller and Fairbanks, 1985; Miller, 1992; Wright and Miller, 1993].

Although Miller [1992] and Wright and Miller [1993] suggested that this may be evidence that the Antarctic was the sole source of bottom water during this time, they also noted that the Oligocene ocean was oligotrophic, which may have led to low input of organic carbon from the photic zone. As a result, there would be little carbon isotopic evidence for aging of bottom water during this time period. There may also have been multiple sources of bottom water during this time [Zachos, personal comm.; Wright and Miller, 1993]. This would not allow significant ageing of any water mass and could be another reason for the lack of global $\delta^{13}C$ gradients in deep water.

Miller [1992] and Wright and Miller [1993] compared Oligocene to Miocene benthic foraminiferal $\delta^{13}C$ records from the North and South Atlantic, Southern, and equatorial Pacific Oceans, and noted an increase in north Atlantic $\delta^{13}C$ values from 35.5 to 34.5 Ma, above values at that time in other sites. Based on this $\delta^{13}C$ maximum and on seismic stratigraphic data [Miller and Fairbanks, 1983, 1985, Miller et al., 1985b, Miller, 1992], they inferred that a pulse of Northern Component water, similar to North Atlantic Deep Water (NADW) in origin, occurred near 35.5 to 34.5 Ma.

I suggest that it is possible that the $\delta^{13}C$ maximum at 35.5 to 34.5 Ma [Miller et al., 1985a; Miller, 1992] may instead be correlated more correctly to the ubiquitous 36-35 Ma $\delta^{13}C$ maximum which occurs just after the $\delta^{18}O$ shift at 35.8 Ma in records from the Atlantic, Pacific, Indian, and

Southern Oceans (Figure 3-7). This logic stems in part from a comparison of the two reasonably complete Oligocene North Atlantic isotopic records (DSDP Sites 558 and 563; Miller and Fairbanks, 1985]. Only one, Site 563, shows the early Oligocene carbon isotopic maximum. Although Miller et al. [1985a] suggest that Site 558 may be diagenetically altered within the lower Oligocene, diagenesis in fact tends to affect carbon isotopic records to a small degree due to the low concentration of dissolved non-carbonate derived carbon in pore water. Yet the $\delta^{13}C$ record from Site 558 does not exhibit the maximum seen at Site 563 [Miller and Fairbanks, 1985], despite the fact that Site 558 has a longer record, and despite the close proximity and similar depths [Bougault, Cande et al., 1985], suggesting that there may be a problem with dating of these records. It should be noted that, with the exception of the carbon isotope correlation I am suggesting, the bio- and magnetostratigraphy used by Miller et al. [1985] and Miller [1992] is internally consistent [Wright and Miller, 1993]. If these suggestions are correct, revisions of the bio- and magnetostratigraphy of Site 563 will be necessary.

My alternate interpretation results in the following observations. First, the $\delta^{18}O$ values from the Site 563 record are relatively low and generally comparable to values from Site 699. Secondly, the $\delta^{13}C$ maximum seen in Site 563 is larger than any other cited in this paper, with the single exception again of Site 699, indicating that Site 563

Figure 3-7: Carbon isotopic ratios for DSDP and ODP sites from the North Atlantic (Site 563; Miller and Fairbanks, 1985), intermediate Southern Ocean (Sites 689, 690, and 703; Kennett and Stott, 1990, this paper), deep Southern Ocean (Site 699; this paper), Indian Ocean (Site 748; Zachos et al., 1992a), and equatorial Pacific (Site 574; Miller and Thomas, 1985).

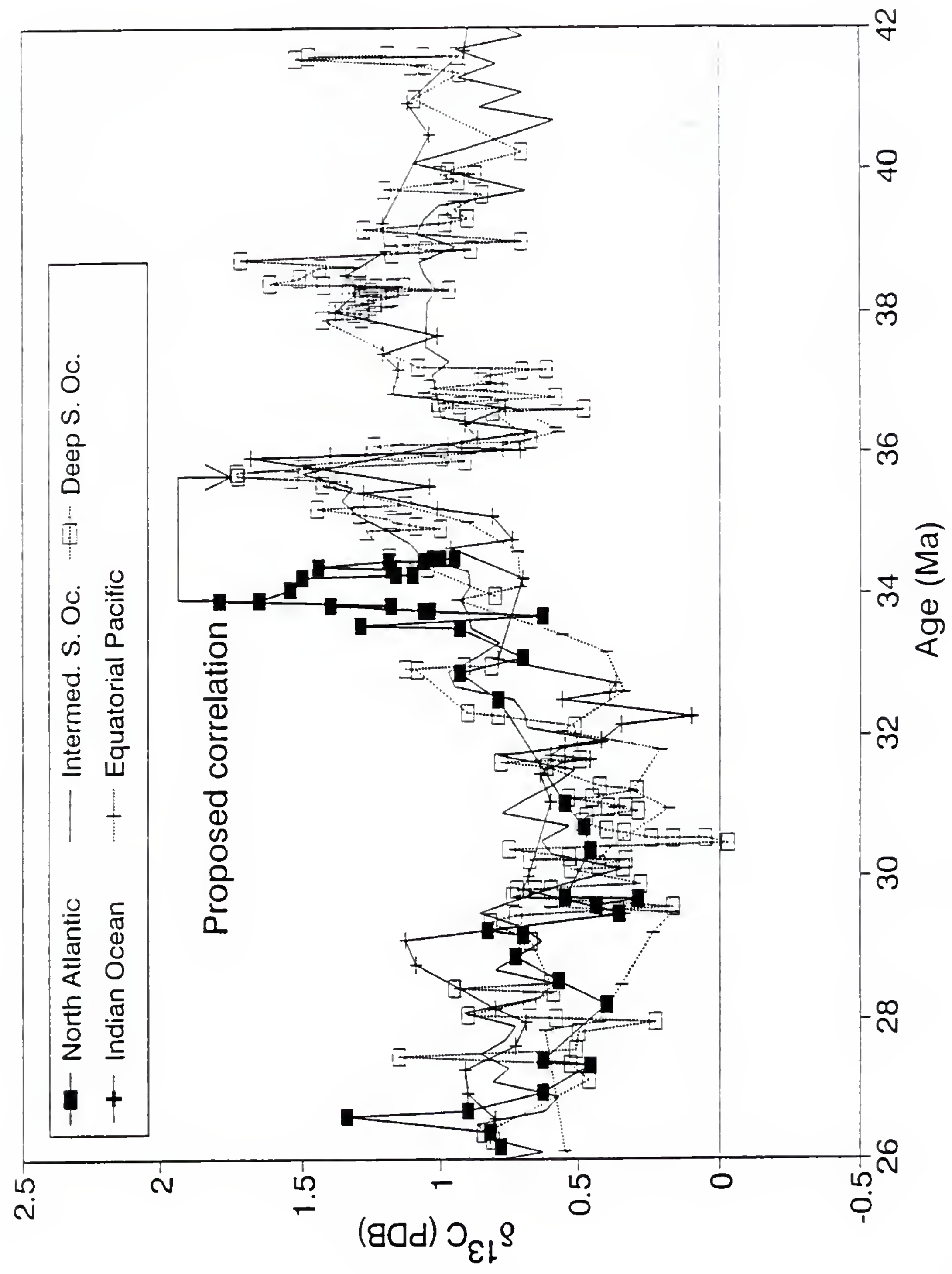
North Atlantic
Indian Ocean
Intermed. S. Oc.
Equatorial Pacific
Deep S. Oc.
Proposed correlation
δ13C (PDB)
Age (Ma)
2.5
2
1.5
1
0.5
0
-0.5
26
28
30
32
34
36
38
40
42

is closest to the source of deep water. This raises the possibility that the pulse of NCW suggested by Miller [1992] and Wright and Miller [1993] is in fact the source of WSDW suggested by this paper.

There is abundant stratigraphic evidence that bottom current speeds increased near the Eocene/Oligocene boundary. Unconformities near this time are common world-wide [Kennett et al., 1972; Moore and Heath, 1977; Moore et al., 1978; Miller et al., 1985a,b, 1987]. There are also unconformities at this time in two of the sections discussed in this study, Sites 690 and 703. The general increase in $\delta^{13}C$ at all depths in this area is also seen in other ocean basins [Miller and Fairbanks, 1985; Keigwin and Corliss, 1986; Miller and Thomas, 1986; Miller et al., 1988; Zachos et al., 1992a,b], but is not found in surface waters [Zachos et al., 1992a,b]. This suggests that there was a generalized increase in the rate of overturn in the deep sea, including bottom, deep, and intermediate water masses as well.

Magnetic anomaly patterns indicate that a connection between the Arctic Ocean and North Atlantic may have been opened at the time of the $\delta^{13}C$ maximum [Rowley and Lottes, 1988]. This, combined with extensive North Atlantic unconformities of this age [Miller et al., 1985a,b] indicates that the opening of the Arctic may have contributed to the increased rates of overturn of deep water.

Salinity and Temperature in WSDW

The pattern seen in the contoured $\delta^{18}O$ data can assist in estimating possible temperatures of the WSDW and in the colder core of seawater overlying it. We can use the paleotemperature equation of Shackleton [1974] ($T = 16.9 - 4.38(\delta_c - \delta_o) + 0.10(\delta_c - \delta_o)^2$), to calculate the temperatures of these water masses during this time period, provided that the $\delta^{18}O$ of deep water (δ_o) is determined.

The values of δ_o we need will be different from the present average value (-0.28^o/oo) for two reasons. First, the amount of continental ice present during the Eocene and Oligocene was less than that of today. Second, the oxygen isotopic composition throughout the water column must have changed, because of the greater salinity of the deeper, warmer water. The determination of the proper values of δ_o used is critical to the calculation of correct bottom waters temperatures.

To determine the average oceanic $\delta^{18}O$ value, I assume that the Eocene ocean was ice-free (with an average $\delta^{18}O$ of -1.2^o/oo [Shackleton and Kennett, 1975]). Keigwin and Corliss [1986], Miller et al. [1987a] and Zachos et al. [1992a] found that the shift in lower latitude planktonic foraminiferal $\delta^{18}O$ in the earliest Oligocene was ~0.3 to 0.4^o/oo. Assuming constancy of tropical oceanic temperatures [Matthews and Poore, 1980]; Adams et al., 1990], this increase was due to an increase in Antarctic ice volume. Zachos et al. [1992a,b] found a similar oxygen isotopic shift in benthic (1.2^{o}/oo) and planktonic (0.5^{o}/oo) foraminifera at high latitudes (58°S) on the Kerguelen Plateau at ODP Site 748 coincident with the first appearance of ice rafted debris. They concluded, from comparison with lower latitude sites, that 0.3^{o}/oo to 0.4^{o}/oo of the isotopic signal was due to ice-volume effect. Assuming that the Eocene polar regions were ice-free, I conclude that the average oceanic $\delta^{18}O$ after the earliest Oligocene would be -0.85^{o}/oo (= -1.2^{o}/oo + 0.35^{o}/oo). Thus 60-70% of the 1^{o}/oo shift in benthic foraminifera was due to a decrease in temperatures of about 2.0-2.5°C in most of the water column and the remaining 30-40% was due to build-up of ice on Antarctica. Table 3-5 presents the temperature estimates based on using δ_o = -1.2^{o}/oo during the Eocene, and δ_o = -0.85^{o}/oo after the earliest Oligocene.

Several features are illustrated by these data. First, bottom water temperatures at Site 689 averaged 3.28^{o}C in the late Eocene, while Site 699 temperatures averaged 5.32^{o}C (2.0^{o}C warmer). During the first 6 m.y. of the Oligocene, temperature differences are similar, with Site 689 temperatures averaging 0.51^{o}C, and Site 699 temperatures averaging 2.70^{o}C, a difference of 2.2^{o}C. However, between 30-28 Ma, isotopic temperatures calculated for Site 689 dropped radically, to an unrealistically low temperature of -1.5^{o}C. This argues for additional ice volume effects at this time, as suggested by Miller et al. [1985b], Keigwin

TABLE 3-5

Oxygen isotopic temperatures of bottom water at Sites 689 and 699.

	Site 689		Site 699		
Age (Ma)	Equil. $\delta^{18}O$	Temp. (°C)	Equil. $\delta^{18}O$	Temp. (°C)	$T_{699}-T_{689}$ (°C)
26.5	3.225	0.71	2.771	2.35	1.64
27.5	3.295	0.46	2.604	2.96	2.50
28.5	3.871	-1.55	2.797	2.26	3.81
29.5	3.863	-1.52	2.826	2.15	3.67
30.5	3.523	-0.34	2.704	2.60	2.94
31.5	3.279	0.52	2.744	2.45	1.93
32.5	3.205	0.78	2.571	3.09	2.30
34.5	3.178	0.88	2.586	3.03	2.15
35.5	3.424	0.01	2.781	2.31	2.31
36.5	2.374	2.52	1.898	4.29	1.77
38.5	2.008	3.88	1.497	5.81	1.94
39.5	2.333	2.67	1.722	4.96	2.28
41.5	1.963	4.05	1.389	6.23	2.18

Estimates based on $\delta^{18}O$ of average ocean water being -1.2°/oo (ice-free conditions) in the Eocene and -0.85°/oo (limited glaciation conditions) in the Oligocene. Temperatures calculated using Shackleton [1974] paleotemperature equation. Because of an unconformity in Site 699 at 34-33 Ma, a lack of data in Site 689 at 38-37 Ma, and lack of data in Site 699 at 41-42 Ma, no calculations are shown for these time periods.

and Keller [1984], Miller and Thomas [1985], Keigwin and Corliss [1986] and subsequent studies.

Because the deeper water at Site 699 most probably originated at least in part in low latitudes through evaporation in enclosed basins [Brass et al., 1982], it would have had a higher $\delta^{18}O$ than the overlying cooler water due to enrichment during evaporation. The correct temperature offset between the WSDW and the colder overlying water will therefore be greater than that calculated by simply assuming an average oceanic oxygen isotopic composition.

By offsetting today's deep salinity vs. $\delta^{18}O$ relationship using different values of average δ_o, and examining the relationship between temperature, salinity, and density, we can explore the range of possible temperatures and salinities necessary to produce a stable water column. The technique of Railsback et al. [1989] to generate curves of constant density and constant calcite $\delta^{18}O$ in temperature - salinity space was used in order to constrain these temperatures and salinities at Site 699, assuming that average oceanic values of δ_o and salinity are present at Site 689. In these calculations, I assume that the modern, empirically determined $\delta^{18}O$/salinity ratio of $0.35^{o}/oo$/ppt [Railsback et al., 1989] still holds (ppt will be used for parts per thousand when referring to salinity in this discussion instead of the commonly used $^{o}/oo$, in order to avoid confusion with the per mil terminology of stable isotopes). I have assumed that the δ_0 values at Site 689 are representative of average ocean water, calculated the temperature at that point, and then calculated the minimum salinity and maximum temperature at Site 699 needed to produce a stable water column. I used Railsback et al.'s [1989] technique to determine the salinity and temperature required for a minimally stable water column assuming (1) an average salinity of 34.0 ppt and an average oceanic $\delta^{18}O$ of $-1.2^{o}/oo$ (42-36 Ma); and (2) average values of 34.266 ppt and $-0.85^{o}/oo$ (36-26 Ma) at Site 689 to approximate the properties of the water mass bathing Site 699 between 42 and 26 Ma (Table 3-6). Results from these calculations show that greater thermal gradients are indeed found; gradients range from 1.9 to 4.2°C, and average 2.8°C, 0.4°C higher than if salinity changes are not considered. Salinities at Site 699 average 0.29 ppt greater than those at Site 689.

One final modification to this model needs to be made. During the Messinian Salinity Crisis in the late Miocene, about 6 % of the ocean's salt was removed [Ryan, 1973], leading to a freshening of the oceans. To calculate oceanic salinity before this event, the average salinity values (34.0 ppt for the Eocene and 34.266 ppt for the Oligocene) were divided by 0.94. The Railsback et al. [1989] technique was again applied to calculate temperatures, salinities, and $\delta^{18}O_w$ at Site 699 necessary for a stable water column (Table 3-7). With the exception of higher absolute salinities at Site 699 as well, the model is robust: temperatures increase

TABLE 3-6

Estimated hydrographic properties of Site 689 and 699

	Site 689		Site 699					
Age (Ma)	Equil. $\delta^{18}O$	Temp. (°C)	Equil. $\delta^{18}O$	Temp. (°C)	Salin. (ppt)	$\delta^{18}O_w$ (^{o}/oo)	T_{699}- T_{689}	S_{699}- S_{689}
26.5	3.225	0.71	2.771	2.58	34.44	-0.788	1.87	0.18
27.5	3.295	0.46	2.604	3.33	34.55	-0.750	2.87	0.29
28.5	3.871	-1.55	2.797	2.66	34.58	-0.740	4.21	0.31
29.5	3.863	-1.52	2.826	2.53	34.57	-0.745	4.06	0.30
30.5	3.523	-0.34	2.704	2.98	34.56	-0.747	3.32	0.29
31.5	3.279	0.52	2.744	2.72	34.47	-0.777	2.20	0.21
32.5	3.205	0.78	2.571	3.44	34.54	-0.754	2.66	0.27
34.5	3.178	0.88	2.586	3.36	34.52	-0.760	2.48	0.26
35.5	3.424	0.01	2.781	2.61	34.50	-0.769	2.60	0.23
36.5	2.374	2.52	1.898	4.65	34.27	-1.105	2.13	0.27

TABLE 3-6--continued

	Site 689		Site 699					
Age (Ma)	Equil. $\delta^{18}O$	Temp. (°C)	Equil. $\delta^{18}O$	Temp. (°C)	Salin. (ppt)	$\delta^{18}O_w$ (^{o}/oo)	$T_{699}-T_{689}$	$S_{699}-S_{689}$
38.5	2.008	3.88	1.497	6.32	34.37	-1.069	2.44	0.37
39.5	2.333	2.67	1.722	5.46	34.38	-1.067	2.79	0.38
41.5	1.963	4.05	1.389	6.83	34.44	-1.045	2.79	0.44

Estimates based on $\delta^{18}O$ and salinity of ocean water at Site 689 being 1.2^o/oo and 34.0 ppt in the Eocene and -0.85^o/oo and 34.266 in the Oligocene. Temperature at Site 689 calculated using Shackleton [1974] paleotemperature equation. Temperature and salinity at Site 699 estimated assuming a minimally stable water column (i. e. approximately the same density as at Site 689), following Railsback et al. [1989]. $\delta^{18}O$ of ocean water at Site 699 calculated from equilibrium $\delta^{18}O$ of calcite and estimated temperature from paleotemperature equation.

TABLE 3-7

Estimated hydrographic properties of Site 689 and 699 after adding 6% additional salt extracted during the Messinian Salinity Crisis

	Site 689		Site 699					
Age (Ma)	Equil. $\delta^{18}O$	Temp. (^{o}C)	Equil. $\delta^{18}O$	Temp. (^{o}C)	Salin. (ppt)	$\delta^{18}O_w$ ($^{o}/oo$)	$T_{699}-T_{689}$	$S_{699}-S_{689}$
26.5	3.225	0.71	2.771	2.60	36.65	-0.781	1.89	0.20
27.5	3.295	0.46	2.604	3.37	36.77	-0.740	2.91	0.32
28.5	3.871	-1.55	2.797	2.72	36.81	-0.725	4.26	0.36
29.5	3.863	-1.52	2.826	2.59	36.79	-0.731	4.11	0.34
30.5	3.523	-0.34	2.704	3.02	36.78	-0.735	3.36	0.33
31.5	3.279	0.52	2.744	2.74	36.68	-0.770	2.22	0.23
32.5	3.205	0.78	2.571	3.48	36.76	-0.744	2.70	0.30
34.5	3.178	0.88	2.586	3.40	36.74	-0.751	2.52	0.28
35.5	3.424	0.01	2.781	2.65	36.71	-0.760	2.64	0.26
36.5	2.374	2.52	1.898	4.68	36.46	-1.097	2.16	0.29

TABLE 3-7--continued

	Site 689		Site 699					
Age (Ma)	Equil. $\delta^{18}O$	Temp. (^{o}C)	Equil. $\delta^{18}O$	Temp. (^{o}C)	Salin. (ppt)	$\delta^{18}O_w$ ($^{o}/oo$)	$T_{699}-T_{689}$	$S_{699}-S_{689}$
38.5	2.008	3.88	1.497	6.36	36.57	-1.059	2.48	0.40
39.5	2.333	2.67	1.722	5.50	36.58	-1.056	2.83	0.41
41.5	1.963	4.05	1.389	6.87	36.64	-1.034	2.83	0.47

Salinity of ocean water at Site 689 would have been 36.170 ppt during the Eocene under ice free conditions and 36.453 ppt in the Oligocene. $\delta^{18}O_w$ was $-1.2^{o}/oo$ during the Eocene and $-0.85^{o}/oo$ during the Oligocene.

by less than 0.07°C, $\delta^{18}O_w$ decreases by less than $0.02^o/oo$, and salinity gradients increase by less than 0.06 ppt, to a maximum of 0.47 ppt.

The temperatures (Eocene: 4-7°C, Oligocene: 2-4°C) and salinities (less than 0.5 ppt greater than mean ocean values) calculated at Site 699 from the isotopic data are too low to characterize a Warm Saline Deep Water sensu strictu. Seawater produced today from excess evaporation, such as Mediterranean Outflow Water (MOW), has much more extreme properties than the calculations suggest, with temperatures and salinities on the order of 9°C and 36 ppt (1.3 ppt greater than average oceanic salinity) at the Straits of Gibraltar, to 13-15°C and 37-39 ppt within the Mediterranean [Reid, 1979, Pickard and Emery, 1982].

Therefore, it is evident that the source of this WSDW cannot be direct production from excess evaporation in semi-enclosed basins in low to mid latitudes. MOW today is entrained into the North Atlantic gyre and flows northward into the Norwegian Greenland Sea. North Atlantic Deep Water is produced by the cooling of saline water derived in part from MOW [Reid, 1979]. One possible scenario for the production of WSDW is that during the late Eocene and early Oligocene, a similar process occurred, with either a larger component of the warm saline intermediate water, or less efficient cooling, producing a "Warmer Saline Deep Water" rather than "Warm Saline Deep Water" in high northern latitudes instead of low to mid latitudes. Bipolar cooling at high latitudes during the earliest Oligocene could thus result in cooling of the entire deep water column without affecting low latitude surface temperatures. However, this scenario may not be justified, especially in the Eocene, in light of suggested warm Arctic temperatures [Estes and Hutchinson, 1980; McKenna, 1980; Wolfe, 1980] during the Paleogene.

This scenario may also be contradicted by the carbon isotopic data, which do not show any decreased $\delta^{13}C$ values in the warmer Site 699 relative to the cooler Site 689 which would be expected if WSDW was produced in the more distant northern hemisphere; rather, the reverse is true. Another scenario is possible, which would both make it possible to derive cooler WSDW from more proximate sources. It is possible that the warm saline water does in fact sink near the point of origin, and during its passage through cooler, less saline waters, entrains and mixes with that water to decrease the temperature and salinity to the values measured at Site 699. This scenario would adequately explain the observed data but would not explain why temperatures decreased equally in intermediate and deep waters in the earliest Oligocene unless they in fact decreased equally at polar and lower latitudes.

Evidence from benthic foraminiferal assemblages is difficult to reconcile with the calculated salinity and temperature gradients. Sites 689 and 699 [Thomas, 1989, 1990, 1992] benthic foraminiferal faunas show essentially the same patterns over the interval studied here rather than showing the effect of differing water masses. No benthic foraminiferal faunal analyses have been made to date over this age interval in Site 699, but my observations are that the faunas are broadly similar to those described from Sites 689 and 690. It is possible that benthic foraminiferal faunas do not respond to the relatively low temperature gradients identified here but rather to other factors such as rain-rates of organic particles or to concentration differences in CO_2. Given the relatively low overall productivity [Miller, 1992] during the late Eocene-Oligocene, and the low CO_2 gradients implied by the low total dissolved $\delta^{13}C$ gradients, differences in bottom water characteristics may not have been large enough to induce different benthic foraminiferal faunas at the different sites.

Keigwin and Corliss [1986] examined thermal gradients in surface water in the Eocene, Oligocene, and Recent based on planktonic isotopic gradients and found low thermal gradients in the late Eocene and early Oligocene. However, little data were present from high latitudes. Additional data from the Kerguelen Plateau and Maud Rise has been interpreted [Zachos et al., 1992a] to mean that the surface water latitudinal thermal gradient was higher at high southern latitudes. My interpretation of the isotopic data from Sites 689 to 699 indicates that either an additional increase in the planetary thermal gradient took place across the earliest Oligocene oxygen isotope shift, and that a bipolar cooling of about 2.5°C occurred, or that an overall, world-wide temperature decrease of about 2.5°C occurred.

Conclusions

Analysis of new benthic foraminiferal oxygen isotopic data from high southern latitude ODP Sites 699 (Eocene/Oligocene paleodepth ~3400 m) and 703 (Eocene/Oligocene paleodepth ~950 m) have led to three advances in the interpretation of Paleogene paleoceanography. The first supports the hypothesis [Kennett and Stott, 1990] that a warm saline water mass was produced during much of the Paleogene. These two sites, together with Kennett and Stott's previously published isotopic data from ODP Sites 689 (paleodepth ~1500 m) and 690 (paleodepth ~2300 m), define a maximum in calcite $\delta^{18}O$ in Site 689 (~1500 m). The decreases above and below indicate a temperature minimum near 1400 m, with water temperature increasing steadily in the three sites from 1500 to 3400 m. A second finding of this study is a near-constant oxygen isotopic gradient before and after the earliest Oligocene oxygen isotope enrichment event. When considered in the light of suggestions of an approximately 0.3-0.4^{o}/oo ice volume effect, I suggest that there was a cooling at the time of the oxygen isotope shift of about 2.5°C. Finally, I suggest that the immediate source of the "WSDW" was not directly from subtropical, semi-enclosed basins with high evaporation rates, as has been suggested by Brass et al. [1982]. After initial production in that environment, warm, saline intermediate waters were cooled and/or mixed with cooler water at high northern latitudes to form "Warmer Saline Deep Water", similar in genesis to the North Atlantic Deep Water today, or during downward advection of the warm saline water. Two factors support this. First, the same level of cooling occurred in both the cooler intermediate waters and the deeper, warmer waters during the earliest Oligocene. Second, the water properties defined by oxygen isotope ratios in Paleogene sediments at Site 699 are neither warm enough nor saline enough to have been produced by direct evaporation and sinking at low to mid latitude source regions.

Two contrasting conclusions may be drawn from the different possible generation mechanisms: either an increase in the planetary thermal gradient occurred, with bipolar cooling of about 3°C, or an overall planetary decrease in temperatures of the same amount occurred. Warm Arctic temperatures during the Paleogene support the latter interpretation.

Benthic foraminiferal studies [Corliss, 1981, Thomas, 1989, 1990, 1992] find no significant change in faunas across the Eocene/Oligocene oxygen isotopic shift or between sites, suggesting little geographic or temporal temperature change. It is possible that benthic faunas may not respond to the low temperature gradients (mostly 2-3^{o}C) calculated here. However, low inter-ocean $\delta^{13}C$ gradients suggest little difference in age of bottom water or rain rate of organic carbon, and benthic foraminiferal faunas may be more sensitive to those factors than to small changes in temperature or salinity.

A maximum in $\delta^{13}C$ occurs near 36-35 Ma in virtually all benthic deep-sea records from the world ocean. This, in combination with the development of widespread unconformities at this time, leads us to suggest an increase in deep-sea circulation rates, possibly related to a pulse of warm saline water from the North Atlantic.

CHAPTER 4

OLIGOCENE BRAARUDOSPHAERA OOZES AND CHALKS: GENESIS AND PALEOCEANOGRAPHIC IMPLICATIONS FROM ISOTOPIC ANALYSES OF FINE FRACTION AND FORAMINIFERA

Introduction

Braarudosphaera oozes and chalks are deposits usually composed almost entirely of pentaliths of the single calcareous nannofossil genus *Braarudosphaera*. These deposits are unusual because most deep sea calcareous oozes contain a diverse assemblage of different foraminiferal and calcareous nannofossil species, and because the *Braarudosphaera* oozes and chalks have very specific temporal and spatial ranges.

The distribution of *Braarudosphaera* oozes and chalks is unusual because of the restricted nature of these deposits. Fischer and Arthur [1977] found that *Braarudosphaera* oozes and chalks have occurred at very specific times, at the Jurassic-Cretaceous boundary, just after the Cretaceous-Tertiary boundary, during the Oligocene, and during Recent times. At any given time, the spatial distribution has been limited. This pilot study addresses the *Braarudosphaera* oozes deposited in the South Atlantic during the Oligocene.

In the Oligocene, it has been noted that Braarudosphaera oozes are found in both the North and South Atlantic in bands at about 30° of latitude in cores from Deep Sea Drilling Project (DSDP) Legs 3, 40, 73, 74, and 82 [Parker et al., 1985], in the Gulf of Mexico in DSDP Leg 77 cores [Lang and Watkins, 1984] and in the western Indian Ocean near the equator in DSDP Leg 24 cores [Roth, 1974]. It is important to note that these 30° bands may be sampling artifacts because of a large concentration of drill sites along 30° north and south, with few sites within 20° of latitude outside of these bands, especially in the South Atlantic (Figure 4-1). Braarudosphaera oozes were not found in DSDP Leg 39 (western South Atlantic) sediments, but may have been missed due to spot coring [Perch-Nielsen, 1977]. Most of the Oligocene occurrences have been from the early Oligocene, but reports have come from all parts of the Oligocene, and multiple Braarudosphaera levels have usually been reported. LaBrecque et al. [1983] noted that the DSDP Site 522 and 523, Braarudosphaera oozes fell within nannofossil zone NP23 (as had similar deposits found during other DSDP legs: Leg 3 [Saito and Percival, 1970], Leg 24 [Roth, 1974], Leg 40 [Bukry, 1978], Leg 74 (zone NP24 - [Manivit, 1984]), Leg 77 [Lang and Watkins, 1984], Leg 82 [Parker et al., 1985], and have been placed within paleomagnetic chrons C10R and C12R, at about 29 Ma and 31-33 Ma (Berggren et al. [1985] time scale), respectively, in the DSDP Leg 73 cores. Up to 34 separate Braarudosphaera chalks

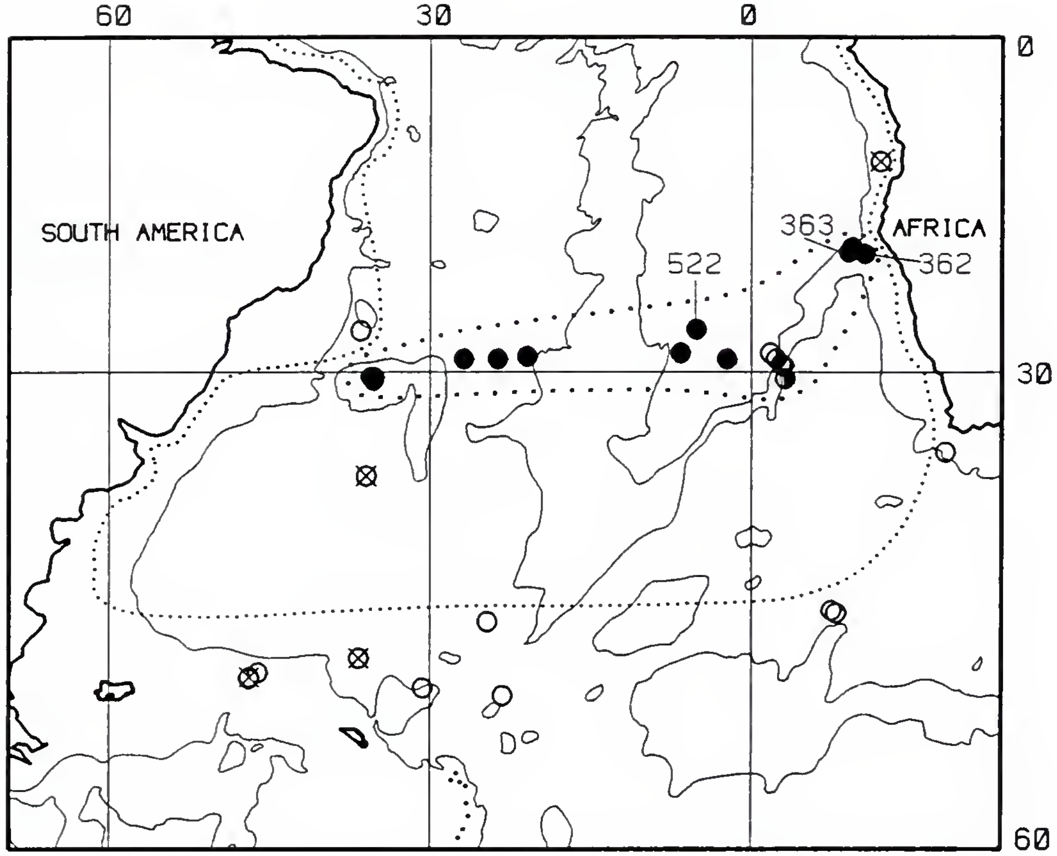

Figure 4-1: Distribution of Braarudosphaera oozes in South Atlantic Ocean DSDP and ODP drill sites which recovered Oligocene sediments. Empty circles denote sites with carbonate sections but lacking Braarudosphaerids, circles with Xs denote Oligocene sections that are carbonate free, half-filled circles indicate Oligocene sections that have common Braarudosphaera pentaliths but no oozes, and solid circles indicate Oligocene sections containing Braarudosphaera oozes. Note that although all of the sites containing Braarudosphaera lie near 30°S, very little drilling has been done within ±10° of 30°S. The heavy dotted line outlines the minimum possible extent of the oozes (similar to Parker et al. [1985]), while the light dotted line outlines the maximum possible extent of the oozes.

were recovered in DSDP Site 362 cores from the southwest African continental shelf, where they occur throughout the Oligocene [Bukry, 1978].

Genesis of Braarudosphaera Deposits

Two different types of theories have evolved to explain the presence of deep-sea *Braarudosphaera* deposits, one based on the environmental and ecologic preferences of the organism, the other based on the possible effects of sedimentary processes.

Braarudosphaerids are not normally found in abundance in marine waters. Fischer and Arthur [1977] have suggested that they are "disaster forms"; i.e., that they only attain appreciable abundances when the environment has changed suddenly, eliminating the more normally diverse pelagic assemblages. This would allow *Braarudosphaera* blooms to occur without competition. Thus during the periodic oligotaxic (low diversity) episodes which Fischer and Arthur propose, normally abundant and diverse taxa disappear, allowing *Braarudosphaera* to dominate. This is an incomplete answer at best, however, as the *Braarudosphaera* oozes represent fairly short periods of time within the long oligotaxic periods, and because they are repetitive, interspersed with layers of normal deep-sea oozes. This also does not explain why the periods of oligotaxy occur.

Bukry [1974] examined Recent occurrences of *Braarudosphaera* from the Black Sea, the Gulf of Maine [Gran and Braarud, 1935], the Gulf of Panama [Smayda, 1966], and several open ocean areas (Table 4-1). In open ocean areas of normal salinity (>34^{o}/oo), concentrations never reached more than 34 cells/liter, while in areas of reduced salinity such as the Gulf of Maine (31.8-32.7^{o}/oo) and Gulf of Panama (26.8-32.5^{o}/oo), cell concentrations in the water column reached 680 and 1500 c/l, respectively. Bukry suggested that the widespread occurrence of _Braarudosphaera_ in Black Sea sediments and other coastal areas was due to a preference by _Braarudosphaera_ of low salinity conditions (17-18^{o}/oo in the case of the Black Sea) which other species cannot tolerate. _Braarudosphaera_ has also been found in waters of unusually high salinity (34-40^{o}/oo, in the Persian Gulf - Roth, [1974]), however, and thus the salinity dependence of this taxon is not yet entirely clear.

Wise and Hsü [1971] and Lloyd and Hsü [1972] analyzed the carbon and oxygen isotopic composition of bulk carbonates of from DSDP Leg 3 (in the _Braarudosphaera_ chalks, mostly fine fraction). This work revealed enriched $\delta^{18}O$ isotopic ratios in _Braarudosphaera_ chalks from DSDP Leg 3, which indicated temperatures of about 6°C. Wise and Hsü [1971] noted that modern _Braarudosphaera_ have not been found at temperatures less than 10°C and suggested that the chalks analyzed were diagenetically altered. Wise and Hsü [1971] and Lloyd and Hsü [1972] therefore concluded that the isotopic ratios measured in the chalks probably reflected diagenesis in cold bottom water temperatures on the sea

TABLE 4-1

Salinity Dependence Of _Braarudosphaera_
(from Bukry, 1974)

Location	Cell Count	Salinity in $^{o}/oo$	Reference
Black Sea	present*	17-18	Bukry, 1974
Gulf of Maine	≤680 c/l	31.8-32.7	Gran and Braarud, 1935
Gulf of Panama	≤1500 c/l	26.8-32.5	Smayda, 1966
North Atlantic	>1 c/l	"open ocean"	Gaarder, 1954
SW Atlantic	<20 c/l	36.8-37.2	Hulburt, 1962
Btw. S. New Engl. & Bermu.	≤34 c/l	present only <34	Hulburt and Rodman, 1963
Pacific	absent	>34.7	Hasle, 1959, 1960
Indian & Pac.	absent	"open ocean"	Ushakova, 1967, 1969

*in sediment

floor rather than initial production in cool upwelled surface waters. Berger [1979] suggested that Braarudosphaera deposits were due to mid-ocean upwelling, based on the oxygen isotopic work of Wise and Hsü [1971] and Lloyd and Hsü [1972]. Fine fraction carbon and oxygen isotopic values have been shown to be affected by changes in the faunal and floral composition [Paull and Thierstein, 1987], however, and thus bulk carbonate $\delta^{18}O$ analyses are suspect. In any event, an upwelling hypothesis does not resolve the question of the cause of low diversity present in the oozes.

Decreased open ocean near-surface salinity has been proposed as an environmental trigger for blooms of Braarudosphaera by several authors from DSDP Leg 40 [Bukry, 1978; Siesser, 1978; Melguen, 1978]. The multiple beds in DSDP Site 362 are cyclic, with a maximum interbed period of 100,000 years or less [Bukry, 1978], suggesting to Hsü [1977, personal communication to Bukry, 1978] that blooms might have occurred due to pulses of low salinity water caused by periodic infusions of glacial meltwater. Siesser [1978] and Melguen [1978] suggested that upwelled low salinity water during the initiation of the Benguela current could have caused blooms of Braarudosphaera to occur.

It has been suggested that sedimentary processes of dissolution and/or redeposition have helped form the Braarudosphaera oozes. Saito and Percival [1970] and Berger [1972] suggested that since Braarudosphaera is more typically found in near-shore waters (because of the low salinity preference outlined above), deep-sea deposits may have been redeposited from shallow water, either near-shore or from the Mid-Atlantic Ridge. However, a number of problems exist for this hypothesis. No shallow water source is known [Wise and Kelts, 1972]. In addition, some of the sites in which the Braarudosphaera deposits are known are above the turbidite deposition layer [Wise and Kelts, 1972], and the chalks lack the graded bedding expected of such redeposited sediments [Lloyd and Hsü, 1972]. Third, the low diversity, widespread [Roth, 1974], and nearly synchronous [Wise and Kelts, 1972] nature of the deposits argue against a sporadic redeposition process.

Wise and Hsü [1971] suggested that Braarudosphaera is a dissolution resistant taxa and that concentration by dissolution of more susceptible taxa may have occurred. However, they note that the terrigenous content of the South Atlantic Braarudosphaera ooze is low, indicating that little dissolution has occurred. In addition, other authors [Bukry, 1971; Wise and Kelts, 1972] have noted that Braarudosphaera is actually a dissolution susceptible taxon which would be selectively removed by dissolution rather than concentrated. Therefore, it seems likely that the deposits are formed autochthonously rather than through concentration by redeposition [Wise and Kelts, 1972] or dissolution.

To summarize, the immediate cause of high concentrations of Braarudosphaera in open ocean deposits are probably not due to redeposition from shallow, near shore sites, nor due to dissolution of other components. A more probable cause is unusual environmental conditions in overlying waters. Although the work of Bukry [1974] and others indicates that low salinity may play a part in the production of Braarudosphaera oozes, the actual causal mechanism is not known.

Paleoceanographic Considerations

LaBrecque et al. [1983] attributed the production of the Braarudosphaera ooze to a "biological crisis" brought on by the opening of the Drake Passage. The date of the opening of the Drake Passage is somewhat equivocal, and depends on how the Western Scotia Sea magnetic anomalies are interpreted [LaBrecque and Rabinowitz, 1977]. If the Barker and Burrell [1977] interpretation is used, the opening occurred during paleomagnetic chron C8, while if the interpretation of LaBrecque and Rabinowitz [1977] is used the opening occurred during chrons C10-C13. The latter date correlates well with the presence of the Braarudosphaera oozes. LaBrecque et al. [1983] also note that this time period correlates well with the mid-Oligocene erosional event identified by Vail et al. [1977]. LaBrecque et al. [1983] suggested that the opening of the Drake Passage led to the development of circum-Antarctic winds, which in turn caused atmospheric instabilities and enhanced oceanic circulation. This enhanced oceanic circulation would be responsible for both the Vail et al. [1977] erosional events and increased mid-ocean upwelling postulated by Berger [1979] to have caused Braarudosphaera blooms in the South Atlantic. However, this does not explain the reason for the dominance of Braarudosphaera in the bloom. In addition, this scenario does not explain why both the Braarudosphaera ooze and the erosional events were temporary and why the Braarudosphaera oozes are repetitive.

A factor that has been little considered is the effects of Antarctic ice on the production of Braarudosphaera oozes. Miller and Fairbanks [1983] and Miller et al. [1985] proposed that temporary accumulation of Antarctic ice occurred at several times during the Oligocene, including an accumulation event at 31 Ma (Berggren et al. [1985] (BKFV85) time scale; 29.2 Ma on the Cande and Kent [1992] (CK92) time scale), based mostly on oxygen isotopic data. A high resolution bulk carbonate $\delta^{18}O$ record from DSDP Legs 73 and 74 shows 3 distinct early, middle, and late Oligocene cool episodes [Shackleton, 1986] which correlate well with the data of Miller and co-workers. The middle Oligocene cool episode is dated paleomagnetically at 31 Ma, shortly before the occurrence of the Braarudosphaera bloom. The effects of the eventual deglaciation after the Oligocene glacial episodes on the world ocean, however, have not been addressed. A widespread meltwater spike has been proposed by Kennett and Shackleton [1975] and Berger et al. [1977] for the most recent Pleistocene deglaciation, based on a significant decrease in foraminiferal $\delta^{18}O$ ratios in cores from the Gulf of Mexico and western equatorial Pacific. This indicates the presence of a widespread low salinity layer during that time. If temporary Antarctic glaciation did exist during the Oligocene, then rapid melting of the ice might very well provide a low salinity pulse to the southern oceans. This low salinity water, entrained in the ancestral Benguela Current suggested by Hsü et al. [1984b] or in AAIW would be brought up to the mid-latitudes in which the Braarudosphaera oozes are found. The growth of Braarudosphaera would be encouraged and the growth of other coccolithophorids would be inhibited, resulting in the production of pure Braarudosphaera oozes. This explanation is also applicable for the high concentrations of Braarudosphaera found in the Indian Ocean. It would not, however, be applicable to the North Atlantic occurrences mentioned previously unless Northern hemisphere Oligocene glaciation is postulated as well.

It is perhaps surprising that, since the initial measurements of bulk carbonates [Wise and Hsü, 1971; Lloyd and Hsü, 1972], few if any additional isotopic studies have been attempted on Braarudosphaera oozes. Indeed, carbon and oxygen isotopic analyses of these oozes have been actively avoided [Shackleton, 1986].

This paper addresses two questions associated with these sedimentary units, specifically: what environmental and ecologic conditions caused their production and what events led to the establishment of these conditions? In order to examine the possibility that unusual environmental conditions led to the production of Braarudosphaera oozes, the oxygen and carbon isotopic composition of planktic and benthic foraminifera from within these oozes and immediately adjoining sediments above and below were measured in DSDP Sites 363 and 522.

There are three specific goals. First, I seek to determine the ages of at least some of the numerous Braarudosphaera oozes present in DSDP Site 363. For this reason, $^{87}Sr/^{86}Sr$ analyses of selected samples from each core were made in order to compare to existing $^{87}Sr/^{86}Sr$ stratigraphies. Second, I wish to determine the cause of reported high $\delta^{18}O$ values measured from bulk carbonate within these oozes. Possible causes I consider include changes in temperature, salinity, vital effects, or seafloor diagenesis, or some combination thereof. Third, I seek to determine the cause of the Braarudosphaera oozes (including both enhancement of Braarudosphaera productivity and suppression of other taxa). I address the second and third goals by the analysis of fine fraction, planktic, and benthic foraminiferal oxygen and carbon isotopes. I also examined the fine fraction using a scanning electron microscope (SEM) to evaluate the approximate composition and state of preservation of the fine fraction.

Methods

Sample Descriptions

Two DSDP Sites were selected for this study (Figure 4-1). DSDP Site 363 (Angola Basin, on the flank of the Walvis Ridge, offshore Africa, at a depth of 2248 m) was selected as an example of a more near-shore deposit. Both Site 363 and the nearby Site 362 contain numerous Braarudosphaera ooze beds, with Site 362 actually containing a greater number. However, Site 363 was selected because the burial depth of the Oligocene section (90-175 mbsf) was much less than that of Site 362 (830-920 mbsf), lessening the possibility of diagenetic alteration of samples. Both sites were discontinuously cored (Figure 4-2), and the Braarudosphaera ooze beds found within them may not correlate to each other. Since these were rotary drilled cores, no magnetostratigraphy exists, and they were dated biostratigraphically.

Site 522 (Walvis ridge, central South Atlantic, 4441 mbsf) was selected as an example of a more mid-ocean deposit. This is a very complete section, recovered with the hydraulic piston core, and has been dated both magnetostratigraphically and biostratigraphically (Figure 4-2). Only three Braarudosphaera oozes have been identified in this section.

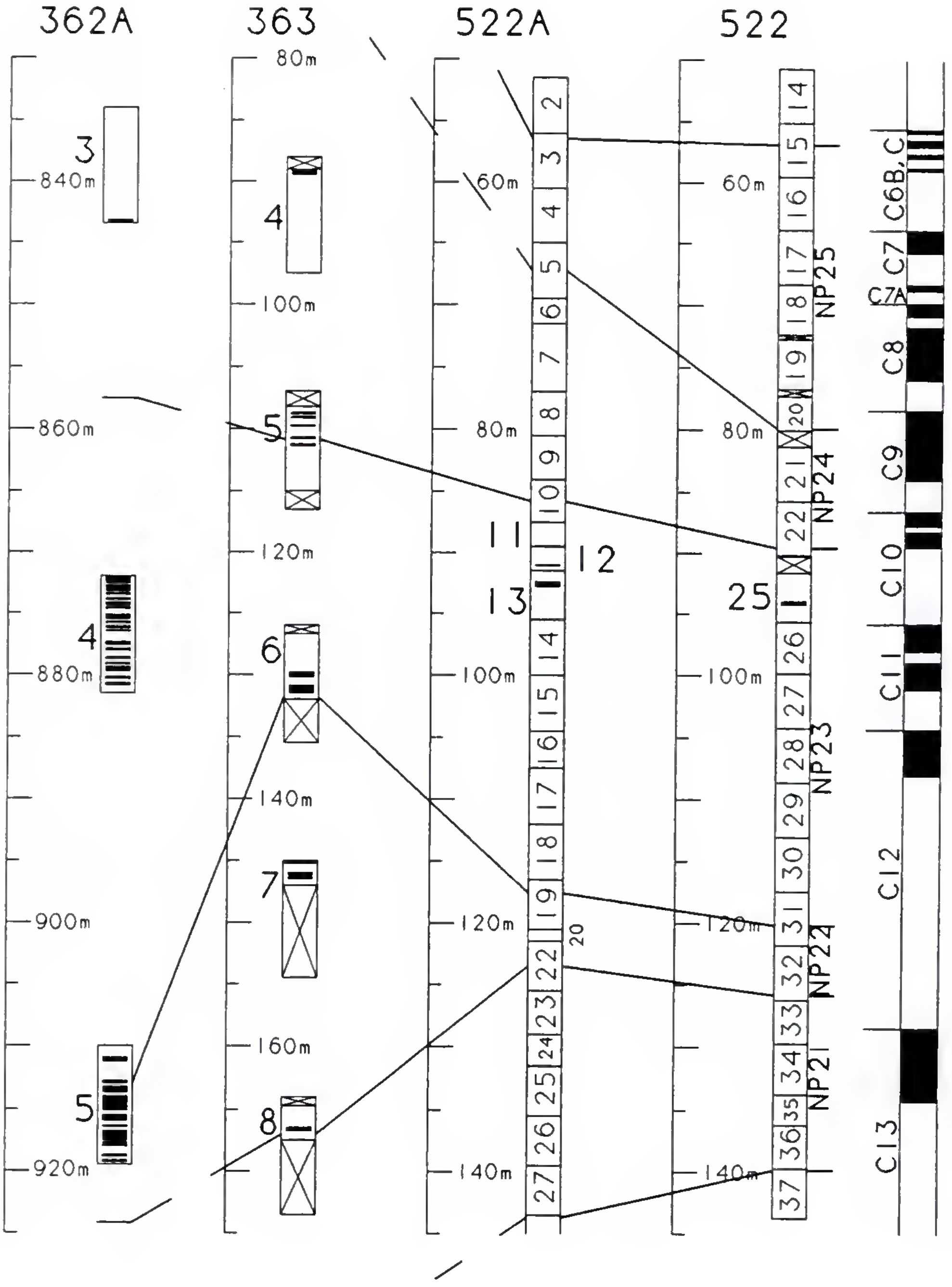

Figure 4-2: Comparison of Braarudosphaera ooze occurrence in DSDP Holes 362, 363, 522, and 522A. Calcareous nannofossil biostratigraphy is indicated by lines (dashed where uncertain) connecting the cores, and magnetostratigraphy of Hole 522 is indicated on the right. Cores are designated by numbers within or beside them. Braarudosphaera ooze occurrences are indicated by black boxes within cores designated by bold-faced numbers. Incomplete recovery is indicated by large Xs.

Three different cores from DSDP Site 363 were sampled. Core 7 (lower Oligocene, zone NP22) contained one *Braarudosphaera* ooze bed; core 6 ("middle" Oligocene, base of zone NP23) contained two *Braarudosphaera* ooze beds although only one was sampled, and Core 5 (upper Oligocene, base of zone NP24) contained five *Braarudosphaera* ooze beds, two of which were sampled. Thus a total of 8 *Braarudosphaera* ooze beds were identified at this site.

Of the three *Braarudosphaera* oozes identified at Site 522, only the thickest layer was sampled. Initially, Hole 522A (Core 13-1) was sampled, but because this core had already been sampled using U-channels [Mead et al., 1986], samples were taken from near the core liner. To alleviate the possibility that contamination from higher stratigraphic intervals might exist near the core wall, additional samples were taken from the correlative interval in Hole 522 (Core 25-2). The correlative *Braarudosphaera* oozes are at slightly different subbottom depths and of slightly different thicknesses in the different holes (Hole 522: 93.85-94.20 mbsf, Hole 522A: 92.40-92.85 mbsf [Shipboard Scientific Party, 1984]). As a result, depths from Hole 522A were corrected by adding 1.45 m.

Oxygen and Carbon Isotopes

The strategy of sampling was to measure the oxygen and carbon isotopic composition of several different fractions from each sample, with close sampling through a number of different Braarudosphaera layers. The fine fraction was measured for comparison to the work of previous investigations. The benthic foraminiferal genus Cibicidoides was measured because its isotopic behavior is well understood, for comparison to numerous Oligocene deep water isotopic studies, and to obtain deep water isotopic values. The planktic foraminifer Chiloguembelina cubensis (Palmer) was measured because it is considered to be a shallow-living taxon [Poore and Matthews, 1984, Boersma and Premoli-Silva, 1986]; the 104-125, 125-150, and 150-250μm size fractions of this taxon were measured to investigate ontogenetic changes in depth. Catapsydrax dissimilis (Cushman and Bermudez) was analyzed as a representative deep-living planktic taxon [Poore and Matthews, 1984, Boersma and Premoli-Silva, 1986].

The oxygen and carbon isotopic composition of the fine fraction and different foraminiferal taxa were measured using standard techniques (see Appendix B4). Organic carbon was removed from all samples either by roasting at 375°C for 1 hour (fine fraction) or by reacting with H_2O_2 for 0.5 to 1 hour (foraminifera). A previous study established that these methods give similar results (see Chapter 3). Foraminiferal samples were then cleaned ultrasonically to remove adhering debris. Carbonates were dissolved at two different temperatures (70°C and 90°C). This resulted in an offset of $0.5^{o}/oo$ and $0.2^{o}/oo$ in the $\delta^{18}O$ and $\delta^{13}C$ values, respectively, for the working standard (Carrara Marble).

For 70°C, the precision (1 standard deviation) of $\delta^{18}O$ and $\delta^{13}C$ was 0.06^{o}/oo and 0.15^{o}/oo (n=35), respectively, while at 90°C, the precision of $\delta^{18}O$ and $\delta^{13}C$ was 0.08^{o}/oo and 0.10^{o}/oo (n=45), respectively. All values were corrected to PDB and to the offset in standards. Replicate samples run at the two temperatures showed no significant differences after being corrected for the offset in standards.

Strontium Isotopes

All Sr samples were analyzed in a VG Micromass 354 thermal ionization mass spectrometer in dynamic mode. Samples were loaded onto oxidized Ta single filaments by dissolving the extracted Sr in 2-3μl of 0.5 N H_3PO_4 acid (see chapter 2).

An analysis of NBS-987 is run with each turret of samples. Analyses of 3 NBS-987 standards averaged 0.710237, with an uncertainty (2 standard deviations or 2σ) of ±0.000032. All samples are normalized to NBS-987 = 0.710235 and $^{86}Sr/^{88}Sr = 0.1194$. Samples for which the $^{86}Sr/^{88}Sr$ ratio was determined to be less than 0.1194 are assumed to have been fractionated and those values were not reported.

Scanning Electron Microscopy

Approximately 200 mg of bulk sample from within a Braarudosphaera ooze and from above or below the ooze was used from each of the three cores sampled from Site 363. The six samples were disaggregated in deionized water, and after allowing the coarse fraction to settle for about one minute, the suspended fine fraction was poured off. After allowing another 1 hour of settling, the suspended clay fraction was poured off. The remaining fine fraction was re-suspended in a 2 l beaker and allowed to settle onto mica plates glued with silver paint onto standard SEM mounting stubs. They were coated with a gold-palladium alloy and examined with a JEOL Scanning Electron Microscope at magnifications of from 700x to 2500x.

Results

General Comments

Comparison of the records of the *Braarudosphaera* oozes from each of the 3 Site 363 cores reveals that these deposits are not all identical; they vary significantly in carbonate content and in the magnitude of the carbon and oxygen isotopic excursion of the fine fraction (Figure 4-3). Similarities include the surprising lack of response of foraminiferal isotopic composition to the conditions leading to the deposition of the oozes, and the consistently higher carbonate composition of *Braarudosphaera* oozes. Foraminifera from Site 522 were generally visibly altered, and *Chiloguembelina cubensis* was essentially absent; as a result, only the fine fraction from Site 522 was analyzed isotopically.

Figure 4-3: Isotopic, percent carbonate, and percent fine fraction results from DSDP Site 363 cores 5, 6, and 7, plotted against depth. (a), (c), and (e): $\delta^{13}C$ and $\%CaCO_3$. (b), (d), and (f): $\delta^{18}O$ and % fine fraction. (a) and (b), (c) and (d), and (e) and (f) are cores 5, 6, and 7, respectively. Isotopic analyses of fine fraction are indicated by B's within *Braarudosphaera* oozes and plus signs (+) elsewhere, *Catapsydrax dissimilis* is indicated by solid boxes, and *Cibicidoides* is indicated by empty boxes. Several size fractions of *Chiloquembelina cubensis* were measured: 104-125μm (c), 104-150μm (C), 125-150μm (Ch), 150-250μm (CH), and 104-250μm (cC). In Core 7, bulk planktic foraminifera from 125-150μm are indicated by P. Calcium carbonate determinations are denoted by the solid line, and percent fine fraction by the dotted line.

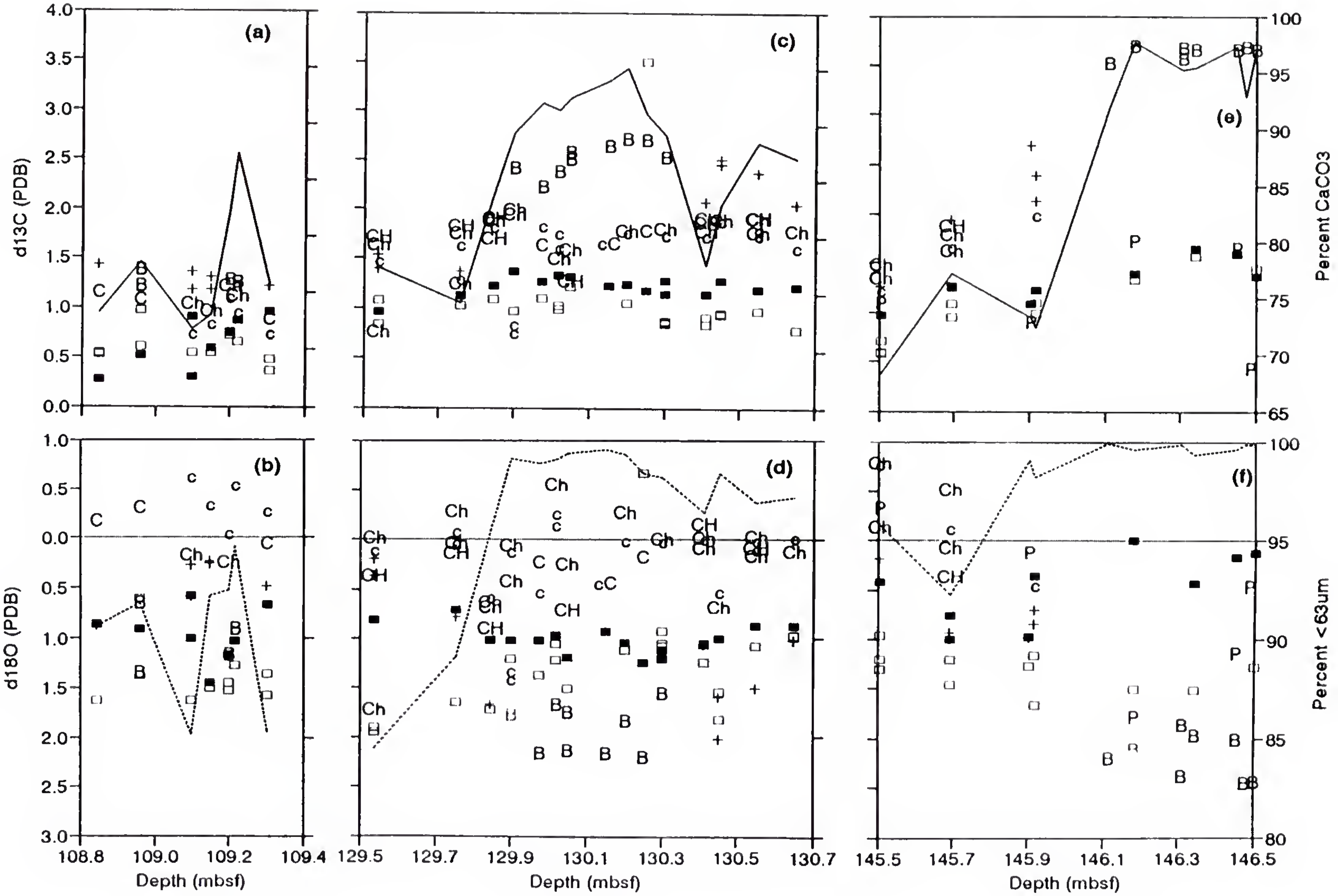
(a)
(b)
(c)
(d)
(e)
(f)
d13C (PDB)
4.0
3.5
3.0
2.5
2.0
1.5
1.0
0.5
0.0
d18O (PDB)
1.0
0.5
0.0
0.5
1.0
1.5
2.0
2.5
3.0
Percent CaCO3
100
95
90
85
80
75
70
65
Percent <63um
100
95
90
85
80
108.8
109.0
109.2
109.4
129.5
129.7
129.9
130.1
130.3
130.5
130.7
145.5
145.7
145.9
146.1
146.3
146.5
Depth (mbsf)
Depth (mbsf)
Depth (mbsf)

Carbonate Content and Percent Fine Fraction

Site 363

The carbonate content of Braarudosphaera oozes was always higher than in adjoining non-Braarudosphaera ooze intervals, although the difference between the two decreased up-section (Table 4-2, Figure 4-3). In core 7, the difference between the two types of ooze was 22.5%, decreasing to 10.2% in core 6 and 8.9% in core 5. Overall, the difference was 14.6%. Similarly, the percentage of fine fraction (<63μm) uniformly increased within the Braarudosphaera oozes, although the differences are not as extreme. Fine fraction percentages ranged from 84.4% to 99.9%, a reflection of the general nanno-foram ooze nature of these sediments [Shipboard Scientific Party, 1978], with the coarse fraction increasing up-section.

Site 522

The carbonate results were generally similar to those from Site 363, averaging 10.4% greater in the Braarudosphaera ooze than in the surrounding nannofossil ooze (Table 4-3, Figure 4-4). Fine fraction percentages, however, were lower within the Braarudosphaera "ooze", reflecting the partial lithification of this chalky layer in Site 522. Later observation of the coarse fraction in Site 522 samples confirmed that nearly all of the particles >63μm within the Braarudosphaera ooze were chalk rather than

Figure 4-4: Isotopic, percent carbonate, and percent fine fraction results from DSDP Site 522, plotted against depth (corrected depth for Hole 522A). (a): $\delta^{13}C$ and %$CaCO_3$. (b): $\delta^{18}O$ and % fine fraction. Isotopic analyses of fine fraction are indicated by Bs within Braarudosphaera oozes and plus signs (+) elsewhere. Percent carbonate and percent fine fraction are indicated by lines without symbols. Solid lines refer to data from Hole 522 and dotted lines refer to data from Hole 522A.

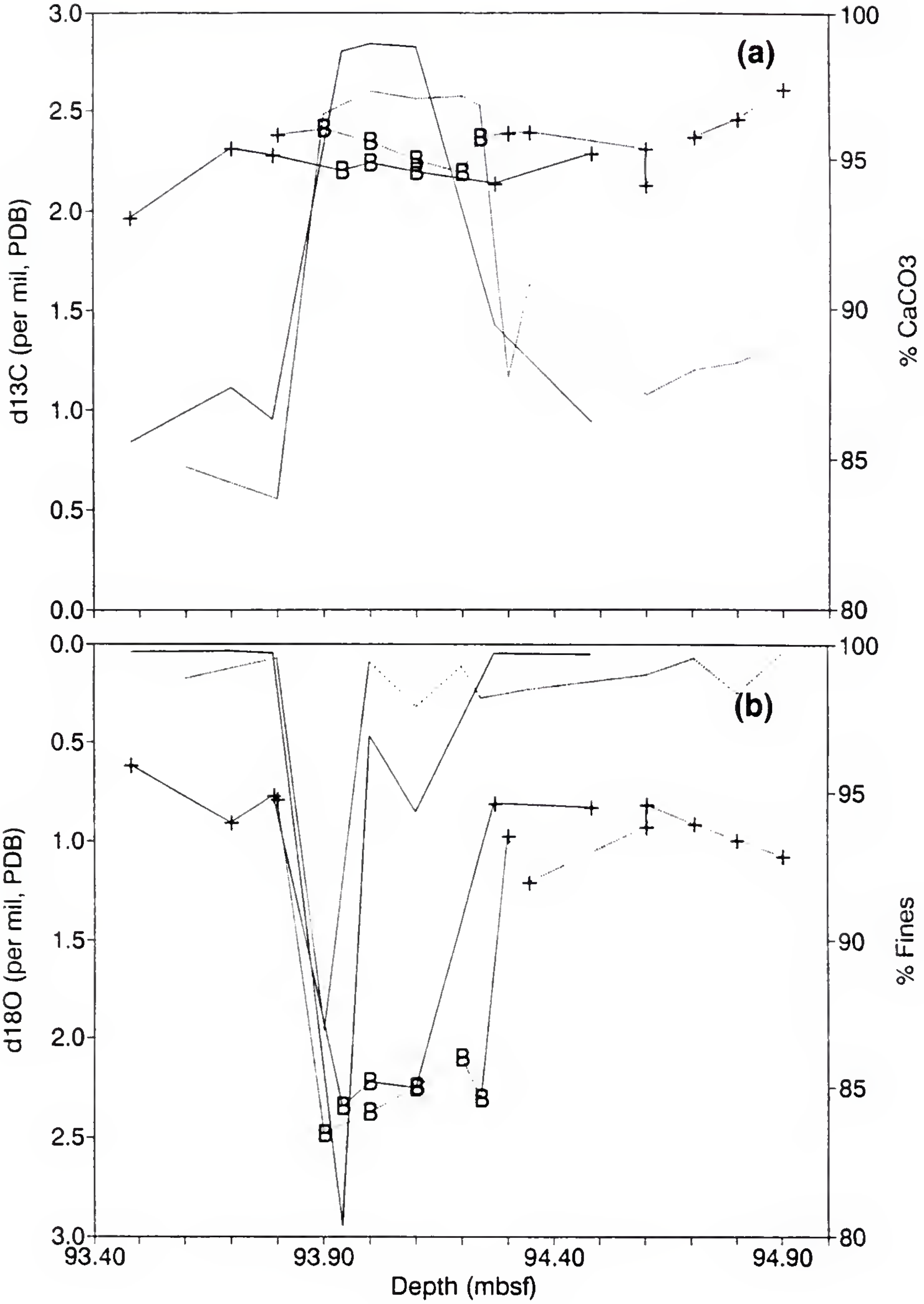
(a)
(b)
d13C (per mil, PDB)
% CaCO3
d18O (per mil, PDB)
% Fines
Depth (mbsf)
93.40
93.90
94.40
94.90
3.0
2.5
2.0
1.5
1.0
0.5
0.0
100
95
90
85
80
B
+

TABLE 4-2

Subbottom Depth, Age, % $CaCO_3$, and % Fine Fraction From DSDP Site 363, Cores 5, 6, and 7

Sample c-s- z	*	sub-bottom depth (mbsf)	Age (nannos, CK92)	Linear Regress. Sr Age	Bulk % $CaCO_3$	% Fine Fract. (<63um)
5-2- 34.5	+	108.845	28.549	29.795	73.3	90.6
5-2- 46	B	108.960	28.553	29.803	77.7	91.7
5-2- 60	+	109.100	28.559	29.813	71.8	85.2
5-2- 65	+	109.150	28.561	29.816	73.1	92.1
5-2- 70	B	109.200	28.563	29.820	82.2	92.4
5-2- 72	B	109.220	28.564	29.821	87.3	94.6
5-2- 80.5	+	109.305	28.568	29.827	75.8	85.3
6-3- 54	+	129.540	32.104	31.267	77.3	84.4
6-3- 75.5	+	129.755	32.144	31.282	74.2	89.1
6-3- 84.5	+	129.845	32.160	31.289	83.7	95.5
6-3- 90	B	129.900	32.170	31.293	89.3	99.1
6-3- 97.5	B	129.975	32.184	31.298	91.9	98.8
6-3-102	B	130.020	32.193	31.301	91.3	99.0
6-3-105	B	130.050	32.198	31.303	92.4	99.3
6-3-115.5	B	130.150	32.217	31.310	93.9	99.5
6-3-120	B	130.200	32.226	31.314	95.1	99.3

TABLE 4-2--continued

Sample c-s- z	*	sub-bottom depth (mbsf)	Age (nannos, CK92)	Linear Regress. Sr Age	Bulk % $CaCO_3$	% Fine Fract. (<63um)
6-3-125.5	B	130.250	32.235	31.318	90.9	98.3
6-3-130	B	130.300	32.245	31.321	89.1	98.1
6-3-141	+	130.410	32.265	31.329	77.5	96.4
6-3-145	+	130.450	32.272	31.332	82.8	98.3
6-4- 5	+	130.550	32.291	31.339	88.4	96.9
6-4- 15	+	130.650	32.310	31.346	87.0	97.1
7-1- 50.5	+	145.505	32.613	32.403	68.2	95.8
7-1- 69	+	145.690	32.615	32.416	77.2	92.3
7-1- 90	+	145.900	32.618	32.431	73.3	99.1
7-1- 91.5	+	145.915	32.618	32.432	72.4	98.2
7-1-111	B	146.110	32.620	32.446	91.9	99.9
7-1-117.5	B	146.175	32.621	32.451	97.7	99.6
7-1-130.5	B	146.305	32.623	32.460	95.1	99.9
7-1-134	B	146.340	32.623	32.462	95.4	99.3
7-1-145	B	146.450	32.625	32.470	97.3	99.6
7-1-147.5	B	146.475	32.625	32.472	92.8	99.8
7-CC	B	146.500	32.625	32.474	97.2	99.9

*: B indicates a sample from a _Braarudosphaera_ ooze; + indicates a non-_Braarudosphaera_ ooze sample.

TABLE 4-3

Subbottom Depth, Age, % $CaCO_3$, % Fine Fraction, and Oxygen and Carbon Isotopic Data from DSDP Site 522

Sample c-s- z	*	sub-bottom depth (mbsf)	Corrected sub-bottom depth (mbsf)	Age (Ma, CK92)	Bulk % $CaCO_3$	% Fine Fract. (<63um)	Fine Fraction $\delta^{13}C$ (PDB)	Fine Fraction $\delta^{18}O$ (PDB)
Hole 522A								
13-1- 65	+	92.15	93.60	28.996	84.8	98.9		
13-1- 85	+	92.35	93.80	29.017	83.7	99.5	2.377	0.782
13-1- 95	B	92.45	93.90	29.027	96.6	86.9	2.407	2.479
13-1-105	B	92.55	94.00	29.038	97.3	99.4	2.345	2.374
13-1-115	B	92.65	94.10	29.048	97.1	97.9	2.253	2.246
13-1-125	B	92.75	94.20	29.058	97.2	99.2	2.190	2.097
13-1-129	B	92.79	94.24	29.062	96.8	98.2	2.364	2.303
13-1-135	+	92.85	94.30	29.068	87.8	98.4	2.389	0.970
13-1-140	+	92.90	94.35	29.073	90.8	98.5	2.393	1.207
13-2- 15	+	93.15	94.60	29.099	87.2	99.0	2.308	0.920
							2.127	0.809
13-2- 25	+	93.25	94.70	29.110	88.0	99.5	2.371	0.907
13-2- 35	+	93.35	94.80	29.120	88.3	98.4	2.456	0.989
13-2- 45	+	93.45	94.90	29.130	88.9	99.7	2.611	1.075

TABLE 4-3--continued

Sample c-s- z	*	sub-bottom depth (mbsf)	Corrected sub-bottom depth (mbsf)	Age (Ma, CK92)	Bulk % $CaCO_3$	% Fine Fract. (<63um)	Fine Fraction $\delta^{13}C$ (PDB)	Fine Fraction $\delta^{18}O$ (PDB)
Hole 522								
25-2- 38	+	93.48		28.984	85.6	99.7	1.967	0.612
25-2- 60	+	93.70		29.007	87.4	99.7	2.312	0.904
25-2- 69	+	93.79		29.016	86.3	99.7	2.274	0.764
25-2- 84	B	93.94		29.031	98.7	80.4	2.198	2.341
25-2- 90	B	94.00		29.038	98.9	96.9	2.237	2.220
25-2-100	B	94.10		29.048	98.8	94.3	2.191	2.249
25-2-117	+	94.27		29.065	89.5	99.7	2.134	0.805
25-2-138	+	94.48		29.087	86.3	99.7	2.288	0.822

*: B indicates a sample from a Braarudosphaera ooze; + indicates a non-Braarudosphaera ooze sample.

foraminifera. Note that the 1.45 m correction to the depths of Hole 522A relative to Hole 522 causes the curves of percent carbonate and percent fine fraction of both sites to be in phase (Figure 4-4), confirming the validity of the correction.

Oxygen and Carbon Isotopes

Fine fraction

Site 363. The fine fraction $\delta^{13}C$ values found in Site 363 non-Braarudosphaera oozes are generally comparable to those found in South Atlantic bulk carbonate from DSDP Legs 73 and 74 [Shackleton, 1986]; however, $\delta^{18}O$ values are up to 0.5°/oo lower, not surprising considering the more northern position of DSDP Site 363. Consistent with previous results [Wise and Hsü, 1971; Lloyd and Hsü, 1972], the $\delta^{18}O$ values of fine fraction within the layers of Braarudosphaera oozes was greater than fine fraction outside of the Braarudosphaera oozes. The difference in fine fraction $\delta^{18}O$ inside and outside of Braarudosphaera oozes was greatest in Core 7 of Site 363 (1.46 °/oo), and decreased up-section (Appendix A5, Figure 4-3). Fine fraction $\delta^{18}O$ values average 0.79°/oo greater within the Braarudosphaera ooze in Core 6 than in sediments on either side, and 0.58°/oo greater within the two Braarudosphaera oozes in Core 5 than in sediments on either side of the oozes. Fine fraction $\delta^{13}C$ values within Braarudosphaera oozes also generally increased relative to fine fraction outside of the Braarudosphaera oozes, with the largest increase in Core 7 as well ($1.54^{o}/oo$), decreasing to $0.55^{o}/oo$ in Core 6. Within Core 5, fine fraction $\delta^{13}C$ values are essentially the same throughout the sequence, with the Braarudosphaera ooze $\delta^{13}C$ values at $0.01^{o}/oo$ less than the non-Braarudosphaera sediments. Often, $\delta^{18}O$ and $\delta^{13}C$ values increased over several tens of centimeters below the Braarudosphaera oozes, reached maxima within the Braarudosphaera oozes, and decreased over several tens of centimeters above the Braarudosphaera oozes, rather than having a sharp isotopic demarcation between Braarudosphaera oozes and non-Braarudosphaera oozes.

Site 522. The behavior of fine fraction $\delta^{18}O$ in Site 522 was similar to that in Site 363. Within the Braarudosphaera ooze, $\delta^{18}O$ averaged $2.29^{o}/oo$, $1.40^{o}/oo$ greater than the average $\delta^{18}O$ value of $0.89^{o}/oo$ above and below the Braarudosphaera ooze (Table 3, Figure 4-4). The behavior of fine fraction $\delta^{13}C$ in Site 522, however, is quite different from that in Site 363. In Site 522, for reasons which are not understood, no significant variability in $\delta^{13}C$ occurs, averaging $2.27^{o}/oo$ within the Braarudosphaera ooze and $2.31^{o}/oo$ in the non-Braarudosphaera sediments.

Foraminifera

Site 363. In general, results of $\delta^{18}O$ and $\delta^{13}C$ analyses of foraminifera (Appendix A5) confirm results from previous studies [Poore and Matthews, 1984, Boersma and

Premoli-Silva, 1986]. The benthic foraminiferal genus Cibicidoides consistently gave the lowest $\delta^{13}C$ values (averaging 0.90±0.27^{o}/oo (1σ)) and highest $\delta^{18}O$ values (1.36±0.28^{o}/oo), confirming its benthic habitat. Conversely, Chiloguembelina cubensis was measured with the highest $\delta^{13}C$ values (averaging 1.51±0.43^{o}/oo) and lowest $\delta^{18}O$ values (0.10±0.47^{o}/oo), consistent with its reported shallow planktic habitat. Measurement of the isotopic composition of Catapsydrax dissimilis resulted in intermediate $\delta^{13}C$ (1.10±0.32^{o}/oo) and $\delta^{18}O$ (0.85±0.34^{o}/oo) values, consistent with a deep-living planktic habitat. $\delta^{13}C$ values of C. dissimilis were only slightly higher than Cibicidoides $\delta^{13}C$ values, suggesting that only a small $\delta^{13}C$ gradient existed between the depth habitat of C. dissimilis and the seafloor.

Little in the way of long term trends is visible throughout this record (Figure 4-3). A slight increase in $\delta^{18}O$ values of C. dissimilis seems to be present up-section, accompanied by a slight decrease in $\delta^{13}C$ values. A similar trend is not visible in analyses of C. cubensis or Cibicidoides.

Chiloguembelina cubensis. Despite suggestions that planktic foraminifera live in progressively deeper water as they develop ontogenetically, no consistent relationship between size fraction of C. cubensis and $\delta^{18}O$ or $\delta^{13}C$ was observed (Appendix A5, Figure 4-3). This suggests that either different size fractions of C. cubensis calcify at the same water depth, or that the size fractions were not sufficiently different to observe these differences.

With the possible exception of Core 7, no significant difference between C. cubensis $\delta^{18}O$ or $\delta^{13}C$ values from within and outside of Braarudosphaera oozes was observed (Figure 4-3). In core 5, the $\delta^{18}O$ values of samples from within the two Braarudosphaera oozes averaged 0.06°/oo greater than the non-Braarudosphaera sediments, while $\delta^{13}C$ values were 0.19°/oo greater in the Braarudosphaera oozes. In core 6, the C. cubensis $\delta^{18}O$ values of the Braarudosphaera ooze averaged 0.02°/oo greater than the non-Braarudosphaera sediments, while $\delta^{13}C$ values were 0.20°/oo lower in the Braarudosphaera oozes. Because of a lack of specimens, no C. cubensis analyses were possible within the Core 7 Braarudosphaera ooze. Instead, bulk planktic foraminifera from the 125-150μm size fraction were measured. Above the Braarudosphaera ooze, $\delta^{18}O$ values of the bulk planktic foraminifera (0.10°/oo) were similar to those measured from C. cubensis (0.18°/oo). However, within the Braarudosphaera ooze, $\delta^{18}O$ values were larger and more variable, at 1.12±0.66°/oo (1σ). In the interval above the Braarudosphaera ooze, bulk planktic $\delta^{13}C$ values were somewhat lower (1.00°/oo) than C. cubensis $\delta^{13}C$ values (1.63°/oo), and were variable and slightly higher within the Braarudosphaera ooze (1.28±0.73°/oo). Unfortunately, as is always the case when multiple taxa are measured, it is unclear whether this is a result of changing faunas or changes in isotopic response.

Catapsydrax dissimilis. Analyses of the isotopic composition of C. dissimilis, as noted above, show a slight increasing trend in $\delta^{18}O$ and decreasing trend in $\delta^{13}C$ (Appendix A5, Figure 4-3). Most of the change occurs in Core 7. The $\delta^{18}O$ of C. dissimilis in the upper part of core 7 (0.71±0.31^{o}/oo) is 0.52^{o}/oo greater than in the lower part (which contains the Braarudosphaera ooze; 0.19±0.18^{o}/oo), opposite the trend seen in the fine fraction. The $\delta^{13}C$ of C. dissimilis in the upper part of core 7 is 0.34^{o}/oo lower than in the lower part, similar to the trend seen in the fine fraction. In the other cores, differences between Braarudosphaera ooze and non-Braarudosphaera ooze C. dissimilis $\delta^{18}O$ and $\delta^{13}C$ analyses are within one standard deviation of each other. Between cores, however, average $\delta^{13}C$ values increase (1.31±0.22^{o}/oo to 1.21±0.10^{o}/oo to 0.64±27^{o}/oo for cores 7, 6, and 5, respectively). Average $\delta^{18}O$ values in Cores 5 and 6 are the same (0.96±0.27^{o}/oo and 1.00±0.14^{o}/oo, respectively), and increased relative to Core 7 (0.48±0.37^{o}/oo).

Cibicidoides. The benthic $\delta^{18}O$ and $\delta^{13}C$ record from Cibicidoides shows the same low variability seen in the planktic records of C. cubensis and C. dissimilis relative to the fine fraction records (Appendix A5, Figure 4-3). Overall, Cibicidoides $\delta^{18}O$ values were extremely constant, at 1.32±0.20^{o}/oo, 1.35±0.32^{o}/oo, and 1.41±0.29^{o}/oo for Cores

7, 6, and 5, respectively. Cibicidoides $\delta^{13}C$ values decreased slightly up section from 1.04±0.33^{o}/oo to 0.97±0.13 to 0.61±0.16^{o}/oo for Cores 7, 6, and 5, respectively. Within each core, no consistent trend between $\delta^{18}O$ values within and outside of the Braarudosphaera oozes was observed, with differences all within one standard deviation of each other. However, while in Cores 5 and 6 the same was true for $\delta^{18}O$, in Core 7, Cibicidoides $\delta^{18}O$ within the Braarudosphaera ooze was 0.56^{o}/oo greater than in Cibicidoides above the Braarudosphaera ooze. This trend is similar to that seen in the C. dissimilis $\delta^{13}C$ results.

Site 522. As previously stated, due to the clear evidence of alteration of foraminifera within Site 522, and the general low abundance of foraminifera (especially C. cubensis), no isotopic analyses of Site 522 foraminifera were performed.

Strontium Isotopes

Within each core, $^{87}Sr/^{86}Sr$ values were very consistent, averaging 0.707867±0.000022 (1σ), 0.707915±0.000013, and 0.707971±0.000023 for Hole 363, cores 7, 6, and 5, respectively, and 0.708018±0.000019 for Hole 522A, core 13 (Table 4-4). Ages were calculated from these values using the $^{87}Sr/^{86}Sr$ to age model of Chapter 2, and uncertainties were calculated based on the number of samples measured within each core using the statistical technique outlined in Chapter 2.

TABLE 4-4

Strontium isotopic data from DSDP Sites 363 and 522

Hole	C - S	Avg Int.	*	Avg. Depth (mbsf)	$^{87}Sr/^{86}Sr$	Age (Ma,CK92)	Model Age (Ma,CK92)
363	5 - 2	34.5	+	108.85	0.708001	28.594	29.076
363	5 - 2	65	+	109.15	0.707955	28.606	30.236
363	5 - 2	70	B	109.20	0.707977	28.608	29.681
363	5 - 2	80.5	B	109.31	0.707951	28.613	30.337
363	6 - 3	54	+	129.54	0.707917	32.049	31.194
363	6 - 3	90	B	129.90	0.707905	32.114	31.497
363	6 - 3	97.5	B	129.98	0.707905	32.129	31.497
363	6 - 3	105	B	130.05	0.707916	32.141	31.219
363	6 - 3	105	B	130.05	0.707928	32.141	30.917
363	6 - 3	125.5	B	130.25	0.707903	32.177	31.547
363	6 - 3	141	+	130.41	0.707937	32.206	30.690
363	6 - 4	15	+	130.65	0.707905	32.250	31.497
363	7 - 1	50.5	+	145.51	0.707895	32.575	31.749
363	7 - 1	69	+	145.69	0.707861	32.578	32.606
363	7 - 1	90	+	145.90	0.707883	32.581	32.051
363	7 - 1	111	B	146.11	0.707853	32.584	32.808
363	7 - 1	130.5	B	146.31	0.707842	32.587	33.085

TABLE 4-4--continued

Hole	C - S	Avg Int.	*	Avg. Depth (mbsf)	$^{87}Sr/^{86}Sr$	Age (Ma,CK92)	Model Age (Ma,CK92)
522A	13 - 1	105	B	92.55	0.708005	29.038	28.975
522A	13 - 1	125	B	92.75	0.708032	29.058	28.294

Averages:	Average Depth (mbsf)	Average $^{87}Sr/^{86}Sr$	Average Age (Ma,CK92)	Model Age (Ma,CK92)
Core 363-5	109.08	0.707971	28.603	29.832±0.538
Core 363-6	130.10	0.707915	32.149	31.257±0.393
Core 363-7	145.91	0.707867	32.581	32.460±0.495
Core 522A-13	92.65	0.708018	29.048	28.635±0.754

*: B indicates a sample from a Braarudosphaera ooze while + indicates a non-Braarudosphaera ooze sample.
Age: Age calculated from calcareous nannofossil biostratigraphy (Site 363) or magnetostratigraphy (Site 522).
Model Age: Age calculated from $^{87}Sr/^{86}Sr$ age model of Chapter 2.
Average Model Ages: The uncertainty listed is the 95% confidence interval as calculated using the technique of Miller et al. [1991] as modified in Chapter 2, which is based on the number of analyses. A linear regression of these averages was used to construct the age model for Site 363, and gives a sedimentation rate of 1.41 m/m.y.

The results suggest a linear sedimentation rate in Site 363 of 14.06 m/m.y. (Figure 4-5). The ages for cores 5 and 6 are not compatible with ages calculated from nannofossil biostratigraphy (Table 4-4; see Age Model below), being 29.83±0.54 Ma and 31.26±0.39 Ma for cores 5 and 6 respectively, vs. nannofossil ages of about 28.6 Ma and 32.1 Ma for cores 5 and 6 respectively. The age calculated for core 7 (32.46±0.50 Ma) and for core 13 of Hole 522A (28.63±0.0.75 Ma) agree within uncertainty with the nannofossil age of core 7 (32.6 Ma) and the magnetostratigraphic age of core 13 (29.05 Ma).

Scanning Electron Microscopy

The sample of Braarudosphaera ooze from Core 7 of Site 363 contained no complete pentaliths, only the quadrangular fragments of them, but in large numbers (Figure 4-6a,b). A few placoliths from coccolithophores were also present, which were well preserved. This contrasts with the sample above the Braarudosphaera ooze in Core 7, which contained primarily poorly preserved coccolithophore placoliths (Figure 4-6d). Both samples from Core 7 also contained common aggregates of platy crystals termed "lepispheres" (Figure 4-6c) which have been previously identified from Braarudosphaera oozes but not from the normal oozes surrounding them [Wise and Kelts, 1972; Lloyd and Hsü, 1972].

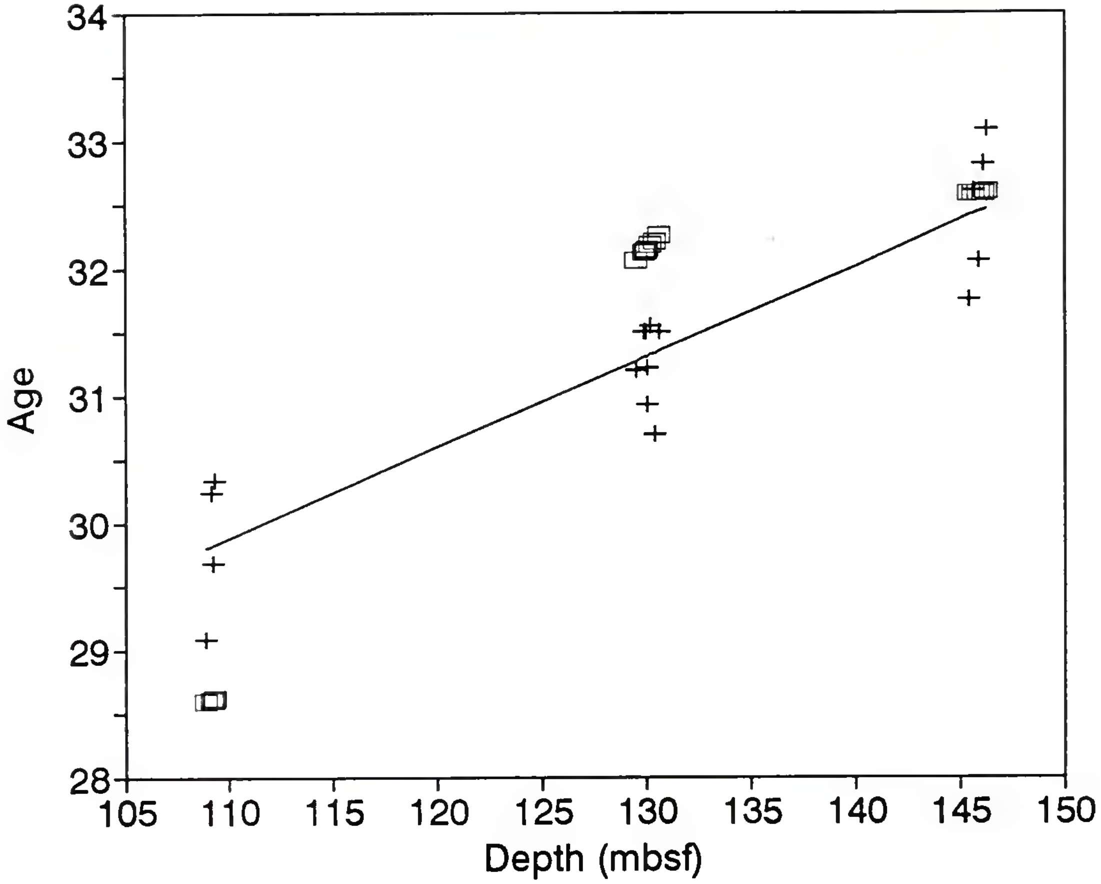

Figure 4-5: Ages (according to Cande and Kent [1992]) defined from $^{87}Sr/^{86}Sr$ stratigraphy and calcareous nannofossil biostratigraphy plotted vs. subbottom depth in Site 363. Note that the $^{87}Sr/^{86}Sr$ ages suggest a linear sedimentation rate. Biostratigraphic ages are indicated by boxes, and $^{87}Sr/^{86}Sr$ ages are indicated by plus signs (+).

The samples from Cores 6 (Figure 4-7) and 5 (Figure 4-8) of Site 363 were similar. Within the Braarudosphaera oozes, the most common grains were fragmentary Braarudosphaera pentaliths, with, however, frequent complete pentaliths (Figures 4-7a,b, 8a,b). Placoliths were somewhat more common in the Core 5 Braarudosphaera ooze, consistent with the less extreme carbonate and isotopic values obtained from it (Figure 4-8a,b). Above the Braarudosphaera oozes, well preserved placoliths were dominant, with a few scattered whole and fragmentary Braarudosphaera pentaliths. A few discoasters were present in both samples from Core 5, which exhibited calcareous overgrowths (Figure 4-8a,c). These overgrowths have been identified previously in samples from a DSDP Site 22 Braarudosphaera ooze [Wise and Kelts, 1972].

Age Models

Site 363

The depths of nannofossil datums in Proto-Decima et al. [1978] were used as the boundaries for the nannofossil zones NP22 through NP24. Ages were picked from Hsü et al. [1984a], who used the magnetostratigraphy of Tauxe et al. [1984], and converted to the Cande and Kent [1992] time scale. Sedimentation was assumed to be linear between these tie points, and ages were calculated with linear interpolation. A second set of ages was calculated using $^{87}Sr/^{86}Sr$ stratigraphy, and calculated using an assumption of a linear sedimentation rate through the entire section. This

Figure 4-6: DSDP Site 363, core 7, section 1. (a) 144-146 cm x1783; (b) 114-117 cm x810. Note the complete absence of *Braarudosphaera* pentaliths but the dominance of quadrangular pentalith fragments. (c) 67-71 cm x891; (d) 67-71 cm x1216. *Braarudosphaera* fragments are much less common while placoliths are dominant in this sample from outside the *Braarudosphaera* ooze. Note also in (c) the presence of lepispheres about 10μm in diameter.

Figure 4-7: DSDP Site 363, core 6, section 3. (a) 114-117 cm x2030; (b) 114-117 cm x568. Note a complete *Braarudosphaera* pentaliths surrounded dominantly by quadrangular pentalith fragments. (c) 74-77 cm x609. This sample from above the *Braarudosphaera* ooze still contains some pentaliths and pentalith fragments but in far fewer numbers than the from within the *Braarudosphaera* ooze. The sample is dominated by placoliths.

Figure 4-8: DSDP Site 363, core 5, section 2. (a) 69-75 cm x1778; (b) 69-75 cm x606. The concentration of complete and fragmented Braarudosphaera pentaliths is lower in this sample even though it is also from a Braarudosphaera ooze. (c) 59-61 cm x606. Pentalith fragments are less common in this sample from above a Braarudosphaera ooze. Note also the presence of discoasters with crystal overgrowths in this sample and the sample from 69-75 cm.

assumption is justified by the high regression coefficients (0.998, calculated from a linear regression of the depth vs. average $^{87}Sr/^{86}Sr$, or 0.845 from depth vs. all $^{87}Sr/^{86}Sr$ data, with depth as the independent variable). The regression from the averaged data was used to construct the age model, although the regression from all $^{87}Sr/^{86}Sr$ data gives ages within 21 kyr of the averaged-data age model. The average sedimentation rate calculated in this way is 1.41 cm/yr, or 14.1 m/m.y.

It is not clear why ages calculated from nannofossil biostratigraphy [Proto-Decima et al., 1978] are so different from ages calculated using $^{87}Sr/^{86}Sr$ stratigraphy of Site 363. The depths of the nannofossil datums used are well constrained, so uncertainty in depth cannot be a factor. It has been shown that some nannofossil datums at higher latitudes are diachronous [Wei, 1991; Wei and Wise, 1992], and one of these (Reticulofenestra umbilica) is a marker for the NP22/NP23 boundary. The other datums were not discussed in Wei [1991] and Wei and Wise [1992], so it is not possible to evaluate the presence or absence of diachroneity of those datums. In any case, the latitudes of Site 363 and Site 522 differ by only a few degrees. I tentatively use the linear regression of the $^{87}Sr/^{86}Sr$ data for the age model.

Site 522

An excellent magnetostratigraphy of this site allows reliable dating to the geomagnetic polarity time scale [Tauxe et al., 1984]. The age model of Mead et al. [1986]

was used, with ages of polarity intervals calibrated to the Cande and Kent [1992] time scale. In the part of the section containing the Braarudosphaera ooze, the sedimentation rate averages 0.97 cm/ky or 9.7 m/m.y.

Durations of Braarudosphaera oozes

The durations of the sampled sections are very short, consistent with the small range of variability exhibited in the $^{87}Sr/^{86}Sr$ data. Within Hole 363, the times represented by the sampled parts of cores 7 (100 cm), 6 (111 cm), and 5 (46 cm) were only 71, 79, and 33 kyr, respectively, assuming constant sedimentation rates. The sampled part of Core 25 of Hole 522 and Core 13 of Hole 522A (142 cm) was 146 kyr in duration.

An assumption of constant sedimentation within these sections is probably an oversimplification, as the high carbonate content of the Braarudosphaera oozes suggests accelerated sedimentation. I estimate the change in sedimentation rates by assuming (1) that the sedimentation rate for the non-carbonate fraction is constant and (2) that the density of the carbonate and non-carbonate fractions are constant. In this case, the rate of non-carbonate deposition can be calculated as follows:

$$R_{nC} = \frac{(Z_B * FF_{CS} + Z_S * FF_{CB}) * R_{avg}}{FF_{CB} * FF_{CS} * Z_T} \qquad (1)$$

where R_{nC} is the rate of non-carbonate deposition, Z_B and Z_S are the thicknesses of the Braarudosphaera oozes and normal sediments, respectively, (Z_T/R_{avg}) is the total thickness of the section in question (in this case, the thickness of the sampled section) divided by the average sedimentation rate (e.g., the total length of time represented by Z_T). FF_{CB} and FF_{CS} are factors calculated from the average fraction of carbonate in the Braarudosphaera ooze and normal sediments, respectively:

$$FF_{CM} = \frac{1}{1 - f_{CM}} \qquad (2)$$

where f_{CM} is the carbonate fraction of layer M (i.e., $\%CaCO_3/100$). When R_{nC} is calculated, the rate of carbonate accumulation R_{CM} in a layer M can be calculated:

$$R_{CM} = \frac{f_{CM}}{1 - f_{CM}} * R_{nC} \qquad (3)$$

The total sedimentation rate in layer M is $R_{TM} = R_{CM} + R_{nC}$, and it is a simple matter to calculate the length of time necessary to deposit a layer, given its thickness (see Appendix B5 for derivations of equations 1 to 3).

The results of these calculations do indeed show accelerated sedimentation rates during Braarudosphaera ooze deposition (Table 4-5). The sedimentation rates in the Site 363, Core 5, 6, and 7 Braarudosphaera oozes rise 28%, 72%, and 216%, respectively, over the average 1.41 cm/kyr rate derived from linear regression, while the corresponding non-Braarudosphaera ooze sedimentation rates drop by 15%, 23%, and 46%, respectively. The non-carbonate sedimentation rates as calculated for the three cores are low and only differ by 60%, fairly small in comparison to the changes seen in the carbonate sedimentation rates, and suggests that the approximation of constant non-carbonate sedimentation rates are valid. The sedimentation rate in the Site 522 Braarudosphaera ooze jumps by 306% over the average sedimentation rate of 0.97 cm/kyr derived from magnetostratigraphy, and the non-carbonate sedimentation rate is distinctly lower than in Site 363, perhaps a reflection of its more distal position from the African continent.

In all cases, no matter which type of calculation is used, the durations of the events causing deposition of the Braarudosphaera oozes are short. Using constant sedimentation rates, the durations range from 7.1 kyr to 46.4 kyr. Using non-constant sedimentation rates, the durations range only between 5.5 kyr and 18.6 kyr (Table 4-5).

TABLE 4-5

Calculations of Braarudosphaera Sedimentation Rates Based on %$CaCO_3$

		Hole: 363			522/522A
	Units	Core: 5*	6	7	25/13
Avg. Sed. Rate	(cm/kyr)	1.406	1.406	1.406	0.9703
Overall Section Thickness	(cm)	46	111	100	142
Overall Section Duration	(kyr)	33	78	71.12	146.35
Braarudo. Thickness	(cm)	20	45	55	45
non-Braarudo. Thickness	(cm)	26	66	45	97
Avg. %$CaCO_3$, Braarudo.	(%)	82.4	91.7	95.3	97.7
Avg. %$CaCO_3$, non-Braarudo.	(%)	73.5	81.6	72.8	87.3
Braarudo. $CaCO_3$ factor		5.678	12.048	21.427	42.992
non-Braarudo. $CaCO_3$ factor		3.773	5.435	3.675	7.847
non-$CaCO_3$ Sed. Rate	(cm/kyr)	0.318	0.201	0.208	0.092
Braa. $CaCO_3$ Sed. Rate	(cm/kyr)	1.489	2.222	4.254	3.847
Braa. Total Sed. Rate	(cm/kyr)	1.807	2.423	4.462	3.939

TABLE 4-5--continued

		Hole:	363			522/522A
	Units	Core:	5*	6	7	25/13
non-Braa. $CaCO_3$ Sed. Rate	(cm/kyr)		0.883	0.892	0.557	0.627
non-Braa. Total Sed. Rate	(cm/kyr)		1.201	1.093	0.765	0.719
Duration of Braarudo., Constant Sed. Rate	(kyr)		14.2	32.0	39.1	46.4
Duration of Braarudo., non-Const. Sed. Rat	(kyr)		11.1	18.6	12.3	11.4

*: Core 5 contains two 10 cm Braarudosphaera oozes; the duration of each is half of the listed value.

Discussion

Cause of Fine Fraction $\delta^{18}O$ and $\delta^{13}C$ Excursions

A comparison of the foraminiferal and fine fraction isotopic compositions is revealing. Foraminiferal isotopic rankings are as expected, with lowest $\delta^{13}C$ values and highest $\delta^{18}O$ values in benthic (Cibicidoides) foraminiferal calcite, and progressively higher $\delta^{13}C$ and lower $\delta^{18}O$ values in shallower living planktic foraminifera. This is due to the effects of biological pumping of organic carbon to deep water and of lower deep water temperatures, respectively. Within and between each core, however, there is little variation in the isotopic composition of each foraminiferal component, implying that little change in physical parameters occurred over the time represented by this sequence. Fine fraction isotopic behavior is very different, however. The extremes of $\delta^{13}C$ and $\delta^{18}O$ values of fine fraction outside of Braarudosphaera oozes are similar to or slightly greater than those of Chiloguembelina cubensis, although because of the gradual increase below and gradual decrease above the Braarudosphaera oozes of isotopic values, the average $\delta^{13}C$ and $\delta^{18}O$ values of fine fraction in non-Braarudosphaera oozes are somewhat greater than those of Chiloguembelina cubensis. However, within the Braarudosphaera oozes, in every case, fine fraction $\delta^{18}O$ (as noted in earlier studies) and $\delta^{13}C$ rise. In cores 6 and 7 of Site 363, the $\delta^{18}O$ values rise to nearly 1^{o}/oo more than maximum foraminiferal (benthic) values, while the $\delta^{13}C$ values rise to as much as $1^{o}/oo$ and $1.5^{o}/oo$ in cores 6 and 7, respectively. The increases also occur within the Braarudosphaera oozes within core 5 of Site 363, but are of lesser magnitude. As a general rule, the $\delta^{13}C$ and $\delta^{18}O$ values of fine fraction are linearly correlated with percent $CaCO_3$, while foraminiferal isotopic data are uncorrelated with percent $CaCO_3$ (Figure 4-9).

There are three ways in which the fine fraction isotopic values may be interpreted. They may be interpreted as resulting from seafloor diagenesis, from vital effects due to changing floral assemblages or changing rates of productivity, or due to paleoceanographic effects.

The first possibility, that $\delta^{18}O$ values are due to a diagenetic effect, with recrystallization of fine fraction giving $\delta^{18}O$ values characteristic of deep water, is more likely in Core 7, because it has the largest isotopic enrichment and because diagenetic overgrowths on Braarudosphaera pentaliths have been observed [Noël and Melguen, 1978]. The fact that the $\delta^{18}O$ of the fine fraction is up to $1^{o}/oo$ greater than the $\delta^{18}O$ of Cibicidoides (in Core 7) does not necessarily argue against this hypothesis, because Cibicidoides is known to fractionate oxygen isotopes by from $0.64^{o}/oo$ [Shackleton and Opdyke, 1973] to $1.02^{o}/oo$ [Graham et al., 1981] less than equilibrium values. If the smaller value ($0.64^{o}/oo$) is accepted, then seafloor diagenesis can be ruled out, because the fine fraction $\delta^{18}O$

Figure 4-9: Isotopic results from Site 363 plotted against percent $CaCO_3$. Legend as in Figure 4-3, except that fine fraction analyses also indicate the core from which they were taken. Note that no consistent relationship to $CaCO_3$% is visible except for the fine fraction $\delta^{13}C$ and $\delta^{18}O$, which increase as $CaCO_3$% increases. a: $\delta^{13}C$ vs $CaCO_3$%. b: $\delta^{18}O$ vs $CaCO_3$%.

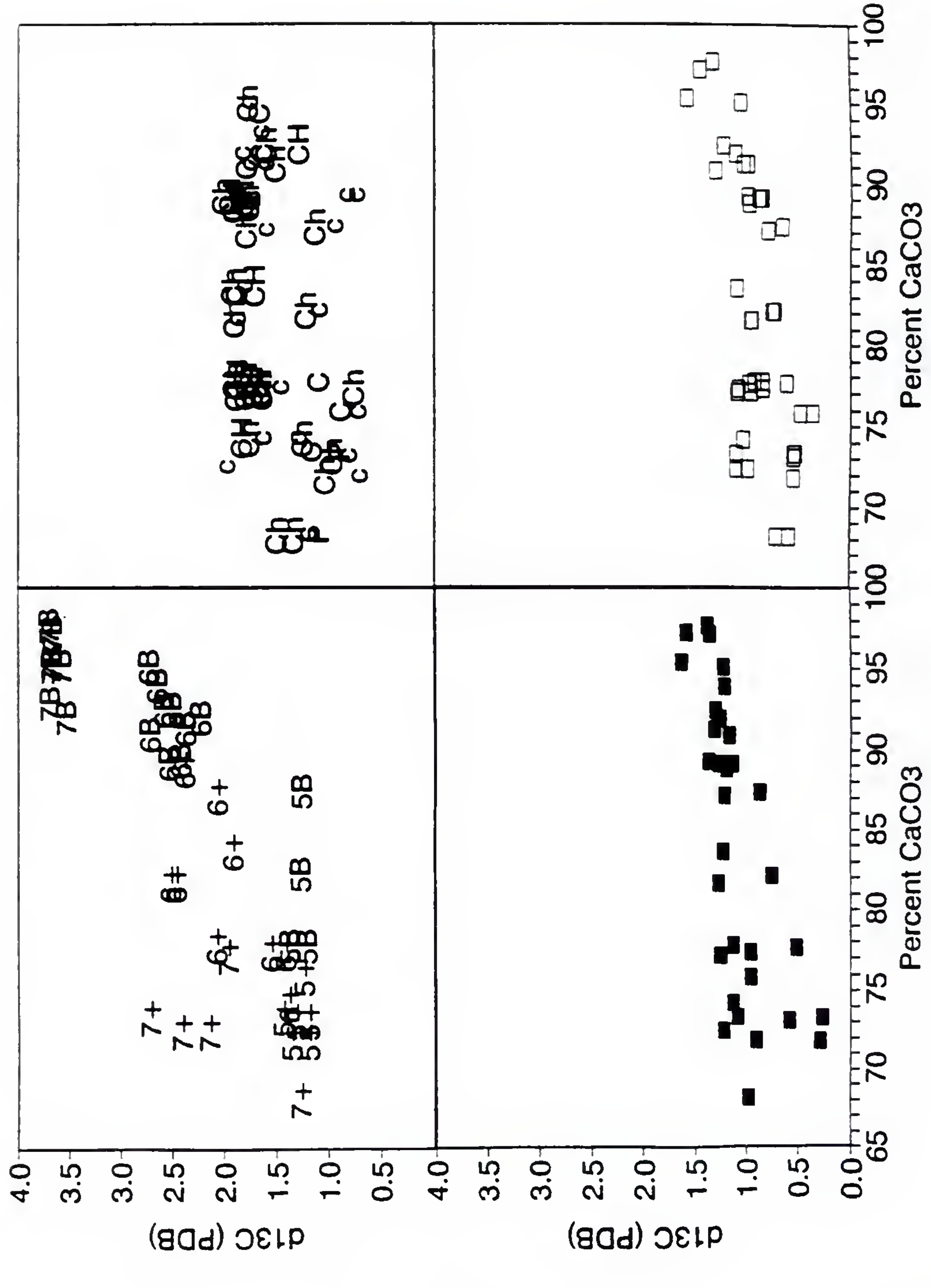
d13C (PDB)
d13C (PDB)
4.0
3.5
3.0
2.5
2.0
1.5
1.0
0.5
0.0
Percent CaCO3
Percent CaCO3
65
70
75
80
85
90
95
100
7B
6B
5B
7+
6+
5+
Ch
CH
C
c
P

Figure 4-9--continued

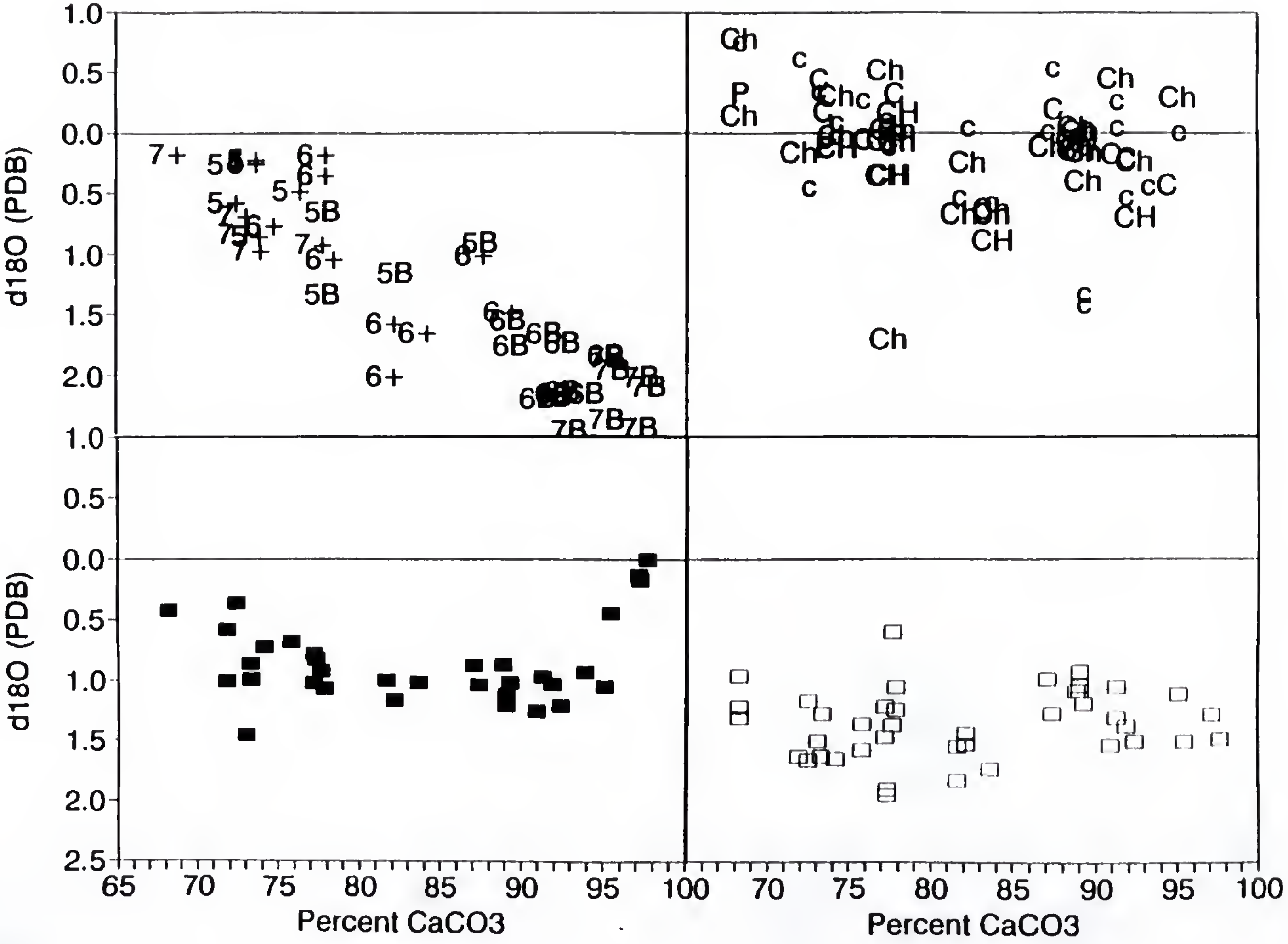

values remain greater than equilibrium Cibicidoides values. However, adding 1.02^{o}/oo to the Cibicidoides measurements (Figure 4-10) brings the fine fraction and benthic $\delta^{18}O$ values of Core 7 into correspondence, allowing seafloor diagenesis of the fine fraction to be a viable hypothesis. In the SEM examination of the Core 7 Braarudosphaera ooze, no overgrowths were observed except on the few discoasters present (Figure 4-6). If the high $\delta^{18}O$ values were due to diagenesis, extensive diagenetic effects should be visible. The lack of pervasive calcitic overgrowths on nannofossils observed with the SEM in either of the other two cores (Figures 4-7, 4-8), with lower $\delta^{18}O$ values within the Braarudosphaera oozes, is additional evidence against seafloor diagenesis. In addition, the lack of any apparent diagenetic effect on the planktonic foraminifera argue against this. Furthermore, examination of the $\delta^{13}C$ record gives little evidence of seafloor diagenesis. If seafloor diagenesis were responsible for the increase in $\delta^{18}O$ values within the Braarudosphaera oozes, a convergence of fine fraction $\delta^{13}C$ with the benthic $\delta^{13}C$ record might also be expected. Seawater has much less carbon than oxygen in it, and thus in general diagenetic effects on carbon isotopes are less pervasive than on oxygen isotopes. However, we might at least expect $\delta^{13}C$ values of the fine fraction to drift in the direction of benthic (low) $\delta^{13}C$ values. Failing that, we would expect fine fraction to track with planktic foraminiferal $\delta^{13}C$ values. Instead, fine fraction

Figure 4-10: Isotopic results from DSDP Site 363 cores 5, 6, and 7, plotted against age derived from $^{87}Sr/^{86}Sr$ stratigraphy. (a), (c), and (e): $\delta^{13}C$ and $\%CaCO_3$. (b), (d), and (f): $\delta^{18}O$ and % fine fraction. (a) and (b), (c) and (d), and (e) and (f) are cores 5, 6, and 7, respectively. Cibicidoides is corrected by $1.02^{o}/oo$ to give equilibrium values. See Figure 4-3 for legend.

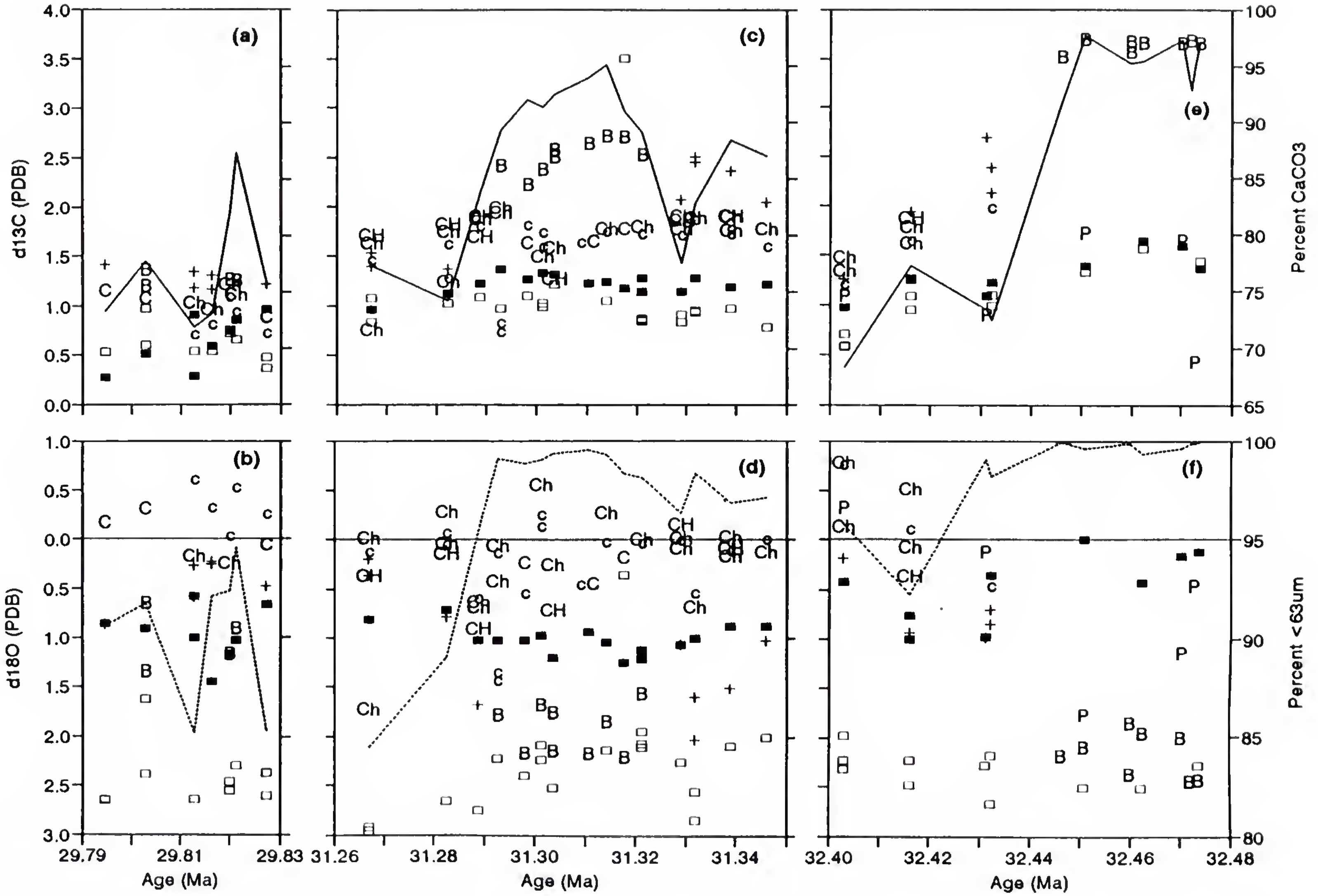
(a)
(b)
(c)
(d)
(e)
(f)
d13C (PDB)
4.0
3.5
3.0
2.5
2.0
1.5
1.0
0.5
0.0
d18O (PDB)
1.0
0.5
0.0
0.5
1.0
1.5
2.0
2.5
3.0
Percent CaCO3
100
95
90
85
80
75
70
65
Percent <63um
100
95
90
85
80
29.79
29.81
29.83
31.26
31.28
31.30
31.32
31.34
32.40
32.42
32.44
32.46
32.48
Age (Ma)
Age (Ma)
Age (Ma)
C
B
Ch
CH
c
P
+

$\delta^{13}C$ values rise to values as much as 1.8°/oo greater than planktic $\delta^{13}C$ values, which cannot be explained as a result of diagenesis.

Since the transition into and out of Braarudosphaera oozes by definition involves large changes in the fine fraction floral assemblage, another possibility to be considered is that different vital effects are responsible for the changes seen in the oxygen isotope composition of the fine fraction. The fact that percent $CaCO_3$, percent fine fraction ($<63\mu m$), $\delta^{13}C$, and $\delta^{18}O$ are strongly correlated suggests that $\delta^{13}C$ and $\delta^{18}O$ of fine fraction may be controlled by vital effects, and that the magnitude of the vital effect on $\delta^{13}C$ and $\delta^{18}O$ signals in the Braarudosphaera oozes is controlled by the proportion of Braarudosphaera pentaliths in the fine fraction. Covariance of $\delta^{13}C$ and $\delta^{18}O$ in coccolithophoridae has been observed previously [Paull and Theirstein, 1987]. Covariance in biogenic carbonates has also been observed in several calcite-precipitating taxa, including corals, foraminifera, echinoids, and calcareous algae during rapid skeletonogenesis as a "kinetic" vital effect [McConnaughey, 1989a,b]. However, this type of vital effect invariably results in depleted $\delta^{13}C$ and $\delta^{18}O$ values as the rate of calcification increases. Since the most rapid production of calcite is probably within the Braarudosphaera oozes, when $\delta^{13}C$ and $\delta^{18}O$ values are enriched relative to the other sediments rather than depleted, it is unlikely that kinetic vital effects are responsible for the trends seen in these isotopic data. Metabolic enrichment of $\delta^{13}C$ ratios are indeed seen in photosynthetic organisms, but no equivalent effect is seen in $\delta^{18}O$ [McConnaughey, 1989a,b]. This analysis is complicated by the fact that there are clearly assemblage changes between the Braarudosphaera oozes and non-Braarudosphaera ooze, whereas the productivity-induced depletion in $\delta^{18}O$ and $\delta^{13}C$ refers to single taxa. With respect to different taxa, both culture studies [Dudley and Goodney, 1979; Dudley et al., 1980] and studies of different size fractions within the fine fraction [Paull and Theirstein, 1987] indicate taxon-specific vital effects in both $\delta^{13}C$ and $\delta^{18}O$. These effects also form a positive correlation between $\delta^{13}C$ and $\delta^{18}O$, so it may be difficult to separate productivity effects, paleoceanographic effects, and taxon-specific vital effects.

Paleoceanographic Considerations

The covariance of percent $CaCO_3$, percent fine fraction ($<63\mu m$), $\delta^{13}C$, and $\delta^{18}O$ may also be due to response to varying intensities of the paleoceanographic conditions leading to a Braarudosphaera ooze. We may next examine paleoceanographic changes as an alternative to diagenesis and vital effects as controls on Braarudosphaera $\delta^{13}C$ and $\delta^{18}O$ values. Given the ecological preferences of Braarudosphaera and the isotopic patterns observed, two effects will be examined here: runoff of cold, low salinity water, and upwelling of cold, low salinity mid-waters.

The foraminiferal record is characterized by its uniformity rather than its variability through this section, leaving little evidence of possible causes of the Braarudosphaera oozes. In fact, the uniformity of the foraminiferal isotope record suggests that little in the way of oceanographic changes occurred during the times of Braarudosphaera ooze deposition. We can, however, discuss suggested causes in the context of the foraminiferal record, as these possible causes should have left isotopic traces.

There is little evidence for decreased near-surface salinity due to continental runoff during the time when Braarudosphaera oozes were deposited. In this case, the oxygen isotopic composition of near-surface waters (and hence near-surface planktic foraminifera) would tend to decrease during mixing of normal marine surface water with low-$\delta^{18}O$ fresh water. The only possible way for this to be a viable hypothesis would be if a cooling (about 4°C for every $1^{o}/oo$ decrease in surface water $\delta^{18}O$ composition [Shackleton, 1974]) was coupled with a decrease in salinity. Salinity and seawater isotopic composition are empirically related by the ratio of about 1.6 ppt/$1^{o}/oo$ [Railsback et al., 1989]. This means that a coupling of a 4.38°C temperature drop [Shackleton, 1974] with a salinity decrease of 1.6 ppt, would be needed to result in a net $0^{o}/oo$ change in isotopic composition of planktic foraminifera growing within that water.

Given these parameters, we can calculate the amount of freshwater input allowable. We can use the equation of Shackleton [1974]

$$T = 16.9 - 4.38(\delta_c - \delta_o) + 0.10(\delta_c - \delta_o)^2 \qquad (4)$$

to calculate temperature of the surface water to be 12.6°C given an assumed Oligocene seawater $\delta^{18}O$ of $-0.85^o/oo$ (see chapter 3) and the average $\delta^{18}O$ of surface planktic foraminifera (Chiloguembelina) of about 0.15 [this study].

Africa has drifted about 10° north since the Oligocene [Tauxe et al., 1983]. That would place DSDP Site 363 at about 30°S at the time of the deposition of the Braarudosphaera oozes. Assuming normal salinity of about 34.5 ppt [Pickard and Emery, 1982] at this paleolatitude, we can then calculate temperature, salinity, and seawater $\delta^{18}O$ for varying inputs of fresh water ($\delta^{18}O = -21^o/oo$, salinity = 0). Holding planktic foraminiferal $\delta^{18}O$ constant, a temperature of 0°C is reached at a seawater $\delta^{18}O$ of $-4.07^o/oo$ according to Equation 4, implying 16.3% fresh water and a salinity of 28.9 ppt. Since fresh water cannot reach temperatures of less than 0°C, a cooling to 0°C through mixing alone is impossible. This implies that if a decrease in surface salinity is responsible for the production of Braarudosphaera oozes, additional cooling would have to have taken place to keep planktic foraminiferal $\delta^{18}O$ values constant. Even if temperatures do not reach 0°C, the curve of the temperature vs. freshwater input demands additional cooling.

As an alternative to runoff of fresh water, the fine fraction data would also be consistent with an upwelling origin, with higher $\delta^{18}O$ values due to upwelling of cold water, higher $\delta^{13}C$ due to extraction of isotopically light ^{12}C by high rates of primary production, and higher carbonate content due to high rates of production of Braarudosphaera pentaliths. There are two problems associated with this that must be explained before ascribing the origin of Braarudosphaera oozes to upwelling.

First, since Braarudosphaera is usually associated with unusually low (or perhaps high) salinity, we need to determine whether possible candidates for cold, nutrient rich, and unusually low or high salinity waters for upwelling are available. Antarctic Intermediate Water is in fact a likely candidate. AAIW is formed from the mixing of cold, low salinity Antarctic Surface Water (formed by summer ice melting and winter cooling near ice shelves) below the Antarctic Polar Front Zone. It reaches depths of 800 to 1000 m by 40°S, remaining at this depth during northward movement [Pickard and Emery, 1982]. This low salinity water moreover would not contain the low $\delta^{18}O$ signal that continental runoff would, because no isotopic fractionation occurs during freezing or thawing of sea ice. High preformed nutrient contents [Broecker and Takahashi, 1981] would lead to high rates of primary production if upwelling occurred.

This might even help explain the bi-hemispheric distribution of Braarudosphaera oozes. Charles and Fairbanks [1992] have suggested that based on $\delta^{13}C$ data, in the Pleistocene, nutrient-rich water from the Southern Ocean was drawn northward across the equator at mid-depths. This movement was caused by the removal of surface and thermocline waters during formation of North Atlantic Deep Water. If, as has been suggested [Miller and Fairbanks, 1983; Miller, 1992; Chapter 3], some form of deep or bottom water was being formed in the North Atlantic during the Oligocene, then conservation of water would demand that some northward flow would occur, perhaps through a similar mechanism.

If fine fraction $\delta^{18}O$ correctly represents surface equilibrium calcite, the surface temperature may be calculated using the Shackleton [1974] paleotemperature equation (Equation 4) and $-0.85^{o}/oo$ for seawater $\delta^{18}O$. The average temperatures in Braarudosphaera oozes within cores 7, 6, and 5, respectively are 4.6, 5.6, and 9.1°C (Table 4-6). Average temperatures in non-Braarudosphaera oozes are considerably higher, at 10.3, 8.7, and 11.5°C for cores 7, 6, and 5, respectively.

The calculated temperatures within the Braarudosphaera oozes are lower than the 10°C minimum that has been reported

TABLE 4-6

Calculated Temperatures for *Braarudosphaera* oozes and non-*Braarudosphaera* oozes

		Fine Frac.	Chilo-guemb.	Catap-sydrax	Cibicid-oides	Corrected Cibicid-oides
Core 5						
non-*Braarudo*.	$\delta^{18}O$	0.429	0.458	0.910	1.550	2.570
	T(°C)	11.460	15.199	9.499	6.964	3.090
Braarudo.	$\delta^{18}O$	1.008	0.483	1.034	1.241	2.261
	T(°C)	9.108	15.308	9.001	8.179	4.242
Core 6						
non-*Braarudo*.	$\delta^{18}O$	1.111	0.232	0.905	1.472	2.492
	T(°C)	8.695	12.279	9.522	7.270	3.380
Braarudo.	$\delta^{18}O$	1.905	0.237	1.080	0.984	2.004
	T(°C)	5.591	12.256	8.821	9.204	5.215
Core 7						
non-*Braarudo*.	$\delta^{18}O$	0.712	0.189	0.702	1.278	2.298
	T(°C)	10.304	14.049	10.342	8.034	4.105
Braarudo.	$\delta^{18}O$	2.167		0.178	1.424	2.444
	T(°C)	4.596		12.505	7.458	3.558

for modern Braarudosphaera [Wise and Hsü, 1971]. The ecology of Braarudosphaera is poorly known, however. A better understanding of Braarudosphaerid ecology and biology is clearly necessary to determine whether the temperatures calculated from the Braarudosphaera oozes reflect vital effects, calcification in the photic zone, or calcification in deeper waters.

The second problem, the lack of correspondence between the fine fraction and foraminiferal isotope records makes the suggestion that the isotopic record of the fine fraction (and by extension, the bulk carbonate) is controlled by upwelling-induced productivity difficult to justify. We would expect that during an upwelling event, planktic carbon and oxygen isotopic composition would tend to approach benthic or mid-water values, as cold, nutrient and organic carbon-rich deeper waters were lifted towards the surface. This is not the case, as instead, all foraminiferal $\delta^{18}O$ and $\delta^{13}C$ values remain constant through the intervals in question. A way that fine fraction and planktic foraminiferal isotopic records could be decoupled but still reflect surface water physical properties would be for production of the fine fraction and foraminifera to be separated in time, perhaps seasonally due to monsoonal control over winds and upwelling. This remains speculative at present. Finally, the lack of response in $\delta^{13}C$ of the Site 522 Braarudosphaera ooze remains unexplained by the upwelling model. The lack of $\delta^{13}C$ response suggests a lower productivity event, an explanation at odds with the large increases in $\delta^{18}O$ and percent $CaCO_3$. Given the lack of other viable explanations, however, mid-ocean upwelling of cold, low salinity water originating from a precursor of AAIW is the most likely answer for the origin of _Braarudosphaera_ oozes.

The reasons for the repetitive nature of the _Braarudosphaera_ oozes in the South Atlantic are not known; however, given the short-term cyclicity of these oozes in DSDP Sites 362, and 363, and other sites, it seems likely that some Milankovitch-scale processes are responsible. Oligocene Milankovitch periodicities have been identified in the South Atlantic [Mead et al., 1986; Salamy et al., 1994]. Certainly massive meltback of the Antarctic ice shelf during a deglacial event could lead to a less saline version of AAIW which would be more likely to encourage the growth of _Braarudosphaera_. Indeed, a waxing and waning of the Antarctic ice shelf would not even require changes in glacial volume, only changes in polar temperatures. With more complete sections and better dating of the _Braarudosphaera_ sequences, time-series analysis might be illuminating in this respect.

Conclusions

Braarudosphaera oozes and chalks are unusually pure, low-diversity calcareous deposits which occur within very restricted temporal and spatial ranges. They occur at the

Jurassic/Cretaceous boundary, Cretaceous/Tertiary boundary, mid Oligocene, and Recent times. During the Oligocene they are especially widespread, occurring in the North and South Atlantic and in the Indian Ocean. Their genesis seems to be due to unusual, persistent environmental conditions, which leads to restriction of other taxa and to blooms of Braarudosphaera. Redeposition and dissolution do not seem to play a major part. The events which led to these conditions are not well known, but the opening of the Drake Passage, Oligocene glaciation, and mid-ocean upwelling have been suggested.

Isotopic analysis of fine fraction samples from Braarudosphaera oozes and adjacent normal marine samples show that both $\delta^{18}O$ and $\delta^{13}C$ are enriched within the Braarudosphaera oozes. The degree of enrichment varies with the carbonate content. Seafloor diagenesis is probably not a factor either, because little evidence of diagenesis is visible in SEM observation, changes in fine fraction $\delta^{13}C$ are opposite what would be expected from diagenetic alteration, and no diagenetic effects are present in the foraminifera. Productivity-induced vital effects can probably be ruled out because the enrichment in $\delta^{18}O$ and $\delta^{13}C$ within the Braarudosphaera oozes is opposite that which would be expected. However, this doesn't take into account the effects on $\delta^{18}O$ and $\delta^{13}C$ of changes in floral assemblages, which cannot be quantified because as yet the isotopic fractionation by Braarudosphaera are not known.

Isotopic analysis of benthic and planktic foraminifera reveal surprisingly uniform $\delta^{18}O$ and $\delta^{13}C$ records, with little or no difference between analyses of foraminifera within the *Braarudosphaera* oozes and outside the *Braarudosphaera* oozes. Analysis of the foraminiferal $\delta^{18}O$ signal rules out continental runoff as a source of low salinity water which could have led to the formation of *Braarudosphaera* ooze. If vital effects are assumed to be negligible, then the best explanation is that upwelling of cold, low salinity AAIW led to the generation of these oozes. However, because the vital effects of changing floral assemblages in the fine fraction are unknown, the set of conditions which led to the deposition of *Braarudosphaera* oozes still "remains a mystery" [Van Andel et al., 1977].

APPENDIX A

LARGE DATA TABLES

APPENDIX A1

Correlated Geomagnetic Polarity Time Scales from 1968 to 1994

	HOHPL 1968	TM 1976	LKC 1977	MD 1979	NLC 1980	LA 1981	GTS 1982	BKFV 1985	HHV 1988	GTS 1989	CK 1992	CK 1994	
t	0.00 1	0.00 1	0.00 1	0.00 1	0.00 1	0.00 1	0.00 1	0.00 1	0.00 C1	0.00 1	0.000 C1n	0.000 C1n	Present
b	0.69	0.68	0.70	0.73	0.72	0.72	0.73 1r	0.73		0.72	0.780	0.780	Brunhes/Matuyama
t	0.89	0.89	0.89	0.90	0.91 1'	0.91	0.90 1r-1	0.91		0.91 1R-1	0.984 C1r.1n	0.990 C1r.1n	\ Jaramillo
b	0.93	0.95	0.95	0.97	0.97	0.97	0.97 1r	0.98		0.97	1.049	1.070	/
t												1.201 C1r.2r-1n	
b												1.211	
t	1.78 2	1.58 2	1.62 2	1.67 2	1.66 2	1.66 2	1.67 2	1.66 2	1.65 C2	1.65 2	1.757 C2n	1.770 C2n	\ Olduvai
b		1.70											
t		1.75											
b	1.93	1.83	1.83	1.87	1.87	1.87	1.87 2r	1.88		1.88	1.983	1.950	/
t		2.01		2.01	2.01		2.01 2r-1			2.06 2R-1	2.197 C2r.1n	2.140 C2r.1n	\ Reunion
b		2.02		2.04	2.04		2.04 2r			2.09	2.229	2.150	/
t				2.12	2.12		2.12 2r-2				2.420 C2r.2r-1	2.420 C2r.2r-1	
b				2.14	2.14		2.14 2r				2.441	2.441	
t	2.48	2.41 2^{1}	2.41 2A	2.48 2A	2.47 2.1'	2.47 2A	2.48 2A	2.47 2A	2.50 C2A	2.45 2A	2.600 C2An.1n	2.581 C2An.1n	Matuyama/Gauss
b	2.93	2.84	2.84	2.92	2.91	2.91	2.92 2A-1	2.92		2.91	3.054	3.040	\ Kaena

APPENDIX A1--continued

	HOHPL 1968	TM 1976	LKC 1977	MD 1979	NLC 1980	LA 1981	GTS 1982	BKFV 1985	HHV 1988	GTS 1989	CK 1992	CK 1994	
t		2.91	2.91 2A	3.01 2A	2.98 2.2'	2.98 2A	3.01 2A	2.99 2A		2.98 2A	3.127 C2An.2n	3.110 C2An.2n	/
b		3.00	3.00	3.05	3.07	3.07	3.05 2A-2	3.08		3.07	3.221	3.220	\ Mammoth
t	3.06	3.10	3.10 2A	3.15 2A	3.17 2.3'	3.17 2A	3.15 2A	3.18 2A		3.17 2A	3.325 C2An.3n	3.330 C2An.3n	/
b	3.37	3.32	3.32	3.40	3.40	3.40	3.40 2Ar	3.40		3.40	3.553	3.580	Gauss/Gilbert
t	4.04	3.79	3.76 3	3.80 3	3.86 3.1	3.87 3	3.86 3.1	3.88 3	3.90 C3	3.87 3.1	4.033 C3n.1n	4.180 C3n.1n	\ Cochiti
b	4.22	3.89	3.85	3.90	3.98	3.97	3.98 3.1r	3.97		3.99	4.134	4.290	/
t	4.35	4.02	3.97 3	4.05 3	4.12 3.2	4.10 3	4.12 3.2	4.10 3		4.12 3.2	4.265 C3n.2n	4.480 C3n.2n	\ Nunivak
b	4.53	4.16	4.10	4.20	4.26	4.24	4.26 3.2r	4.24		4.26	4.432	4.620	/
t	4.66	4.31	4.24 3	4.32 3	4.41 3.3	4.39 3	4.41 3.2r-1	4.40 3		4.41 3.2R-1	4.611 C3n.3n	4.800 C3n.3n	\ Sidufjall
b	4.77	4.38	4.31	4.47	4.49	4.46	4.49 3.2r	4.47		4.48	4.694	4.890	/
t	4.81 3	4.48 3	4.40 3	4.85 3	4.59 3.4	4.56 3	4.59 3.3	4.57 3		4.79 3.3	4.812 C3n.4n	4.980 C3n.4n	\ Thvera
b	5.01	4.68	4.59	5.00	4.79	4.76	4.79 3r	4.77		5.08	5.046	5.230	/
t	5.61	5.20 3^{1}	5.12 3A	5.26 3A	5.41 3.1'	5.33 3A	5.41 3A	5.35 3A	5.40 C3A	5.69 3A	5.705 C3An.1n	5.894 C3An.1n	
b	5.88	5.43	5.29	5.43	5.70	5.52	5.70 3A-1	5.53		5.96	5.946	6.137	
t	5.96	5.58	5.43 3A	5.57 3A	5.98 3.2'	5.67 3A	5.78 3A	5.68 3A		6.04 3A	6.078 C3An.2n	6.269 C3An.2n	
b	6.24	5.85	5.62	5.77	6.07	5.87	6.07 3Ar	5.89		6.33	6.376	6.567	

APPENDIX A1--continued

	HOHPL	TM	LKC	MD	NLC	LA	GTS	BKFV	HHV	GTS	CK	CK
	1968	1976	1977	1979	1980	1981	1982	1985	1988	1989	1992	1994
t	6.57	6.28	6.06	6.22	6.42 3.3'	6.34	6.42 3B	6.37		6.66 3B	6.744 C3Bn	6.935 C3Bn
b	6.70	6.39	6.18	6.34	6.55	6.47	6.55 3Br	6.50		6.79	6.901	7.091
t											6.946 C3Br.1n	7.135 C3Br.1n
b											6.981	7.170
t											7.153 C3Br.2n	7.341 C3Br.2n
b											7.187	7.375
t	6.91	6.59	6.37 4	6.54 4	6.77 4	6.68 4	6.77 4	6.70 4	6.70 C4	7.01 4	7.245 C4n.1n	7.432 C4n.1n
b	7.00	6.68	6.44	6.61	6.86	6.75	6.86 4-1	6.78		7.10	7.376	7.562
t	7.07 4	6.75 4	6.51 4	6.68 4	6.94 4	6.83 4	6.94 4	6.85 4		7.17 4	7.464 C4n.2n	7.650 C4n.2n
b	7.46	7.17	6.90	7.08	7.32	7.25	7.34 4-2	7.28		7.56	7.892	8.072
t	7.51	7.24	6.97 4	7.16 4	7.39 4	7.32 4	7.39 4	7.35 4		7.62 4	8.047 C4r.1n	8.225 C4r.1xn
b	7.55	7.30	7.02	7.21	7.44	7.38	7.44 4r	7.41		7.66	8.079	8.257
t	7.91	7.39 4'	7.39 4A	7.59 4A	7.81 4.1'	7.77 4A	7.81 4A	7.90 4A	7.80 C4A	8.02 4A	8.529 C4An	8.699 C4An
b	8.28	7.80	7.68	7.88	8.18	8.09	8.18 4Ar	8.21		8.29	8.861	9.025
t	8.37	8.06	7.87 4A	8.08 4A	8.40 4.2'	8.29 4A	8.40 4Ar-1	8.41 4A		8.48 4AR-1	9.069 C4Ar.1n	9.230 C4Ar.1n
b	8.51	8.16	7.95	8.16	8.49	8.38	8.49 4Ar	8.50		8.54	9.149	9.308

APPENDIX A1--continued

	HOHPL 1968	TM 1976	LKC 1977	MD 1979	NLC 1980	LA 1981	GTS 1982	BKFV 1985	HHV 1988	GTS 1989	CK 1992	CK 1994
t		8.51	8.15	8.37	8.80 4.3'	8.59	8.80 4Ar-2	8.71		8.78 4AR-2	9.428 C4Ar.2n	9.580 C4Ar.2n
b		8.59	8.23	8.45	8.87	8.68	8.87 4Ar	8.80		8.83	9.491	9.642
t	8.79 5	8.71 5	8.34 5	8.56 5	8.98 5.1	8.80 5	8.98 5	8.92 5	8.95 C5	8.91 5	9.592 C5n.1n	9.740 C5n.1n
b		8.88	8.50	8.73	9.13		9.13 5-1			9.09	9.735	9.880
t		8.93	8.54 5	8.77 5	9.17 5.2		9.17 5			9.14 5	9.777 C5n.2n	9.920 C5n.2n
b		9.25	8.86	9.10	9.47		9.47 5-2			9.48	10.060 C5n.2n-1	10.197 C5n.2n-1
t		9.27	8.87 5	9.11 5	9.48 5.3		9.48 5			9.49 5	10.069	10.205
b		9.58	9.15	9.39	9.75		9.75 5-3			9.80	10.317 C5n.2n-2	10.446 C5n.2n-2
t		9.61	9.18 5	9.42 5	9.78 5.4		9.78 5			9.83 5	10.342	10.470
b		9.91	9.46	9.71	10.03		10.03 5-4			10.13	10.589 C5n.2n-3	10.710 C5n.2n-3
t		9.93	9.48 5	9.73 5	10.05 5.5		10.05 5			10.15 5	10.605	10.726
b	9.94	10.21	9.74	10.00	10.30	10.30	10.30 5r	10.42		10.43	10.834	10.949
t		10.34	9.86	10.12	10.42 5'	10.42	10.43 5r-1	10.54		10.57 5R-1	10.940 C5r.1n	11.052 C5r.1n
b		10.40	9.91	10.17	10.47	10.47	10.48 5r	10.59		10.63	10.989	11.099
t	10.77	10.75	10.36	10.64	10.89	10.91	10.91 5r-2	11.03		11.11 5R-2	11.378 C5r.2n	11.476 C5r.2n
b	11.14	11.05	10.43	10.71	10.96	10.98	10.99 5r	11.09		11.18	11.434	11.531

APPENDIX A1--continued

	HOHPL	1M	LKC	MD	NLC	LA	GTS	BKFV	HHV	GTS	CK	LK
	1968	1976	1977	1979	1980	1981	1982	1985	1988	1989	1992	1994
t	11.72	11.47 5[1]	10.91 5A	11.20 5A	11.42	11.46 5A	11.47 5A.1	11.55 5A	11.70 C5A	11.71 5A.1	11.852 C5An.1n	11.935 C5An.1n
b	11.85	11.63	11.09	11.38	11.58	11.64	11.63 5A.1r	11.73		11.90	12.000	12.078
t	11.93	11.73	11.22 5A	11.52 5A	11.71 5A	11.76 5A	11.77 5A.2	11.86 5A		12.05 5A.2	12.108 C5An.2n	12.184 C5An.2n
b	12.43	12.01	11.49	11.79	11.96	12.03	12.03 5Ar	12.12		12.34	12.333	12.401
t	12.72	12.30	11.84	12.15	12.28		12.36 5Ar-1	12.46		12.68 5AR-1	12.618 C5Ar.1n	12.678 C5Ar.1n
b		12.50	11.87	12.18	12.32		12.41 5Ar	12.49		12.71	12.649	12.708
t		12.60	11.96	12.28	12.40	12.50	12.49 5Ar-2	12.58		12.79 5AR-2	12.718 C5Ar.2n	12.775 C5Ar.2n
b	13.09	12.70	12.01	12.33	12.45	12.54	12.54 5Ar	12.62		12.84	12.764	12.819
t	13.29	12.88	12.23	12.55	12.66	12.76	12.76 5AA	12.83 5AA		13.04 5AA	12.941 C5AAn	12.991 C5AAn
b	13.71	13.08	12.41	12.74	12.83	12.94	12.94 5AAr	13.01		13.21	13.094	13.139
t	13.96	13.35	12.61	12.94	13.03	13.14	13.15 5AB	13.20 5AB		13.40 5AB	13.263 C5ABn	13.302 C5ABn
b	14.28	13.52	12.87	13.21	13.28	13.40	13.41 5ABr	13.46		13.64	13.476	13.510
t	14.51	13.75	13.11	13.46	13.51	13.63	13.65 5AC	13.69 5AC		13.87 5AC	13.674 C5ACn	13.703 C5ACn
b		14.00										
t		14.01										
b	14.82	14.28	13.52	13.88	13.89	14.04	14.04 5ACr	14.08		14.24	14.059	14.076

APPENDIX A1--continued

	HOHPL	TM	LKC	MD	NLC	LA	GTS	BKFV	HHV	GTS	CK	CK
	1968	1976	1977	1979	1980	1981	1982	1985	1988	1989	1992	1994
t	14.98	14.40	13.64	14.00	14.00	14.16	14.16 5AD	14.20 5AD		14.35 5AD	14.164 C5A0n	14.178 C5A0n
b		14.69										
t		14.71										
b	15.45	14.87	14.11	14.48	14.45	14.62	14.63 5ADr	14.66		14.79	14.608	14.612
t	15.71	15.13 5^{II}	14.32 5B	14.70 5B	14.64 5B	14.83 5B	14.82 5B.1	14.87 5B	14.20 C5B	14.98 5B.1	14.800 C5Bn.1n	14.800 C5Bn.1n
b	16.00	15.24	14.42	14.80	14.74	14.93	14.93 5B.1r	14.96		15.07	14.890	14.888
t	16.03	15.34	14.59 5B	14.98 5B	14.90 5B	15.10 5B	15.09 5B.2	15.13 5B		15.23 5B.2	15.038 C5Bn.2n	15.034 C5Bn.2n
b		15.45										
t		15.52										
b	16.41	15.57	14.73	15.12	15.03	15.23	15.23 5Br	15.27		15.35	15.162	15.155
t	17.33	16.49 5^{III}	15.72 5C	16.14 5C	15.96 5C	16.21 5C	16.20 5C	16.22 5C	16.10 C5C	16.27 5C	16.035 C5Cn.1n	16.014 C5Cn.1n
b		16.77	16.02	16.44	16.25		16.50 5C-1	16.52		16.55	16.318	16.293
t		16.81	16.06 5C	16.48 5C	16.29 5C		16.54 5C	16.56 5C		16.59 5C	16.352 C5Cn.2n	16.327 C5Cn.2n
b	17.80	16.97	16.24	16.67	16.46	16.73	16.72 5C-2	16.73		16.75	16.515	16.488
t	17.83	17.04	16.31 5C	16.74 5C	16.53 5C	16.80 5C	16.79 5C	16.80 5C		16.82 5C	16.583 C5Cn.3n	16.556 C5Cn.3n
b	18.02	17.21	16.50	16.94	16.71	16.99	16.98 5Cr	16.98		16.99	16.755	16.726

APPENDIX A1--continued

	HDHPL	TM	LKC	MD	NLC	LA	GTS	BKFV	HHV	GTS	CK	CK
	1968	1976	1977	1979	1980	1981	1982	1985	1988	1989	1992	1994
t	18.91	17.78 5^{IV}	17.11 5D	17.56 50	17.28 50	17.59 5D	17.58 50	17.57 50	17.50 C5D	17.55 50	17.310 C50n	17.277 C5Dn
b		17.90										
t		17.92										
b	19.26	18.10	17.45	17.91	17.60	17.92	17.91 50r	17.90		17.87	17.650	17.615
t		18.26	17.67 50	18.14 50	17.81		18.13 50r-1	18.12 5D		18.07 5DR-1	17.860 C5Dr-1	
b		18.32	17.69	18.16	17.83		18.15 50r	18.14		18.09	17.888	
t	19.62	18.80 5^{V}	18.13 5E	18.61 5E	18.25 5E	18.60 5E	18.59 5E	18.56 5E	18.50 C5E	18.50 5E	18.317 C5En	18.281 C5En
b	19.96	19.23	18.67	19.16	18.76	19.13	19.12 5Er	19.09		19.00	18.817	18.781
t	20.19 6	19.50 6	18.95 6	19.24 6	19.04 6	19.41 6	19.41 6	19.35 6	19.30 C6	19.26 6	19.083 C6n	19.048 C6n
b	21.31	20.54	20.07	20.60	20.09	20.52	20.50 6r	20.45		20.23	20.162	20.131
t	21.65	20.95	20.52 6A	21.06 6A	20.52	20.96 6A	20.95 6A.1	20.88 6A	20.80 C6A	20.52 6A.1	20.546 C6An.1n	20.518 C6An.1n
b	21.91	21.21	20.80	21.35	20.78	21.24	21.22 6A.1r	21.16		20.74	20.752	20.725
t	22.17	21.43	21.03 6A	21.58 6A	21.00	21.47 6A	21.45 6A.2	21.38 6A		20.97 6A.2	21.021 C6An.2n	20.996 C6An.2n
b	22.64	21.73	21.36	21.92	21.31	21.79	21.78 6Ar	21.71		21.37	21.343	21.320
t	22.90	21.92	21.56	22.13	21.50	21.99	21.97 6AA	21.90 6AA		21.60 6AA	21.787 C6AAn	21.768 C6AAn
b	23.08	22.07	21.72	22.29	21.66	22.15	22.14 6AAr	22.06		21.75	21.877	21.859

APPENDIX A1--continued

	HOHPL	TM	LKC	MD	NLC	LA	GTS	BKFV	HHV	GTS	CK	CK
	1968	1976	1977	1979	1980	1981	1982	1985	1988	1989	1992	1994
t	23.29	22.25	21.92	22.50	21.85	22.35	22.34 6AAr-1	22.25 6AA		21.93 6AAR-1	22.166 C6AAr.1n	22.151 C6AAr.1n
b	23.40	22.35	22.02	22.60	21.94	22.44	22.43 6AAr	22.35		22.03	22.263	22.248
t											22.471 C6AAr.2n	22.459 C6AAr.2n
b											22.505	22.493
t	23.63	22.54	22.24 6B	22.83 6B	22.15	22.66 6B	22.65 6B	22.57 6B	22.60 C6B	22.23 6B	22.599 C6Bn.1n	22.588 C6Bn.1n
b											22.760	22.750
t											22.814 C6Bn.2n	22.804 C6Bn.2n
b	24.07	22.91	22.65	23.25	22.54	23.07	23.06 6Br	22.97		22.60	23.076	23.069
t	24.41	23.20	22.96 6C	23.56 6C	22.84	23.37 6C	23.37 6C.1	23.27 6C	23.75 C6C	22.90 6C.1	23.357 C6Cn.1n	23.353 C6Cn.1n
b	24.59	23.36	23.13	23.74	23.00	23.54	23.54 6C.1r	23.44		23.05	23.537	23.535
t	24.82	23.55	23.25 6C	23.86 6C	23.21	23.66 6C	23.76 6C.2	23.55 6C		23.25 6C.2	23.678 C6Cn.2n	23.677 C6Cn.2n
b	24.97	23.68	23.49	24.11	23.35	23.90	23.90 6C.2r	23.79		23.38	23.800	23.800
t	25.25	23.92	23.75 6C	24.37 6C	23.59	24.15 6C	24.15 6C.3	24.04 6C		23.62 6C.3	23.997 C6Cn.3n	23.999 C6Cn.3n
b	25.43	24.07	23.92	24.55	23.75	24.32	24.32 6Cr	24.21		23.78	24.115	24.118
t	26.86 7	25.29 7	25.24 7	25.90 7	25.02 7	25.74 7	25.75 7	25.50 7	25.53 C7	25.01 7	24.722 C7n.1n	24.730 C7n.1n
b	26.98	25.39	25.35	26.02	25.13	25.86	25.88 7-1	25.60		25.11	24.772	24.781

APPENDIX A1--continued

	HDHPL	TM	LKC	MD	NLC	LA	GTS	BKFV	HHV	GTS	CK	CK
	1968	1976	1977	1979	1980	1981	1982	1985	1988	1989	1992	1994
t	27.05	25.45	25.42 7	26.09 7	25.19 7	25.94 7	25.94 7	25.67 7		25.17 7	24.826 C7n.2n	24.835 C7n.2n
b	27.37	25.72	25.72	26.40	25.47	26.27	26.27 7r	25.97		25.45	25.171	25.183
t	27.83	26.11	26.14 7A	26.83 7A	25.88	26.73 7A	26.74 7A	26.38 7A		25.84 7A	25.482 C7An	25.496 C7An
b	28.03	26.28	26.33	27.02	26.06	26.94	26.95 7Ar	26.56		26.01	25.633	25.648
t	28.35 8	26.55 8	26.63 8	27.33 8	26.34	27.27 8	27.27 8	26.86 8	26.76 C8	26.29 8	25.807 C8n.1n	25.823 C8n.1n
b	28.44	26.63	26.71	27.41	26.42	27.36	27.36 8-1	26.93		26.37	25.934	25.951
t	28.52	26.70	26.79 8	27.49 8	26.49 8	27.44 8	27.44 8	27.01 8		26.44 8	25.974 C8n.2n	25.992 C8n.2n
b	29.33	27.39	27.54	28.26	27.21	28.27	28.27 8r	27.74		27.13	26.533	26.554
t	29.78 9	27.77 9	27.96 9	28.69 9	27.61 9	28.73 9	28.73 9	28.15 9	28.23 C9	27.52 9	27.004 C9n	27.027 C9n
b	30.42	28.31	28.56	29.31	28.18	29.39	29.39 9-1	28.74		28.07		
t	30.48	28.36	28.62 9	29.37 9	28.23	29.45 9	29.45 9	28.80 9		28.12 9		
b	30.93	28.75	29.04	29.80	28.63	29.92	29.91 9r	29.21		28.51	27.946	27.972
t	31.50 10	29.23 10	29.57 10	30.34 10	29.13 10	30.50 10	30.48 10	29.73 10	29.70 C10	29.00 10	28.255 C10n.1n	28.283 C10n.1n
b	31.84	29.52	29.88	30.66	29.44	30.84	30.84 10-1	30.03		29.29	28.484	28.512
t	31.90	29.57	29.94 10	30.72 10	29.49 10	30.90 10	30.90 10	30.09 10		29.35 10	28.550 C10n.2n	28.578 C10n.2n
b	32.17	29.80	30.19	30.98	29.73	31.18	31.17 10r	30.33		29.58	28.716	28.745

APPENDIX A1--continued

	HDHPL	TM	LKC	MD	NLC	LA	GTS	BKFV	HHV	GTS	CK	CK
	1968	1976	1977	1979	1980	1981	1982	1985	1988	1989	1992	1994
t	33.16 11	30.64 11	31.11 11	31.92 11	30.61 11	32.19 11	32.19 11	31.23 11	31.36 C11	30.42 11	29.373 C11n.1n	29.401 C11n.1n
b	33.55	30.97	31.47	32.29	30.95	32.59	32.58 11-1	31.58		30.77	29.633	29.662
t	33.61	31.02	31.53 11	32.35 11	31.01 11	32.65 11	32.65 11	31.64 11		30.82 11	29.727 C11n.2n	29.765 C11n.2n
b	34.07	31.41	31.96	32.80	31.41	33.12	33.11 11r	32.06		31.21	30.071	30.098
t	34.52 12	31.80 12	32.37 12	33.22 12	31.81 12	33.57 12	33.57 12	32.46 12	32.50 C12	31.60 12	30.452 C12n	30.479 C12n
b	35.00	32.21	32.82	33.68	32.24	34.07	34.06 12r	32.90		32.01	30.915	30.939
t	37.61 13	34.42 13	35.26 13	36.18 13	34.56 13	36.75 13	36.73 13	35.29 13	35.43 C13	34.26 13	33.050 C13n	33.058 C13n
b	37.82	34.60	35.45	36.37	34.75	36.96	36.95 13-1	35.47		34.44	33.261 C13n-1	
t	37.89	34.66	35.52 13	36.45 13	34.81 13	37.03 13	37.02 13	35.54 13		34.50 13	33.277	
b	38.26	34.88	35.86	36.80	35.14	37.41	37.40 13r	35.87		34.82	33.543	33.545
t	38.68 14	35.13 14										
b	38.77	35.19										
t	38.83	35.22										
b	38.92	35.28										
t	39.03	35.34										
b	39.11	35.39										

APPENDIX A1--continued

	HOHPL	TM	LKC	MD	NLC	LA	GTS	BKFV	HHV	GTS	CK	CK
	1968	1976	1977	1979	1980	1981	1982	1985	1988	1989	1992	1994
t	39.42	35.58										
b	39.47	35.61										
t	39.77 15	35.79	37.26 15	38.23 15	36.48 15	38.51 15	38.64 15	37.24 15	37.10 C15	36.12 15	34.669 C15n	34.655 C15n
b	40.00	35.93	37.48	38.46	36.68	38.77	38.80 15-1	37.46		36.32		
t	40.03	35.94	37.50 15	38.48 15	36.71 15		38.83 15	37.48 15		36.35 15		
b	40.25	36.08	37.71	38.69	36.90		38.98 15r	37.68		36.54	34.959	34.940
t	40.71	36.35 16	38.14 16	39.13 16	37.31	39.02 16	39.30 15A	38.10 16	38.06 C16	36.93 15A	35.368 C16n.1n	35.343 C16n.1n
b	40.97	36.51	38.38	39.38	37.54	39.16	39.48 15Ar	38.34		37.16	35.554	35.526
t	41.15	36.62	38.55 16	39.55 16	37.70 16	39.26 16	39.60 16	38.50 16		37.31 16	35.716 C16n.2n	35.685 C16n.2n
b	41.46	36.80	38.84	39.85	37.97	39.43	39.82 16-1	38.79		37.58		
t	41.52 16	36.84	38.89 16	39.90 16	38.03 16	39.47 16	39.86 16	38.83 16		37.63 16		
b	41.96	37.10	39.31	40.33	38.42	39.71	40.17 16r	39.24		38.01	36.383	36.341
t	42.28 17	37.29 17	39.60 17	40.63 17	38.70 17	39.88 17	40.39 17	39.53 17	38.96 C17	38.28 17	36.665 C17n.1n	36.618 C17n.1n
b	43.26	37.88	40.52	41.57	39.57	40.42	41.07 17-1	40.43		39.13	37.534	37.473
t	43.34	37.93	40.59 17	41.64 17	39.64	40.46 17	41.13 17	40.50 17		39.20 17	37.667 C17n.2n	37.604 C17n.2n
b	43.56	38.06	40.80	41.86	39.84	40.59	41.29 17-2	40.70		39.39	37.915	37.848

APPENDIX A1--continued

	HOHPL	IM	LKC	MD	NLC	LA	GTS	BKFV	HHV	GTS	CK	CK
	1968	1976	1977	1979	1980	1981	1982	1985	1988	1989	1992	1994
t	43.64	38.11	40.87 17	41.93 17	39.91	40.63 17	41.34 17	40.77 17		39.45 17	37.988 C17n.3n	37.920 C17n.3n
b	44.01	38.33	41.22	42.29	40.24	40.84	41.60 17r	41.11		39.77	38.183	38.113
t	44.21	38.45	41.40 18	42.48 18	40.42	40.94 18	41.74 18	41.29 18	40.20 C18	39.94 18	38.500 C18n.1n	38.426 C18n.1n
b	44.69	38.74	41.85	42.94	40.85	41.30	42.08 18-1	41.73		40.36		
t	44.77	38.79	41.93 18	43.02 18	40.92	41.36 18	42.14 18	41.80 18		40.43 18		
b	45.24	39.07	42.37	43.47	41.34	41.74	42.47 18-2	42.23		40.83	39.639	39.552
t	45.32 18	39.12	42.44 18	43.54 18	41.40 18	41.79 18	42.51 18	42.30 18		40.90 18	39.718 C18n.2n	39.631 C18n.2n
b	45.79	39.40	42.88	43.99	41.82	42.17	42.84 18r	42.73		41.31	40.221	40.130
t	46.76 19	39.98 19	43.77 19	44.90 19	42.68 19	42.92 19	43.52 19	43.60 19	42.23 C19	42.14 19	41.353 C19n	41.257 C19n
b	47.26	40.28	44.24	45.39	43.13	43.32	43.87 19r	44.06		42.57	41.617	41.521
t	47.91 20	40.67 20	44.85 20	46.01 20	43.69 20	43.83 20	44.31 20	44.66 20	43.10 C20	43.13 20	42.629 C20n	42.536 C20n
b	49.58	41.67	46.70	47.60	45.18	45.14	45.49 20r	46.17		44.57	43.868	43.789
t	52.41 21	43.37 21	49.04 21	50.31 21	47.69 21	47.37 21	47.46 21	48.75 21	46.56 C21	47.01 21	46.284 C21n	46.264 C21n
b	54.16	44.42	50.67	51.98	49.25	48.75	48.69 21r	50.34		48.51	47.861	47.906
t	55.92 22	45.48 22	52.31 22	53.66 22	50.81 22	50.14 22	49.91 22	51.95 22	48.86 C22	50.03 22	48.947 C22n	49.037 C22n
b	56.66	45.92	53.00	54.36	51.47	50.70	50.43 22r	52.62		50.66	49.603	49.714

APPENDIX A1--continued

	HDHPL	TM	LKC	MD	NLC	LA	GTS	BKFV	HHV	GTS	CK	CK
	1968	1976	1977	1979	1980	1981	1982	1985	1988	1989	1992	1994
t	58.04 23	46.75 23	54.29 23	55.69 23	52.69 23	51.74 23	51.39 23	53.88 23	50.36 C23	51.85 23	50.646 C23n.1n	50.778 C23n.1n
b			54.44	55.84	52.92	51.87	51.57 23-1	54.03		52.08	50.812	50.946
t			54.50 23	55.90 23	52.95 23	51.91 23	51.60 23	54.09 23		52.13 23	50.913 C23n.2n	51.047 C23n.2n
b	58.94	47.29	55.13	56.55	53.49	52.42	52.02 23r	54.70		52.83	51.609	51.743
t					53.74		52.22 23r-1			53.15 23R 1		
b					53.79		52.26 23r			53.20		
t	59.43 24	47.58 24	55.58	57.01 24	53.92	52.79 24	52.36 24.1	55.14 24	51.70 C24	53.39 24	52.238 C24n.1n	52.364 C24n.1n
b	59.69	47.74	55.81	57.24	54.16	52.97	52.55 24.1r	55.37		53.69	52.544	52.663
t											52.641 C24n.2n	52.757 C24n.2n
b											52.685	52.801
t	60.01	47.93	56.11 24	57.55 24	54.44 24	53.21 24	52.77 24.2	55.66 24		54.05 24	52.791 C24n.3n	52.903 C24n.3n
b	60.53	48.88	56.60	58.05	54.90	53.61	53.13 24r	56.14		54.65	53.250	53.347
t	62.75 25	52.66 25	58.67 25	60.17 25	57.81 25	55.76 25	55.60 25	58.64 25	55.03 C25	57.19 25	55.981 C25n	55.904 C25n
b	63.28	53.56	59.16	60.68	58.50	56.66	56.33 25r	59.24		57.80	56.515	56.391
t	64.14 26	55.02 26	59.97 26	61.51 26	59.63 26	58.15 26	57.52 26	60.21 26	57.28 C26	58.78 26	57.800 C26n	57.554 C26n
b	64.62	55.84	60.41	61.96	60.26	58.95	58.19 26r	60.75		59.33	58.197	57.911

APPENDIX A1--continued

	HDHPL	TM	LKC	MD	NLC	LA	GTS	BKFV	HHV	GTS	CK	CK
	1968	1976	1977	1979	1980	1981	1982	1985	1988	1989	1992	1994
t	66.65 27	59.29 27	62.30 27	63.89 27	62.92 27	62.31 27	61.00 27	63.03 27	61.36 C27	61.65 27	61.555 C27n	60.920 C27n
b	67.10	60.05	62.72	64.32	63.50	63.00	61.62 27r	63.54		62.17	61.951	61.276
t	67.77 28	61.19 28	63.34 28	64.96 28	64.38 28	64.00 28	62.55 28	64.29 28	63.13 C28	62.94 28	63.303 C28n	62.499 C28n
b	68.51	62.45	64.03	65.67	65.35	65.12	63.57 28r	65.12		63.78	64.542	63.634
t	68.84 29	63.01 29	64.34 29	65.98 29	65.78 29	65.63 29	64.03 29	65.50 29	64.91 C29	64.16 29	64.911 C29n	63.976 C29n
b	69.44	64.03	64.90	66.56	66.57	66.54	64.86 29r	66.17		64.85	65.732	64.745
t	69.93 30	64.86 30	65.37 30	67.04 30	67.18 30	66.98 30	65.39 30	66.74 30	66.96 C30	65.43 30	66.601 C30n	65.578 C30n
b	71.12	66.89	66.76	68.46	69.00	68.01	66.88 30r	68.42		67.14	68.625	67.610
t	71.22 31	67.06 31	66.84 31	68.54 31	69.11 31	68.07 31	66.97 31	68.52 31		67.23 31	68.745 C31n	67.735 C31n
b	72.11	68.40	67.57	69.29	70.06	68.62	67.74 31r	69.40		68.13	69.683	68.737
t	74.17 32	71.80 32	69.20 32	70.96 32	72.19	69.84 32	69.48 32.1	71.37 32		70.14 32.1	71.722 C32n.1n	71.071 C32n.1n
b	74.30	72.14	69.43	71.20	72.49	70.01	69.72 32.1r	71.65		70.42	71.943	71.338
t	74.64	72.38	69.65 32	71.42 32	72.78 32	70.17 32	69.96 32.2	71.91 32		70.69 32.2	72.147 C32n.2n	71.587 C32n.2n
b	76.33	74.95	71.00	72.80	74.55	71.18	71.40 32r	73.55		72.35	73.288	73.004
t		75.29	71.34	73.15	74.99	71.43	71.76 32r-1	73.96		72.77 32R-1	73.517 C32r.1n	73.291 C32r.1n
b		75.37	71.38	73.19	75.05	71.46	71.81 32r	74.01		72.82	73.584	73.374

APPENDIX A1--continued

	HDHPL	TM	LKC	MD	NLC	LA	GTS	BKFV	HHV	GTS	CK	CK
	1968	1976	1977	1979	1980	1981	1982	1985	1988	1989	1992	1994
t		75.64	71.62 33	73.44 33	75.39 33	71.64 33	72.06 33	74.30 33		73.12 33	73.781 C33n	73.619 C33n
b			76.48	78.41	81.72	78.82	78.53 33r	80.17		79.09	78.781	79.075
t			79.65 34	81.66 34	85.86 34	84.02 34	82.93	84.00 34		83.00 34	83.000 C34n	83.000 C34n
b			108.19	110.86			118.21	118.00		118.00	118.000	118.000

HDHPL 1968: Heirtzler et al., 1968.

TM 1976: Tarling and Mitchell, 1976.

LKC 1977: LaBrecque et al., 1977.

MD 1979: Mankinen and Dalrymple, 1979.

NLC 1980: Ness et al., 1980.

LA 1981: Lowrie and Alvarez, 1981.

t: Top of a normal polarity interval.

GTS 1982: Harland et al., 1982.

BKFV 1985: Berggren et al., 1985.

HHV 1988: Haq et al., 1988.

GTS 1989: Harland et al., 1988.

CK 1992: Cande and Kent, 1992.

CK 1994: Cande and Kent, 1994.

b: Base of a normal polarity interval.

APPENDIX A2

Sr, O, C Isotope and Sr/Ca Data, ODP Hole 689B

C S	Int.	Depth (mbsf)	Age (Ma) BKFV85	Age (Ma) CK92	Mass (mg)	Composition	87/86	Internal Error (10^{-6})	Sr/Ca $\mu g/mg$	Ratio mmol/mol	$\delta^{18}O$ (PDB)	$\delta^{13}C$ (PDB)
8-1	35-39	62.85	18.714	18.463	1.7	P	0.708525	8				
8-1	110-114	63.60	18.821	18.563	3.0	M	0.708501	6	5.23	2.39		
									5.00	2.29		
8-2	35-39	64.35	18.927	18.663	4.4	P	0.708502	8	5.27	2.41		
					3.7	B	0.708498	5				
8-2	110-114	65.10	19.033	18.764	6.9	B,wp	0.708511	8				
					9.9	B,pp	0.708504	6				
8-3	35-39	65.85	20.153	19.871	3.1	M	0.708435	6				
8-3	110-114	66.60	20.374	20.087	6.0	B,wp	0.708421	5	4.58	2.09	2.384	0.839
					4.4	B,pp	0.708424	6				
8-4	35-39	67.35	25.726	24.872	3.5	B	0.708193	5	4.03	1.84		

APPENDIX A2--continued

C S	Int.	Depth (mbsf)	Age (Ma) BKFV85	Age (Ma) CK92	Mass (mg)	Comp-osi-tion	87/86	Internal Error (10^{-6})	Sr/Ca µg/mg	Ratio mmol/mol	$\delta^{18}O$ (PDB)	$\delta^{13}C$ (PDB)
8-4	110-114	68.10	25.901	25.017	4.3	B	0.708176	5	4.96	2.27	2.294	0.510 *
									4.79	2.19		
8-5	35-39	68.85	26.077	25.161	5.2	B	0.708115	5	4.79	2.19		
8-5	110-114	69.60	26.252	25.306	2.1	M	0.708138	6				
8-6	35-39	70.35	26.427	25.450	5.3	B	0.708110	6				
8-6	110-114	71.10	26.602	25.595	5.8	B	0.708110	5				
8-7	12-17	71.62	26.724	25.695	3.8	B,wp	0.708130	5	4.77	2.18	2.387	0.492
					4.5	B,pp	0.708113	6				
9-1	35-39	72.45	26.918	25.855	2.9	B	0.708123	8				
9-1	110-114	73.20	27.093	25.999	2.9	B,wp	0.708092	6	4.27	1.95	2.411	0.735 *
					3.9	B,pp	0.708086	6				
9-2	35-39	73.95	27.268	26.144	2.3	M	0.708103	5				
9-2	110-114	74.70	27.443	26.288	2.4	M	0.708085	6				

APPENDIX A2--continued

C S	Int.	Depth (mbsf)	Age (Ma) BKFV85	Age (Ma) CK92	Mass (mg)	Comp-osi-tion	87/86	Internal Error (10^{-6})	Sr/Ca µg/mg	Ratio mmol/mol	$\delta^{18}O$ (PDB)	$\delta^{13}C$ (PDB)
9-3	35-39	75.45	27.619	26.433	3.8	B	0.708090	6	4.48	2.05		
									4.86	2.22		
9-3	110-114	76.20	27.767	26.564	2.7	M	0.708095	5				
9-4	35-39	76.95	27.855	26.665	2.2	P	0.708112	6				
					2.3	B	0.708106	9				
9-4	110-114	77.70	27.943	26.766	1.8	P	0.708123	6				
					2.4	B	0.708093	7				
9-5	35-39	78.45	28.031	26.868	1.3	P	0.708096	7				
					3.5	B	0.708104	5				
9-5	110-114	79.20	28.119	26.969	2.1	P	0.708085	5				
					2.6	B	0.708098	6				
9-6	35-39	79.95	28.236	27.071	6.4	B	0.708093	6			2.522	0.719 *
10-1	35-39	82.05	28.603	27.360	2.6	B	0.708107	7	5.33	2.44		

APPENDIX A2--continued

C S	Int.	Depth (mbsf)	Age (Ma) BKFV85	Age (Ma) CK92	Mass (mg)	Comp- osi- tion	87/86	Internal Error (10-^{6})	Sr/Ca μg/mg	Ratio mmol/mol	$\delta^{18}O$ (PDB)	$\delta^{13}C$ (PDB)
10-1	110-114	82.80	28.734	27.463	4.7	B	0.708091	6	4.78	2.19		
									3.62	1.65		
10-2	47-51	83.67	28.886	27.582	3.3	M	0.708057	5				
10-2	110-114	84.30	28.996	27.668	1.4	P	0.708063	6				
					2.7	B	0.708027	6				
10-3	35-39	85.05	29.127	27.771	4.4	M	0.708078	7	6.81	3.12		
									6.66	3.04		
10-3	110-114	85.80	29.258	27.874	5.6	P	0.708082	6				
10-4	35-39	86.55	29.389	27.977	9.0	M	0.708039	6	4.88	2.23		
10-4	110-114	87.30	29.521	28.080	2.6	M	0.708052	6				
10-5	35-39	88.05	29.652	28.183	6.8	M	0.708028	6				
10-5	110-114	88.80	29.783	28.286	1.9	M	0.707989	8				
10-6	35-39	89.55	29.914	28.389	3.1	M	0.708020	7				

APPENDIX A2--continued

C S	Int.	Depth (mbsf)	Age (Ma) BKFV85	Age (Ma) CK92	Mass (mg)	Comp-osi-tion	87/86	Internal Error (10^{-6})	Sr/Ca µg/mg	Ratio mmol/mol	$\delta^{18}O$ (PDB)	$\delta^{13}C$ (PDB)	
11-1	35-39	91.65	30.281	28.678	7.5	M	0.708014	6	5.56	2.54	2.537	0.414	*
11-1	109-113	92.39	30.400	28.770	6.6	M	0.708022	6					
11-2	35-39	93.15	30.514	28.861	8.6	M	0.708018	6	4.88	2.23			
11-2	109-113	93.89	30.626	28.948	5.1	M	0.708020	6					
11-3	35-39	94.65	30.741	29.038	4.0	P	0.708054	6					
					2.8	B	0.708025	5					
11-3	109-113	95.39	30.853	29.126	2.3	M	0.708050	12					
11-4	35-39	96.15	30.968	29.216	3.5	M	0.708009	6					
11-4	109-113	96.89	31.080	29.303	5.0	M	0.707983	6			2.394	0.357	
11-5	35-39	97.65	31.195	29.394	6.6	M	0.707966	6	5.46	2.50	2.335	0.331	*
									5.36	2.45			
11-5	109-113	98.39	31.307	29.481	4.6	M	0.70797	6			2.286	0.515	
12-1	35-39	101.35	31.755	29.832	3.8	M	0.707986	7					

APPENDIX A2--continued

C S	Int.	Depth (mbsf)	Age (Ma) BKFV85	Age (Ma) CK92	Mass (mg)	Composition	87/86	Internal Error (10^{-6})	Sr/Ca µg/mg	Ratio mmol/mol	$\delta^{18}O$ (PDB)	$\delta^{13}C$ (PDB)
12-1	110-114	102.10	31.868	29.921	3.1	M	0.707972	7			2.387	0.374 *
12-2	35-39	102.85	31.981	30.009	3.7	M	0.707929	7				
12-2	110-114	103.60	32.115	30.126	3.1	M	0.707957	7				
12-3	35-39	104.35	32.295	30.307	6.2	P	0.707972	6				
					5.3	B	0.707964	6				
12-3	110-114	105.10	32.475	30.488	3.2	M	0.707932	6				
12-4	34-39	105.84	32.653	30.667	7.2	M	0.707926	8	4.91	2.25		
12-4	110-114	106.60	32.835	30.850	10.0	M	0.707953	6	4.59	2.10		
12-5	35-39	107.35	33.017	31.019	7.0	M	0.707969	6				
12-5	110-114	108.10	33.199	31.182	5.9	M	0.707896	6				
12-6	34-39	108.84	33.378	31.342	3.2	M	0.707898	5				
12-6	110-114	109.60	33.563	31.507	1.9	M	0.707916	8				
12-7	35-39	110.35	33.745	31.670	6.3	M	0.707923	6	4.71	2.15		

APPENDIX A2--continued

C S	Int.	Depth (mbsf)	Age (Ma) BKFV85	Age (Ma) CK92	Mass (mg)	Comp-osi-tion	87/86	Internal Error (10^{-6})	Sr/Ca Ratio µg/mg	Sr/Ca Ratio mmol/mol	$\delta^{18}O$ (PDB)	$\delta^{13}C$ (PDB)
13-1	35-39	110.95	33.891	31.800	3.2	M	0.707890	6				
13-1	110-115	111.70	34.073	31.963	3.0	M	0.707896	6			2.140	0.764 *
13-2	35-39	112.45	34.255	32.126	6.7	M	0.707908	11				
13-2	111-116	113.21	34.440	32.291	5.6	M	0.707894	6				
13-3	35-39	113.95	34.620	32.451	2.5	M	0.707872	6				
13-3	111-116	114.71	34.804	32.616	3.9	M	0.707860	5				
13-4	34-38	115.44	34.982	32.774	4.0	M	0.707843	7				
13-4	111-116	116.21	35.169	32.942	4.3	M	0.707830	6				
13-5	34-38	116.94	35.335	33.088	6.6	M	0.707843	5				
13-5	111-116	117.71	35.485	33.215	3.3	M	0.707857	7			2.392	1.336 *
13-6	34-38	118.44	35.627	33.336	2.6	M	0.707822	6			2.507	1.406 *
13-6	111-116	119.21	35.777	33.464	1.7	P	0.707822	6			1.897	1.495
					7.0	B	0.707826	6				

APPENDIX A2--continued

C S	Int.	Depth (mbsf)	Age (Ma) BKFV85	Age (Ma) CK92	Mass (mg)	Comp-osi-tion	87/86	Internal Error (10^{-6})	Sr/Ca Ratio µg/mg	mmol/mol	$\delta^{18}O$ (PDB)	$\delta^{13}C$ (PDB)
14-1	37-39	120.57	36.144	33.768	5.3	M	0.707789	6			1.675	0.916 *
14-1	110-114	121.30	36.371	33.955	6.5	M	0.707791	6				
14-2	36-40	122.06	36.608	34.150	4.2	M	0.707767	6				
14-2	110-114	122.80	36.838	34.339	5.7	M	0.707782	6				
14-3	36-39	123.56	37.075	34.533	4.3	M	0.707781	8				
14-3	110-114	124.30	37.334	34.731	6.2	M	0.707775	6			1.324	0.850
14-4	36-40	125.06	37.676	34.956	4.4	M	0.707772	7			1.376	0.773
14-4	110-114	125.80	37.774	35.051	4.9	M	0.707732	6			1.384	1.085
14-5	36-40	126.56	37.873	35.147	4.0	M	0.707753	6			1.603	1.191
14-5	110-114	127.30	37.968	35.240	3.3	M	0.707768	6			1.329	1.118
14-6	36-40	128.06	38.066	35.335	3.4	M	0.707740	7			1.267	1.206
14-6	110-114	128.80	38.158	35.419	6.2	M	0.707756	6			0.970	1.195
15-1	35-39	130.25	38.334	35.574	3.7	M	0.707781	12			0.994	1.036

APPENDIX A2--continued

C S	Int.	Depth (mbsf)	Age (Ma) BKFV85	Age (Ma) CK92	Mass (mg)	Comp-osi-tion	87/86	Internal Error (10^{-6})	Sr/Ca µg/mg	Ratio mmol/mol	$\delta^{18}O$ (PDB)	$\delta^{13}C$ (PDB)
15-1	107-112	130.97	38.421	35.651	4.7	M	0.707775	5	5.26	2.41	1.055	1.186
									5.39	2.46		
15-2	35-39	131.75	38.515	35.734	6.5	M	0.707778	5	5.19	2.38	1.167	1.051 *
									5.27	2.41		
15-2	107-112	132.47	38.602	35.811	6.1	M	0.707787	7			1.099	1.101 *
15-3	35-39	133.25	38.697	35.895	7.1	M	0.707749	6	4.42	2.02		
15-3	107-112	133.97	38.784	35.972	6.3	P	0.707750	6	4.20	1.92	1.037	1.155 *
					3.7	B,wp	0.707722	6	5.42	2.48		
					4.7	B,pp	0.707739	5				
15-4	35-39	134.75	39.102	36.267	5.3	M	0.707751	5				
15-4	107-112	135.47	39.410	36.554	7.4	P	0.707719	6				
					3.6	B	0.707746	7				

APPENDIX A2--continued

C S	Int.	Depth (mbsf)	Age (Ma) BKFV85	Age (Ma) CK92	Mass (mg)	Comp-osi-tion	87/86	Internal Error (10^{-6})	Sr/Ca Ratio µg/mg	Sr/Ca Ratio mmol/mol	$\delta^{18}O$ (PDB)	$\delta^{13}C$ (PDB)
15-5	35-39	136.25	39.577	36.710	5.6	M	0.707747	7	4.65	2.13	0.835	1.345
									4.77	2.18		
15-5	107-112	136.97	39.644	36.774	5.6	M	0.707740	6	5.24	2.40	0.558	1.066
15-6	35-39	137.75	39.716	36.844	5.5	M	0.707748	7	4.97	2.27	0.629	1.187
15-6	107-112	138.47	39.783	36.908	5.0	M	0.707732	6			0.559	1.255 *
15-7	35-39	139.25	39.856	36.978	5.6	M	0.707716	7				
16-1	35-37	139.75	39.902	37.023	5.7	M	0.707736	6	5.63	2.58	0.784	1.082
16-1	110-114	140.50	39.972	37.090	4.8	M	0.707750	6	4.90	2.24	0.780	1.265
16-2	35-37	141.25	40.042	37.157	5.2	M	0.707729	6				
16-2	110-114	142.00	40.112	37.224	6.5	M	0.707708	6	4.58	2.09	0.866	1.289
									4.91	2.25		
16-3	35-37	142.75	40.181	37.291	4.6	P	0.707729	7				
16-4	35-37	144.25	40.321	37.425	4.7	M	0.707733	7				

APPENDIX A2--continued

C S	Int.	Depth (mbsf)	Age (Ma) BKFV85	Age (Ma) CK92	Mass (mg)	Comp-osi-tion	87/86	Internal Error (10^{-6})	Sr/Ca Ratio µg/mg	Sr/Ca Ratio mmol/mol	$\delta^{18}O$ (PDB)	$\delta^{13}C$ (PDB)
16-5	35-37	145.75	40.461	37.559	5.7	M	0.707733	6				
16-6	35-37	147.25	40.600	37.693	5.0	M	0.707712	7				
16-7	35-37	148.75	40.740	37.827	4.3	M	0.707732	6				
17-1	87-89	149.97	40.853	37.936	10.0	P	0.707743	6				
					3.0	B	0.707729	6				
17-2	35-37	150.95	40.944	38.024	6.4	M	0.707718	5				
17-3	35-37	152.45	41.084	38.158	5.2	M	0.707704	6				
17-4	35-37	153.95	41.338	38.558	5.9	M	0.707726	5	4.89	2.24		
17-5	35-37	155.45	41.627	38.903	5.4	M	0.707718	6				
17-6	35-37	156.95	41.917	39.249	3.1	P	0.707728	6				
					3.2	B	0.707710	6				
17-6	110-112	157.70	42.061	39.422	6.5	M	0.707709	5	4.45	2.04		

APPENDIX A2--continued

C S	Int.	Depth (mbsf)	Age (Ma) BKFV85	Age (Ma) CK92	Mass (mg)	Comp-osi-tion	87/86	Internal Error (10^{-6})	Sr/Ca µg/mg	Ratio mmol/mol	$\delta^{18}O$ (PDB)	$\delta^{13}C$ (PDB)
17-7	35-37	158.45	42.206	39.594	6.5	M	0.707719	6	4.66	2.13		
									4.57	2.09		
18-1	36-38	159.16	42.343	39.758	2.1	M	0.707712	6				
18-1	110-113	159.90	42.485	39.928	4.5	M	0.707714	7				
18-2	36-38	160.66	42.632	40.104	5.5	M	0.707695	5				
18-2	110-113	161.40	42.774	40.278	6.0	M	0.707717	6	5.45	2.49		
									5.19	2.38		
18-3	110-113	162.90	43.996	41.580	5.8	M	0.707735	7	5.10	2.33		
									5.06	2.32		
18-4	110-113	164.40	44.371	42.142	3.7	P	0.707724	6				
					4.5	B	0.707730	6				
18-5	110-113	165.90	44.755	42.707	5.7	M	0.707747	7	5.19	2.37		
									4.93	2.25		

APPENDIX A2--continued

C S	Int.	Depth (mbsf)	Age (Ma) BKFV85	Age (Ma) CK92	Mass (mg)	Comp-osi-tion	87/86	Internal Error (10^{-6})	Sr/Ca μg/mg	Ratio mmol/mol	$\delta^{18}O$ (PDB)	$\delta^{13}C$ (PDB)
19-1	35-39	168.85	45.556	43.364	3.1	M	0.707744	7				
19-2	35-39	170.35	45.964	43.699	5.7	M	0.707746	6	5.52	2.52		
									5.16	2.36		
19-3	35-39	171.85	46.328	44.016	6.0	M	0.707767	10	5.35	2.45		
									5.04	2.30		
19-4	35-39	173.35	46.647	44.315	6.6	P	0.707752	8				
					1.5	B	0.707762	5				
19-5	35-39	174.85	46.966	44.614	4.7	M	0.707761	6				
19-6	35-39	176.35	47.285	44.913	2.6	Sh	0.707759	5				
					5.3	M	0.707743	7				
20-1	109-113	179.19	47.890	45.479	5.9	M	0.707771	5	4.53	2.07		
									4.41	2.02		

APPENDIX A2--continued

C S	Int.	Depth (mbsf)	Age (Ma) BKFV85	Age (Ma) CK92	Mass (mg)	Composition	87/86	Internal Error (10^{-6})	Sr/Ca Ratio µg/mg	Sr/Ca Ratio mmol/mol	$\delta^{18}O$ (PDB)	$\delta^{13}C$ (PDB)
20-2	109-113	180.69	48.209	45.778	6.9	M	0.707736	5	5.36	2.45		
									5.15	2.36		
20-3	109-113	182.19	48.529	46.077	5.4	M	0.707768	6	5.24	2.39		
									5.06	2.31		
20-4	35-39	182.95	48.690	46.228	6.7	P	0.707768	6				
					5.3	B	0.707725	8				

*: Replicates of data from Kennett and Stott [1990]. $\delta^{18}O$ values average 0.070 (σ=0.287) higher than the 1990 data, while $\delta^{13}C$ values average 0.026 (σ=0.184) lower than the 1990 data.

wp: well preserved, as determined by optical microscopy.

pp: poorly preserved, as determined by optical microscopy.

B: Benthic Foraminifera

P: Planktic Foraminifera

M: Mixed Foraminifera

Sh: Shell material

APPENDIX A3

Oxygen and carbon isotope analyses of *Cibicidoides* spp. for ODP Hole 703A

c-s	int	Depth (mbsf)	Age (Ma)	$\delta^{13}C$	$\delta^{18}O$
4-5,	82	30.72	20.370	0.982	1.854
4-6,	41	31.81	20.610	0.868	1.724
4-6,	132	32.72	20.889	0.821	1.592
5-1,	82	34.22	20.996	1.467	2.275
5-1,	127	34.67	21.027	1.078	2.441
5-3,	82	37.22	21.218	0.762	1.741
5-3,	127	37.67	21.256	0.952	1.979
5-4,	40	38.30	21.309	0.979	1.765
5-4,	43	38.33	21.311	1.585	0.897 *
5-4,	127	39.17	21.382	1.017	1.568
5-5,	82	40.22	23.290	1.457	2.092
5-5,	127	40.67	23.330	1.109	1.757
5-6,	43	41.33	23.390	1.253	1.736
5-6,	82	41.72	23.425	1.424	1.827
				1.441	1.964
				1.277	2.045
5-6,	127	42.17	23.452	1.083	1.482
5-7,	43	42.83	23.479	1.206	1.696
6-1,	41	43.31	23.499	0.784	1.657
6-1,	99	43.89	23.523	1.655	2.003
6-1,	141	44.31	23.540	1.691	2.164

APPENDIX A3--continued

c-s	int	Depth (mbsf)	Age (Ma)	$\delta^{13}C$	$\delta^{18}O$
6-2,	41	44.81	23.595	1.490	1.950
6-2,	141	45.81	23.760	1.769	2.212
6-3,	41	46.31	23.801	1.458	2.181
6-3,	99	46.89	23.821	1.365	2.031
6-4,	41	47.81	23.853	1.638	2.024
6-4,	99	48.39	23.873	0.680	1.626
				0.900	1.870
6-4,	141	48.81	23.887	1.162	1.611
6-5,	41	49.31	23.904	1.338	1.764
				1.329	1.682
6-5,	99	49.89	23.924	1.336	1.802
6-6,	41	50.81	23.956	0.223	1.682
6-6,	45	50.85	23.958	0.424	1.634
6-7,	6	51.96	23.996	0.750	1.509
6-7,	31	52.21	24.004	1.126	1.673
6-7,	45	52.35	24.009	0.788	1.604
6-7,	66	52.56	24.017	0.802	1.762
7-1,	61	53.01	25.794	1.156	1.970
				1.324	1.831
7-1,	111	53.51	25.823	1.171	1.728
7-2,	31	54.21	25.864	0.972	1.755
7-2,	61	54.51	25.882	0.848	1.618
7-2,	111	55.01	25.912	1.175	1.697
7-3,	3	55.43	25.936	0.784	1.811

APPENDIX A3--continued

c-s	int	Depth (mbsf)	Age (Ma)	$\delta^{13}C$	$\delta^{18}O$
7-3,	61	56.01	25.973	0.776	1.930
7-4,	31	57.21	26.367	0.776	1.969
				0.863	1.681
7-4,	61	57.51	26.615	0.819	1.211
				0.658	1.829
7-4,	111	58.01	26.862	0.573	2.009
7-5,	31	58.71	26.976	0.763	1.581
				0.647	1.615
7-5,	61	59.01	27.025	1.094	2.009
7-5,	97	59.37	27.083	0.941	2.242
7-5,	140	59.80	27.153	0.971	2.142
7-CC,	10	60.12	27.205	0.612	2.069
8-1,	42	62.32	27.564	0.833	1.887
8-1,	64	62.54	27.600	0.707	1.972
8-2,	64	64.04	28.172	0.859	2.405
8-3,	64	65.54	29.014	0.550	2.178
8-4,	42	66.82	29.336	0.677	2.148
8-6,	42	69.82	30.405	0.774	2.431
8-6,	101	70.41	30.462	0.845	2.475
9-1,	75	72.15	30.630	0.777	2.248
9-2,	25	73.15	30.727	0.722	2.290
9-2,	125	74.15	30.824	0.861	2.337
				1.284	2.844
9-3,	25	74.65	30.873	0.877	2.892

APPENDIX A3--continued

c-s	int	Depth (mbsf)	Age (Ma)	$\delta^{13}C$	$\delta^{18}O$	
9-3,	92	75.32	30.937	0.593	2.296	
9-4,	58	76.48	31.050	0.677	1.858	
9-4,	91	76.81	31.082	0.817	1.631	
9-5,	75	78.15	31.212	0.947	2.118	
9-5,	92	78.32	31.228	0.790	2.300	
9-5,	115	78.55	31.303	0.479	1.911	
9-6,	10	79.00	31.459	0.528	2.301	
9-6,	58	79.48	31.588	0.372	1.781	
9-6,	75	79.65	31.599	0.652	1.931	
9-6,	92	79.82	31.610	1.284	2.222	
9-7,	58	80.98	31.690	1.003	1.661	
10-1,	8	80.98	31.690	0.490	1.826	
10-1,	125	82.15	31.776	0.349	1.828	
10-2,	75	83.15	31.849	0.444	1.878	
10-3,	73	84.63	31.958	0.520	1.925	
10-4,	60	86.00	32.059	0.626	1.922	
10-5,	60	87.50	32.179	0.733	1.827	
10-6,	1	88.41	32.252	0.833	2.180	
10-6,	48	88.88	32.290	0.414	1.892	
10-6,	60	89.00	32.300	0.288	0.400	*
10-6,	71	89.11	32.309	0.894	1.892	
10-7,	60	90.50	32.421	0.568	1.968	
11-1,	30	90.70	32.437	0.679	1.823	
11-1,	91	91.31	32.490	0.560	1.589	

APPENDIX A3--continued

c-s	int	Depth (mbsf)	Age (Ma)	$\delta^{13}C$	$\delta^{18}O$
11-2,	30	92.20	32.572	0.942	1.848
11-2,	68	92.58	32.607	0.886	1.787
11-2,	91	92.81	32.629	0.853	1.859
11-3,	68	94.08	32.746	0.989	1.734
				0.823	1.505
11-3,	91	94.31	32.768	1.008	1.502
11-4,	30	95.20	32.850	0.906	1.734
				0.984	1.904
11-4,	68	95.58	32.885	1.041	1.848
				1.142	1.961
11-5,	30	96.70	33.055	0.780	1.363
11-5,	68	97.08	33.116	0.820	1.549
11-5,	91	97.31	33.153	0.817	1.471
11-6,	29	98.19	33.295	0.767	1.713
				0.773	1.965
				0.877	1.745
11-6,	68	98.58	33.358	0.741	1.534
				0.752	1.588
11-7,	30	99.70	33.539	0.982	1.675
11-7,	37	99.77	33.550	1.001	1.603
12-1,	41	100.31	33.637	1.042	1.514
12-1,	85	100.75	33.708	1.032	1.613
				0.972	1.634
12-1,	91	100.81	33.718	0.811	1.908

APPENDIX A3--continued

c-s	int	Depth (mbsf)	Age (Ma)	$\delta^{13}C$	$\delta^{18}O$
12-1,	94	100.84	33.723	1.158	1.709
				1.094	1.731
12-1,	130	101.20	33.781	0.830	1.242
12-2,	3	101.43	33.818	0.846	1.385
12-2,	40	101.80	33.877	0.935	1.312
12-3,	3	102.93	34.060	0.836	1.201
12-3,	40	103.30	34.119	0.843	1.486
12-4,	40	104.80	34.361	0.801	1.528
12-4,	72	105.12	34.413	1.052	1.503
12-5,	40	106.30	34.603	1.309	1.532
				1.062	1.848
12-5,	130	107.20	34.748	1.025	1.515
12-6,	3	107.43	34.785	1.237	1.593
12-6,	118	108.58	34.970	1.193	1.930
12-6,	130	108.70	34.989	1.409	1.964
12-7,	40	109.30	35.086	1.293	2.024
				1.355	1.753
13-1,	45	109.85	37.107	1.308	1.178
13-1,	90	110.30	37.129	0.875	0.989
13-2,	45	111.35	37.179	0.971	1.300
				0.847	0.977
13-2,	145	112.35	37.226	0.980	1.040
13-3,	45	112.85	37.250	1.024	1.097
13-4,	61	114.51	37.329	0.973	0.929

APPENDIX A3--continued

c-s	int	Depth (mbsf)	Age (Ma)	$\delta^{13}C$	$\delta^{18}O$
13-4,	87	114.77	37.341	0.886	0.959
				1.067	1.075
13-4,	133	115.23	37.363	0.876	1.023
13-CC,	36	118.86	37.536	1.054	1.085
15-1,	136	129.76	38.055	1.006	0.637
				1.073	0.702
15-1,	146	129.86	38.060	1.104	0.825
15-2,	41	130.31	38.081	0.860	0.486
15-2,	82	130.72	38.101	1.209	0.703
15-2,	132	131.22	38.123	1.080	0.631
15-3,	41	131.81	38.148	0.986	0.508
15-3,	82	132.22	38.166	0.968	0.616
15-3,	132	132.72	38.188	1.147	0.904
15-4,	82	133.72	38.232	0.949	0.910
15-4,	118	134.08	38.248	1.022	1.070
				0.785	0.894
15-5,	82	135.22	38.297	1.023	1.075
15-5,	132	135.72	38.319	1.164	1.241
				1.086	1.207
15-6,	82	136.72	38.363	1.070	1.086
16-1,	15	138.05	38.421	0.999	1.175
16-1,	82	138.72	38.450	1.142	1.150
				1.144	1.224
16-1,	122	139.12	38.468	1.135	1.143

APPENDIX A3--continued

c-s	int	Depth (mbsf)	Age (Ma)	$\delta^{13}C$	$\delta^{18}O$
16-CC,	23	139.58	38.488	1.034	1.217
				0.986	1.343
17-1,	14	143.54	38.661	0.927	1.043
17-1,	100	144.40	38.698	0.994	0.913
17-2,	32	145.22	38.734	1.026	1.051
				1.079	0.974
17-2,	100	145.90	38.764	1.187	1.149
17-2,	106	145.96	38.766	1.180	1.313
17-2,	110	146.00	38.768	1.053	1.287
				1.217	1.478
17-2,	110	146.00	38.768	1.157	1.383
17-3,	32	146.72	38.802	0.610	0.897
17-3,	61	147.01	38.817	0.787	0.776
17-3,	100	147.40	38.838	1.086	1.275
				1.018	1.315
17-CC,	10	147.60	38.849	0.974	1.210
18-1,	10	153.00	39.136	1.117	1.087
18-1,	38	153.28	39.151	0.907	1.054
18-2,	38	154.78	39.231	0.875	0.939
18-2,	95	155.35	39.278	1.265	1.246
18-2,	140	155.80	39.320	1.237	1.265
				1.236	1.183
18-3,	38	156.28	39.365	0.922	0.936
18-3,	71	156.61	39.396	1.152	1.127

APPENDIX A3--continued

c-s	int	Depth (mbsf)	Age (Ma)	$\delta^{13}C$	$\delta^{18}O$	
18-3,	95	156.85	39.418	1.207	1.130	
18-4,	38	157.78	39.506	0.583	0.707	*
				1.028	1.046	
18-4,	95	158.35	39.559	0.997	1.088	
18-4,	99	158.39	39.563	0.795	0.661	
				0.767	0.839	
18-5,	23	159.13	39.632	0.466	0.232	

Asterisks denote analyses considered to be invalid, and are not plotted or used in calculating million-year averages.

APPENDIX A4

Oxygen and carbon isotope analyses of *Cibicidoides* spp. for ODP Hole 699A

c-s, int	Depth (mbsf)	Age (Ma)	$\delta^{13}C$	$\delta^{18}O$	
15-2, 111	134.71	26.276	0.812	1.919	
15-4, 45	137.05	26.378	0.841	1.582	
16-5, 10	147.70	27.120	0.464	1.667	
16-CC, 20	150.80	27.347	0.530	1.583	
17-1, 145	152.55	27.476	1.153	1.007	
17-2, 110	153.70	27.561	0.509	2.185	
17-5, 103	158.13	27.815	0.501	1.519	
18-1, 140	162.00	27.962	0.230	1.540	
18-2, 115	163.25	28.010	0.582	1.789	
18-3, 80	164.40	28.053	0.899	1.821	
18-5, 92	167.52	28.188	0.093	1.459	*
18-6, 56	168.66	28.265	0.676	2.049	
19-1, 8	170.18	28.368	0.591	1.496	
19-1, 100	171.10	28.429	0.946	1.863	
19-2, 57	172.17	28.502	0.601	1.987	
19-3, 130	174.40	28.652	-0.184	2.045	*
20-1, 133	180.93	29.091	0.673	1.515	
20-2, 100	182.10	29.170	0.143	1.687	*
20-4, 57	184.67	29.365	0.818	2.054	
20-5, 35	185.95	29.465	0.729	1.793	
20-6, 28	187.38	29.577	0.170	1.610	

APPENDIX A4--continued

c-s, int	Depth (mbsf)	Age (Ma)	$\delta^{13}C$	$\delta^{18}O$
21-1, 12	189.22	29.721	0.737	2.115
21-1, 122	190.32	29.822	0.602	2.150
			0.656	2.081
			0.724	2.063
21-2, 37	190.97	29.882	0.283	1.637
21-3, 117	193.27	30.100	0.531	1.168
21-4, 27	193.87	30.127	0.346	1.452
21-4, 107	194.67	30.163	0.431	1.396
21-5, 120	196.30	30.237	0.335	1.779
			0.676	1.927
21-6, 42	197.02	30.270	0.535	1.564
22-1, 30	198.90	30.381	0.751	1.694
22-1, 119	199.79	30.463	-0.029	1.440
22-2, 43	200.53	30.531	0.054	1.518
			0.246	1.551
			0.169	1.502
22-2, 122	201.32	30.604	0.340	1.853
22-3, 10	201.70	30.640	0.402	1.974
22-3, 140	203.00	30.760	0.485	1.706
22-4, 75	203.85	30.838	0.472	1.826
22-5, 15	204.75	30.921	0.292	1.439
23-1, 12	205.22	30.965	0.398	1.798
			0.333	1.674

APPENDIX A4--continued

c-s, int	Depth (mbsf)	Age (Ma)	$\delta^{13}C$	$\delta^{18}O$
23-2, 5	206.65	31.097	0.538	1.724
			0.453	1.677
23-2, 130	207.90	31.212	0.296	1.995
23-3, 36	208.46	31.269	0.427	1.660
23-4, 137	210.97	31.530	0.615	1.619
23-5, 65	211.75	31.612	0.783	1.736
23-5, 98	212.08	31.646	0.494	1.759
24-3, 77	218.37	32.118	0.515	1.689
25-1, 32	224.42	32.269	0.793	1.506
25-2, 31	225.91	32.306	0.900	1.471
27-5, 119	250.29	32.915	1.085	1.523
27-6, 82	251.42	32.944	1.130	1.588
28-1, 15	252.75	32.977	0.916	1.540
28-1, 30	252.90	32.981	0.814	1.499
28-1, 134	253.94	33.959	0.799	1.524
29-1, 125	260.35	34.359	1.049	1.350
29-3, 66	262.76	34.509	1.185	1.772
30-1, 25	268.85	34.890	1.270	1.628
30-1, 66	269.26	34.915	1.002	1.431
30-1, 130	269.90	34.955	1.089	1.593
30-2, 61	270.71	35.006	1.170	1.559
30-2, 120	271.30	35.043	1.179	1.895
30-3, 80	272.40	35.111	1.294	1.624
30-4, 68	273.78	35.198	1.447	1.843

APPENDIX A4--continued

c-s, int	Depth (mbsf)	Age (Ma)	$\delta^{13}C$	$\delta^{18}O$	
30-4, 138	274.48	35.241	1.126	1.876	
31-1, 105	279.15	35.533	1.770	1.744	*
31-1, 112	279.22	35.537	1.428	1.647	
31-2, 40	280.00	35.586	1.360	1.886	
31-2, 107	280.67	35.628	1.538	1.493	
31-3, 30	281.40	35.673	1.721	1.759	
31-3, 112	282.22	35.725	1.639	2.003	*
			1.729	1.699	
31-4, 42	283.02	35.774	1.490	1.971	
			1.507	1.967	
31-5, 50	284.60	35.873	0.909	1.262	
31-5, 129	285.39	35.922	0.996	1.127	
31-6, 130	286.90	36.017	1.152	0.932	
32-1, 65	288.25	36.101	1.242	1.211	
32-1, 110	288.70	36.129	0.902	0.304	*
32-1, 140	289.00	36.147	0.738	1.027	
32-2, 25	289.35	36.169	0.673	0.839	
32-6, 76	295.86	36.575	0.810	0.788	
32-6, 130	296.40	36.609	0.482	0.853	
32-7, 26	296.86	36.637	1.007	0.925	
33-1, 20	297.30	36.665	0.930	0.924	
33-1, 97	298.07	36.713	1.009	0.806	
33-2, 59	299.19	36.783	0.582	0.923	
33-2, 81	299.41	36.796	0.724	0.639	*

APPENDIX A4--continued

c-s, int	Depth (mbsf)	Age (Ma)	$\delta^{13}C$	$\delta^{18}O$	
33-3, 20	300.30	36.852	0.777	0.603	
33-3, 111	301.21	36.909	1.036	1.231	
33-4, 81	302.41	36.984	0.796	0.837	
33-4, 111	302.71	37.002	0.852	0.529	
33-5, 81	303.91	37.077	1.170	0.956	*
33-5, 111	304.21	37.096	0.840	0.679	
33-6, 81	305.41	37.171	0.704	0.654	
33-6, 111	305.71	37.189	0.613	0.692	
33-CC	306.11	37.214	1.083	0.708	
35-1, 86	316.96	37.891	1.428	0.858	
35-1, 90	317.00	37.893	1.283	0.787	
35-2, 30	317.90	37.949	1.233	0.664	
35-2, 86	318.46	37.984	1.316	0.509	
35-2, 145	319.05	38.021	1.378	0.976	
35-3, 86	319.96	38.078	1.528	1.379	*
35-4, 10	320.70	38.124	1.236	0.643	
35-4, 86	321.46	38.165	1.259	0.572	
35-5, 10	322.20	38.183	1.189	0.696	
35-5, 86	322.96	38.203	1.178	0.515	
35-6, 10	323.70	38.222	1.284	0.512	
35-6, 81	324.41	38.240	1.264	0.416	
35-7, 10	325.20	38.260	1.335	0.342	
36-1, 21	325.81	38.275	1.254	0.094	
36-1, 126	326.86	38.302	0.968	0.229	

APPENDIX A4--continued

c-s, int	Depth (mbsf)	Age (Ma)	$\delta^{13}C$	$\delta^{18}O$	
36-2, 73	327.83	38.327	1.234	0.430	
			1.171	0.537	
36-2, 115	328.25	38.338	1.291	0.644	
36-3, 21	328.81	38.352	1.131	0.317	
36-3, 116	329.76	38.376	1.425	0.572	
36-4, 21	330.31	38.390	1.613	0.388	
36-4, 116	331.26	38.473	1.511	-0.023	
36-5, 73	332.33	38.613	1.292	0.564	
			1.438	0.056	
36-6, 21	333.31	38.742	1.713	0.339	
36-6, 75	333.85	38.812	1.177	0.492	
36-6, 116	334.26	38.866	1.051	1.075	
			0.885	0.768	
36-7, 21	334.81	38.938	1.136	0.652	
36-7, 50	335.10	38.976	0.704	0.251	
37-1, 128	336.38	39.144	1.282	0.726	
37-2, 54	337.14	39.243	0.980	0.920	
37-2, 96	337.56	39.298	0.899	0.737	
37-3, 54	338.64	39.439	0.949	0.721	
37-3, 86	338.96	39.481	0.667	0.941	*
37-4, 54	340.14	39.636	0.848	0.645	
37-4, 118	340.78	39.720	1.203	0.808	
37-5, 54	341.64	39.832	0.933	0.593	
			0.871	0.590	

APPENDIX A4--continued

c-s, int	Depth (mbsf)	Age (Ma)	$\delta^{13}C$	$\delta^{18}O$	
37-5, 122	342.32	39.921	1.002	0.584	
37-6, 15	342.75	39.978	0.973	0.597	
37-CC, 22	343.14	40.029	0.765	0.128	*
38-1, 16	344.76	40.241	0.704	0.955	
38-CC	350.60	41.004	1.096	0.887	
39-1, 26	354.36	41.367	0.929	0.379	
39-1, 110	355.20	41.472	1.103	0.027	
			1.053	0.161	
39-2, 26	355.86	41.567	1.521	0.168	
39-2, 51	356.11	41.603	0.936	0.176	
			1.060	0.376	
			1.476	0.267	
39-2, 75	356.35	41.638	1.191	0.360	

Asterisks denote analyses considered to be invalid, and are not plotted or used in calculating million-year averages.

APPENDIX A5

Oxygen and Carbon Isotopic Data from DSDP Site 363, Cores 5, 6, And 7

			Fine Fraction			Chiloguembelina cubensis		Catapsydrax dissimilis		Cibicidoides spp.	
Sample			$\delta^{13}C$	$\delta^{18}O$		$\delta^{13}C$	$\delta^{18}O$	$\delta^{13}C$	$\delta^{18}O$	$\delta^{13}C$	$\delta^{18}O$
c-s-	z	*1	(PDB)	(PDB)	*2	(PDB)	(PDB)	(PDB)	(PDB)	(PDB)	(PDB)
5-2-	34.5	+	1.447	0.841	C	1.159	-0.177	0.269	0.857	0.528	1.623
										0.542	1.626
5-2-	46	B	1.381	1.332	C	1.088	-0.325	0.510	0.912	0.971	0.601
			1.218	0.650						0.602	1.365
5-2-	60	+	1.197	0.564	c	0.736	-0.625	0.291	1.001	0.540	1.623
			1.368	0.255	Ch	1.038	0.160	0.906	0.579		
5-2-	65	+	1.324	0.210	c	0.838	-0.351	0.589	1.445	0.534	1.496
			1.192	0.243	Ch	0.970	-0.443				
5-2-	70	B	1.279	1.146	c	1.108	-0.051	0.754	1.164	0.715	1.527
					Ch	1.219	0.242			0.745	1.441
5-2-	72	B	1.266	0.904	c	0.954	-0.548	0.863	1.028	0.656	1.271

APPENDIX A5--continued

Sample			Fine Fraction			Chiloguembelina cubensis		Catapsydrax dissimilis		Cibicidoides spp.	
			$\delta^{13}C$	$\delta^{18}O$		$\delta^{13}C$	$\delta^{18}O$	$\delta^{13}C$	$\delta^{18}O$	$\delta^{13}C$	$\delta^{18}O$
C-S-	z	*1	(PDB)	(PDB)	*2	(PDB)	(PDB)	(PDB)	(PDB)	(PDB)	(PDB)
5-2-	72	B			Ch	1.124	-0.198				
5-2-	80.5	+	1.236	0.464	c	0.739	-0.282	0.962	0.672	0.356	1.356
					C	0.894	0.049			0.473	1.575
6-3-	54	+	1.420	0.339	c	1.483	0.098	0.956	0.811	0.834	1.948
			1.562	0.174	Ch	0.767	1.705			1.067	1.906
					Ch	1.645	-0.030				
					CH	1.723	0.351				
6-3-	75.5	+	1.389	0.759	c	1.649	0.018	1.127	0.714	1.025	1.643
					c	1.304	-0.092				
					Ch	1.760	0.023				
					Ch	1.255	-0.299				
					CH	1.834	0.121				

APPENDIX A5--continued

Sample			Fine Fraction			Chiloguembelina cubensis		Catapsydrax dissimilis		Cibicidoides spp.	
			$\delta^{13}C$	$\delta^{18}O$		$\delta^{13}C$	$\delta^{18}O$	$\delta^{13}C$	$\delta^{18}O$	$\delta^{13}C$	$\delta^{18}O$
c-s-	z	*1	(PDB)	(PDB)	*2	(PDB)	(PDB)	(PDB)	(PDB)	(PDB)	(PDB)
6-3-	84.5	+	1.918	1.644	c	1.818	0.564	1.226	1.010	1.081	1.730
					Ch	1.880	0.624				
					Ch	1.916	0.666				
					CH	1.705	0.888				
6-3-	90	B	2.419	1.758	c	-0.137	0.106	1.371	1.014	0.976	1.193
					c	0.750	1.411				
					c	0.844	1.322				
					Ch	2.006	0.154				
					Ch	1.943	0.404				
6-3-	97.5	B	2.232	2.153	c	1.838	0.519	1.264	1.019	1.103	1.374
					C	1.641	0.212				
6-3-	102	B	2.379	1.656	c	1.761	-0.273	1.325	0.963	0.983	1.312
					c	1.618	-0.055			1.024	1.051

APPENDIX A5--continued

		Fine Fraction			Chiloguembelina cubensis		Catapsydrax dissimilis		Cibicidoides spp.	
Sample		$\delta^{13}C$	$\delta^{18}O$		$\delta^{13}C$	$\delta^{18}O$	$\delta^{13}C$	$\delta^{18}O$	$\delta^{13}C$	$\delta^{18}O$
c-s- z	*1	(PDB)	(PDB)	*2	(PDB)	(PDB)	(PDB)	(PDB)	(PDB)	(PDB)
6-3-102	B			Ch	1.511	-0.456				
6-3-105	B	2.506	2.131	Ch	1.594	0.235	1.313	1.197	1.218	1.502
		2.582	1.733	CH	1.281	0.698				
6-3-115.5	B	2.648	2.153	cC	1.656	0.431	1.220	0.926		
6-3-120	B	2.727	1.829	c	1.770	-0.015	1.232	1.040	1.047	1.115
				Ch	1.779	-0.294				
6-3-125.5	B	2.710	2.189	C	1.787	0.167	1.168	1.247	1.296	1.533
6-3-130	B	2.531	1.546	c	1.750	0.004	1.136	1.200	0.875	0.920
				Ch	1.811	-0.018	1.277	1.112	0.845	1.082
									0.855	1.046
6-3-141	+	2.085	1.034	c	1.730	-0.014	1.132	1.058	0.828	1.237
				Ch	1.907	0.071			0.832	1.238

APPENDIX A5--continued

		Fine			Chiloguembelina		Catapsydrax		Cibicidoides	
		Fraction			cubensis		dissimilis		spp.	
Sample		$\delta^{13}C$	$\delta^{18}O$		$\delta^{13}C$	$\delta^{18}O$	$\delta^{13}C$	$\delta^{18}O$	$\delta^{13}C$	$\delta^{18}O$
c-s- z	*1	(PDB)	(PDB)	*2	(PDB)	(PDB)	(PDB)	(PDB)	(PDB)	(PDB)
6-3-141	+			Ch	1.784	-0.027			0.909	1.055
				CH	1.874	-0.166				
6-3-145	+	2.464	1.997	c	1.885	0.517	1.272	0.997	0.951	1.545
		2.519	1.568	Ch	1.897	0.665			0.932	1.830
6-4- 5	+	2.386	1.481	c	1.799	0.077	1.192	0.869	0.968	1.078
				c	1.748	-0.001				
				Ch	1.907	0.144				
				Ch	1.766	-0.044				
				CH	1.912	0.061				
6-4- 15	+	2.067	1.005	c	1.617	-0.023	1.214	0.876	0.787	0.979
				Ch	1.790	0.113				

APPENDIX A5--continued

		Fine Fraction			Chiloguembelina cubensis		Catapsydrax dissimilis		Cibicidoides spp.	
Sample		$\delta^{13}C$	$\delta^{18}O$		$\delta^{13}C$	$\delta^{18}O$	$\delta^{13}C$	$\delta^{18}O$	$\delta^{13}C$	$\delta^{18}O$
c-s- z	*1	(PDB)	(PDB)	*2	(PDB)	(PDB)	(PDB)	(PDB)	(PDB)	(PDB)
7-1- 50.5	+	1.280	0.165	c	1.222	-0.771	0.977	0.418	0.708	0.956
				Ch	1.496	-0.146			0.582	1.301
				Ch	1.347	-0.784			0.586	1.208
				P	1.097	-0.328				
7-1- 69	+	1.963	0.917	c	1.664	-0.120	1.253	0.772	1.088	1.206
				Ch	1.633	-0.518	1.258	1.010	0.942	1.463
				Ch	1.797	0.064				
				CH	1.882	0.351				
7-1- 90	+	2.709	0.968	P	0.902	0.119	1.087	0.983	1.089	1.267
7-1- 91.5	+	2.152	0.827	c	1.994	0.440	1.223	0.363	0.979	1.659
		2.404	0.681						1.099	1.160
7-1-111	B	3.527	2.180							
7-1-117.5	B	3.697	2.091	P	1.739	1.773	1.386	0.000	1.325	1.490

APPENDIX A5--continued

		Fine Fraction			Chiloguembelina cubensis		Catapsydrax dissimilis		Cibicidoides spp.	
Sample c-s- z	*1	$\delta^{13}C$ (PDB)	$\delta^{18}O$ (PDB)	*2	$\delta^{13}C$ (PDB)	$\delta^{18}O$ (PDB)	$\delta^{13}C$ (PDB)	$\delta^{18}O$ (PDB)	$\delta^{13}C$ (PDB)	$\delta^{18}O$ (PDB)
7-1-130.5	B	3.675	2.366							
		3.581	1.855							
7-1-134	B	3.663	1.949				1.642	0.438	1.574	1.503
7-1-145	B	3.662	2.009	P	1.651	1.140	1.597	0.171		
7-1-147.5	B	3.686	2.451	P	0.441	0.458				
7-CC	B	3.668	2.436				1.365	0.129	1.441	1.279

---

*1: B indicates a sample from a *Braarudosphaera* ooze; + indicates a non-*Braarudosphaera* ooze sample.

*2: The letter in this column indicates which size fraction of *Chiloquembelina cubensis* was measured: 104-125μm (c), 104-150μm (C), 125-150μm (Ch), 150-250μm (CH), and 104-250μm (cC). In Core 7, bulk planktic foraminifera from 125-150μm are indicated by P.

APPENDIX B

DETAILED METHODS AND DERIVATIONS

APPENDIX B1

Instructions for obtaining and using on-line data tables.

Retrevial from the Internet

Appendix A1 has been archived in digital form at the World Data Center-A for Paleoclimatology, NOAA/NGDC 325 Broadway, Boulder, CO, 80303; (Phone (303) 4977-6513, Internet e-mail: paleo@mail.ngdc.noaa.gov). The files are in the timescales subdirectory within the paleo directory. Instructions for logging on and downloading the necessary files may be found in Webb et al. [1994]. A brief list of instructions follows (from Webb et al. [1994] and Bauer, personal communication):

1. At the system prompt, enter:

```
ftp ngdc1.ngdc.noaa.gov
```

2. When prompted for a username, enter:

```
anonymous
```

3. When prompted for a password, enter your e-mail address:

```
scientist@computer.univ.edu
```

4. To change to the paleo directory, enter:

```
cd paleo
```

5. To change to the timescales directory, enter:

```
cd timescales
```

Three files are present in the paleo\timescales directory: TIMESCALE.README, TIMESCAL.ASC, and TIMESCAL.TAB. TIMESCALE.README is a readme file explaining the contents. TIMESCAL.ASC is a pure-ASCII table which can be taken into word processors for the purpose of making a table of the GPTS's. TIMESCAL.TAB is a tab delimited ASCII (pure text) file, which has successfully been test-imported into the DOS-based spreadsheets Quattro Pro and Lotus 123, and into the MacIntosh-based spreadsheet Excel.

6. To retrieve the files into your computer, with a name you decide, enter:

```
get timescale.readme myname1.doc
get timescal.tab myname2.doc
```

7. At this point, the computer should respond with some information that the files have been transferred.

Loading Into a Spreadsheet:

Quattro Pro v5.0: After starting the program, press the "/" key to access the menu, then the "t" (for Tools), "i" (Import), and "c" (Comma & "" Delimited File) keys. Then enter the file name TIMESCAL.TAB and press the Enter key. The file will be imported into the spreadsheet.

Lotus 123 v2.0: After starting the program, press the "/" key to access the menu, then the "f" (File), "I" (Import), and "N" (Numbers) keys. Then enter the file name TIMESCAL.TAB and press the Enter key. The file will be imported into the spreadsheet.

Excel: After starting the program, use the Load command in the File menu. Enter the file name TIMESCAL.TAB and press the Enter key. Different versions of Excel use different dialogues, but at some point you will be prompted for the type of file. Enter "Tab delimited", or some variant thereof. Enter the file name TIMESCAL.TAB and press the Enter key. The file will be imported into the spreadsheet.

APPENDIX B2

Strontium Extraction Method

1. Pick foraminifera and sonicate samples as for oxygen and carbon isotopes. Peroxide treatment is not necessary. Ultrasonically clean the samples in methanol to remove adhering fine debris and dry in a 60°C oven. Sample sizes successfully extracted range from about 1.3 to 10.0 mg. Strontium concentrations were about 2000 ppm, giving sample Sr masses of 2.6 to 20 μg.

2. Dissolve samples in 1 to 2 ml of 0.25 N HCl for about 1 hour at 200-250°C, then dry under a laminar flow hood with filtered air flow.

3. Carbonate samples previously dissolved in 0.25 N HCl and dried are re-dissolved in 100μl 3.5 N Opticlean HNO_3.

4. Sample is centrifuged for 3 minutes at 14000 RPM in an Eppendorf type 5415 centrifuge to concentrate non-dissolvable components. The supernatant is loaded onto the ion exchange column according to the following schedule:

Purpose	Amount	Agent	Approximate Time
Cleaning	2.5 ml	4X distilled H_2O	2 hrs 45 min
Conditioning	2.0 ml	3.5 N HNO_3	2 hrs
Loading	100μl	sample in 3.5 N HNO_3	15 min
Washing 4 times	100μl	3.5 N HNO_3	1 hr
Washing away Ca	1.0 ml	3.5 N HNO_3	1hr 15 min
Collect Sr	2.0 ml	4X distilled H_2O	2 hrs

APPENDIX B3

Operating Instructions for Thermal Ionization Mass Spectrometer

Shut-Down Procedure

1. Turn off motor power switches.
2. Put Programmable Focus Unit (PFU) on STANDBY.

   Set KV on PFU to 0.
3. Close valves:
   a. BEAM VALVE (hex nut) closed to ≤150 ft-lbs).
   b. GATE VALVE to ion pump
   c. ROUGH PUMP valve.
   d. OCTABIN VALVE.
4. Loosen nuts on face of Mass Spec.
5. Open valves:
   a. GATE VALVE TO ROUGH PUMP (GVRP).
   b. Bleed air in with BLEED VALVE.
6. Close GVRP and BLEED VALVE.
7. To pump down:
   a. Open ROUGH PUMP valve to pump down piping up to the GVRP.
   b. Open OCTABIN VALVE to Analyzer when Thermocouple pressure is ≤60 μm.

Loading Procedure:

8. Remove Faceplate and place with the inside face down on the kimwipe-covered Plexiglass block.
9. Slide in curved plate over Ion Pump opening.
10. Remove old turret and install new turret.
11. Check contacts:
    a. Set Programmable Filament Supply (PFS) to Manual.
    b. Set Motor to Standby.
    c. Set Current to about 4.
    d. Turn the turret with the handle behind the chamber, watching the dial to make sure each sample makes contact. If there is a problem with contacts, remove turret and fix.
    e. Set current back to 0.
    f. Set PFS back to Auto.
    g. Set Motor back to On.

Initial Pump-down:

12. Remove curved plate from over Ion Pump opening.
13. Check to make sure there is no dust on O-ring or Faceplate.
14. Put Faceplate back on with all 4 bolts finger tight only.
15. Check to make sure Bleed Valve is closed.

16. Start pumping down:
    a. Close OCTABIN VALVE.
    b. Open GVRP and wait 5 minutes or for Thermocouple pressure to reach ≤400 µm, whichever is first.
    c. Turn on TURBO PUMP. It will have to be on 1.5 to 2 hrs (or more on humid days) before the pressure is low enough for the next step.
    d. Open OCTABIN VALVE to Analyzer when Thermocouple pressure is ≤60 µm.
    e. Measure pressure:
        i. Put Process Control on Override (pull out switch to change its position).
        ii. Turn Emission to OFF.
        iii. Switch Filament to 1 (Source Pressure, P_S).
        iv. Turn Emission back to EMISSION.
        v. GATE VALVE can be opened only if P_S is $\leq 4x10^{-5}$. If P_S is $>4x10^{-5}$, leave on Filament 1 until $\leq 4x10^{-5}$.
        vi. Turn off Emission.
        vii. Switch back to filament 2 (Analyzer Pressure, P_A).
        viii. Turn on Emission again.
        ix. Switch from Override back to middle position again once P_A $\leq 5x10^{-8}$.
17. When P_S is $<4x10^{-5}$, close GVRP.

18. Then open GATE VALVE.
19. Open BEAM VALVE when P_S is $\leq 1x10^{-6}$.
20. Turn off TURBO PUMP.
21. The mass spec may be started when $P_A \leq 2x10^{-8}$ and $P_S \leq 1x10^{-6}$. Data may be input at any time. Instructions are at the end of the current section.
22. Reset all switches changed during shut-down:
    a. Turn on motor power switches.
    b. Put Programmable Focus Unit (PFU) on ON from STANDBY.
    c. Set KV switch on PFU to 8.
23. Make sure that there's enough paper before starting the Mass Spectrometer!!!
24. Start Mass Spec by pressing CONTINUE after the last sample.
25. On PFU, dial in with the dial on the far right side of the PFU until KV = 8 on the 3rd LED readout. The value most recently used is 7.42.
26. After the 8KV is accepted, turn back to the most recent correct value (6.3 KV as of 5/17/93).

Inputting Data/Computer Operation

27. Press the <Shift> and <Reset> (Pause) keys simultaneously to reset the computer.

28. Type LOAD "MENU" and press the <Execute> key. After the disk drive finishes accessing the disk, press the <Run> key.
29. Press <k_0> ("Select" on the menu).
30. Press <Continue> at the next question.
31. Turn the disk-shaped paddle until "SR High P(2V)" is highlighted, and press k_5 ("Choose" on the menu) for each carousel position for which you have a sample. Press k_6 ("Skip" on the menu) for position 6 and any other spots which don't have samples. This tells the computer what kind of sample you have so that it knows what protocol to use in running them.
32. When you're done, press k_9 ("Complete" on the menu).
33. Answer the questions about date and time, pressing <Continue> after each one.
34. Enter your sample ID's one at a time, pressing <Continue> after each one. The computer will start the run after you've entered the last sample ID, so wait until Step 23 is done.

APPENDIX B4

Preparation of Foraminifera for Oxygen and Carbon Isotopic Analysis:

1. Pick well preserved foraminifera from washed samples. A minimum of about 200 μg of sample is needed for a successful bellows run in the Prism mass spectrometer. For Cibicidoides, the average masses of the >150μm, >212μm, and >250μm fractions respectively are 28.2μg, 43.6μg, and 129.1μg. From these averages, we need an average of 8, 5, and 2 specimens for a successful run. These numbers of course are biased by large specimens in each fraction. At >150μm, >212μm, and >250μm, minimums of over 30, 17, and 8, respectively, are needed to be sure of getting a bellows run. For other taxa, of course, the numbers will differ.
2. After picking enough samples for a mass spec run (16-22, usually), place the picked foraminiferal samples in 2 ml glass vials, label them, and tape the labels to avoid having them fall off during the cleaning process.
3. The samples then must be cleansed of organic material. This is usually done 1-2 days before a run. React the organic material with about 1-1.5 ml of 15% H_2O_2 placed in the vial with a hypodermic syringe or squirt bottle for about 1 hour or until any reaction ceases. Do not cap the vials. If there is a significant amount of

organic material in the sample, the reaction will produce an increase in pressure.

4. The hydrogen peroxide is withdrawn by a syringe with a 1.5", 18G needle attached. The tip of the needle is dulled and crimped to a very narrow slot to avoid sucking up any of the specimens.
5. The sample is then rinsed with distilled water in the vial a couple of times to remove any traces of H_2O_2. This is necessary because of the potential of reaction with methanol used in a later step.
6. The sample vials are then filled about half way with distilled water and sonicated one at a time to remove adhering debris for 10-20 seconds. The vial is held by hand half-submerged in the sonicator. Use an ultrasonicator with a rheostat to control the strength of the sonication. The strength of sonication will have to be empirically determined. If the level is too low, nothing happens. If the level is too high, there is a puff, and your sample is destroyed. At the right level, the sample "dances" in the vial, often leaving a thin trail or cloud of dust. For Cibicidoides, generally use 30-40% of the maximum on the rheostat. Planktonic foraminifera will be more delicate, and larger specimens of benthic foraminifera are more durable than smaller specimens. When in doubt, use a low value, then gradually increase the level.

7. The water is then extracted with the syringe and modified needle. It is a good idea to examine the sample microscopically at this point to make sure it has been sufficiently cleaned. If not, repeat the sonication process.
8. The next step is to rinse the sample with methanol to allow it to dry more quickly and to avoid fractionation with the distilled water. Put the methanol into the vial with a squirt bottle. Extract half of the methanol with the syringe and modified needle and squirt back into the vial. Allow the specimens to settle for a moment, then extract the methanol. This tends to suspend and remove any of the debris still in the vial, resulting in a cleaner sample. Do this a couple of times with fresh methanol.
9. Next, place the sample vials, uncapped, into a 60°C oven for drying. It takes a couple of hours for the sample to dry properly. Once the samples are dry, cap the vials.
10. The day before the run, place the samples, one sample at a time, into sample boats. Note: at this time, cleanliness is critical in obtaining good results. Clean the preparation area to remove any dust, and clean pans, forceps, etc. with acetone and Kimwipes. At no time should the sample or sample boat be touched with fingers. You are now ready to begin. First, pour the sample into a brass pan. It may be necessary to

tap the vial in case any of the specimens are stuck to the bottom of the vial. Examine the specimens microscopically to make sure that there is no debris in the vial and to make sure that there are no other problems. Weigh each sample and record the mass for later reference. Place a specimen boat into a Sartorius micro-scale with forceps and tare it. Remove the boat and place it on a piece of weighing paper or in another tray or pan. Carefully tap and pour your sample into the boat. Place the boat back into the scale to get the net mass of the sample. Do not react more than $600\mu g$ in the mass spec. After recording the mass, take the boat out, and place one of the small Teflon ball bearings on it to keep it in place while in the carousel and while falling into the reaction vessel. Place the boat into a numbered boat holder for storage. After the samples are all put into boats, store the boat holder in a desiccator until the morning of the run.

APPENDIX B5

Derivation of equations.

In a stratigraphic section, if the rate of non-carbonate deposition is assumed to be constant, then changes in overall sedimentation rate is determined by carbonate content. Thus, if the overall sedimentation rate, carbonate content of 2 different layers, and thicknesses of these layers are known, the rate of carbonate and non-carbonate deposition can be calculated:

Variables:

R_{XM} - the sedimentation rate of a particular component X and/or some layer M.

f_M - the carbonate fraction of layer M.

Z_M - the thickness of layer M

T_M - the time to deposit a layer M.

$_{nC}$ - non-carbonate fraction.

$_C$ - carbonate fraction.

$_B$ - layer of Braarudosphaera ooze.

$_S$ - layer of non-Braarudosphaera sediments

$_T$ - total thickness or overall rate.

Assumptions:

1. That R_{nC} is constant.
2. That the densities of carbonate and non-carbonate components are constant. This allows us to use sedimentation rates instead of mass accumulation rates.

3. Z_T, Z_B, Z_S, and R_T are known.

Then:

$$f_M = \frac{R_{CM}}{R_{CM} + R_{nC}} \tag{a}$$

Solving for R_{CM}:

$$R_{CM} = \frac{f_M}{1 - f_M} * R_{nC} \tag{3}$$

Since the densities of the components are assumed to be constant:

$$R_M = R_{nC} + R_{CM} = R_{nC} + \frac{f_M}{1 - f_M} * R_{nC} \tag{b}$$

or:

$$R_M = R_{nC} * \left[1 + \frac{f_M}{1 - f_M} \right] \tag{c}$$

Simplifying:

$$R_M = \frac{R_{nC}}{1 - f_M} \tag{d}$$

FF_{CM} can now be defined:

$$FF_{CM} = \frac{1}{1 - f_M} \tag{2}$$

which is actually just the inverse of the non-carbonate fraction of layer M. Therefore:

$$R_M = R_{nC} * FF_{CM} \tag{e}$$

Which is a function of R_{nCM} and f_M. Also:

$$T_T = T_B + T_S \tag{f}$$

and:

$$R_M = Z_M / T_M \tag{g}$$

Therefore:

$$\frac{Z_T}{R_T} = \frac{Z_B}{R_B} + \frac{Z_S}{R_S} \qquad \text{(h)}$$

Putting (h) in terms of R_{nC} and f_M:

$$\frac{Z_T}{R_T} = \frac{Z_B}{R_{nC} * FF_{CB}} + \frac{Z_S}{R_{nC} * FF_{CS}} \qquad \text{(i)}$$

or:

$$\frac{Z_T}{R_T} = \frac{Z_B * FF_{CS} + Z_S * FF_{CB}}{R_{nC} * FF_{CB} * FF_{CS}} \qquad \text{(j)}$$

Solving for R_{nC}:

$$R_{nC} = \frac{(Z_B * FF_{CS} + Z_S * FF_{CB}) * R_T}{FF_{CB} * FF_{CS} * Z_T} \qquad \text{(1)}$$

REFERENCES

Adams, C. G., Lee, D. E., and Rosen, B. R., Conflicting isotopic and biotic evidence for tropical sea-surface temperatures during the Tertiary, Palaeogeogr., Palaeoclimatol., Palaeoecol., 77(3/4):289-313, 1990.

Armstrong, R. L., Glacial erosion and the variable isotopic composition of Stontium in sea water, Nature Physical Science, 230(14):132-133, 1971.

Bainbridge, A., GEOSECS Atlantic Expedition, Vol. 1, Hydrographic Data 1972-1973, NSF, 121 pp., 1981a.

Bainbridge, A., GEOSECS Atlantic Expedition, Vol. 2, Sections and Profiles, NSF, 198 pp., 1981b.

Barker, P. F. and Burrell, J., The opening of Drake Passage, Mar. Geol., 25(1/2):15-34, 1977.

Barker, P. F., Kennett, J. P., et al., Proc. Ocean Drill. Program Initial Rep., 113, 1033 pp., Ocean Drilling Program, College Station, TX, 1988a.

Barker, P. F., Kennett, J. P., and Scientific Party, Weddell Sea palaeoceanography: Preliminary results of ODP Leg 113, Palaeogeogr., Palaeoclimatol., Palaeoecol., 67(1/2):75-102, 1988b.

Barker, P. F., Kennett, J. P., et al., Proc. Ocean Drill. Program Sci. Results, 113, 1033 pp., Ocean Drilling Program, College Station, TX, 1990.

Barrera, E., Barron, J., and Halliday, A., Strontium isotope stratigraphy of the Oligocene-Lower Miocene section at Site 744, Southern Indian Ocean, in Proc. Ocean Drill. Program Sci. Results, edited by J. Barron, B. Larson, et al., 119(40):731-738, Ocean Drilling Program, College Station, TX, 1991.

Barrera, E. and Huber, B. T., Eocene to Oligocene oceanography and temperatures in the Antarctic Indian Ocean, in The Antarctic Paleoenvironment: A perspective on global change, Part 2, edited by J. P. Kennett and D. A. Warnke, Antarctic Research Series, 60:49-65, Amer. Geophys. Union, Washington, DC, 1993.

Belanger, P. E., Curry, W. B., and Matthews, R. K., Core-top evaluation of benthic foraminiferal isotopic ratios for paleo-oceanographic interpretations, Palaeogeogr., Palaeoclimatol., Palaeoecol., 33(1-3):205-220, 1981.

Berger, W. H., Deep sea carbonates: dissolution facies and age-depth constancy, Nature, 236(5347):392-395, 1972.

Berger, W. H., Impact of deep drilling on paleoceanography, in *Deep Drilling Results - Atlantic Ocean: Continental Margins and Paleoenvironment*, edited by M. Talwani, W. W. Hay, and W. B. F. Ryan, *Maurice Ewing Series*, *3*:297-314, AGU, Washington, D. C, 1979.

Berger, W. H., Johnson, R. F., and Killingley, J. S., 'Unmixing' of the deep-sea record and the deglacial meltwater spike, *Nature*, *269*(5630):661-663, 1977.

Berggren, W. A., Kent, D. V., and Flynn, J. J., Jurassic to Paleogene: Part 2. Paleogene geochronology and chronostratigraphy, in *The chronology of the geologic record*, edited by N. J. Snelling, *Geol. Soc. London Mem.*, *10*:141-195, 1985b.

Berggren, W. A., Kent, D. V., Flynn, J. J., and Van Couvering, J. A., Cenozoic geochronology, *Geol. Soc. Am. Bull.*, *96*(11):1499-1510, 1985a.

Berggren, W. A., Kent, D. V., and Van Couvering, J. A., Neogene geochronology and chronostratigraphy, in *The chronology of the geologic record*, edited by N. J. Snelling, *Geol. Soc. London Mem.*, *10*:211-260, 1985c.

Blakely, R. J., Geomagnetic reversals and crustal spreading rates during the Miocene, *J. Geophys. Res.*, *79*(20):2979-2985, 1974.

Blum, J. D. and Erel, Y., A silicate weathering mechanism linking increases in marine ^{87}Sr/^{86}Sr with global glaciations, *Nature*, *373*(6513):415-418, 1995.

Boersma, A. and Premoli-Silva, I., Terminal Eocene events: Planktonic foraminifera and isotopic evidence, in *Terminal Eocene Events*, edited by C. Pomeral, and I. Premoli-Silva, pp.213-223, Elsevier Science Publ. B. V., Amsterdam, 1986.

Bougault, H., Cande, S. C., et al., *Initial Rep. Deep Sea Drill. Proj.*, *82*, 667 pp., U.S. Gov't Printing Office, Washington, DC, 1985.

Brass, G. W., Southam, J. R., and Peterson, W. H., Warm saline bottom water in the ancient ocean, *Nature*, *296*(5858):620-623, 1982.

Breza, J. R. and Wise, S. W., Jr., Lower Oligocene ice-rafted debris on the Kerguelen Plateau: Evidence for East Antarctic continental glaciation, in *Proc. Ocean Drill. Program Sci. Results*, edited by S. W. Wise, R. Schlich, et al., *120*(12):161-178, Ocean Drilling Program, College Station, TX, 1992.

Broecker, W. S., A revised estimate for the radiocarbon age of North Atlantic Deep Water, J. Geophys. Res., 84(C6):3218-3226, 1979.

Broecker, W. S. and Takahashi, T., Hydrography of the central Atlantic-IV. Intermediate waters of Antarctic origin, Deep-Sea Res., 28(3A):177-193, 1981.

Bukry, D., Cenozoic calcareous nannofossils from the Pacific Ocean, San Diego Soc. Nat. Hist. Trans., 16(14):303-328, 1971.

Bukry, D., Coccoliths as paleosalinity indicators - Evidence from Black Sea, in The Black Sea - Geology, Chemistry, and Biology, edited by E. T. Degens, and D. A. Ross, A. A. P. G. Mem., 20:353-363, 1974.

Bukry, D., Cenozoic silicoflagellate and coccolith stratigraphy, southeastern Atlantic Ocean, Deep Sea Drilling Project Leg 40, in Initial Rep. Deep Sea Drill. Proj., edited by H. M. Bolli, W. B. F. Ryan, et al., 40(13):775-805, U.S. Gov't Printing Office, Washington, DC, 1978.

Burke, W. H., Denison, R. E., Hetherington, E. A., Koepnick, R. B., Nelson, H. F., Otto, J. B., Variation of seawater ^{87}Sr/^{86}Sr throughout Phanerozoic time, Geology, 10(11):516-519, 1982.

Cande, S. C. and Kent, D. V., A New geomagnetic polarity time scale for the late Cretaceous and Cenozoic, J. Geophys. Res., 97(B10):13,917-13,951, 1992.

Cande, S. C. and Kent, D. V., Revised calibration of the geomagnetic polarity time scale for the late Cretaceous and Cenozoic, J. Geophys. Res., in press 1995.

Cande, S. C., LaBrecque, J. L., and Haxby, W. F., Plate kinematics of the South Atlantic: Chron C34 to present, J. Geophys. Res., 93:13479-13492, 1988.

Capo, R. C. and DePaolo, D. H., Seawater strontium isotopic variations from 2.5 million years ago to the Present, Science, 249(4964):51-55, 1990.

Chamberlin, T. C., On a possible reversal of deep-sea circulation and its influence on geological climates, J. Geol., 14(5):363-373, 1906.

Charles, C. D. and Fairbanks, R. G., Evidence from Southern Ocean sediments for the effect of North Atlantic deep-water flux on climate, Nature, 355(6359):416-419, 1992.

Ciesielski, P. F., Kristofferson, Y., et al., Proc. Ocean Drill. Program Initial Rep., 114, 815 pp., Ocean Drilling Program, College Station, TX, 1988.

Clague, D. A., Dalrymple, G. B., and Moberly, R., Petrogrpahy and K-Ar ages of dredged volcanic rocks from the Western Hawaiian Ridge and the Southern Emperor Seamount Chain, Geol. Soc. of Amer. Bull., 86(7):991-998, 1975.

Clemens, S. C., Farrell, J. W., and Gromet, L. P., Synchronous changes in seawater strontium isotope composition and global climate, Nature, 363(6430):607-610, 1993.

Coplen, T. B., Kendall, C., and Hopple, J., Comparison of stable isotope reference samples, Nature, 302(5904):236-238, 1983.

Corliss, B. H., Deep-sea benthonic foraminiferal faunal turnover near the Eocene/Oligocene boundary, Mar. Micropaleont., 6(4):367-384, 1981.

Corliss, B. H., Aubry, M.-P., Berggren, W. A., Fenner, J. M., Keigwin, L. D., and Keller, B., The Eocene/Oligocene boundary event in the deep sea, Science, 226(4676):806-810, 1984.

Corliss, B. H. and Keigwin, L. D., Jr., Eocene-Oligocene paleoceanography, in Mesozoic and Cenozoic Oceans, edited by K. J. Hsü, Geodynamics Series, 15, 101-118, AGU, Washington, D. C, 1986.

Dalrymple, G. B., Potassium-argon dating of geomagnetic reversals and North American glaciations, in Calibration of Hominoid Evolution, edited by W. W. Bishop and J. A. Miller, pp. 107-134, Scottish Academic Press, Edinburgh, 1972.

Delaney, M. L. and Boyle, E. A., Tertiary paleoceanic chemical variability: unintended consequences of simple geochemical models, Paleoceanography, 3(2):137-156, 1988.

DePaolo, D. J. and Ingram, B. L., High-resolution stratigraphy with strontium isotopes, Science, 227(4689):938-941, 1985.

Dercourt, J., Zonenshain, L. P., Ricou, L. E., Kazmin, V. G., Le Pichon, X., Knipper, A. L., Grandjacquet, C., Sbortshikov, I. M., Geyssant, J., Lepvrier, C., Pechersky, D. H., Boulin, J., Sibuet, J.-C., Savostin, L. A., Sorokhtin, O., Westphal, M., Bazhenov, M. L., Lauer, J. P., and Biju-Duval, B., Geological evolution of the Tethys belt from the Atlantic to the Pamirs since the Lias, in Evolution of the Tethys, edited by J. Abouin, X. Le Pichon, and A. S. Monin, Tectonophysics, 123(1-4):241-315, 1986.

Dia, A. N., Cohen, A. S., O'Nions, R. K., and Shackleton, N. J., Seawater Sr isotope variation over the past 300 kyr and influence of global climate cycles, Nature, 356(6372):786-788, 1992.

Doell, R. R., Dalrymple, G. B., and Cox, A., Geomagnetic polarity epochs: Sierra Nevada data, 3, J. Geophys. Res., 71:531-541, 1966.

Douglas, R. G. and Savin, S. M., Oxygen and carbon isotope analyses of Tertiary and Cretaceous microfossils from Shatsky Rise and other sites in the north Pacific Ocean, Initial Rep. Deep Sea Drill. Proj., 32(15):509-520, U.S. Gov't Printing Office, Washington, DC, 1975.

Dudley, W. C., Duplessy, J. C., Blackwelder, P. L., Brand, L. E., and Guillard, R. R. L., Coccoliths in Pleistocene-Holocene nannofossil assemblages, Nature, 285(5762):222-223, 1980.

Dudley, W. C. and Goodney, D. E., Oxygen isotope content of coccoliths grown in culture, Deep-Sea Res., 26(5A):495-503, 1979.

Duplessy, J. C., Labou, C., and Vinot, A. C., Differential isotopic fractionation in benthic foraminifera and paleotemperatures reassessed, Science, 168(3928):250-251, 1970.

Edmond, J. M., Himalayan tectonics, weathering processes, and the strontium isotope record in marine limestones, Science, 258(5087):1594-1597, 1992.

Edmond, J. M., Measures, C., McDuff, R. E., Chan, L. H., Collier, R., and Grant, B, Ridge crest hydrothermal activity and the balances of the major and minor elements, Earth and Planet. Sci. Letters, 46(1):1-18, 1979.

Egeberg, P. K., Smalley, P. C., and Aagaard, P., Strontium isotope geochemistry of Leg 113 interstitial waters and carbonates, in Proc. Ocean Drill. Program Sci. Results, edited by P. F. Barker, J. P. Kennett, et al., 113(11):147-157, Ocean Drilling Program, College Station, TX, 1990.

Ehrmann, W. U., Hambrey, M. J., Baldauf, J. G., Barron, J., Larsen, B., Mackensen, A., Wise, S. W., Jr., and Zachos, J. C., History of Antarctic glaciation: An Indian Ocean perspective, in Synthesis of Results from Scientific Drilling in the Indian Ocean, edited by R. A. Duncan, D. K. Rea, R. B. Kidd, U. von Rad, and J. K. Weissel, Geophysical Monograph, 70:423-446, Amer. Geophys. Union, (Washington, D.C.), 1992.

Ehrmann, W. U. and Mackensen, A., Sedimentological evidence for the formation of an East Antarctic ice sheet in Eocene/Oligocene time, *Palaeogeogr., Palaeoclimatol., Palaeoecol.*, *93*(1/2):85-112, 1992.

Elderfield, H., Strontium isotope stratigraphy, *Palaeogeogr., Palaeoclimatol., Palaeoecol.*, *57*(1):71-90, 1986.

Estes, R. and Hutchinson, J. H., Eocene lower vertebrates from Ellesmere Island, Canadian Arctic Archipelago, *Palaeogeogr., Palaeoclimatol., Palaeoecol.*, *30*(3/4):325-347, 1980.

Fischer, A. G. and Arthur, M. A., Secular variations in the pelagic realm, *Soc. Econ. Paleontol. Mineral. Spec. Publ.*, *25*:19-50, 1977.

Garrison, R., Diagenesis of Ocean Carbonate Sediments: A Review of the DSDP Perspective, in *The Deep Sea Drilling Project: A Decade of Progress*, edited by J. E. Warme, R. G. Douglas, and E. L. Winterer, *Soc. Econ. Paleontol. Mineral. Spec. Publ.*, *32*:181-207, 1981.

Gersonde, R. and Burckle, L. H., Neogene diatom biostratigraphy of ODP Leg 113, Weddell Sea (Antarctic Ocean), in *Proc. Ocean Drill. Program Sci. Results*, edited by P. F. Barker, J. P. Kennett, et al., *113*(43):761-789, Ocean Drilling Program, College Station, TX, 1990.

Graham, D. W., Corliss, B. H., Bender, M. L., and Keigwin, L. D., Jr., Carbon and oxygen isotopic disequilibria of Recent deep-sea benthic foraminifera, *Mar. Micropaleont.*, *6*(5/6):483-497, 1981.

Gran, H. H and Braarud, T., A qualitative study of the phytoplankton in the Bay of Funday and the Gulf of Maine, *Biol. Board of Canada Jour.*, *1*:279-467, 1935.

Hailwood, E. A. and Clement, B. M., Magnetostratigraphy of Sites 699 and 700, East Georgia Basin, in *Proc. Ocean Drill. Program Sci. Results*, edited by P. F. Ciesielski, Y. Kristofferson, et al., *114*(19):337-357, Ocean Drilling Program, College Station, TX, 1991a.

Hailwood, E. A. and Clement, B. M., Magnetostratigraphy of Sites 703 and 704, Southeastern South Atlantic, in *Proc. Ocean Drill. Program Sci. Results*, edited by P. F. Ciesielski, Y. Kristofferson, et al., *114*(21):367-385, Ocean Drilling Program, College Station, TX, 1991b.

Hamilton, N., Mesozoic magnetostratigraphy of Maud Rise, Antarctica, in Proc. Ocean Drill. Program Sci. Results, edited by P. F. Barker, J. P. Kennett, et al., 113(20):255-260, Ocean Drilling Program, College Station, TX, 1990.

Haq, B. U., Hardenbol, J., and Vail, P. R., Mesozoic and Cenozoic chronostratigraphy and cycles of sea-level change, in Sea-Level Changes - An Integrated Approach, edited by C. K. Wilgus et al., Soc. Econ. Paleontol. Mineral. Spec. Publ., 42:71—108, 1988.

Harland, W. B., Armstrong, R. L., Cox, A. V., Craig, L. E., Smith, A. G., and Smith, D. G., A geologic time scale 1989, Cambridge Univ. Press, 263 pp., 1990.

Harland, W. B., Cox, A. V., Llewellyn, P. G., Pickton, C. A. G., Smith, A. G., and Walters, R., A Geologic Time Scale, Cambridge Univ. Press, 131 pp., 1982.

Harrison, T. M., Copeland, P., Kidd, W. S. F., and Yin, A., Raising Tibet, Science, 255(5052):1663-1670, 1992.

Harrison, T. M., Yin, A., Chen, W., Ryerson, F. J., Kidd, W. S. F., and Copeland, P., The Neogene thrust, uplift and denudation history of southern Tibet, GSA Abstracts with Programs, 25(6):A-175, 1993.

Hayes, D. E., Age-depth relationships and depth anomalies in the southeast Indian Ocean and South Atlantic Ocean, J. Geophys. Res., 93(B4):2937-2054, 1988.

Heirtzler, J. R., Dickson, G. O., Herron, E. M., Pitman, W. C., III, and Le Pichon, X., Marine magnetic anomalies, geomagnetic field reversals, and motions of the ocean floor and continents; J. Geophys. Res., 73(6):2119-2136, 1968.

Hess, J., Bender, M. L., and Schilling, J.-G., Evolution of the ratio of Strontium-87 to Strontium-86 in seawater from Cretaceous to Present, Science, 231(4741):979-984, 1986.

Hess, J., Stott, L. D., Bender, M. L., Kennett, J. P., Schilling, J.-G., The Oligocene marine microfossil record: high resolution age assessments using strontium isotopes, Paleoceanography, 4(6):655-679, 1989.

Hilgen, F. J., Extension of the astronomically calibrated (polarity) time scale to the Miocene/Pliocene boundary, Earth and Planet. Sci. Letters, 107(2):349-368, 1991.

Hodell, D. A., Progress and paradox in strontium isotope stratigraphy, Paleoceanography, 9(3):395-398, 1994.

Hodell, D. A., Benson, R. H., Kennett, J. P., and Rakic-El Bied, K., Stable isotope stratigraphy of Latest Miocene sequences in northwest Morocco: The Bou Regreg section, Paleoceanography, 4(4):467-482, 1989.

Hodell, D. A., Mead, G. A., and Mueller, P. A., Variation in the strontium isotopic composition of seawater (8 Ma to present): Implications for chemical weathering rates and dissolved fluxes to the oceans, Isotope Geoscience, 80(4):291-307, 1990.

Hodell, D. A., Mueller, P. A., McKenzie, J. A., and Mead, G. A., Strontium isotope stratigraphy and geochemistry of the late Neogene Ocean, Earth and Planet. Sci. Letters, 92(2):165-178, 1989.

Hodell, D. A. and Woodruff, F., Variations in the strontium isotopic ratio of seawater during the Miocene: Stratigraphic and geochemical implications, Paleocenanography, 9(3):405-426, 1994.

Hsü, K. J., LaBrecque, J., and Pisciotto, K. A., Numerical ages of magnetostratigraphically calibrated bistratigraphic zones, in Initial Rep. Deep Sea Drill. Proj., edited by K. J. Hsü, J. L., LaBrecque, J. L., et al., 73(24):623-635, U.S. Gov't Printing Office, Washington, DC, 1984a.

Hsü, K. J., McKenzie, J. A., Oberhänsli, H. J., Weissert, H., and Wright, R. C., South Atlantic Cenozoic paleoceanography, in Initial Rep. Deep Sea Drill. Proj., edited by K. J. Hsü, J. L., LaBrecque, J. L., et al., 73(38):771-785, U.S. Gov't Printing Office, Washington, DC, 1984b.

Keigwin, L. D., Paleoceanographic change in the Pacific at the Eocene-Oligocene boundary, Nature, 287(5784):722-725, 1980.

Keigwin, L. D. and Corliss, B. H., Stable isotopes in late middle Eocene to Oligocene foraminifera, Geol. Soc. America Bull., 97(3):335-345, 1986.

Keigwin, L. D. and Keller, G., Middle Oligocene cooling from equatorial Pacific DSDP Site 77B, Geology, 12(1):16-19, 1984.

Kennett, J. P, Burns, R. E., Andrews, J. E., Churkin, M., Jr., Davies, T. A., Dumitrica, P., Edwards, A. R., Galehouse, J. S., Packham, G. H., And van der Lingen, G. J., Australian-Antarctic continental drift, palaeocirculation changes and Oligocene deep-sea erosion, Nature Physical Science, 239(91):51-55, 1972.

Kennett, J. P. and Shackleton, N. J., Laurentide Ice Sheet Meltwater Recorded in Gulf of Mexico Deep-Sea Cores, Science, 188(4184):147-150, 1975.

Kennett, J. P. and Shackleton, N. J., Oxygen isotopic evidence for the development of the psychrosphere 38 Myr ago, Nature, 260(5551):513-515, 1976.

Kennett, J. P. and Stott, L. D., Proteus and Proto-Oceanus: ancestral Paleogene oceans as revealed from Antarctic stable isotopic results, ODP Leg 113, in Proc. Ocean Drill. Program Sci. Results, edited by P. F. Barker, J. P. Kennett, et al., 113(49):865-880, Ocean Drilling Program, College Station, TX, 1990.

Kennett, J. P., von der Borch, C. C., Baker, P. A., Barton, C. E., Boersma, A., Cauler, J. P., Dudley, W. C., Jr., Gardner, J. V., Jenkins, D. G., Lohman, W. H., Martini, E., Merrill, R. B., Morin, R., Nelson, C. S., Robert, C., Srinivasan, M. S., Stein, R., Takeuchi, A., and Murphy, M. G., Palaeotectonic impications of increased late Eocene-early Oligocene volcanism from South Pacific DSDP sites, Nature, 316(6028):507-511, 1985.

Kent, D. V. and Gradstein, F. M., A Jurassic to recent chronology, in The Western North Atlantic Region, edited by P. Vogt and B. E. Tucholke, pp.45-50, The Geology of North America, v. M, Geological Society of America, Boulder, CO, 1986.

Klitgord, K. D., Huestis, S. P., Mudie, J. D., and Parker, R. L., An analysis of near-bottom magnetic anomalies: Sea-floor spreading and the magnetized layer, Geophys. J. R. astr. Soc., 43(2):387-424, 1975.

Koepnick, R. B., Burke, W. H., Denison, R. E., Hetherington, E. A., Nelson, H. F., Otto, J. B., and Waite, L. E., Construction of the seawater ^{87}Sr/^{86}Sr curve for the Cenozoic and Cretaceous: Supporting Data, Chem. Geol. (Isot. Geosci. Sect.), 58(1/2):55-81, 1985.

Kominz, M. A., Oceanic Ridge Volumes and Sea-Level Change - An Error Analysis, in Interregional unconformities and hydrocarbon accumulation, edited by J. S. Schlee, A. A. P. G. Mem., 36:109-127, 1984.

Kristoffersen, Y. and LaBrecque, J., On the tectonic history and origin of the Northeast Georgia Rise, in Proc. Ocean Drill. Program Sci. Results, edited by P. F. Ciesielski, Y. Kristofferson, et al., 114(2):23-38, Ocean Drilling Program, College Station, TX, 1991.

Kroopnick, P., The distribution of ^{13}C in the Atlantic Ocean, Earth and Planet. Sci. Letters, 49(2):469-484, 1980.

Kroopnick, P., The distribution of ^{13}C of ΣCO_2 in the world oceans, Deep-Sea Res., 32(1):57-84, 1985.

LaBrecque, J. L., Hsü, K. J., Carman, M. F., Jr., Karpoff, A.-M.,. McKenzie, J. A., Percival, S. F., Jr., Petersen, N. P., Pisciotto, K. A., Schreiber, E., Tauxe, L., Tucker, P., Weissert, H. J., and Wright, R., DSDP Leg 73: Contributions to Paleogene stratigraphy in nomenclature, chronology and sedimentation rates; Palaeogeogr., Palaeoclim., Palaeoecol., 42(1/2):91-125, 1983.

LaBrecque, J. L., Kent, D. V., and Cande, S. C., Revised magnetic polarity time scale for Late Cretaceous and Cenozoic time; Geology, 5(6):330-335, 1977.

LaBrecque, J. L., and Rabinowitz, P. D., Magnetic anomalies bordering the continental margin of Argentina, A. A. P. G. Spec. Map Ser., 1977.

Lang, T. H. and Watkins, D. K., Cenozoic calcareous nannofossils from DSDP Leg 77: biostratigraphy and delineation of hiatuses, in Initial Rep. Deep Sea Drill. Proj., edited by R. T. Buffler, W. Schlager, et al., 77(26):629-648, U.S. Gov't Printing Office, Washington, DC, 1984.

Larson, R. L., Golovchenko, X., and Pitman, W. C., III, Geomagnetic polarity time scale, AAPG Plate-Tectonic Map Circum-Pacific Region, Pacific Basin sheet, scale 1:20,000,000, 1982.

Larson, R. L. and Hilde, T. W. L., A revised time scale of magnetic reversals for the Early Cretaceous and Late Jurassic, J. Geophys. Res., 80(17):2586, 1975.

Larson, R. L. and Pitman, W. C., III, World-wide correlation of Mesozoic magnetic anomalies, and its implications; G. S. A. Bull., 83(12):3645-3662, 1972.

Leinen, M., The origin of paleochemical signatures in North Pacific pelagic clays: Partitioning experiments, Geochimica Cosmochimica Acta, 51(2):305-319, 1987.

Leinen, M., The pelagic clay province of the North Pacific Ocean, in The Eastern Pacific Ocean and Hawaii, in The Geology of North America, edited by E. L. Winterer, D. M. Hussong, and R. W. Decker, N(16):323-335, Geol. Soc. Amer., Boulder, CO, 1989.

Lloyd, R. M. and Hsü, K. J., Stable-isotope investigations of sediments from the DSDP III cruise to South Atlantic, Sedimentology, 19(1/2):45-58, 1972.

Lorens, R. B., Sr, Cd, Mn, and Co distribution coefficients in calcite as a function of calcite precipitation rate, Geochimica Cosmochimica Acta, 45(4):553-561, 1981.

Lowrie, W. and Alvarez, W., One hundred million years of geomagnetic polarity history, Geology, 9(9):392-397, 1981.

Lowrie, W., Alvarez, W., and Premoli Silva, I., Late Cretaceous geomagnetic reversal sequence, EOS (Am. Geophys. Un. Trans.) 57:238, 1976.

Lyle, M., Leinen, M., Owen, R. M., and Rea, D. K., Late Tertiary history of hydrothermal deposition at the East Pacific Rise, 19°S: Correlation to volcano-tectonic events, Geophys. Res. Lett., 14(6):595-598, 1987.

Manivit, Paleogene and Upper Cretaceous calcareous nannofossils from Deep Sea Drilling Project Leg 74, in Initial Rep. Deep Sea Drill. Proj., T. C. Moore, P. D. Rabinowitz, et al., 74(8):475- 499, U.S. Gov't Printing Office, Washington, DC, 1984.

Mankinen, E. A. and Dalrymple, G. B., Revised geomagnetic polarity time scale for the interval 0-5 m.y. B.P. J. Geophys. Res., 84(B2):615-626, 1979.

Matthews, R. K. and Poore, R. Z., Tertiary del^{18}O record and glacio-eustatic sea-level fluctuations, Geology, 8(10):501-504, 1980.

McConnaughey, T., ^{13}C and ^{18}O isotopic disequilibrium in biological carbonates: I. Patterns, Geochimica Cosmochimica Acta, 53:151-162, 1989.

McConnaughey, T., ^{13}C and ^{18}O isotopic disequilibrium in biological carbonates: II. In vitro simulation of kinetic isotope effects, Geochimica Cosmochimica Acta, 53:163-171, 1989.

McFarlane, A. M., Timing constraints on the tectonic events in the crystalline core of the Himalaya, Langtang National Park, central Nepal, GSA Abstracts with Programs, 25(6):A174, 1993.

McKenna, M. C., Eocene paleolatitude, climate, and mammals of Ellesmere Island, Palaeogeogr., Palaeoclimatol., Palaeoecol., 30(3/4):349-362, 1980.

Mead, G. A., Tauxe, L., and LaBrecque, J. L., Oligocene Paleoceanography of the South Atlantic: Paleoclimatic implications of sediment accumulation rates and magnetic susceptibility measurements, Paleoceanography, 1(3):273-284, 1986.

Melguen, M., Facies evolution, carbonate dissolution cycles in sediments from the eastern South Atlantic (DSDP Leg 40) since the Early Cretaceous, in *Initial Rep. Deep Sea Drill. Proj.*, edited by H. M. Bolli, W. B. F. Ryan, et al., *40*(29):981-1022, Washington, DC. U.S. Gov't Printing Office), 1978.

Miller, K. G., Middle Eocene to Oligocene stable isotopes, climate, and deep-water history: The Terminal Eocene Event?, in *Eocene-Oligocene Climatic and Biotic Evolution*, edited by D. R. Prothero, and W. A. Berggren,, Princeton Univ. Press, Princeton, NJ, pp.160-177, 1992.

Miller, K. G., Aubry, M-P., Khan, M. J., Melillo, A. J., Kent, D. V., and Berggren, W. A., Oligocene-Miocene biostratigraphy, magnetostratigraphy, and isotopic stratigraphy of the western North Atlantic, *Geology*, *13*(4):257-261, 1985a.

Miller, K. G. and Fairbanks, R. G., Evidence for Oligocene-Middle Miocene abyssal circulation changes in the western North Atlantic, *Nature*, *306*(5940):250-253, 1983.

Miller, K. G. and Fairbanks, R. G., Oligocene-Miocene global carbon and abyssal circulation changes, in *The Carbon Cycle and Atmospheric CO2: Natural Variations, Archaean to Present*, edited by E. Sundquist and W. S. Broecker, *American Geophysical Union Geophysical Monograph Series*, *32*, 469-486, 1985.

Miller, K. G., Fairbanks, R. G., and Mountain, G. S., Tertiary oxygen isotope synthesis, sea level history, and continental margin erosion, *Paleoceanography*, 2(1):1-19, 1987.

Miller, K. G., Feigenson, M. D., Kent, D. V., and Olsson, R. K., Upper Eocene to Oligocene isotope (87Sr/86Sr, δ18O, δ13C) Standard Section, Deep Sea Drilling Project Site 522, *Paleoceanography*, *3*(2):223-233, 1988.

Miller, K. G., Feigenson, M. D., Wright, J. D., and Clement, B. M., Miocene isotope reference section, Deep Sea Drilling Project Site 608: An evaluation of isotope and biostratigraphic resolution, *Paleoceanography*, *6*(1):33-52, 1991a.

Miller, K. G., Mountain, G. S. and Tucholke, B. E., Oligocene glacio-eustasy and erosion on the margins of the North Atlantic, *Geology*, *13*(1):10-13, 1985b.

Miller, K. G. and Thomas, E., Late Eocene to Oligocene benthic foraminiferal isotopic record, Site 574, equatorial Pacific, in Initial Rep. Deep Sea Drill. Proj., edited by L. Mayer, F. Theyer, et al., 85, 771-777, U.S. Gov't Printing Office, Washington, DC, 1985.

Miller, K. G., Wright, J. D., and Fairbanks, R. G., Unlocking the Ice House: Oligocene-Miocene oxygen isotopes, eustasy, and margin erosion, J. Geophys. Res., 96(B4):6829-6848, 1991b.

Moore, T. C. and Heath, G. R., Survival of deep-sea sedimentary sections, Earth and Planet. Sci. Letters, 37(1):71-80, 1977.

Moore, T. C., van Andel, T. H., Sancetta, C., and Pisias, N., Cenozoic hiatuses in pelagic sediments, Micropaleontology, 24(2):113-138, 1978.

Ness, G., Levi, S., and Couch, R., Marine magnetic anomaly time scales for the Cenozoic and Late Cretaceous: a Précis, critique, and synthesis, Rev. Geophys. and Space Physics, 18(4):753-770, 1980.

Noël, D. and Melguen, M., Nannofacies of Cape Basin and Walvis Ridge sediments, lower Cretaceous to Pliocene (Leg 40), in Initial Rep. Deep Sea Drill. Proj., edited by H. M. Bolli, W. B. F. Ryan, et al., 40(7):487-524, U.S. Gov't Printing Office, Washington, DC, 1978.

Oberhänsli, H., McKenzie, J., Toumarkine, M., and Weissert, H., A paleoclimatic and paleoceanographic record of the Paleogene in the central South Atlantic (Leg 73, Sites 522, 523, and 524), in Initial Rep. Deep Sea Drill. Proj., edited by K. J. Hsü, J. L., LaBrecque, et al., 73(34):737-747, U.S. Gov't Printing Office, Washington, DC, 1984.

Oberhänsli, H. and Toumarkine, M., The Paleogene oxygen and carbon isotope history of Sites 522, 523, and 524 from the central South Atlantic, in South Atlantic Paleoceanography, edited by K. J. Hsü and H. J. Weissert, Cambridge Univ. Press, pp. 125-147, 1985.

Oppo, D. W., and Fairbanks, R. G., Variability in the deep and intermediate water circulation of the Atlanic Ocean during the past 25,000 years: Northern Hemisphere modulation of the Southern Ocean, Earth and Planet. Sci. Letters, 86(1):1-15, 1987.

Oslick, J. S., Miller, K. G., Feigenson, M. D., and Wright, J. D., Oligocene-Miocene strontium isotopes: Stratigraphic revisions and correlations to an inferred glacioeustatic record, Paleoceanography, 9(3):427-443, 1994.

Ostlund, H. G., Craig, H., Broecker, W. S., and Spencer, D., GEOSECS Atlantic, Pacific, and Indian Ocean Expeditions, Vol. 7, Shorebased data and graphics, IDOE, NSF, 198 pp., 1987.

Owen, R. M. and Rea, D. K., Sea-floor hydrothermal activity links climate to tectonics: The Eocene Carbon Dioxide Greenhouse, Science, 277(4683):166-169, 1985.

Owen, R. M. and Zimmerman, A. R. B., Geochemistry of Broken Ridge sediments, in Proc. Ocean Drill. Program Sci. Results, edited by J. Weissel, J. Peirce, E. Taylor, J. Alt, et al., 121(21):437-445, Ocean Drilling Program, College Station, TX, 1991.

Palmer, M. R. and Edmond, J. M., The strontium isotope budget of the modern ocean, Earth and Planet. Sci. Letters, 92(1):11-26, 1989.

Palmer, M. R. and Edmond, J. M., Controls over the strontium isotope composition of river water, Geochimica Cosmochimica Acta, 56(5):2099-2111, 1992.

Palmer, M. R. and Elderfield, H., Sr isotope composition of sea water over the past 75 Myr, Nature, 314(6011):526-528, 1985.

Parker, M. E., Clark, M., and Wise, S. W., Jr., Calcareous nannofossils of Deep Sea Drilling Project Sites 558 and 563, North Atlantic Ocean: biostratigraphy and the distribution of Oligocene Braarudosphaerids, in Initial. Rep. Deep Sea Drill. Proj., edited by H. Bougault, S. C. Cande, et al., 82(34):559-589, U.S. Gov't Printing Office, Washington, DC, 1985.

Parrish, R. R. and Hodges, K. V., Miocene (22±1) Ma metamorphism and two stage thrusting in the Greater Himalayan sequence, Annapurna Sanctuary, Nepal, GSA Abstracts with Programs, 25(6):A174, 1993.

Parsons, B. and Sclater, J. G., An analysis of the variation of ocean floor bathymetry and heat flow with age, J. Geophys. Res., 82(5):803-827, 1977.

Paull, C. K. and Theirstein, H. R., Stable Isotopic Fractionation Among Particles in Quaternary Coccolith-Sized Deep-Sea Sediments, Paleoceanography, 2(4):423-429, 1987.

Perch-Nielson, K., Albian to Pleistocene calcareous nannofossils from the western South Atlantic, DSDP Leg 39, in Initial Rep. Deep Sea Drill. Proj., edited by P. R. Supko, K. Perch-Nielson, et al., 39(31):699-823, U.S. Gov't Printing Office, Washington, DC, 1977.

Pickard, G. L. and Emery, W. J., Descriptive Physical Oceanography: an introduction, Pergamon Press, Elmsford, NY, 249 pp., 1982.

Pin, C. and Bassin, C., Evaluation of a strontium-specific extraction chromatographic method for isotopic analysis in geologic materials, Anal. Chimica Acta, 269(2):249-255, 1992.

Poore, R. Z. and Matthews, R. K., Late Eocene-Oligocene oxygen- and carbon-isotope record from South Atlantic Ocean, Deep Sea Drilling Project Site 522, in Initial Rep. Deep Sea Drill. Proj., edited by K. J. Hsü, J. L., LaBrecque, et al., 73(33):725-735, U.S. Gov't Printing Office, Washington, DC, 1984.

Poore, R. Z. and Matthews, R. K., Oxygen isotope ranking of Late Eocene and Oligocene planktonic foraminifers: implications for Oligocene sea-surface temperatures and global ice volume, Mar. Micropaleont., 9(2):111-134, 1984.

Prentice, M. L. and Matthews, R. K., Cenozoic ice-volume history: Development of a composite oxygen isotope record, Geology, 16(11):963-966, 1988.

Proto Decima, F., Medizza, F., and Todesco, L., Southeastern Atlantic Leg 40 calcareous nannofossils, in Initial Rep. Deep Sea Drill. Proj., edited by H. M. Bolli, W. B. F. Ryan, et al., 40(12):571-634, U.S. Gov't Printing Office, Washington, DC, 1978.

Railsback, L. B., Anderson, T. F., Ackerly, S. C., and Cisne, J. L., Paleoceanographic modeling of temperature - salinity profiles from stable isotopic data, Paleoceanography, 4(5):585-591, 1989.

Raymo, M. E., and Ruddiman, W. F., Tectonic forcing of late Cenozoic climate, Nature, 359(6391):117-122, 1992.

Raymo, M. E., Ruddiman, W. F., and Froelich, P. N., Influence of late Cenozoic mountain building on ocean geochemical cycles, Geology, 16(7):649-653, 1988.

Raymond, C. A., LaBrecque, J. L. and Kristofferson, Y., Islas Orcadas Rise and Meteor Rise: the tectonic and depositional history of two aseismic plateaus from ODP sites 702, 703, and 704, Proc. Ocean Drill. Program Sci. Results, edited by P. F. Ciesielski, Y. Kristofferson, et al., 114(1):5-22, Ocean Drilling Program, College Station, TX, 991.

Rea, D. K., Delivery of Himalayan sediment to the northern Indian Ocean and its relation to global climate, sea level, uplift, and seawater Strontium, in Synthesis of Results from Scientific Drilling in the Indian Ocean, edited by R. A. Duncan, D. K. Rea, R. B. Kidd, U. von Rad, and J. K. Weissel, Geophysical Monograph, 70:387-402, Appendix 1, Amer. Geophys. Union, (Washington, D.C.), 1992.

Reid, J. L., On the contribution of the Mediterranean Sea outflow to the Norwegian-Greenland Sea, Deep-Sea Res., 26(11A):1199-1223, 1979.

Reynolds, R. C. and Johnson, N. M., Chemical weathering in the temperate glacial environment of the North Cascade Mountains, Geochim. Cosmochim. Acta, 36:537-554, 1972.

Richter, F. M., Rowley, D. B., and DePaolo, D. J., Sr isotope evolution of seawater: the role of tectonics, Earth and Planet. Sci. Letters, 109(1/2):11-23, 1992.

Robert, C. and Chamley, H., Late Eocene-Early Oligocene evolution of climate and marine circulation: Deep-sea clay mineral evidence, in The Antarctic Paleoenvironment: A perspective on global change, edited by J. P. Kennett and D. A. Warnke, Antarctic Research Series, 56:97-117, Amer. Geophys. Union, Washington, DC, 1992.

Roth, P. H., Calcareous nannofossils from the Northwestern Indian Ocean, Leg 24, Deep Sea Drilling Project, in Initial Rep. Deep Sea Drill. Proj., edited by A. G. Fischer, E. T. Bunce, et al., 24(23):969-994, U.S. Gov't Printing Office, Washington, DC, 1974.

Rowley, D. B. and Lottes, A. L., Plate-kinematic reconstructions of the North Atlantic and Arctic: Late Jurassic to Present, Tectonophysics, 155(1/4):73-120, 1988.

Ryan, W. B. F., Geodynamic implications of the Messinian Crisis of salinity, in Messinian events in the Mediterranean, edited by C. W. Drooger, pp. 26-38, North-Holland, Amsterdam, 1973.

Saito, T. and Percival, S. F., Mid-Atlantic Ridge Sequence" in Maxwell, A. E. et al., 1970, Summary and Conclusions, in Initial Rep. Deep Sea Drill. Proj., edited by A. E. Maxwell, R. P. Von Herzen, et al., 3(13):441-471, U.S. Gov't Printing Office, Washington, DC, 1970.

Salamy, K. A., Zachos, J. C., Quinn, T. M., and Diester-Haass, L., High frequency variations in ice volume, calcite dissolution, and primary productivity in the early Oligocene as inferred from deep sea sediment records, EOS (Am. Geophys. Un. Trans.) 75(44):393, 1994.

Savin, S. M., Douglas, R. G., and Stehli, F. G., Tertiary marine paleotemperatures, Geol. Soc. of Amer. Bull., 86(11):1499-1510, 1975.

Shackleton, N. J., Attainment of isotopic equilibrium between ocean water and the benthonic foraminifera genus Uvigerina: isotopic changes in the ocean during the last glacial, Colloques Internationaux du Centre National del la Recherche Scientifique, 219:203-209, Les Methodes Quantitatives d'Etude des Variations du Climat au Cours du Pleistocene, 1974.

Shackleton, N. J., Paleogene stable isotope events, Palaeogeogr., Palaeoclimatol., Palaeoecol., 57(1):91-102, 1986.

Shackleton, N. J., Berger, A., and Peltier, W. R., An alternative astronomical calibration of the lower Pleistocene timescale based on ODP Site 677, Trans. R. Soc. Edinburgh: Earth Sci., 81(4):251-261, 1990.

Shackleton, N. J. and Kennett, J. P., Paleotemperature history of the Cenozoic and the initiation of Antarctic glaciation: oxygen and carbon isotope analysis in DSDP Sites 277, 279, and 281, in Initial. Rep. Deep Sea Drill. Proj., edited by J. P. Kennett, R. E. Houtz, et al., 29(17):743-755, U.S. Gov't Printing Office, Washington, DC, 1975.

Shackleton, N. J. and Opdyke, N. D., Oxygen isotope and palaeomagnetic stratigraphy of Equatorial Pacific Core V28-238: Oxygen isotope temperatures and ice volumes on a 10^5 year and 10^6 year scale, Quat. Res., 3(1):39-55, 1973.

Shipboard Scientific Party, Walvis Ridge - Sites 362 and 363, in Initial Rep. Deep Sea Drill. Proj., edited by H. M. Bolli, W. B. F. Ryan, et al., 40:183-356, U.S. Gov't Printing Office, Washington, DC, 1978.

Shipboard Scientific Party, Site 522, in Initial Rep. Deep Sea Drill. Proj., edited by K. J. Hsü, J. L. LaBrecque, et al., 73:187-270, U.S. Gov't Printing Office, Washington, DC, 1984.

Shipboard Scientific Party, Site 689, in Proc. Ocean Drill. Program Initial Rep., edited by P. F. Barker, J. P. Kennett, et al., 113(5):89-181, Ocean Drilling Program, College Station, TX, 1988a.

Shipboard Scientific Party, Site 690, in Proc. Ocean Drill. Program Initial Rep., edited by P. F. Barker, J. P. Kennett, et al., 113(6):183-292, Ocean Drilling Program, College Station, TX, 1988b.

Shipboard Scientific Party, Site 699, in Proc. Ocean Drill. Program Initial Rep., edited by P. F. Ciesielski, Y. Kristofferson, et al., 114(6):621-795, Ocean Drilling Program, College Station, TX, 1988c.

Siesser, W. G., Leg 40 results in relation to continental shelf and onshore geology, in Initial Rep. Deep Sea Drill. Proj., edited by H. M. Bolli, W. B. F. Ryan, et al., 40(28):965-979, U.S. Gov't Printing Office, Washington, DC, 1978.

Smayda, T. J., A quantitative analysis of the phytoplankton of the Gulf of Panama - III. General Ecological conditions, and the phytoplankton dynamics at 8 deg 45'N, 79 deg 23'W from November 1954 to May 1957, Inter-Am. Tropical Tuna Comm. Bull., 11(5):353-612, 1966.

Spieβ, V., Cenozoic magnetostratigraphy of Leg 113 drill sites, Maud Rise, Weddell Sea, Antarctica, in Proc. Ocean Drill. Program Sci. Results, edited by P. F. Barker, J. P. Kennett, et al., 113(21):261-315, Ocean Drilling Program, College Station, TX, 1990.

Steiger, R. H. and Jäger, E., Subcomission on geochronology: Convention on the use of decay constants in geo- and cosmochronology, Earth and Planet. Sci. Letters, 36:359-362, 1977.

Stott, L. D. and Kennett, J. P., Antarctic Paleogene planktonic foraminifer biostratigraphy: ODP Leg 113, Sites 689 and 690, in Proc. Ocean Drill. Program Sci. Results, edited by P. F. Barker, J. P. Kennett, et al., 113(34):549-569, Ocean Drilling Program, College Station, TX, 1990.

Tarling, D. H. and Mitchell, J. G., Revised Cenozoic polarity time scale, Geology, 4(3):133-136, 1976.

Tauxe, L., Besse, J., and LaBrecque, J. L., 1983, Palaeolatitudes from DSDP Leg 73 sediment cores: implications for the apparent polar wander path for Africa during the late Mesozoic and Cenozoic, Geophys. J. R. astr. Soc., 73:315-324.

Tauxe, L., Tucker, P., Petersen, N. P., and LaBrecque, J. L., Magnetostratigraphy of Leg 73 Sediments, in Initial Rep. Deep Sea Drill. Proj., edited by K. J. Hsü, J. L., LaBrecque, et al., 73(23):609-621, U.S. Gov't Printing Office, Washington, DC, 1984.

Thomas, E., Development of Cenozoic deep-sea benthic foraminiferal faunas in Antarctic waters, in Origins and Evolution of the Antarctic Biota, edited by J. A. Crame, Geol. Soc. Spec. Publ., 47, 283-296, 1989.

Thomas, E., Late Cretaceous through Neogene deep-sea benthic foraminifers (Maud Rise, Weddell Sea, Antarctica), in Proc. Ocean Drill. Program Sci. Results, edited by P. F. Barker, J. P. Kennett, et al., 113(35):571-594, Ocean Drilling Program, College Station, TX, 1990.

Thomas, E., Middle Eocene - late Oligocene bathyal benthic foraminifera (Weddell Sea): faunal changes and implications for ocean circulation, in Eocene - Oligocene Climatic and Biotic Evolution, edited by D. A. Prothero and W. A. Berggren, Princeton Univ. Press, Princeton, NJ, pp. 245-271, 1992.

Thomas, E., Barrera, E., Hamilton, N., Huber, B. T., Kennett, J. P., O'Connell, S. B., Pospichal, J. J., Speiβ, V., Stott, L. D., Wei, W., and Wise, S. W., Jr., Upper Cretaceous-Paleogene stratigraphy of sites 689 and 690, Maud Rise, Antarctica), in Proc. Ocean Drill. Program Sci. Results, edited by P. F. Barker, J. P. Kennett, et al., 113(51):901-914, Ocean Drilling Program, College Station, TX, 990.

Vail, P., Mitchum, R. M., Jr., and Thompson, S., Seismic Stratigraphy and Global Changes of Sea Level, Part 4. Global Cycles of Relative Changes of Sea Level, in Seismic Stratigraphy - Applications to hydrocarbon exploration, edited by C. E. Payton, A. A. P. G. Mem., 26:83-97, 1977.

Van Andel, T. H., Heath, G. R., and Moore, T. C., Cenozoic history and paleoceanography of the Central Equatorial Pacific Ocean, Geol. Soc. of Amer. Mem., 143, 134 pp., 1975.

Van Andel, T. H., Thiede, J., Sclater, J. G., and Hay, W. W., Depositional history of the South Atlantic Ocean during the last 125 Million Years, J. Geol., 85(6):651-698, 1977.

Van Hinte, J. E., A Cretaceous time scale, A. A. P. G. Bull., 60:489-497, 1976a.

Van Hinte, J. E., A Jurassic time scale, A. A. P. G. Bull., 60:498-516, 1976b.

Vine, F. J. and Matthews, D. H., Magnetic anomalies over oceanic ridges, Nature, 199:947-949, 1963.

Vogt, P. R, Changes in geomagnetic reversal frequency at times of tectonic change: Evidence for coupling between core and upper mantle processes, Earth and Planet. Sci. Letters, 25(3):313-321, 1975.

Wadleigh, M. A., Veizer, J., and Brooks, C., Strontium and its isotopes in Canadian rivers: Fluxes and global implications, Geochimica Cosmochimica Acta, 49(8):1727-1736, 1985.

Webb, R. S., Anderson, D. M., and Overpeck, J. T., Archiving data at the World Data Center-A for Paleoclimatology, Paleoceanography, 9(3):391-393, 1994.

Wei, W., Middle Eocene-lower Oligocene calcareous nannofossil magnetobiochronology of ODP Holes 699A and 703A in the subantarctic South Atlantic, Mar. Micropaleont., 18(1/2):143-165, 1991.

Wei, W., Paleogene chronology of southern ocean drill holes: An update, in The Antarctic Paleoenvironment: A perspective on global change, edited by J. P. Kennett and D. A. Warnke, Antarctic Research Series, 56:75-96, Amer. Geophys. Union, Washington, DC, 1992.

Wei, W., and Wise, S. W., Jr., Middle Eocene to Pleistocene calcareous nannofossils recovered by Ocean Drilling Program Leg 113 in the Weddell Sea, in Proc. Ocean Drill. Program Sci. Results, edited by P. F. Barker, J. P. Kennett, et al., 113(38):639-666, Ocean Drilling Program, College Station, TX, 1990.

Wei, W., and Wise, S. W., Jr., Eocene-Oligocene calcareous nannofossil magnetobiochronology of the Southern Ocean, Newsl. Stratigr., 26:119-126, 1992.

Wise, S. W., Jr., Breza, J. R., Harwood, D. M., and Wei, W., Paleogene glacial history of Antarctica, in Controversies in Modern Geology, edited by D. W. Müller, J. A. McKenzie, and H. Weissert, pp. 133-171, Academic Press, Ltd., Academic Press, Inc., San Diego, CA., 1991.

Wise, S. W., Jr., Breza, J. R., Harwood, D. M., Wei, W., and Zachos, J. C., Paleogene glacial history of Antarctica in light of Leg 120 drilling results, in Proc. Ocean Drill. Program Sci. Results, edited by S. W. Wise, R. Schlich, et al., 120(31):1001-1030, Ocean Drilling Program, College Station, TX, 1992.

Wise, S. W., Jr., and Hsü, K. J., Genesis and Lithification of a Deep Sea Chalk, Ecologae geol. Helv., 64(2):273-278, 1971.

Wise, S. W., Jr., and Kelts, K. R., Inferred diagenetic history of a weakly silicified deep sea chalk, Gulf Coast Assoc. Geol. Soc. Trans., 22:177-203, 1972.

Wolfe, J. A., Tertiary climates and floristic relationships at high latitudes in the Northern Hemisphere, Palaeogeogr., Palaeoclimatol., Palaeoecol., 30(3/4):313-323, 1980.

Wright, J. D. and Miller, K. G., Miocene stable isotope stratigraphy, Site 747, Kerguelen Plateau, in _Proc. Ocean Drill. Program Sci. Results_, edited by S. W. Wise, R. Schlich, et al., _120_(45):855-866, Ocean Drilling Program, College Station, TX, 1992.

Wright, J. D. and Miller, K. G., Southern Ocean influences on late Eocene to Miocene deep-water circulation, in _The Antarctic Paleoenvironment: A Perspective on Global Change, Part 2_, edited by J. P. Kennett and D. A. Warnke, _Antarctic Research Series_, _60_:1-26, Amer. Geophys. Union, Washington, DC, 1993.

Zachos, J. C., Berggren, W. A., Aubry, M.-P., and Mackensen, A., Isotope and trace element geochemistry of Eocene and Oligocene foraminifers from Site 748, Kerguelen Plateau, in _Proc. Ocean Drill. Program Sci. Results_, edited by S. W. Wise, R. Schlich, et al., _120_(44):839-854, Ocean Drilling Program, College Station, TX, 1992a.

Zachos, J. C., Breza, J. R., and Wise, S. W., Early Oligocene ice-sheet expansion on Antarctica: Stable isotope and sedimentological evidence from Kerguelen Plateau, southern Indian Ocean, _Geology_, _20_(6):569-573, 1992b.

Zachos, J. C., Opdyke, B. N., Jones, C. E., Quinn, T. M., and Halliday, A. N., Estabishing a link between Antarctic glaciation and early Cenozoic variations in seawater ^{87}Sr/^{86}Sr, in preparation.

BIOGRAPHICAL SKETCH

Greg Mead was born in Los Angeles, CA, and grew up in Connecticut. He earned a Bachelor of Arts (cum laude) in Geology at the University of Pennsylvania in 1978, and a Master of Science in Geological Oceanography at the Graduate School of Oceanography at the University of Rhode Island before heading south to New Orleans to work for Gulf Oil Exploration and Production Co. for a year. Wising up, he returned to school and work in San Diego, CA, before deciding that his future lay in Florida, where he has worked on his doctorate since 1987.

I certify that I have read this study and that in my opinion it conforms to acceptable standards of scholarly presentation and is fully adequate, in scope and quality, as a dissertation for the degree of Doctor of Philosophy.

David A. Hodell

David A. Hodell, Chair
Associate Professor of Geology

I certify that I have read this study and that in my opinion it conforms to acceptable standards of scholarly presentation and is fully adequate, in scope and quality, as a dissertation for the degree of Doctor of Philosophy.

Paul F. Ciesielski
Associate Professor of Geology

I certify that I have read this study and that in my opinion it conforms to acceptable standards of scholarly presentation and is fully adequate, in scope and quality, as a dissertation for the degree of Doctor of Philosophy.

Douglas S. Jones
Professor of Geology

I certify that I have read this study and that in my opinion it conforms to acceptable standards of scholarly presentation and is fully adequate, in scope and quality, as a dissertation for the degree of Doctor of Philosophy.

Neil D Opdyke

Neil D. Opdyke
Professor of Geology

I certify that I have read this study and that in my opinion it conforms to acceptable standards of scholarly presentation and is fully adequate, in scope and quality, as a dissertation for the degree of Doctor of Philosophy.

Claire L. Schelske
Carl S. Swisher Eminent
Scholar in Water Resources

This dissertation was submitted to the Graduate Faculty of the Department of Geology in the College of Liberal Arts and Sciences and to the Graduate School and was accepted as partial fulfillment of the requirements for the degree of Doctor of Philosophy.

May, 1995

Karen A. Holbrook

Dean, Graduate School

LD
1780
1995
.M479

UNIVERSITY OF FLORIDA
3 1262 08554 1729